Functional characterization of *Drosophila* sturkopf in cell proliferation and endocrine physiology regulation

Inaugural-Dissertation

zur Erlangung des Doktorgrades
der Mathematisch-Naturwissenschaftlichen Fakultät
der Heinrich-Heine-Universität Düsseldorf

vorgelegt von

Irfan Akhtar
aus Wuppertal

Düsseldorf, März 2023

aus dem Institut für Mathematische Modellierung biologischer Systeme
Arbeitsgruppe Systembiologie des Fettstoffwechsels
der Heinrich-Heine-Universität Düsseldorf

Gedruckt mit der Genehmigung der
Mathematisch-Naturwissenschaftlichen Fakultät der
Heinrich-Heine-Universität Düsseldorf

Berichterstatter:
1. Jun.-Prof. Dr. Mathias Beller
2. Prof. Dr. Thomas Klein

Tag der mündlichen Prüfung:
31.10.2023

“Come what may, all bad fortune is to be conquered by endurance.”
Vergil

INDEX

Abstract

Lipid droplets (LDs) are highly dynamic organelles involved in many physiological and pathophysiological processes. Especially the LD-associated proteome affects health and disease. Deregulation of lipid droplet associated proteins (LDAPs) is linked to obesity, diabetes, and several types of cancer, including prostate cancer (PCa). The LDAP protein LDAH (lipid droplet-associated hydrolase) and its homologs were shown to impact a broad spectrum of physiological processes including cell proliferation and endocrine regulation. Loss of *LDAH* promotes PCa in mice and humans. The molecular mechanism of how *LDAH* loss of function (LOF) promotes prostate carcinogenesis is, however, not understood.

The aim of this study was, hence, to investigate whether the function of the *Drosophila* LDAH homolog sturkopf affects proliferation and endocrine physiology regulation *in vitro* and *in vivo*. The results of cell proliferation assays in cultured *Drosophila* cells confirm a role of sturkopf on cell proliferation. Protein-protein interaction (PPI) studies suggest that sturkopf participates in the regulation of protein stability and the ubiquitination machinery. Deregulation of androgen signaling is a hallmark of PCa. Regulation of ecdysone signaling in the accessory gland (AG), the functional analog of the mammalian prostate, and androgen signaling in the prostate were shown to partially underly conserved mechanisms. A deregulation of ecdysone signaling in *sturkopf* mutant males was hypothesized previously. *In vitro* and *in vivo* analyses of a putative sturkopf-mediated regulation of ecdysone signaling indicate a stabilizing role of sturkopf in EcR protein stability. Significantly reduced ecdysone hemolymph titers in male *sturkopf* LOF animals signify a profound role of sturkopf in ecdysone signaling. Moreover, *in vivo* analyses of *sturkopf* LOF animals revealed a remarkable loss of secondary cells (SCs) in the AG in a sturkopf- and likely SC-dependent manner. Data of this work further proposes alterations in apoptotic processes in *sturkopf* LOF animals causing the loss of SCs. Cell survival and proliferation due to loss of apoptosis promotes tumorigenesis ultimately leading to PCa.

Altogether, the results of this work reveal a crucial role of sturkopf in proliferation, endocrine physiology regulation, as well as protein stability regulation. As all these aspects have a high significance in PCa, the study aids in gaining a mechanistic insight of *LDAH* loss and prostate carcinogenesis in the mammalian system.

Vorveröffentlichungen der Dissertation

Teilergebnisse aus dieser Arbeit und Mitarbeit in anderen Projekten wurden mit Genehmigung der Mathematisch-Naturwissenschaftlichen Fakultät der Heinrich-Heine-Universität Düsseldorf, vertreten durch die Institutsleitung und Mentoren, in folgenden Beiträgen vorab veröffentlicht:

Publikation: Schönborn J. W., Stewart F. A., Maas-Enriquez K., **Akhtar I.**, Droste A., Waschina S., Beller M. Modeling *Drosophila* gut microbe interactions reveals metabolic interconnectivity. iScience, 2021.

Irfan Akhtar hat zu dieser Publikation beigetragen:

- Bakterielle Wachstumsmessungen
- am Schreibprozess beteiligt

Publikation: **Akhtar I.**, Stewart F. A., Härle A., Droste A., Beller M. Visualization of endogenous gut bacteria in *Drosophila melanogaster* using fluorescence *in situ* hybridization. PLOS ONE, 2021.

Irfan Akhtar hat zu dieser Publikation beigetragen:

- einen Großteil der *in vitro* und *in vivo* Daten:
    - Hybridisierung und fluoreszenzmikroskopische Aufnahmen bakterieller Zellsuspensionen, bakterieller Isolate aus *Drosophila*, *Drosophila* Fäzes
    - Präparation, Hybridisierung und fluoreszenzmikroskopische Aufnahmen aller larvalen und adulten *Drosophila* Därme
- Aufbau, Formale Analyse, Datenerhebung und -auswertung
- entscheidend am Schreibprozess beteiligt

Publikation: Chartschenko E., Hugenroth M., **Akhtar I.**, Droste A., Kolkhof P., Bohnert M., Beller M. CG32803 is the fly homolog of LDAF1 which influences lipid storage *in vivo*. Insect Biochemistry and Molecular Biology, 2021.

Irfan Akhtar hat zu dieser Publikation beigetragen:

- Präparation, Prozessierung und Antikörper- und Lipidfärbungen larvaler Fettkörper
- Fluoreszenzmikroskopische Aufnahme und Analyse des präparierten Gewebes

Tagungsbeiträge:

Werthebach M., Stewart F. A., Gahlen A., Mettler-Altmann T., **Akhtar I.**, Maas-Enriquez K., Droste A., Eichmann T. O., Poschmann G., Stuhler K., Beller M. Control of *Drosophila* growth and survival by the lipid droplet-associated protein CG9186/Sturkopf. Poster, European *Drosophila* Research Conference (EDRC) Lausanne, Schweiz, 2019.

Stewart F. A., **Akhtar I.**, Kuder K., Droste A., Beller M. Host interoperability and stability of the *Drosophila melanogaster* gut microbiome. Poster, European *Drosophila* Research Conference (EDRC) Lausanne, Schweiz, 2019.

Chartschenko E., Hugenroth M., **Akhtar I.**, Droste A., Kolkhof P., Bohnert M., Beller M. CG32803 is the fly homolog of LDAF1 which influences lipid storage *in vivo*. Vortrag, Lipid Droplet Workshop, Düsseldorf, 2020.

Eingereichte Beiträge:

Weitreichende Teilergebnisse aus dieser Arbeit wurden in einem fertigen Manuskript zusammengefasst und vorab zur Begutachtung eingereicht:

Manuskript: **Akhtar I.**, Kolkhof P., Bursa D., Seidel S., Beller M. Loss of *Drosophila sturkopf* regulates prostate cancer-relevant processes.

1 Introduction

In biology, energy homeostasis is defined as the balance between energy influx and efflux. Storage macromolecules, encompassing carbohydrates and lipids especially, serve as buffers in case energy expenditure exceeds energy influx. Energy homeostasis is a fundamental process which needs to be tightly regulated both on a cellular and organismic scale as its deregulation can have severe consequences for the organism. This requires the capability of each cell and organ to store energy in times of energy excess and to remobilize the stored energy, in turn, if needed. Adenosine triphosphate (ATP) is the major organic compound providing energy to fuel diverse cellular processes such as intracellular signaling (Novak 2003; Li et al. 2013), DNA/RNA synthesis (Enomoto et al. 1981; Joyce and Steitz 1995; Martin and MacNeill 2002), and amino acid activation in protein synthesis (Pang et al. 2014) in all living organisms. It is intracellularly present in only small amounts due to a rapid turnover rate and generated on demand from either glycogen or neutral lipids such as triacylglycerols (TAG) (Flatt 1995). While ATP is quickly generated from hydrated glycogen for a fast response, the main energy storage form of cells are lipids as these macromolecules are the most energy-dense molecules yielding much more energy than hydrated glycogen (Flatt 1987).

In humans, lipids are primarily stored in dedicated cells, named adipocytes, forming the adipose tissue. This tissue is compartmentalized in white adipose tissue (WAT) and brown adipose tissue (BAT) (Cinti 2005; Tseng 2023). The far more abundant WAT is mainly comprised of large univaculoar adipocytes harboring a large single lipid droplet (LD) (Saely et al. 2012) and serves several functions such as lipid storage (Saely et al. 2012), thermal insulation (Alexander et al. 2015), and functioning as endocrine organ via hormone secretion (Scherer 2006; Martínez-Sánchez 2020). BAT, on the other hand, is made up of plurivacuolar adipocytes rich in smaller, numerous LDs (Saely et al. 2012) and mitochondria (Cinti 2009). Its main role serves the generation of heat, a process known as thermogenesis (Cannon and Nedergaard 2004). Storage and remobilization of lipids is, however, not restricted to the adipose tissue. LDs can be found in almost every cell within an organism in order to facilitate localized cellular lipid storage and remobilization (Krahmer et al. 2013a). Besides their main function of storing neutral lipids, LDs are highly dynamic cellular organelles which participate in a lot of processes beyond mere lipid metabolism

(Welte and Gould 2017; Olzmann and Carvalho 2019). Their highly diverse functionality is determined by the proteins attached to their surface, termed the LD-associated proteins (LDAPs) (Zhang and Liu 2019). While most of these proteins participate in LD biogenesis or lipid metabolism (Welte and Gould 2017; Olzmann and Carvalho 2019), more LDAPs are progressively identified operating outside lipid metabolism (Welte and Gould 2017; Currall et al. 2018; Werthebach et al. 2019). Deregulation of the delicate interplay between LDAPs and their associated functions has been identified in several pathophysiological conditions covering metabolic diseases such as obesity (Xu et al. 2018), diabetes (Xu et al. 2018), non-alcoholic fatty liver disease (Xu et al. 2018; Ikura and Caldwell 2015), cardiomyopathy (Huang et al. 2022), as well as different types of cancers (Currall et al. 2018; Bai et al. 2021; Luo et al. 2022) highlighting the general importance of LD and LDAPs in physiology as well as their proper regulation.

1.1 Lipid droplet biology

Lipid droplets (LDs) constitute cellular organelles which serve the regulated deposition and remobilization of storage lipids, mainly neutral lipids such as triacylglycerols and sterol esters. These multifunctional organelles can be found among almost every form of life all sharing the same architecture: a hydrophobic core comprising storage lipids enveloped by a phospholipid monolayer, which mostly consist of phosphatidylcholine and phosphoethanolamine and a diverse proteomic set decorating its surface (Murphy 2001; Farese and Walther 2009; Wilfling et al. 2014; Thiam and Beller 2017). Being considered as static cellular lipidic accumulations for a very long time (Fawcett 1966), it is now known that LDs are fully entitled cellular organelles interacting with a variety of different organelles such as mitochondria, peroxisomes, lysosomes among others (Liu et al. 2004; Farese and Walther 2009; Olzmann and Carvalho 2019).

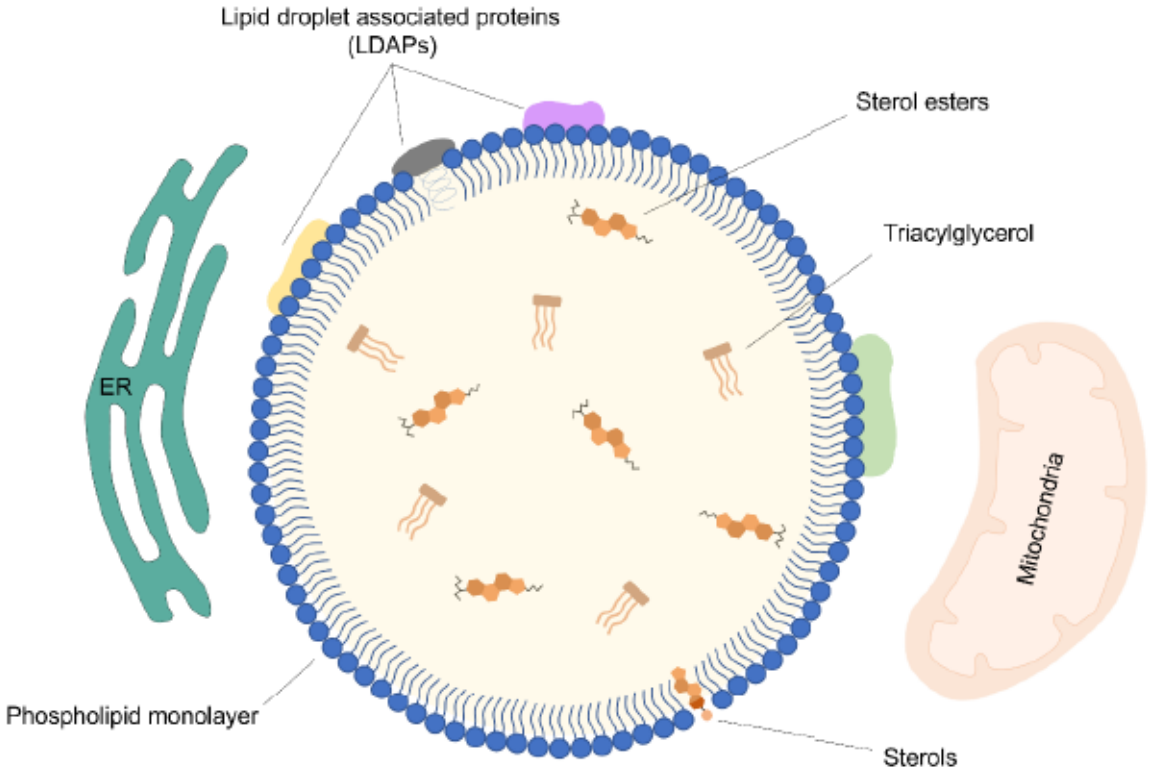

Figure 1: Basic lipid droplet (LD) morphology. LDs are comprised of a hydrophobic core of neutral lipids (triacylglycerol, sterol esters) surrounded by a phospholipid monolayer with a diverse set of lipid droplet associated proteins (LDAPs) attached. Hydrophobic acyl chains of the phospholipid monolayer are oriented towards the neutral lipid core, whereas the polar head groups face the aqueous cytosol. LDs are known to interact with a variety of other cellular organelles such es mitochondria or the endoplasmic reticulum (ER), where LDs originate from.

Although universal in their architecture, LDs can differ in size depending on their cellular origin. In most cases, the size of LDs ranges from 20-40 nm (Guo et al. 2009). However, in adipocytes, they reach a size of up to 200 µm, occupying almost the entire cellular volume (Suzuki et al. 2011; Heid and Franke 2014). Still, independent from their size, the major function of these organelles is the storage of triacylglycerols and sterol esters in times of nutrient excess and the remobilization of the stored neutral lipids on energy demand, respectively.

The most widely recognized model of LD biogenesis proposes a *de novo* LD origin at the leaflet of the ER membrane through localized lipogenesis and lipid nucleation (Thiam and Beller 2017; Henne et al. 2018) Ongoing lipogenesis results in the formation of a lipid lens which bends towards the cytosol. The cytosolic phospholipid monolayer of the endoplasmic reticulum envelops the growing droplet which finally

buds into the cytosol as nascent LD (Thiam and Beller 2017; Henne et al. 2018; Jackson 2019).

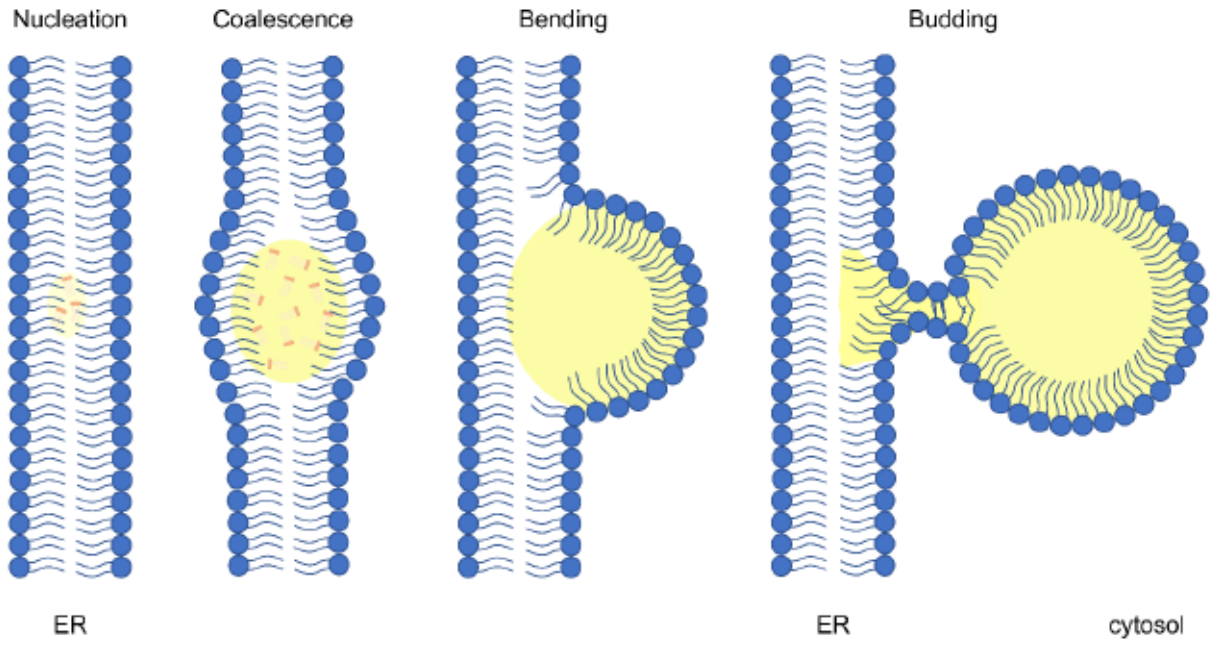

Figure 2: Lipid droplet biogenesis. A lipid lens nucleates in the ER intermembrane space due to *de novo* triglyceride synthesis and accumulation. Triglycerides coalesce over time which results in growth of the lipid lens. The ER membrane bends towards the cytosol due to ongoing growth of the lipid lens and envelops the arising droplet. Finally, the nascent LD buds off into the cytosol.

The major enzymes necessary for lipid synthesis also localize to the ER membrane (Buhman et al. 2001). Triacylglycerol (TAG) synthesis is mediated by the enzymatic conversion of glycerol-3-phosphate to phosphatidic acid via acetylation by the glycerol phosphate acyltransferase (GPAT) as well as the acylglycerolphosphate acyltransferase (AGPAT) (Takeuchi and Reue 2009). Phosphatidic acid phosphatase (lipin)-mediated conversion of phosphatidic acid results in the generation of diacylglycerol which, in turn, gets esterified to triacylglycerol via the diacylglycerol acyltransferase. Thus, lipins influence the regulation of triacylglycerol formation (Carman and Han 2009; Siniossoglou 2013). There is growing evidence that lipins are also regulating triacylglycerol synthesis at the origin of LD biogenesis (Adeyo et al. 2011). Other proteins have been identified as major regulators of *de novo* LD biogenesis such as seipin (Szymanski et al. 2007) and fat storage-inducing (FIT) proteins (Kadereit et al. 2008). Seipin is a homo-oligomeric integral membrane protein in the ER concentrating at the ER-LD junction (Salo et al. 2016; Salo et al. 2019). At this interorganellar contact site, Seipin modulates LD abundance and size

by facilitating continuous triglyceride transfer to LDs (Szymanski et al. 2007; Fei et al. 2008; Wang et al. 2018; Salo et al. 2019). FIT proteins belong to a conserved ER-localized transmembrane protein family capable of binding triglycerides which is important for LD formation (Gross et al. 2011). A potential role of these proteins in the generation of nascent LDs via concentration of triglycerides at the ER leaflet and, thus, promotion of the LD budding process has been hypothesized (Goh and Silver 2013). Recent findings suggest a role of these proteins in organization of LD biogenesis (Chen et al. 2021) and were found to be essential for maintenance of lipid homeostasis at the ER and LD morphology (Yap et al. 2020). Cholesteryl esters are the second most abundant neutral lipid species found in LDs. Their synthesis is mediated by the intracellular esterification of cholesterol via sterol-O-acyltransferases (ACAT) (Wilfling et al. 2014).

Throughout the different steps of LD biogenesis, LDs obtain their functional diversity which is primarily characterized by their lipid composition as well as the proteomic set attached in their surface (Beller et al. 2006; Hsieh et al. 2012). The proteinaceous composition of LDs is highly variable as several proteins only bind to special LD subsets (Kory et al. 2016; Thul et al. 2017) with regard to their neutral lipid composition (Hsieh et al. 2012), their phospholipid composition, or their size (Fei et al. 2008). The LD proteome dramatically influences the regulation and function of the respective droplet (Thiam and Beller 2017). Upon lipolysis-mediated reduction of size, for instance, the LD surface reduces proportionally resulting in the displacement of proteins with lower binding affinities (Kory et al. 2015).

Due to differential protein binding affinities, LD associated proteins (LDAPs) can be categorized into two protein classes (Kory et al. 2015). The first protein class exhibit a dual localization, both to the ER and LDs. One example of these protein class is the *Drosophila* LDAP sturkopf (Thiel et al. 2013; Song et al. 2022) or its mammalian homologs LDAH (lipid droplet associated hydrolase) (Goo et al. 2014). Proteins of these class either bind to the phospholipid monolayer by means of an amphipathic helix via translocation from the ER during LD biogenesis or via a hydrophobic hairpin loop in the interaction of mature LDs and the ER (Kory et al. 2016). Proteins of the second LDAP class bind to LDs in the cytosol via amphipathic or hydrophobic helices (Kory et al. 2016). The removal of class I LDAPs has not been investigated yet, although they are thought to translocate back to the ER (Kory et al. 2016). Class II

LDAPs get either removed due to displacement on the basis of low binding affinities through the ubiquitin-proteasome-system or autophagy (Kory et al. 2016).

1.2 LDs and LDAPs in health and disease

LDs fulfil a fundamental role in lipid metabolism by storing excess lipids ensuring constant supply of energy-dense molecules independent of exogenous nutrient uptake. However, some lipid entities such as cholesterol can induce cytotoxicity (Kellner-Weibel et al. 1998; Kellner-Weibel et al. 1999) although they are essential e.g., for membrane assembly and function (Grouleff et al. 2015). Cellular cholesterol gets esterified and is safely stored in LDs to neutralize the cytotoxic effects. It is known that LDs form organelle contact sites (Valm et al. 2017; Shai et al. 2018; Bohnert 2020; Herker et al. 2021) mediating the interaction with a variety other cellular organelles such as mitochondria, peroxisomes, the ER amongst others (Olzmann and Carvalho 2019). These contact sites mediate, for instance, the interorganellar exchange of lipids and ions by means of locally concentrated lipid transfer proteins or ion channels (Herker et al. 2021). Besides the sheer transport function, these contact sites were shown to be involved in various fundamental physiological processes such as lipid metabolism, LD biogenesis, signaling events, or cellular stress response (Prinz et al. 2020). The generation of these contact sites is mediated by a broad range of different proteins (Bohnert 2020). However, in the meantime, it became clear that these contact sites also play a role in pathophysiological events of genetic, infectious and metabolic diseases (Herker et al. 2021).

An example for a genetic disease is, for instance, congenital generalized lipodystrophy caused by the loss of function of seipin, a central player in LD biogenesis, which, in turn, results in irregular LD morphology (Wang et al. 2016) as well as impaired LD-ER contact sites (Salo et al. 2016). Congenital generalized lipodystrophy is an autosomal recessive disorder which manifests with insulin resistance, lack of subcutaneous fat as well as muscular hypertrophy (Friguls et al. 2009).

Several types of intracellular pathogens, including bacteria, viruses and parasites were also shown to influence LD contact sites by both rearranging the hosts LD contact sites as well as the formation of new LD contact sites with other organelles to promote pathogen replication (Herker et al. 2021). It could, for instance, be shown

that the viral assembly of the hepatitis C virus (HCV) is dependent on the small GTPase Rab18-mediated trafficking of the viral core protein to LDs (Dansako et al. 2014). Furthermore, interaction between sites of viral replication and LDs was shown to be promoted by binding of Rab18 to the HCV nonstructural protein 5A (NS5A) (Salloum et al. 2013).

Nonalcoholic fatty liver disease is a metabolic disease characterized by an excessive and abnormal accumulation of fat in hepatocytes without any secondary cause of fatty liver such as excessive alcohol use or viral hepatitis (Marjot et al. 2020). Here, a remodeling of LD contact sites promote pathological lipid storage in hepatocytes (Herker et al. 2021) which, in turn, may be promoted by decreased hepatic secretory capacity and organellar reprogramming and cellular dysfunction towards lipid storage (Herker et al. 2021). This changes organelle contact sites and results in dramatic redistribution of secretory pathway proteins such as COPI complex (Krahmer et al. 2018).

LDs are players in hallmarks of cancer including epithelial to mesenchymal transition (EMT), modulation of cancer dependent signaling pathways, cell cycle progression or hypoxia-mediated lipid metabolism alteration (Cruz et al. 2020). Their presence was tightly correlated with different types of cancer including colorectal cancer, glioblastoma, breast cancer, as well as prostate cancer among others (Petan 2020). To date it is, however, still not entirely clear whether LD accumulations are directly involved in the formation or initiation of these malignancies (Cruz et al. 2020). For instance, it was shown that prostate cancer (PCa) cells accumulate cholesteryl ester (CE) droplets as a result of enhanced exogenous lipoprotein uptake and required cholesterol esterification leading to increased PCa cell proliferation, invasiveness, and aggressiveness. (Yue et al. 2014). Additionally, it was shown that a variety of different LD forming and processing genes such as *ACAT1*, *ATGL*, *DGAT1*, and *ABHD5* are differentially overexpressed in PCa cells (Mitra et al. 2017). The latter two were shown to promote growth of PCa cells (Mitra et al. 2017). Recently, a study demonstrated a causal relation between the loss of the LDAP LDAH and PCa (Currall et al. 2018). However, how LDs or LDAPs may initiate, affect, or contribute to these malignancies is poorly understood.

1.3 Lipid metabolism and prostate cancer (PCa)

The dysregulation of lipid metabolism is linked to several pathologies such as cachexia, hyperlipidemia, obesity, and several forms of cancer (Tewari et al. 2014; Aoyagi et al. 2015). Aggressive prostate cancer (PCa) is one type of cancers which is affected by lipid metabolism (Yue et al. 2014; Deep and Schlaepfer 2016). Prostatic carcinomas represent a major health issue and is the second most common malignancy and the fifth leading cause of cancer death among men (Saad and Miller 2015; Le Wang et al. 2022).

Cancer cells have an increased energy demand due to their uncontrolled and disproportioned proliferation. Most solid tumors experience the Warburg effect in order to accommodate their massive energy requirement (Warburg 1925; Liberti and Locasale 2016). Malignant cells tend to shift their dominant ATP producing pathway from the oxidative phosphorylation to the aerobic glycolysis (Asgari et al. 2015). However, prostate cancer cells take a different path. It was shown that especially in early prostate cancers, the energy production relies on lipids and other energetic molecules and not on aerobic respiration (Sadeghi et al. 2014; Twum-Ampofo et al. 2016). The Warburg effect is only involved in late-stage tumors, where numerous mutations cause the need of high glucose uptake (Eidelman et al. 2017). Healthy prostate epithelial cells tend to accumulate zinc and synthetize citrate for the seminal fluid (Franz et al. 2013). The production of citrate is very cost-intensive, which is why the epithelial cells compensate the energy loss with aerobic glycolysis (Eidelman et al. 2017). Cancerous prostate cells, however, show a complementing phenotype, wasting zinc and oxidizing citrate (Franz et al. 2013). These cells use the citric acid cycle and subsequent oxidative phosphorylation generating fatty acids (Eidelman et al. 2017). Additionally, enzymes involved in fatty acid-production, such as the fatty acid synthase, sterol regulatory element binding protein 1 (SREBP1), acetyl-CoA-carboxylase and the ATP citrate lyase are highly upregulated in prostate cancer cells (Wu et al. 2014). By avoiding an increased concentration of zinc, prostate cancer may prevent apoptotic regulation (Costello et al. 2005; Costello and Franklin 2011).

PCa cells can use hormone-derived (androgen) lipids as source of energy via the expression of the androgen receptor (Heinlein and Chang 2004). Furthermore, the presence of extracellular cholesterol was shown to be not only a prognostic marker for PCa (Jamnagerwalla 2017; Murtola 2018), but also to influence PCa cell proliferation (Raftopulos et al. 2022). This effect occurs especially in androgen-

independent PCa, via LDL-derived cholesterol incorporation via endocytosis and storage in cholesteryl esters (CE) as a requirement for the support of PCa cell growth (Raftopulos et al. 2022). Cholesteryl ester accumulation was previously shown to be induced by the loss PTEN with subsequent activation of the PI3K/AKT pathway (Yue et al. 2014). These CE accumulations occur in PCa cells through the enhanced uptake of polyunsaturated fatty acids (PUFAs) such as arachidonic acid (AA) (Yue et al. 2014), which is a known proliferation factor of prostate cancer cells (Ghosh and Myers 1997; Hughes-Fulford et al. 2001). CE is further promoted by the uptake of lipoproteins and required cholesterol esterification (Yue et al. 2014). PTEN is a well-known, ubiquitously expressed tumor suppressor commonly inactivated in many human sporadic cancers (Hollander et al. 2011; Álvarez-Garcia et al. 2019) including PCa (Li et al. 1997).

PCa cells are also capable of utilizing *de novo* lipid synthesis in order to obtain the energy needed (Deep and Schlaepfer 2016). The lipid-producing phenotype, also known as castration resistant PCa (CRPC), does not rely on androgen regulation which is clinically problematic as it is not responsive to androgen-deprivation therapy (Griffin 1992).

1.4 The lipid droplet associated protein sturkopf

Sturkopf, formerly known as CG9186, is a lipid droplet associated protein which was initially identified in a proteomic screen of *Drosophila melanogaster* fat body tissue (Beller et al. 2006). Sturkopf is an evolutionary conserved protein showing high abundance in a variety of different cell types and tissues (Beller et al. 2006; Cermelli et al. 2006; Krahmer et al. 2013b). The gene locus of *sturkopf* is located on the left arm of chromosome 3 at position 616F (3L:1,311,719..1,313,373 [-]). Two transcript variants, namely *sturkopf-RA* and *sturkopf-RB*, code for the same polypeptide, comprising 307 amino acids (FlyBase Version FB2022_04, www.flybase.org). On a transcriptional level, *sturkopf* is expressed in every developmental stage of *Drosophila* and most prominently in fat storing tissues such as the fat body and midgut, but also in the salivary and accessory glands (Chintapalli et al. 2007; Celniker et al. 2009; Thiel et al. 2013; Werthebach et al. 2019).

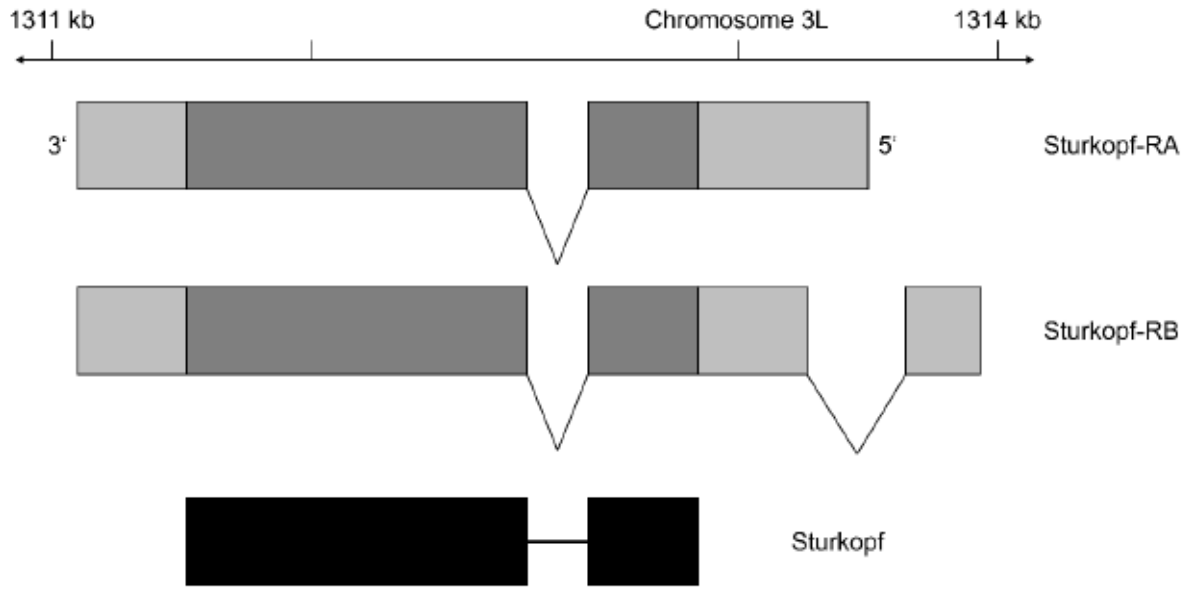

Figure 3: Schematic representation of the sturkopf genomic locus, associated transcripts (grey) and the resulting protein (black) (modified from (Thiel et al. 2013)).

Sturkopf belongs to class I LDAPs known to shuttle between the endoplasmic reticulum (ER) and LDs, once they become available (Thiel et al. 2013; Goo et al. 2014). The protein binds to LDs through an amphipathic helix which is located in the amino acid sequence aa141-200 (Thiel et al. 2013). Sturkopf and its mammalian homologs LDAH contain a highly conserved serine residue (in *Drosophila* at position aa119). Moreover, the protein contains an aspartic acid and histidine residue at position aa254 and aa283, respectively (Thiel et al. 2013).

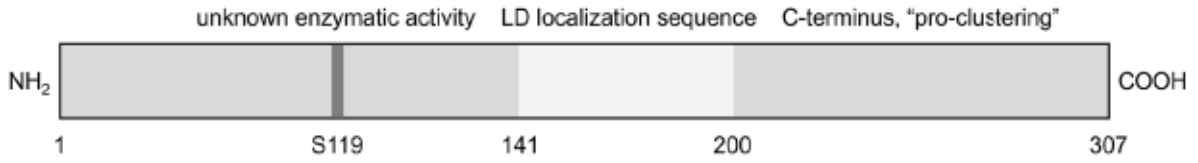

Figure 4: Schematic representation of the sturkopf sequence with functional descriptions of sequence sections (Thiel et al. 2013). The putative catalytically active serine at position aa119 is visualized in dark grey and the LD targeting sequence is shown in light grey. The C-terminus was shown to be necessary for LD clustering.

Based on homology modeling, sturkopf is likely to form a catalytical triad with a typical GXSXG upon proper α/β hydrolase folding (Thiel et al. 2013; Gramates et al. 2017). These folding properties were also hypothesized for its mammalian homolog LDAH (Goo et al. 2014). This catalytical triad is commonly present in acyltransferases or lipases (Rajakumari and Daum 2010; Ploier et al. 2013; Kim

2016; Jaeger et al. 1999). The putative catalytical serine at position 119 is presumably necessary for a nucleophilic attack (Hedstrom 2002; Thiel et al. 2013). Based on these protein properties, a lipase activity has been hypothesized for sturkopf (Thiel et al. 2013).

However, no lipase activity of sturkopf against mono-, di, and triacylglycerols could be demonstrated (Thiel et al. 2013). Overexpression of sturkopf or mammalian LDAH did not result in a reduction of cellular lipids, but instead induced a C-terminus-dependent clustering of LDs, which are usually dispersed in the majority of cell types (Thiel et al. 2013). Overexpression of a sturkopf variant lacking all lysine residues (16K2R), however, fails to induce the LD clustering phenotype (Kolkhof et al. 2017). Lysine residues located in the C-terminus of the protein are ubiquitination sites essential for the LD coalescence (Kolkhof et al. 2017). Furthermore, the RNAi-mediated knockdown of *sturkopf* was shown to decrease triacylglycerol levels *in vivo*, being a counterintuitive finding for a putative lipid-mobilizing enzyme (Thiel et al. 2013). Both lines of evidence argued against an lipase activity of sturkopf.

More recent findings suggest that sturkopf does not play a role in the canonical lipid metabolism, but rather functions on an organismic scale via the involvement in physiological processes and endocrine signaling (Werthebach et al. 2019). A CRISPR/Cas9-derived *sturkopf* null mutant fly line revealed moderately reduced TAG storage levels which was in line with the RNAi-mediated *sturkopf* knockdown data (Thiel et al. 2013). In addition, the male *sturkopf* mutant animals showed reduced lifespan, and altered cuticular hydrocarbon composition (Werthebach et al. 2019). Surprisingly, sturkopf mutant animals showed an enhanced desiccation resistance, which is most likely due to the decrease in locomotion as well as the altered CHC (cuticular hydrocarbon) composition (Werthebach et al. 2019). Furthermore, *sturkopf* mutant larvae show altered expression of *Drosophila insulin like peptides 3* and *6* and the juvenile hormone (JH) signaling target *krüppel-H1* (*kr-H1*) (Werthebach et al. 2019). The JH signaling pathway is the nexus of the found phenotypes. It is not only regulating the composition and abundance of CHCs (Lengyel et al. 2007; Kelstrup et al. 2014; Kelstrup et al. 2017) of many arthropods but it is also involved in locomotion regulation and foraging behavior (Meunier et al. 2007) as well as it directly interacts with the insulin/insulin like growth factor signaling (IIS) pathway (Mirth et al. 2014) bringing the observed phenotypes in agreement (Werthebach et al. 2019). Beyond

that, interactions of sturkopf with a variety of proteins including JH degrading enzymes, i.e., the juvenile hormone epoxide hydrolases (JHEH) (Kolkhof et al. 2017; Werthebach et al. 2019), mediating the degradation of JH in different tissues (Lü et al. 2015; Wisniewski et al. 1987) have been demonstrated. These enzymes complement the activity of the juvenile hormone esterases, which degrade JH in the hemolymph (Kamita and Hammock 2010; Saito et al. 2015). The interaction with JH degrading enzymes suggests an involvement of sturkopf in the regulation of these enzymes. A hypothetical regulation of protein stability is further supported by the interaction of sturkopf and the ubiquitin machinery (Kolkhof et al. 2017). Besides JH, the second major regulator of *Drosophila* development and growth is the steroid hormone 20HE-ecdysone (20HE) (Mirth and Shingleton 2012). A reduction of 20HE signaling was hypothesized for sturkopf loss of function due to the reduction in JH signaling (Werthebach et al. 2019), which is known to regulate 20HE signaling (Mirth et al. 2014). Ecdysone is known to antagonize IIS (Colombani et al. 2005; Delanoue et al. 2010), which was shown to be altered in *sturkopf* mutant flies (Werthebach et al. 2019). The transcriptional regulator *kr-H1* is a direct downstream target of the JH signaling pathway. Its differential expression in *sturkopf* mutant and the corresponding control animals represents, in combination with the observed phenotypes, another indication of the involvement of sturkopf in the JH signaling pathway (Werthebach et al. 2019). The expression of *kr-H1* was downregulated when *sturkopf* mutant animals were raised on low-yeast-diet. However, for mutant animals raised on a low-sugar-diet, no differences in gene expression of *kr-H1* were found, indicating a degradation limiting function of sturkopf, prohibiting upregulation of JH activity, whereas a JH decrease was still possible (Werthebach et al. 2019).

Further findings suggest a role of sturkopf in the adaption of larval developmental timing with regards to varying nutritional conditions. As *sturkopf* null mutant animals showed a decelerated development on low-sugar-diet and an accelerated development on low-yeast-diet, they do not seem to adjust their developmental timing to nutritional conditions (Werthebach et al. 2019). These observations are underpinned by an altered gene expression which can be traced back to the sturkopf mutation. For example, under basal conditions, the *Drosophila insulin like peptide* (*dilp*) *6* well as the *target of brain insulin* (*tobi*) were shown to be strongly downregulated. In addition, a previously reported reduced *tobi* expression on low-yeast-diet (Buch et al. 2008) was confirmed, whereas an upregulation in *tobi*

expression was found in animals on low-sugar-diet. In *sturkopf* mutant animals no differences in the *tobi* expression could be found which further indicates a role of sturkopf as nutritional sensor (Werthebach et al. 2019). Besides that, the sturkopf mutation also affected the expression of the IIS downstream target dFoxO in the fat body of L3 larvae (Werthebach et al. 2019) dFoxO is a well-known important regulator of organismic physiology regulation (Hwangbo et al. 2004; DiAngelo and Birnbaum 2009). Usually, the transcription factor gets phosphorylated upon an insulin stimulus resulting in the nuclear exclusion of dFoxO. *sturkopf* loss of function resulted in an increased nuclear localization of dFoxO, whereas multiple studies state an occasionally nuclear dFoxO signal to be physiological (Buch et al. 2008; Werthebach et al. 2019), hinting towards a reduction in IIS which is in line with the observed phenotypes regarding developmental timing as well as expression profiling and the hypothesized reduction in 20HE signaling (Werthebach et al. 2019). Thus, the molecular function of sturkopf is associated with organismic physiology regulation (Werthebach et al. 2019). However, the underlying molecular mechanisms remain elusive.

1.5 Mammalian lipid droplet associated hydrolase (LDAH)

The mammalian lipid droplet associated hydrolase (LDAH) was initially identified and characterized in murine macrophages in 2014 (Goo et al. 2014). In mice, *mmLDAH* is located on chromosome 12 (Chr12 8258107-8335759 bp, + strand; 3.85 cM) and codes for an 326aa long polypeptide with a predicted α/β hydrolase and the canonical lipase GXSXG motif (Goo et al. 2014) which was also predicted for *Drosophila* sturkopf (Thiel et al. 2013). The mmLDAH hypothetical catalytic triad comprises the conserved, putative catalytic active serine at position aa140, an aspartic acid residue at position aa272 and a histidine residue at position aa291 (Goo et al. 2014). A shuttling form the endoplasmic reticulum to LDs was also demonstrated for mmLDAH as well as a C-terminus-dependent clustering of LDs upon protein overexpression (Thiel et al. 2013). The clustering of LD following protein overexpression was also demonstrated for the *Drosophila* ortholog sturkopf (Thiel et al. 2013) and is presumably independent of a putative enzymatic protein activity (Goo et al. 2017). However, upon testing for a putative lipase activity, unlike sturkopf, mmLDAH exhibits a weak *in vitro* cholesteryl ester (CE) hydrolase activity and significant CE hydrolase activity in HEK-293 cells as well as in raw macrophages

(Goo et al. 2014). This enzymatic activity was traced back to the putative nucleophilic serine at position 140, as an amino acid exchange from serine to cysteine (S140C) did not affect total cholesterol or CE levels while still able to target LDs (Goo et al. 2014). Referring to these studies, other studies have investigated the hypothetical serine hydrolase/lipase activity of mmLDAH (Goo et al. 2017; Kory et al. 2017) but arrived at contradicting conclusions.

While one mmLDAH knockout mouse study found no effect on triacylglycerol storage or other lipid-metabolism related phenotypes (Kory et al. 2017), another knockout mouse study determined a significant weight gain in *mmLDAH* mutant female mice, whereas *mmLDAH* mutant male mice showed invasive prostate lesions with a penetrance of 10 % (Currall et al. 2018). The only data available supporting the CE hydrolase activity is one study characterizing the *Saccharomyces cerevisiae* LDAH ortholog Ypr147cp with regards to a hypothetical lipid-degrading activity (Naresh Kumar et al. 2018). Ypr147cp was found to exhibit both triacylglycerol lipase as well as ester hydrolase activity (Naresh Kumar et al. 2018) which was in agreement with the findings from Goo and colleagues (Goo et al. 2014), however incompatible with data of the other studies mentioned (Thiel et al. 2013; Kory et al. 2017; Werthebach et al. 2019). Due to the contradicting data available, a clear-cut enzymatic function of LDAH in the canonical lipid metabolism remains elusive. One possibility is that the protein functions outside the canonical lipid metabolism as hypothesized for *Drosophila* sturkopf (Werthebach et al. 2019). One study demonstrated that triacylglycerol levels were regulated in a mmLDAH-dependent manner, which, however, was presumably independent from the putative enzymatic activity of mmLDAH (Goo et al. 2017). Here, mmLDAH was shown to play a lipogenic role by enhancing the polyubiquitination and thus the proteasomal degradation of ATGL (adipose triglyceride lipase) pointing towards a role of LDAH in the regulation of protein stability/activity rather than being directly involved in the canonical lipid metabolism (Goo et al. 2017). This putative LDAH function was also hypothesized for *Drosophila* sturkopf (Werthebach et al. 2019) and is in line with the finding that sturkopf interacts with the ubiquitination machinery (Kolkhof et al. 2017).

The data availability for human LDAH (hsLDAH) is even more limited than for mmLDAH or the *Drosophila* ortholog sturkopf. Human *LDAH* is located on the short arm of chromosome 2 (2p24.1, *C2orf43*) and codes for a polypeptide of 325aa of the

canonical isoform in length (Q9H6V9, www.uniprot.org). The protein has a hypothetical α/β hydrolase fold and is also likely to form the aforementioned GXSXG serine hydrolase motif with a serine at position 139, presumably for the enzymatic nucleophilic attack, an aspartic acid residue at position aa271 and a histidine at position aa300 (Q9H6V9, www.uniprot.org). Recently, a study demonstrated an enzymatic activity for hsLDAH for the very first time (Dubey et al. 2020). Here, a LDAH-mediated hydrolysis of lasonolide A, a polyketide-derived macrolide known for its anti-cancer drug properties (Horton et al. 1994) isolated from the marine sponge of the genus *Forcepia* into a cytotoxic metabolite was demonstrated (Dubey et al. 2020). Although LDAH and its orthologs are highly conserved proteins (Thiel et al. 2013; Goo et al. 2014) and their physiological substrates in mammals and other species have not yet been identified, the authors highlight the substrate specificity of lasonolide A to LDAH rather than being the product of a generic ester hydrolysis (Dubey et al. 2020).

Within the scope of various GWAS studies (genome-wide association studies), the gene locus of *hsLDAH*, namely *C2orf43*, was associated with the occurrence of prostate cancer (PCa) (Takata et al. 2010; Innocenti et al. 2011; Lindström et al. 2012; Long et al. 2012; Wang et al. 2013; Shui et al. 2014; Penney et al. 2015; Du et al. 2016). These studies identified a diverse set of prostate cancer risk-associated SNPs (single nucleotide polymorphisms). However, these GWAS studies only provided associations between high risk PCa SNPs in the *LDAH* gene locus *C2orf43*. These associations were first put into causal context in 2018, when Benjamin Currall and colleagues presented a case study of an early onset PCa patient with congenital hearing loss with a *de novo*, germline, balanced chromosomal translocation (Currall et al. 2018). This translocation resulted in a suggested haploinsufficiency effect from the disruption of a single coding *LDAH* allele and thus a heterozygous mutation of *hsLDAH* leading to in lowered *LDAH* mRNA and protein levels (Currall et al. 2018). In the same study, *hsLDAH* was shown to be commonly dysregulated in PCa. Analyses of benign and tumor samples revealed a significant downregulation of *hsLDAH* in both primary and metastatic tumors, in the latter case to an even greater extent as compared to both benign tissue as well as primary PCa (Currall et al. 2018). Further data analysis showed a more frequent downregulation of *hsLDAH* as compared to well-known tumor suppressors in PCa such as *PTEN* (Li et al. 1997; Hollander et al. 2011) and *NKX3-1* (He et al. 1997) both in primary and metastatic prostatic

carcinomas (Currall et al. 2018). In cultured human prostate cell lines, it was demonstrated that transient silencing of *hsLDAH* in RWPE-1 cells, an epithelial cell line with high endogenous *hsLDAH* expression, resulted in a significant increase in cell proliferation, whereas cell migration and invasion were unaffected (Currall et al. 2018). On the other hand, overexpression of hsLDAH in PC3 cells, a highly tumorigenic cell line with a low endogenous hsLDAH expression, led to in a significant decrease in cell proliferation as well as in migration and invasion capability of PC3 cells (Currall et al. 2018). Although all these findings serve as circumstantial evidence that *hsLDAH* loss play a role in PCa tumorigenesis, invasiveness and aggressiveness, the molecular function of the protein is still mostly unknown.

1.6 The *Drosophila* accessory gland (AG) as model for PCa

Drosophila melanogaster has been utilized as model organism to study a variety of pathologies for a very long time. Approximately one century ago, the fly was first used experimentally (Castle 1906). Since then, *Drosophila* has become a widely used, powerful tool to study different biological aspects, including primarily genetics as well as development, metabolism, aging and behavior (Ashburner and Bergman 2005; Tolwinski 2017; Bharucha 2009; Chatterjee and Perrimon 2021; Feinerman 2021; Holtze et al. 2021). Besides basic research, *Drosophila* has further become a convenient tool to study human diseasesdue to the presence of roughly 75 % of functional orthologous genes in *Drosophila* of human disease-related genes (Pandey and Nichols 2011; Yamamoto et al. 2014). The high abundance of these functional human disease gene-related orthologs also explain the broad spectrum of pathologies studied in *Drosophila*, which cover neurodegeneration (Sang and Jackson 2005) including Alzheimer's disease (Tsuda and Lim 2018), obesity and metabolic disease (Musselman and Kühnlein 2018), diabetes (Graham and Pick 2017), infectious diseases (Harnish et al. 2021) including prion disease (Bujdoso et al. 2022) as well as a variety of neoplastic malignancies including, *inter alia*, colorectal cancer (Martorell et al. 2014; Bangi et al. 2016; Zipper et al. 2022), glioblastoma (Kotian et al. 2022; Losada-Pérez et al. 2022), lung cancer (Levine and Cagan 2016), leukemia (Osman et al. 2009; Sinenko et al. 2010), as well as prostate cancer (Ito et al. 2014; Wilson et al. 2017; Rambur et al. 2020; Rambur et al. 2021).

The *Drosophila* accessory gland (AG) has recently gained recognition and was promoted as a model tissue to study diverse aspects of the human prostate including

PCa (Wilson et al. 2017; Rambur et al. 2021). Several studies build on similarities of the AGs and the prostate not only physiologically, but also genetically (Leiblich et al. 2012; Ito et al. 2014; Sitnik et al. 2016; Leiblich et al. 2019). Functionally, the AG operates in a similar manner as the human prostate by contributing to and transferring the seminal fluid during copulation (Bertram et al. 1996; Gilchrist and Partridge 2000). Upon transfer, several components of the seminal fluid induce physiological and behavioral responses in female flies (Liu and Kubli 2003; Chapman et al. 2003; Ravi Ram and Wolfner 2007).

The AGs are secretory glands of the male reproductive tract consisting of two dead-end lobes which branch off of the male genital tract at the anterior end of the ejaculatory duct (Bairati 1967). AGs develop from a special set of cells in the male primordium of the genital disc (Nöthiger et al. 1977) whose developmental fate is determined during the third instar stage via the male sex determination pathway (Chapman and Wolfner 1988). Seminal fluid secretion is ensured by secretory cells and neuronally controlled (Tayler et al. 2012) striated muscle contraction (Susic-Jung et al. 2012). Each gland comprises a simple monolayer epithelium, which is made up by two different cell types, namely main (MC) and secondary cells (SC) (Bertram et al. 1992). Both have an intrinsic gene expression pattern (Bertram et al. 1992). Among the genetically distinct transcriptional profiles of the two postmitotic cell types, they can be distinguished by their morphology and their abundance (Taniguchi et al. 2014). Squamous MCs are flat, hexagonal binucleate cells which line the entire lobe and are numerically most strongly represented with roughly 1000 cells per lobe (Bairati 1967; Bertram et al. 1992). Spherical, binucleate SCs containing large vacuoles are, however, less frequently abundant with roughly 40-60 SCs concentrating at the most distal end of each lobe (Bairati 1967; Bertram et al. 1992).

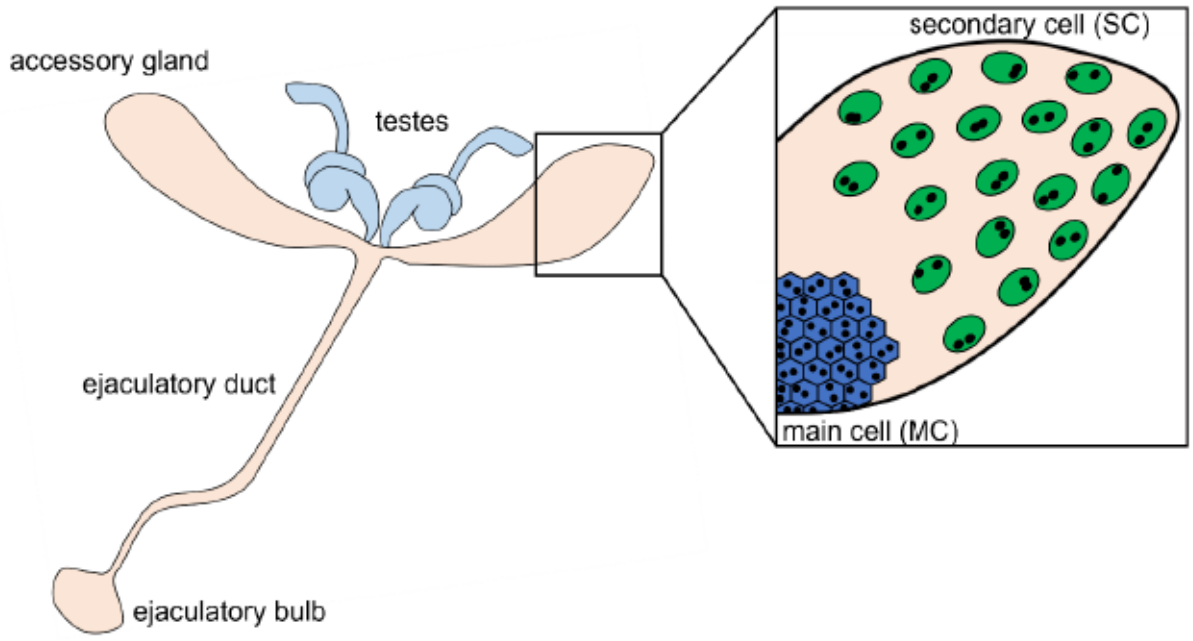

Figure 5: Illustration of the *Drosophila* accessory gland (AG). AGs comprise two dead-end lobes branching off of the ejaculatory duct which in turns is attached to the ejaculatory bulb. Testes (light blue) are located at the proximal region of the AGs. A more detailed representation of the two AG cell types is depicted in the close-up of one AG tip. Hexagonal, binucleate main cells (MCs) are depicted in dark blue and the larger, also binucleated secondary cells (SCs) concentrating in the distal tip of each gland are shown in green. The cell number of both cell types depicted is not accurate and serves only the representation of cell size and shape, as well as cellular location of the SCs.

Although postmitotic, the SCs of the AG are still able to grow in response to mating (Leiblich et al. 2012). A small portion of these cells can also delaminate apically from the epithelium of the AG in multiple mated males, migrate through the ejaculatory duct and get transferred to females upon mating in a SC-specific BMP (bone morphogenic protein) signaling-dependent manner (Leiblich et al. 2012). Both the nuclear growth, also known as endoreplication, as well as cell migration are well known phenomena in cancer (Fox and Duronio 2013; Yamaguchi et al. 2005). BMP signaling has been shown to induce cell growth and migration in different cancers, including PCa (Yuen et al. 2008; Yuen et al. 2012; Giancotti 2013). Interestingly, within the scope of a genetic screen, physiological SC growth and migration were found to be regulated by *Drosophila* orthologs of known PCa regulators such as *paired*, *E-cadherin*, and *N-cadherin* (Ito et al. 2014). Further, three genes were identified promoting SC growth and migration, namely *MrgBP*, *seele*, and *CG11864* (Ito et al. 2014), each of which have human homologs (*MRGBP*, *CNPY2*, *MEP1A*) known to be expressed in PCa cells promoting their replication and invasiveness (Ito

et al. 2014; Ito et al. 2018a; Ito et al. 2018b). CNPY2 was recently shown to inhibit the proteasomal degradation of the androgen receptor (AR), a key regulator in PCa progression, via interference with the ubiquitination machinery (Ito et al. 2018b). The ubiquitination of the steroid receptor by the E3 ubiquitin ligase MYLIP/IDOL (myosin regulatory light chain interacting protein/inducible degrader of the LDL receptor) is inhibited through an interaction of CNPY2 with the E2 conjugating enzyme UBE2D1 (Ito et al. 2018b). Furthermore, a diverse set of E3 ubiquitin ligases is known to ubiquitinate several lysine residues of the AR. Two lysine residues in the C-terminus of the AR (K845 and K847) were shown to be ubiquitinated by SKP2, CHIP, MDM2, RNF6, and Siah2 (Li et al. 2014a; Li et al. 2014b). While the ubiquitination of C-terminal lysine residues by SKP2, MDM2 and CHIP results in the proteasomal degradation of the AR, ubiquitination of the same residues through Siah2 and RNF6 were shown to enhance the transcriptional activity of the receptor (Xu et al. 2009; Li et al. 2014a). A lysine residue (K311) located at the N-terminus of the AR was further demonstrated to be ubiquitinated by SKP2 (McClurg et al. 2017). This post-translational modification was shown to be critical for AR protein stability as well as its transcriptional activity (McClurg et al. 2017).

To date there is no definite AR homolog identified in *Drosophila*. However, several attempts have been made to promote similarities of the ecdysone receptor (EcR) and the human AR (Bender et al. 1997; Leiblich et al. 2019). The EcR is a nuclear steroid receptor which forms a functional heterodimeric protein receptor together with USP (ultraspiracle) (Yao et al. 1993b). The formation of heterodimers between two nuclear receptors was previously also shown for the androgen receptor (Chen et al. 1997; Lee et al. 1999). 20-hydroxyecdysone (20HE) binds to the ligand-activated transcription factor EcR, which, in turn, regulate target gene expression (Riddiford et al. 2000). The EcR is known to control and regulate embryonic and larval development (Koelle et al. 1991). It was shown to also contribute to other processes such as reproduction (Carney and Bender 2000; Meiselman et al. 2017; Sharma et al. 2017). The EcR is crucial for proper AG development and its function (Sharma et al. 2017). Whereas the EcR promotes endoreplication of SCs in virgin male flies, the nuclear growth in mated males is mediated via EcR-independent BMP signaling suggesting mechanistic parallels between the physiological, behavior-induced signaling switch in *Drosophila* male AGs and altered pathological signaling alterations associated with PCa (Leiblich et al. 2019). Moreover, ubiquitination and thus

proteasomal degradation of EcR (isoform A) via the E3 ubiquitin ligase was demonstrated (Gradilla et al. 2011). However, according to FlyBase (version FB2022_04) the most probable human ortholog for the EcR is the liver X receptor α (LXRα) (Reschly et al. 2008). Another nuclear receptor, namely the estrogen-related receptor (ERR), also necessary for larval development (Tennessen et al. 2011) and reproduction success (Misra et al. 2017), is a more probable AR ortholog compared to EcR (FlyBase; version FB2022_04). However, given the fact that a variety of similarities concerning function, genetics and physiology are conserved between the AG and the human prostate renders the AG a robust model to study several, although not entirely, aspects in relation to the human prostate as well as its pathologies.

1.7 Aim of this work

First, this work aims at investigating whether *Drosophila* sturkopf affects cellular processes such as proliferation in a similar manner as it was shown for LDAH in prostate cancer cells. Second, the effect of sturkopf protein abundance alterations *in vivo* in the accessory gland of male *Drosophila* flies is analyzed with regard to proliferation and the regulation of other cellular processes such as apoptosis. Last, research into the mechanism of how the loss of a LDAP promotes or causes malignant neoplastic events was aimed. Here, special focus was put on the putative sturkopf-mediated stability regulation of target proteins. *In vitro* and *in vivo* experiments were conducted to identify the role of the LDAP sturkopf and human LDAH partially, in profound cellular processes as well as accompanying endocrine physiology regulation.

2 Results

Sturkopf and its mammalian homologs, namely LDAH, comprise a conserved group of LDAPs, which have been characterized towards their putative role as serine hydrolases or lipases within the scope of the canonical lipid metabolism (Thiel et al. 2013; Goo et al. 2014). These characterizations were based on the presence of a conserved serine hydrolase/lipase GXSXG motif which all of the protein family members have in common (Thiel et al. 2013; Goo et al. 2014; Naresh Kumar et al. 2018). However, while some studies demonstrated a role in lipid metabolism for murine LDAH (Goo et al. 2014) and for the yeast ortholog Ypr147cp (Naresh Kumar et al. 2018), others were unable to find evidence for a TAG or CE hydrolase/lipase function for murine LDAH or the *Drosophila* ortholog sturkopf, formerly known as CG9186 (Thiel et al. 2013; Kory et al. 2017; Werthebach et al. 2019). Thus, the role of this LDAP family in the canonical lipid metabolism is still in question and not clear yet.

A report from 2018 presented an actual case study of an early-onset PCa patient with a *de novo*, germline, balanced chromosomal translocation resulting in a suggested haploinsufficiency effect from the disruption of a single coding LDAH allele and thus a heterozygous mutation of *hsLDAH* resulting in lowered LDAH mRNA and protein levels was presented (Currall et al. 2018). Currall and colleagues concluded a decisive role of *LDAH* loss in the onset and progression of prostate cancer (Currall et al. 2018). These findings were in line with prostate cancer risk-associated single nucleotide polymorphisms identified previously in the human *LDAH* gene locus *C2ORF43* (Takata et al. 2010; Innocenti et al. 2011; Lindström et al. 2012; Long et al. 2012; Wang et al. 2013; Shui et al. 2014; Penney et al. 2015; Du et al. 2016). Furthermore, a role outside of the canonical lipid metabolism was shown for *Drosophila* sturkopf, affecting profound physiological processes including nutritional sensing, development and accompanying endocrine processes, thus regulating organismal physiology (Werthebach et al. 2019). Additionally, LDAH as well as sturkopf have been associated with the ubiquitination machinery, either by the sheer fact that the protein(s) get ubiquitinated themselves (Kolkhof et al. 2017), or by being involved in protein stability regulation as shown for a LDAH-mediated stability regulation of the adipose triglyceride lipase (ATGL) (Goo et al. 2017) or hypothesized for a sturkopf-mediated protein stability regulation of juvenile hormone degrading enzymes, namely JHEH (Werthebach et al. 2019).

As several lines of evidence converge towards a role of sturkopf and mammalian LDAH in physiological, cellular, and endocrine processes, these aspects were investigated within the scope of this work. Here, the role of these LDAPs in the context of prostate cancer-relevant aspects was investigated particularly. A *Drosophila sturkopf* loss of function (LOF) fly line and cultured cells were used as model systems to scrutinize a potential role of sturkopf in cell proliferation *in vitro* and *in vivo* as the *Drosophila* accessory gland has been recently propagated as model to investigate several aspects of prostate cancer (Wilson et al. 2017; Rambur et al. 2021). Furthermore, biochemical methods were applied to investigate sturkopf's role in endocrine physiology regulation as *sturkopf* LOF is assumed to influence ecdysone signaling (Werthebach et al. 2019) which acts in a similar manner as testosterone in PCa (Leiblich et al. 2019). Last, luciferase complementation experiments were performed to get insight into a potential mechanistic mode of sturkopf action as well as to investigate the hypothetical conservation of protein-protein-interactions in this context.

2.1 Sturkopf affects cell proliferation in cultured cells

There is growing evidence in scientific literature that mammalian LDAH plays a role in cellular processes including proliferation (Currall et al. 2018). A knockdown of *LDAH* in the prostate cell line RWPE-1 was shown to increase proliferation of these cells while other parameters such as cell migration and invasion were unaffected (Currall et al. 2018). Overexpression of LDAH in the highly tumorigenic PCa cell line PC3 (Tai et al. 2011) resulted in a proliferation decrease as well as decreased PC3 cell migration and invasion capacities (Currall et al. 2018) which usually are characteristics of this prostate cancer cell line (Yamazaki et al. 1994; Zi et al. 2005; Huang et al. 2011; Raja Singh et al. 2017).

Thus, it was of interest whether these observations could be recapitulated using the *Drosophila* LDAH ortholog sturkopf in cultured cells. Currently, there is no cell line available originating from the *Drosophila* accessory gland which may be the most accurate cell line to test for the putative role of sturkopf in proliferation with regards to prostate cancer. However, sturkopf as well as various sturkopf variants were stably overexpressed in S2R+ cells (Yanagawa et al. 1998) on top of endogenous sturkopf expression in these cells (FlyBase [version FB2022_05]) which are late-embryonic cells of male origin (Lee et al. 2014). Besides wild type sturkopf (Thiel et al. 2013),

sturkopf(S119A) in which the putative catalytic serine was mutated to alanine (Thiel et al. 2013), as well as sturkopf(16K2R) where 16 lysine residues were changed to arginine (Kolkhof et al. 2017) and human LDAH were used to test for an effect on proliferation. As all constructs were C-terminally eGFP-tagged for detection purposes, a cell line overexpressing eGFP only was also generated as control cell line. The successful generation of these stable sturkopf variants overexpressing cell lines was tested via western blot analysis as depicted in figure 6.

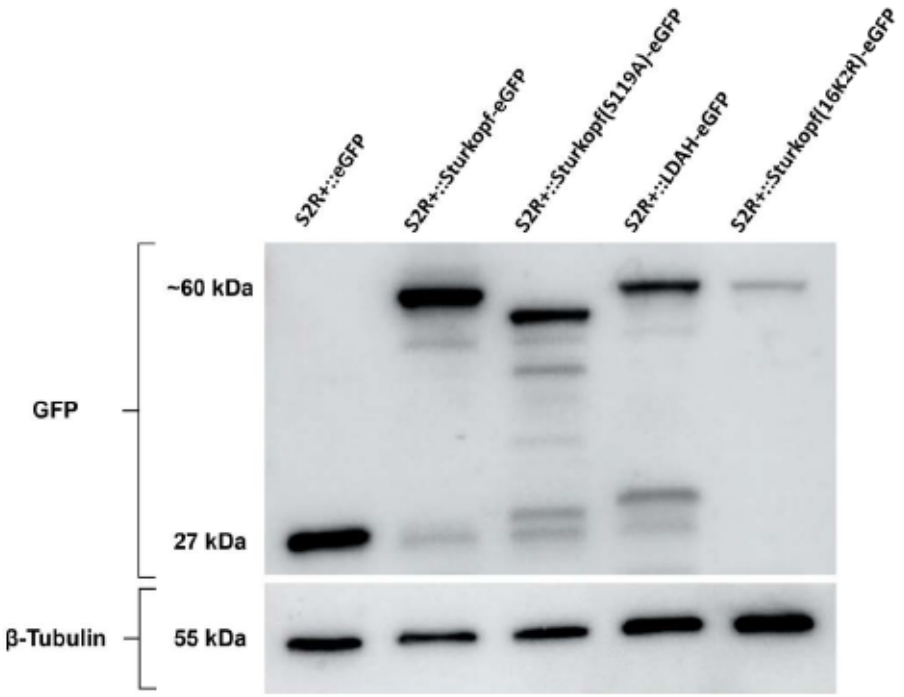

Figure 6: Successful detection of GFP in cell culture extracts from generated S2R+::eGFP, S2R+::sturkopf-eGFP, S2R+::sturkopf(S119A)-eGFP, S2R+::LDAH-eGFP and S2R+::sturkopf(16K2R)-eGFP polyclonal cell lines. Cell lysates were measured for whole protein levels by means of BCA and equal amounts of protein were loaded. The GFP antibody detected several bands in lysates of S2R+::sturkopf-eGFP, S2R+::sturkopf(S119A)-eGFP and S2R+::LDAH-eGFP, which represent most likely proteolytic breakdown of the antigen or the result of insufficient blocking of the western blot membrane. The GFP-specific sturkopf(S119A)-eGFP signal is slightly shifted in comparison to wild type eGFP-tagged sturkopf. The plasmid was re-sequenced to check for the correct construct (appendix, figure 62). Ubiquitously expressed β-tubulin (55 kDa) served as loading control.

The western blot analysis detected a 27 kDa sized signal for the S2R+::eGFP cells, which correspond to the hydrodynamic radius of GFP (Hink et al. 2000). Furthermore, the fusion proteins of sturkopf-eGFP, sturkopf(S119A)-eGFP, LDAH-eGFP and sturkopf(16K2R), which all share a hydrodynamic radius of roughly 60 kDa, were successfully detected (figure 6). Notable is the slight shift in protein size of the

sturkopf(S119A)-eGFP signal, which was, however, not based on the amino acid exchange. This construct was re-sequenced to guarantee the integrity and correctness of it (appendix, figure 62). While all constructs share comparable protein expression level, the sturkopf(16K2R)-eGFP expressing cell line showed the weakest construct overexpression.

Next, the stable cell lines were used within the scope of crystal violet proliferation assays. Crystal violet is a triarylmethane dye which is capable of staining DNA (Klingenberg et al. 2014) and proteins (Krause and Goldring 2019) and is often used as means to evvaluate cell viability and proliferation (Feoktistova et al. 2016; Currall et al. 2018). Cell proliferation was measured over the course of 5 days. The averaged results of three biologically independent experiments are depicted in figure 7.

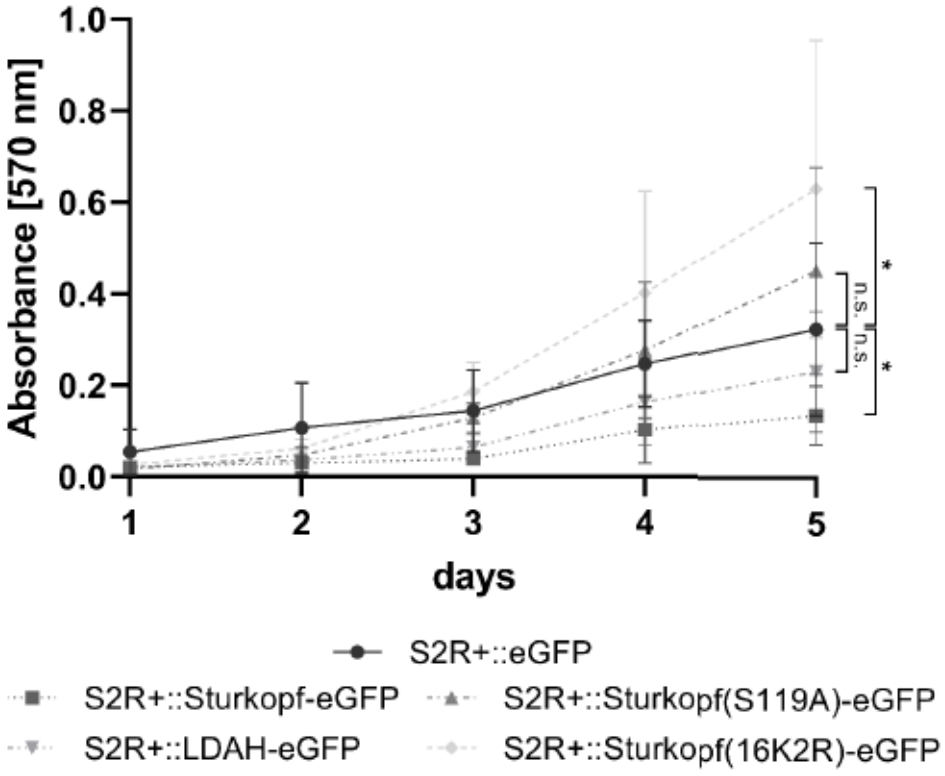

Figure 7: Crystal violet proliferation assay after *in vitro* manipulation of sturkopf (variant) expression. S2R+ cells stably overexpressing C-terminally GFP-tagged wild type sturkopf, sturkopf(S119A), LDAH and sturkopf(16K2R) were measured for proliferation over 5 days by staining the cells with 0.1 % crystal violet solution and followed by subsequent determination of relative absorbance of the methanol-extracted crystal violet dye at a wavelength of 570 nm. Depicted are the mean values of three biologically independent experiments including standard deviation. All p values were obtained by an unpaired two-sample t test with significance levels: p-value >0.05: n.s., <0.05: *, <0.01: **, <0.001:***).

The proliferation assays (figure 7) revealed a significant decrease of proliferation in response to wild type sturkopf overexpression compared to the GFP-only expressing control cell line. While overexpression of the S119A variant as well as human LDAH did not result in significant changes towards proliferation compared to the control cell line, overexpression of the sturkopf variant 16K2R, on the other hand, resulted in a significant increase in proliferation. Data analysis was performed only for day 5, as the differences in proliferation behavior were revealed over time. Additionally, microscopic analysis of the cells from day 5 after crystal violet staining, yet prior to dye extraction, underpin obvious differences in proliferation behavior.

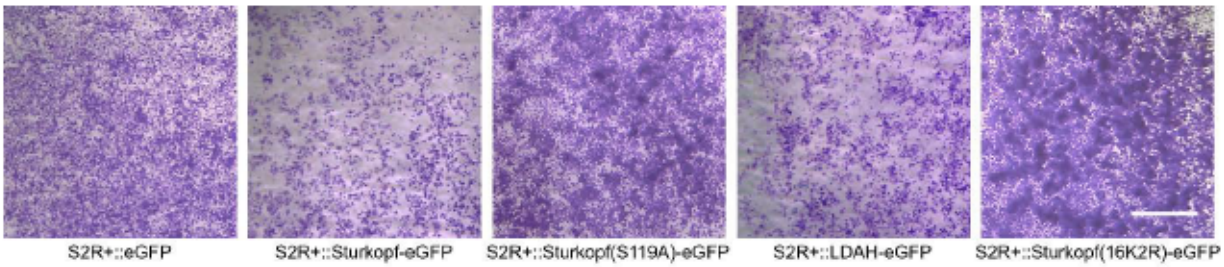

Figure 8: Microscopic analysis of cell proliferation after *in vitro* manipulation of sturkopf (variant) expression of one of the three biologically independent experiments. Crystal violet dyed cells of day 5 were recorded prior to the methanol-based dye extraction using the Leica EZ4D binocular. Scale bar = 1 mm.

While the assessment of proliferation differences by visual means proved difficult for S119A and LDAH overexpressing cell lines, clear-cut differences in proliferation behavior of wild type sturkopf overexpressing cells were apparent as cell density was clearly reduced in comparison to the GFP-only overexpressing control cell line (figure 8). The same applied to overexpression of the 16K2R construct, although the opposite effect was obtained compared to wild type sturkopf overexpression. A confined space of the culture dish was not covered with cells which was likewise in contrast to the GFP-only control cell line.

As sturkopf as well as its mammalian orthologs are LDAPs, it was of interest to see whether the induction of cellular lipid storage via treatment with oleic acid affected proliferation behavior of these stably sturkopf variant overexpressing cell lines. Therefore, the stable cell lines generated were treated with 400 µM oleic acid and measured for proliferation under the same conditions just as for the untreated condition (figure 9).

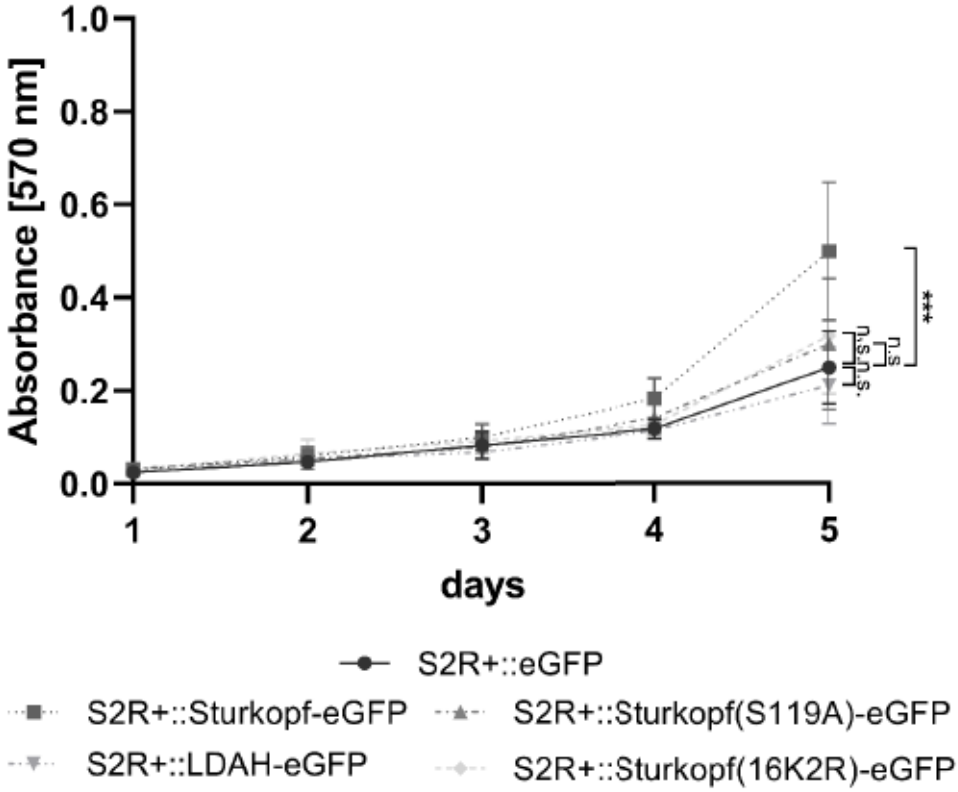

Figure 9: Crystal violet proliferation assay after *in vitro* manipulation of sturkopf (variant) expression upon treatment with 400 µM oleic acid. S2R+ cells stably overexpressing C-terminally GFP-tagged wild type sturkopf, sturkopf(S119A), LDAH and sturkopf(16K2R) were measured for proliferation over 5 days by staining the cells with 0.1 % crystal violet solution and followed by subsequent determination of relative absorbance of the methanol-extracted crystal violet dye at a wavelength of 570 nm. Depicted are the mean values of three biologically independent experiments including standard deviation. All p values were obtained by an unpaired two-sample t test with significance levels: p-value >0.05: n.s., <0.05: *, <0.01: **, <0.001:***).

Upon treatment of stably sturkopf variant overexpressing cell lines with 400 µM oleic acid, the proliferation behavior of the cell lines overexpressing GFP-tagged sturkopf(S119A) as well as LDAH did not change in comparison to both the GFP-only overexpressing control cell line and the untreated condition (compare figures 8 and 9). Interestingly, cells overexpressing wild type sturkopf featured a highly significant increase in cell proliferation compared to the control (figure 9). While the 16K2R sturkopf variant overexpressing cell line showed a significant increase in proliferation under basal conditions (figure 8), this increased proliferation was abolished upon 400 µM oleic acid treatment, resulting in a comparable proliferation behavior as seen for the GFP-only overexpressing control cell line as well as for S119A and LDAH overexpressing cells. Microscopic analysis was also performed for the 400 µM oleic acid treated condition.

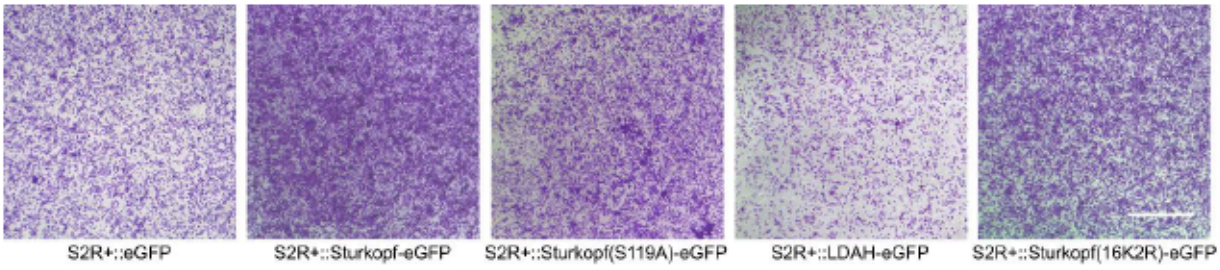

Figure 10: Microscopic analysis of cell proliferation after *in vitro* manipulation of sturkopf (variant) expression upon treatment with 400 µM oleic acid of one of the three biologically independent experiments. Crystal violet dyed cells of day 5 were recorded prior to the methanol-based dye extraction using the Leica EZ4D binocular. Scale bar = 1 mm.

The increase in cell proliferation for overexpressed wild type sturkopf is evident upon visual inspection of the different cell lines (figure 10).

The performed crystal violet proliferation assays revealed an effect of sturkopf (and its variants) on cell proliferation. Overexpression of wild type sturkopf resulted in a significant decrease in proliferation under basal conditions, on the one hand. On the other hand, overexpression of the sturkopf variant 16K2R increased proliferation significantly. Interestingly, neither sturkopf variant S119A, nor human LDAH overexpression affected the proliferation behavior. Treatment with 400 µM oleic acid, however, changed the proliferation behavior of both wild type sturkopf as well as the 16K2R variant. While the latter did not show any differences in proliferation behavior upon induction of lipid storage, overexpression of wild type sturkopf resulted in a highly significant increase in proliferation. Although a sturkopf-mediated effect on proliferation was identified in S2R+ cells, it was, however, still not clear whether sturkopf also affects cellular processes *in vivo* in the AGs of male *Drosophila* which is the functional analog of the human prostate (Wilson et al. 2017; Rambur et al. 2021).

2.2 *sturkopf* loss of function (LOF) affects the number of secondary cells (SCs) in the AG of male *Drosophila*

Male *Drosophila* AGs have been recently promoted as a suitable model to investigate various aspects of human prostate physiology as well as pathophysiological aspects including PCa (Wilson et al. 2017; Rambur et al. 2021). In particular, secondary cells (SCs) can be used to model various aspects of prostate cancer biology, including signaling, growth and biogenesis of exosomes and steroid signaling of the male reproductive system (e.g., reviewed in (Wilson et al. 2017). Amongst others, these

are major aspects of prostate cancer initiation, progression, or aggressiveness and play an important role in therapy options (Culig and Santer 2014).

As shown previously, *Drosophila* sturkopf is expressed in the AGs (Werthebach et al. 2019). It was, thus, of great interest to investigate a putative role for sturkopf in the AGs and in particular in the SCs using both a previously generated CRISPR/Cas9-derived *sturkopf* null mutant fly (Werthebach et al. 2019) as well as a genetic system which was crossed in the *sturkopf* null mutant background. This does not only visualize the SCs by SC-specific GFP expression but also allows for temporal manipulation of transgene expression. The principle of this genetic system (Jiang et al. 2009; Micchelli and Perrimon 2006) requires the development of animals on 18 °C due to the presence of a temperature sensitive Gal80 repressor ensuring a block in transgene expression (McGuire et al. 2004). Upon hatching, animals were transferred to 29 °C to ensure spatial and temporal control of transgene expression.

2.2.1 *sturkopf* LOF results in decreased SC abundance

AGs of 7-days old flies of both genotypes *w;esg-Gal4,UASserGFP,tubGal80^{ts};+* (from now on referred to as *esg;Ctrl*, expressing wild type levels of sturkopf) and *w;esg-Gal4,UASserGFP,tubGal80^{ts};sturkopf[35.7]* (from now on referred to as *esg;35.7*) expressing this genetic construct in the *sturkopf* null mutant background, were dissected, stained, recorded in Z-stacks, and analyzed for morphologic and phenotypic changes regarding the overall AG morphology and in particular SCs. No differences in overall AG morphology as well as SC size, shape, and location (figure 11) have been identified.

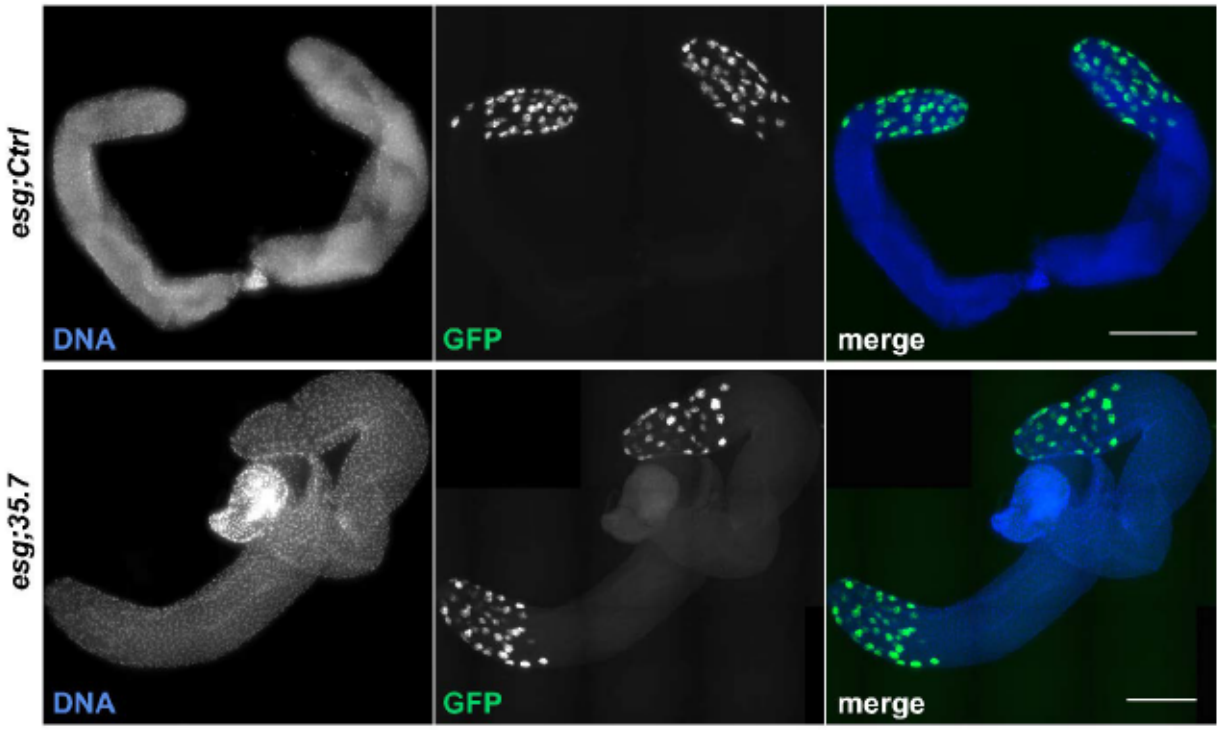

Figure 11: Representative maximum intensity projection of accessory glands of 7-days old, mated flies of the genotypes *esg;Ctrl* and *esg;35.7*. DNA was stained with Hoechst33342 (blue), SCs are marked by endogenous GFP expression (green). Images were recorded with the Operetta CLS High Content Analysis System using a 5x air objective to identify and select tissues and a 40x air objective to obtain high resolution images of the selected fields. Scale bar = 200 µm.

As no apparent phenotypes were visible, SCs of both genotypes were quantified to investigate whether differences in SC number occur. This readout has been used previously by others to study regulators of PCa initiation, progression and invasiveness (Ito et al. 2014). Quantification of SC number revealed a highly significant reduction of SCs in the *sturkopf* null mutant line *esg;35.7* as depicted in figure 12.

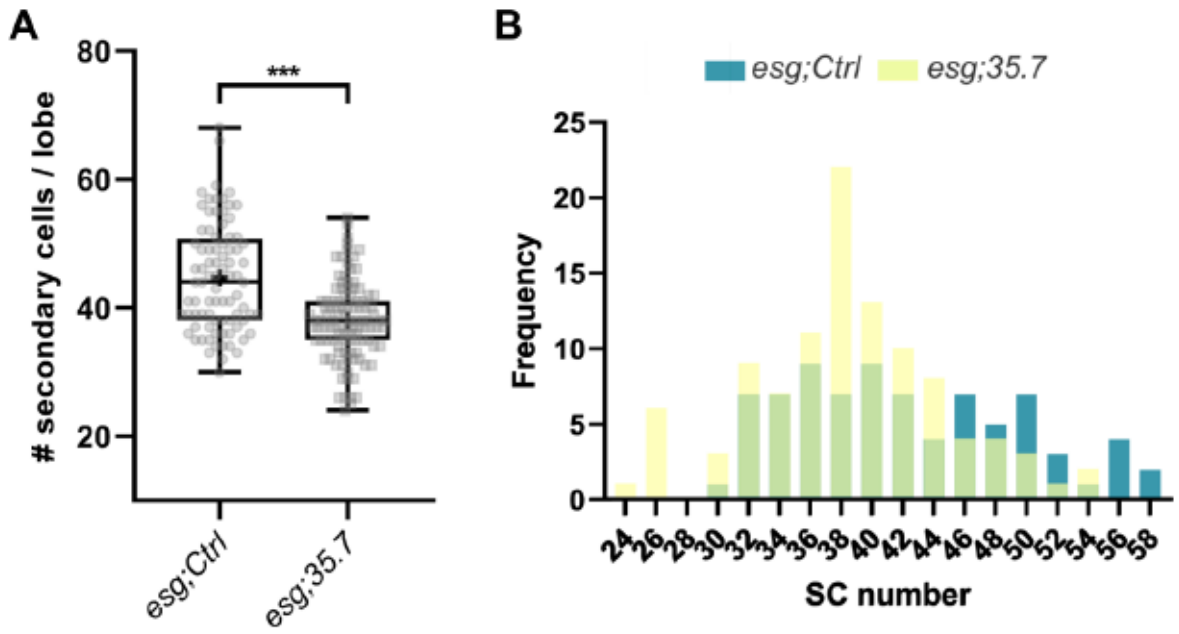

Figure 12: The loss of SC phenotype in AGs of *sturkopf* null mutant male animals. (**A**) Quantification of secondary cells per lobe of 7-days old mated male flies of the genotypes *esg;Ctrl* (n=80 lobes) and *esg;35.7* (n=104 lobes). Analysis was performed based on SC-specific GFP expression of at least three biologically independent experiments. All p values were obtained by an unpaired two-sample t test with significance levels: n.s., $p \geq 0.05$, *$p < 0.05$, **$p < 0.01$, ***$p < 0.001$. (**B**) Corresponding frequency distribution analysis of secondary cell numbers per lobe of 7-days old *esg;Ctrl* and *esg;35.7* animals (same data as in (**A**)).

With an average SC number of roughly 42 cells (mean: 41.6) for *esg;Ctrl* animals and 38 SCs for *esg;35.7* on average (mean: 37.9711) it became clear, that the loss of SC phenotype observed in the *sturkopf* mutant condition, is highly significant. However, it requires the quantification of SCs as well as a sufficiently large sample size (figure 12A). Therefore, the data was used in a superimposed frequency distribution graph to visualize subtility of the phenotype, on the one hand, and the yet two distinguishable populations, on the other hand (figure 12B).

2.2.2 Characterization of the *sturkopf* LOF phenotype

The *sturkopf* LOF-mediated loss of SCs was further characterized regarding parameters which might influence the number of SCs. For instance, it was shown that ongoing aging influences AG physiology profoundly and SC number in particular (Santhosh and Krishna 2013). To investigate a potential influence of age on the observed phenotype, 7- and 14-days old flies were reared, dissected, and subsequently analyzed towards alteration in SC abundance.

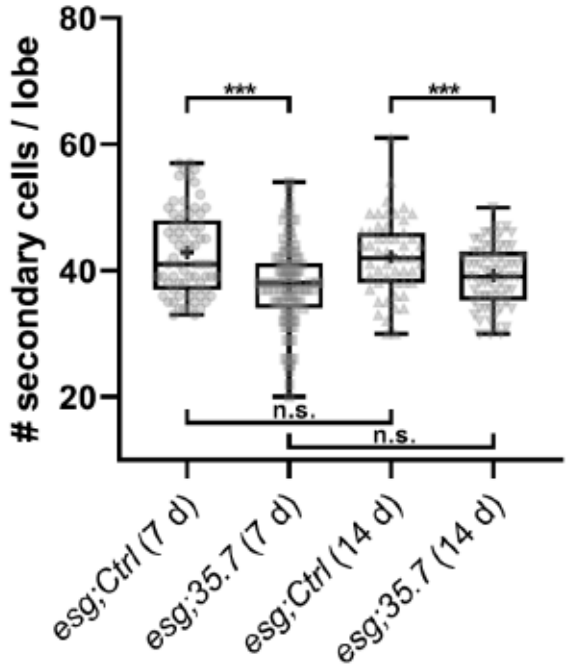

Figure 13: Quantification of SC number per lobe of 7- and 14-days old mated male flies of the genotypes *esg;Ctrl* (7d n=71 lobes; 14d n=52 lobes) and *esg;35.7* (7d n=106 lobes; 14d n=lobes 86). Analysis was performed based on SC-specific GFP expression of at least three biologically independent experiments. All p values were obtained by an unpaired two-sample t test with significance levels: n.s., $p \geq 0.05$, *$p < 0.05$, **$p < 0.01$, ***$p < 0.001$.

As visualized in figure 13, the phenotype of significantly reduced SCs was not affected by age. Both tested fly lines showed no differences in SC abundance between 7 and 14 days of age within each genotype, while comparison between both genotypes showed the previously observed significant reduction of SC number for both ages tested.

Next, it was tested whether mating status affect the number of SCs. Prior studies have shown that SC tend to delaminate apically from the epithelium, migrate through the ejaculatory duct to the proximal end of the gland, and consequently are transferred to females upon further mating eventually (Leiblich et al. 2012; Leiblich et al. 2019). Furthermore, sturkopf protein levels were demonstrated to be increased in the AG upon mating (Werthebach et al. 2019). Therefore, freshly hatched male flies of both genotypes *esg;Ctrl* and *esg;35.7* were collected and separately reared until reaching an age of 7 days.

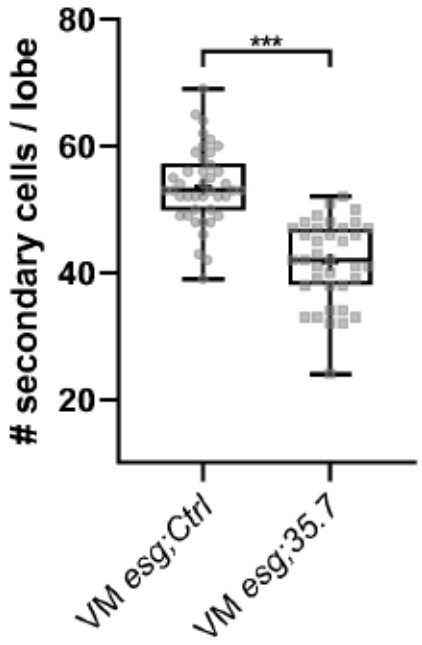

Figure 14: Quantification of SC number per lobe of 7-days old virgin male flies of the genotypes *esg;Ctrl* (n=42 lobes) and *esg;35.7* (n=lobes 38). Analysis was performed based on SC-specific GFP expression of at least three biologically independent experiments. Additionally, SCs were counterstained with an antibody against ANCE for validation purposes. All p values were obtained by an unpaired two-sample t test with significance levels: n.s., $p \geq 0.05$, *$p < 0.05$, **$p < 0.01$, ***$p < 0.001$.

Virgin *sturkopf* LOF animals showed significantly reduced numbers of secondary cells compared to *esg;Ctrl* animals (figure 14). Thus, it could be concluded that the mating status of the flies, and in consequence sturkopf protein levels in virgin males of the control line, did not influence the obtained loss of SC phenotype in *sturkopf* mutant animals, nor did the weaker sturkopf protein expression in the AGs of virgin *esg;Ctrl* males (Werthebach et al. 2019) alter SC abundance compare figures 12A and 14).

The use of genetic systems can also harbor issues and can affect a result under certain circumstances. For certain SC driver lines the problem of decreasing GFP expression over time was described (Leiblich et al. 2012). To rule out potentially incomplete or just partial GFP-expression in the SCs based on the genetic system used, AGs were additionally stained with an SC-specific antibody against the angiotensin-converting enzyme (ANCE) (Houard et al. 1998). These antibody stainings resulted in an entire overlap of ANCE signal and GFP expression in the homozygous conditions (figure 15).

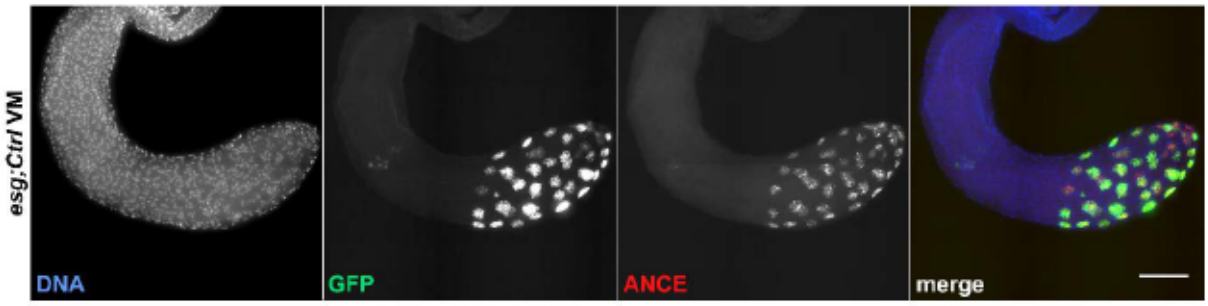

Figure 15: Representative maximum intensity projection of an accessory gland's lobe of a 7-days old virgin fly of the genotype *esg;Ctrl* antibody stained against ANCE of at least three biologically independent experiments. DNA was stained with Hoechst33342 (blue), SCs are marked by endogenous GFP expression (green), and ANCE was detected by usage of an Alexa647-coupled secondary antibody (red). Note that the GFP and ANCE signals show a 1:1 overlap. This exact overlap of SCs (GFP) and ANCE was also found for 7-days old virgin *esg;35.7* Images were recorded with the Operetta CLS High Content Analysis System using a 5x air objective to identify and select tissues and a 40x air objective to obtain high resolution images of the selected fields. Scale bar = 200 µm.

As it was now clear that all SCs were expressing GFP robustly (figure 15) I tested whether the system affected SC abundance. Therefore, the previously generated CRISPR/Cas9-derived *sturkopf* null mutant fly and its genetically matched control (Werthebach et al. 2019) were utilized (from here on referred to as *sturkopf* Ctrl and *sturkopf[35.7]*). Secondary cells of these animals do not express GFP endogenously. Hence, these cells needed to be marked by means of an antibody staining. AGs of both genotypes were stained with antibodies against two SC markers which are ANCE or Abd-B (abdominal-B) to verify the integrity of the loss of SC phenotype. The obtained results revealed comparable numbers of SCs in each genotype, and thus, a significant loss of SCs in the *sturkopf* mutant state (figure 16).

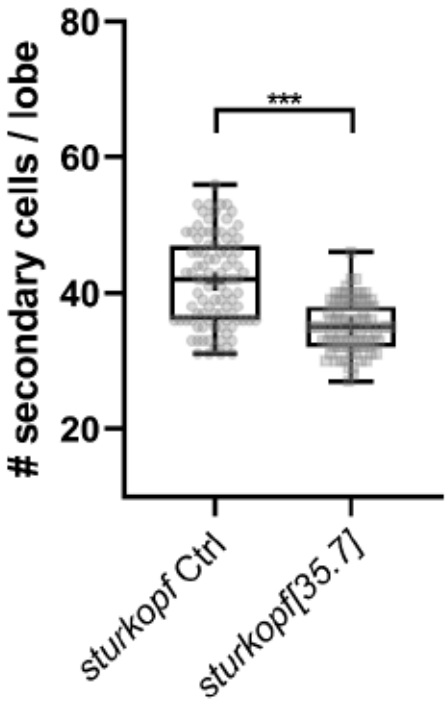

Figure 16: Quantification of SCs per lobe of 7-days old mated male flies of the genotypes *sturkopf* Ctrl (n=91 lobes) and *sturkopf[35.7]* (n=lobes 95). Analysis was performed based on SC-specific antibody stainings against ANCE and Abd-B (data not shown) of at least three biologically independent experiments. All p values were obtained by an unpaired two-sample t test with significance levels: n.s., $p \geq 0.05$, *$p < 0.05$, **$p < 0.01$, ***$p < 0.001$.

The highly significant loss of SC phenotype could be recapitulated using the CRISPR/Cas9-derived *sturkopf* null mutant fly and the corresponding control (figure 16). To finally confirm that the observed phenotype is indeed attributable to the loss of *sturkopf*, SCs were quantified in a transheterozygous background using different *sturkopf* deficiency lines. Crossings of *sturkopf* Ctrl and *sturkopf[35.7]* with w[-] flies served as control in this respect.

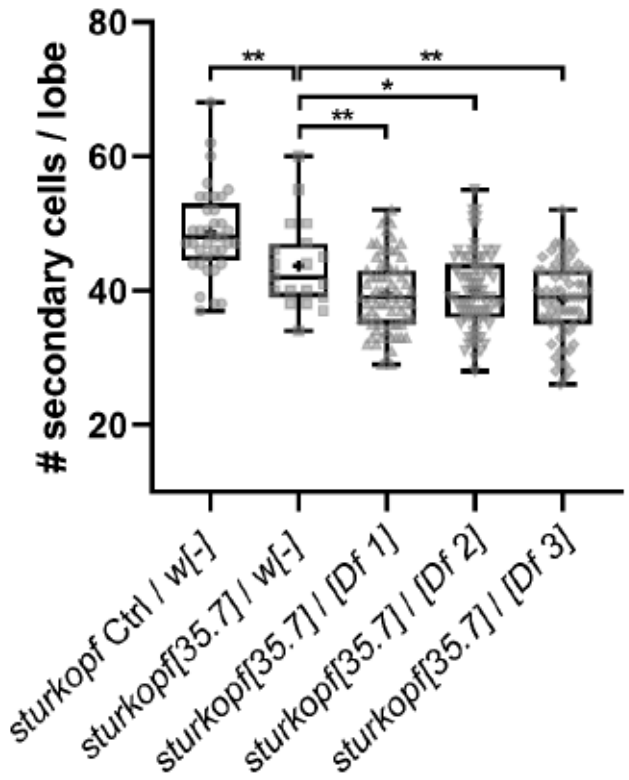

Figure 17: Quantification of SCs per lobe of 7-days old mated male flies in a *sturkopf* transheterozygous background. Analysis of SC abundance in *sturkopf Ctrl / w[-]* (n=37 lobes), *sturkopf[35.7] / w[-]* (n=19 lobes), *sturkopf[35.7] / [Df 1]* (n=72 lobes), *sturkopf[35.7] / [DF 2]* (n=82 lobes), *and sturkopf[35.7] / [Df 3]* (n=68 lobes) was performed based on SC-specific antibody stainings against Abd-B of at least three biologically independent experiments. All p values were obtained by an unpaired two-sample t test with significance levels: n.s., $p \geq 0.05$, *$p < 0.05$, **$p < 0.01$, ***$p < 0.001$.

The different crosses were analyzed for their sturkopf protein expression via western blot ensuring the presence of sturkopf protein signal in crossings with at least one functional *sturkopf* allele and the absence of sturkopf signal in conditions lacking any sturkopf allele (*sturkopf[35.7] / [Df1] – [Df3]*) (figure 18).

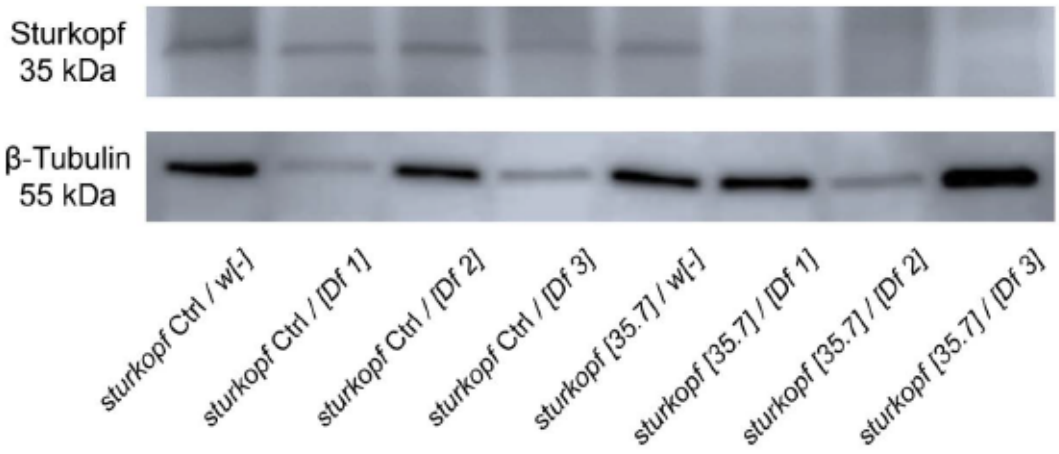

Figure 18: Detection of sturkopf protein levels of 7-days old mated, female flies of each cross in a *sturkopf* transheterozygous background. Whole fly lysates were generated, and total protein levels were determined via BCA. Equal amounts of protein were determined and loaded. Wild type and *sturkopf* heterozygous backgrounds showed a signal when probed with a sturkopf-specific antibody. Loss of two functional *sturkopf* alleles results in the absence of sturkopf protein (last three lanes). Ubiquitously expressed β-tubulin served as loading control. Note that, although equal protein amounts were determined and loaded, a difference in loaded protein levels is visible.

Figure 17 displays the abundance of SCs in different crossings in a *sturkopf* transheterozygous background. While *sturkopf* Ctrl / *w[-]* has two functional *sturkopf* alleles, the abundance of SCs was similar to previously shown results of the different control groups expressing wild type sturkopf protein levels (compare controls of figures 12A,16). The *sturkopf* heterozygous mutant cross of *sturkopf[35.7] / w[-]* revealed a moderately significant decrease of SCs upon loss of one *sturkopf* allele. The utilization of various *sturkopf* deficiency lines [*Df1-3*] in the *sturkopf* mutant background resulted in a highly significant decrease of SCs as compared to the control cross expressing wild type sturkopf levels (*sturkopf* Ctrl / *w[-]*) as well as in comparison to the heterozygous *sturkopf* mutant state (*sturkopf[35.7] / w[-]*). The successful crossings were validated via western blot by the detection of sturkopf protein using a sturkopf-specific antibody (figure 18).

Thus, it can be concluded, that *sturkopf* LOF was responsible for the highly significant reduction in SC abundance. Furthermore, an age-dependent effect of SC number (figure 13), a mating-mediated effect (compare figures 12A and 14), or the genetic system used in these experiments (compare figures 12A and 16) could be ruled out as potential parameters influencing SC abundance.

2.3 The role of *sturkopf* in endocrine physiology regulation

2.3.1 *sturkopf* LOF results in a decrease in endoreplication of SCs

Endoreplication is referred to as the replication of the genome in absence of mitotic divisions (Edgar and Orr-Weaver 2001) and was described as important prognostic marker for PCa (Deitch et al. 1993; Badalament et al. 1991). Endoreplication occurs in the SCs of the AG in male *Drosophila* (Leiblich et al. 2012). This nuclear growth of SCs is mediated by EcR signaling in virgin male *Drosophila* and via BMP (bone morphogenic protein) signaling in mated flies (Leiblich et al. 2019). As a putative effect of sturkopf in ecdysone signaling was previously hypothesized (Werthebach et al. 2019), it was of interest to analyze whether differences in endoreplication occur in *sturkopf* null mutant animals. The method to measure endoreplication is described in 4.2.4.2 (Leiblich et al. 2012).

To determine endoreplication, nuclear areas of both MCs and SCs needed to be measured beforehand. Upon measurement of nuclear areas of MCs and SCs of both *esg;Ctrl* and *esg;35.7* highly significant differences in both MC and SC nuclear area between *esg;Ctrl* and *esg;35.7* were identified (figure 19).

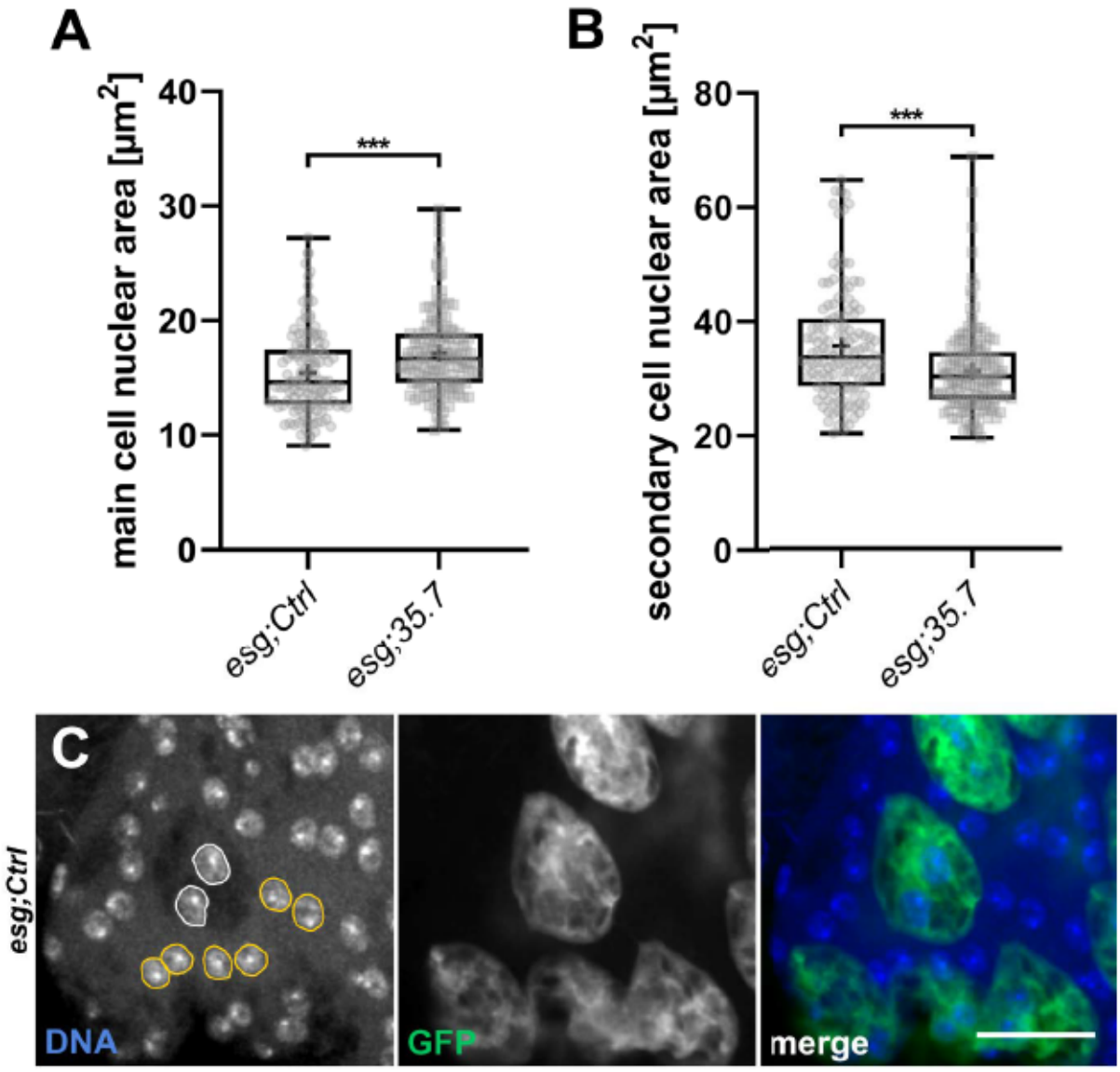

Figure 19: Measurement of main cell (**A**) and secondary cell (**B**) nuclear areas (each n=32 nuclei) of 7-days old, mated flies of the genotypes *esg;Ctrl* and *esg;35.7*. Measurements were based on Hoechst33342 DNA staining to identify nuclei in general and SC-specific GFP expression ensured the identification of SC-specific nuclei. All p values were obtained by an unpaired two-sample t test with significance levels: n.s., $p \geq 0.05$, *$p < 0.05$, **$p < 0.01$, ***$p < 0.001$. (**C**) A typical cluster of nuclei of 3 main cells and 1 secondary cell which were measured to determine endoreplication (Leiblich et al. 2012).

Differences in nuclear area measurements appeared for both cell types. While MC nuclear areas were significantly increased in *esg;35.7* animals compared to *esg;Ctrl* animals, the SC nuclear area measurements showed a highly significant decrease in *sturkopf* mutant animals.

The determination of endoreplication was performed by the calculation of the quotient of both SC and MC nuclear area (Leiblich et al. 2012). The results revealed a highly significant reduction in endoreplication in the *sturkopf* null mutant state (figure 21).

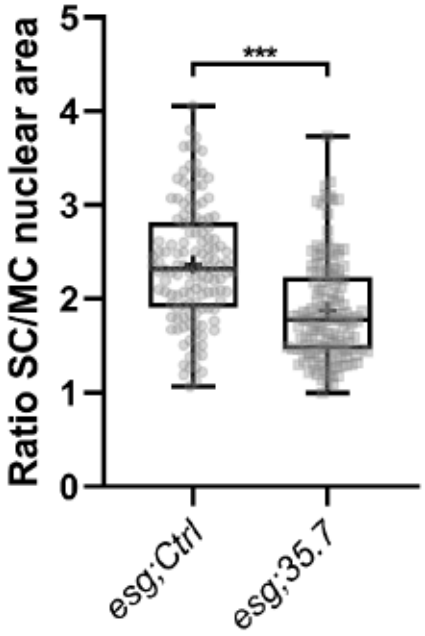

Figure 20: Measurement of endoreplication by calculation of the quotient of SC and MC nuclear area of 7-days old, mated flies of the genotypes *esg;Ctrl* and *esg;35.7*. Nuclear area measurements were based on Hoechst33342 DNA staining to identify nuclei in general and SC-specific GFP expression ensured the identification of SC-specific nuclei. All p values were obtained by an unpaired two-sample t test with significance levels: n.s., $p \geq 0.05$, *$p < 0.05$, **$p < 0.01$, ***$p < 0.001$.

Additionally, it was tested whether SCs of both genotypes differed in their size. Therefore, SC areas of AGs from 7-days old male *esg;Ctrl* and *esg;35.7* animals were measured.

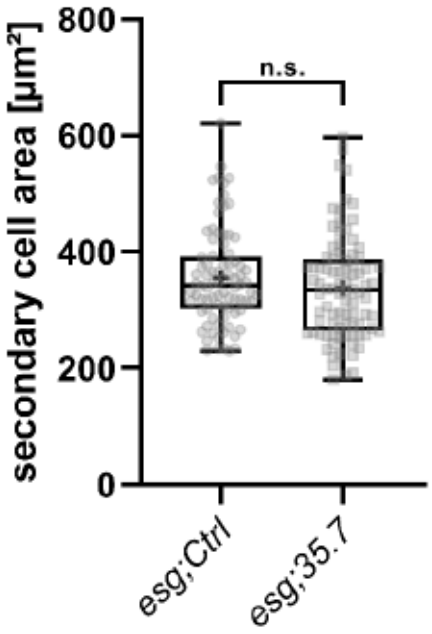

Figure 21: Measurement of whole SC area of 7-days old, mated flies of the genotypes *esg;Ctrl* (n=84 SCs) and *esg;35.7* (n=88 SCs). Measurements were based on SC-specific GFP expression of at least three biologically independent experiments. All p values were obtained by an unpaired two-sample t test with significance levels: n.s., $p \geq 0.05$, *$p < 0.05$, **$p < 0.01$, ***$p < 0.001$.

While nuclear areas of both main and secondary cells differed significantly in size between sturkopf control animals and *sturkopf* mutants, the overall size of SCs between the two genotypes was not altered (figure 20).

Taking these data and the hypothesized impaired/reduced ecdysone signaling for *sturkopf* LOF (Werthebach et al. 2019) into account, it engenders the contemplation that ecdysone signaling is indeed altered in *sturkopf* mutant animals.

2.3.2 *sturkopf* LOF lowers 20-hydroxyecdysone hemolymph titer in male flies

Loss of *sturkopf* affects major endocrine signaling events as juvenile hormone as well as IIS signaling and thereby affecting not only development processes, but also a variety of other physiological parameters such as survival (Werthebach et al. 2019). Thus, the assumption that an effect of sturkopf in ecdysone signaling is not unreasonable, especially considering the fact that juvenile hormone was demonstrated to regulate ecdysone synthesis (Mirth et al. 2014; Zhang et al. 2021) and a reduction in IIS signaling was demonstrated in *sturkopf* mutant animals (Werthebach et al. 2019). This could be explained due to lowered ecdysone signaling

as IIS not only affects ecdysone synthesis (Caldwell et al. 2005; Mirth et al. 2005) but also because ecdysone and IIS signaling were shown to antagonize each other (Colombani et al. 2005; Delanoue et al. 2010). In the fat body of *sturkopf* mutant larvae the localization of dFoxO was shown to be altered (Werthebach et al. 2019). dFoxO is a transcription factor which is a direct downstream target of IIS signaling and regulated by juvenile hormone signaling (Mirth et al. 2014). Lowered IIS signaling results in in increased nuclear localization of dFoxO, as could be detected for *sturkopf* mutant animals (figure 22) (Werthebach et al. 2019).

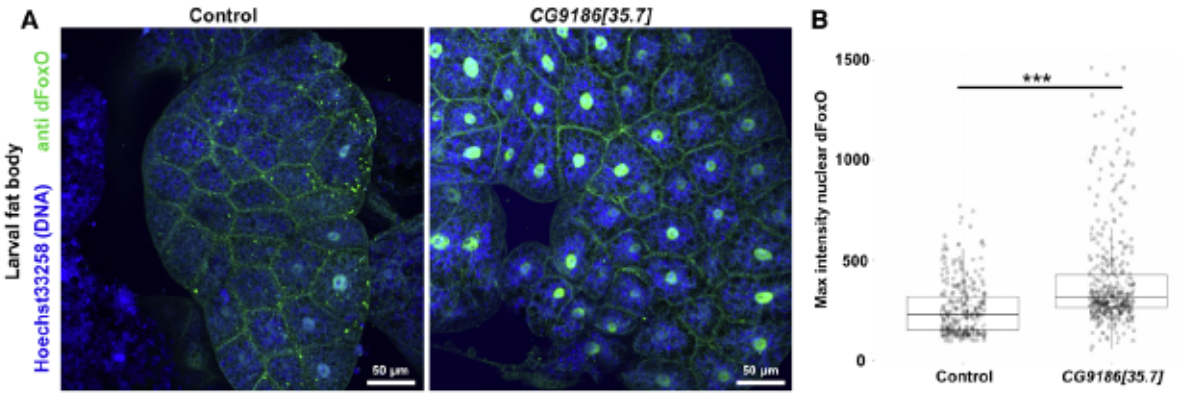

Figure 22: (**A**) Antibody staining against dFoxO (green) of fat bodies of wandering L3 larvae of *sturkopf* Ctrl and *sturkopf[35.7]* animals. Tissues were additionally stained with Hoechst33258 (blue) to mark nuclei. (**B**) Quantification of the nuclear dFoxO levels by measurement of maximal fluorescence intensity. The boxplots represent the data for 315 *sturkopf* Ctrl and 427 *sturkopf[35.7]* nuclei and are an representative example from three biologically independent experiments. All p values were obtained by an unpaired two-sample t test with significance levels: n.s., $p \geq 0.05$, *$p < 0.05$, **$p < 0.01$, ***$p < 0.001$ (adapted from Werthebach et al. (2019) with permission of the journal, as it "is under the terms of Creative Commons CC-BY (CC-BY 4.0) license which permits unrestrictive use […] provided the original work is properly cited" Copyright Clearance Center, Inc.).

sturkopf LOF was hypothesized to alter the stability and, thus, the activity of JHEH enzymes resulting in an elevation in JHEH activity and lowered JH levels as a consequence (Werthebach et al. 2019). Therefore, gene expression changes of *JHEH1-3* transcript levels were tested via qRT-PCR to evaluate the stabilizing role of *sturkopf* LOF with regard to the juvenile hormone epoxide hydrolases (figure 23).

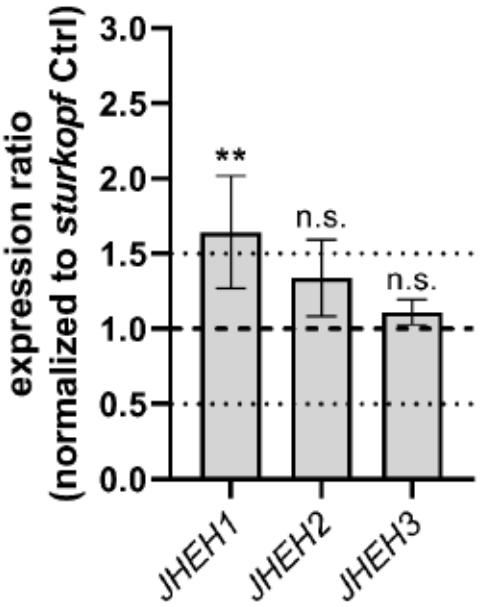

Figure 23: qRT-PCR-based gene expression analysis of accessory gland-derived RNA of 7-days old mated *sturkopf* Ctrl and *sturkopf[35.7]* males of the *JHEH1-3* genes. Gene expression was normalized to expression of the housekeeping gene *rp49* and the genetically matched *sturkopf* Ctrl line of at least three biologically independent experiments. For significant gene expression change, arbitrary thresholds were set to at least 1.5-fold upregulation, or 0.5-fold downregulation as compared to the control. All p values were obtained by an unpaired two-sample t test with significance levels: n.s., $p \geq 0.05$, *$p < 0.05$, **$p < 0.01$, ***$p < 0.001$.

Gene transcript expression ratios for *JHEH1-3* are depicted in figure 23. While *JHEH2* and *JHEH3* were not differentially regulated in the AG of *sturkopf* mutant animals, expression of *JHEH1* was significantly increased as compared to the control. This effect is in line hypothesized increase in JHEH protein activity in sturkopf LOF animals (Werthebach et al. 2019).

Based on an increased *JHEH1* transcript expression as well as lowered IIS signaling and, hence, an increase in nuclear dFoxO localization of *sturkopf* mutant larvae (Werthebach et al. 2019), it was tested whether ecdysone synthesis/signaling is impaired in *sturkopf* loss of function animals. Therefore, qRT-PCR analyses were performed to check for differentially regulated ecdysone downstream target genes (*E74A*, *E75A* and *E75B*) as well as *EcR* transcripts.

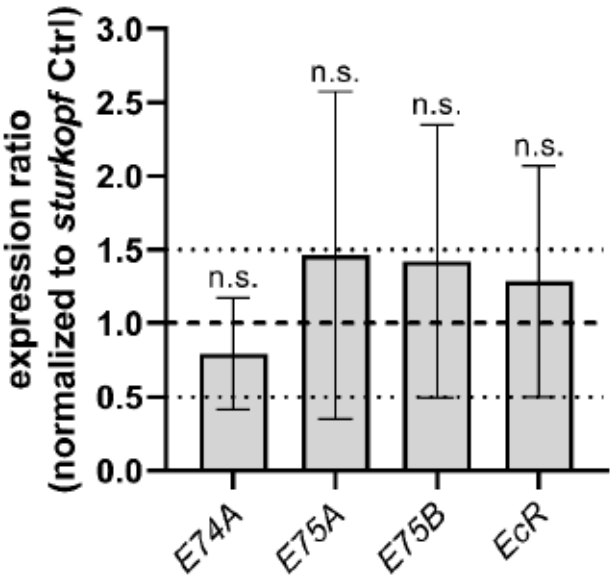

Figure 24: qRT-PCR-based gene expression analysis of accessory gland-derived RNA of 7-days old mated *sturkopf* Ctrl and *sturkopf[35.7]* males of ecdysone target genes *E74A*, *E75A*, *E75B* and the *EcR*. Gene expression was normalized to expression of the housekeeping gene *rp49* and the genetically matched *sturkopf* Ctrl line of at least three biologically independent experiments. For significant gene expression change, arbitrary thresholds were set to at least 1.5-fold upregulation, or 0.5-fold downregulation as compared to the control. All p values were obtained by an unpaired two-sample t test with significance levels: n.s., $p \geq 0.05$, *$p < 0.05$, **$p < 0.01$, ***$p < 0.001$.

The gene expression analysis depicted in figure 24 did not result in any significant or clear-cut transcript expression changes of the tested ecdysone target genes *E74A*, *E75A*, *E75B* or *EcR* between *sturkopf* null mutant animals and their respective control. Based on very high standard deviations, especially for *E75A*, *E75B* as well as *EcR* it was not possible to draw conclusions out of this data set. As a result, gene expression analysis did neither support, nor rule out a potentially impaired ecdysone signaling.

To further evaluate this possibility, an ecdysone ELISA was performed to measure 20-hydroxyecdysone hemolymph levels.

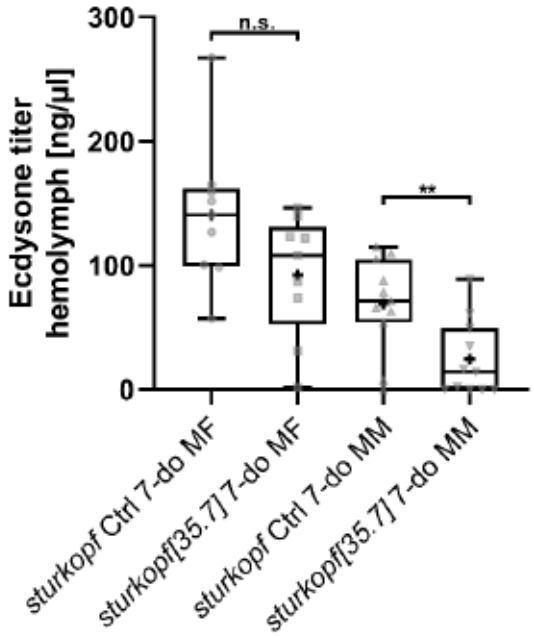

Figure 25: Measurement of ecdysone hemolymph titer [ng/µl] of *sturkopf* Ctrl and *sturkopf[35.7]* mated female and male flies. Measurements were based on extracted hemolymph of 9 (females) and 12 (males) biologically independent experiments. Each biological replicate consisted of extracted hemolymph from 30 flies per sex and genotype. All p values were obtained by an unpaired two-sample t test with significance levels: n.s., $p \geq 0.05$, *$p < 0.05$, **$p < 0.01$, ***$p < 0.001$.

Measurements of ecdysone hemolymph titers of *sturkopf* Ctrl and *sturkopf[35.7]* mated female and male flies are depicted in figure 25. While in females no significant differences in ecdysone titers could be determined, male flies showed significantly decreased ecdysone hemolymph titers in *sturkopf* null mutant animals. Although ecdysone titers differed not significantly between *sturkopf* Ctrl and *sturkopf[35.7]* female flies, titers tended to be decreased in female *sturkopf* mutant flies as well.

Next, it was tested whether sturkopf and the EcR, a nuclear, non-covalent heterodimer of the EcR protein and ultraspiracle USP) (Yao et al. 1993b), physically interact with each other to assess a direct function of sturkopf in ecdysone signaling events by using a split luciferase complementation assay (Kolkhof et al. 2017). Additionally, USP and the estrogen-related-receptor (ERR) were included within this interaction network as both USP and ERR were previously shown to interact with the EcR (Yao et al. 1992; Yao et al. 1993b; Yoo et al. 2021; Kovalenko et al. 2019). According to FlyBase (version FB2022_05), the ERR is more likely an AR ortholog compared to the EcR.

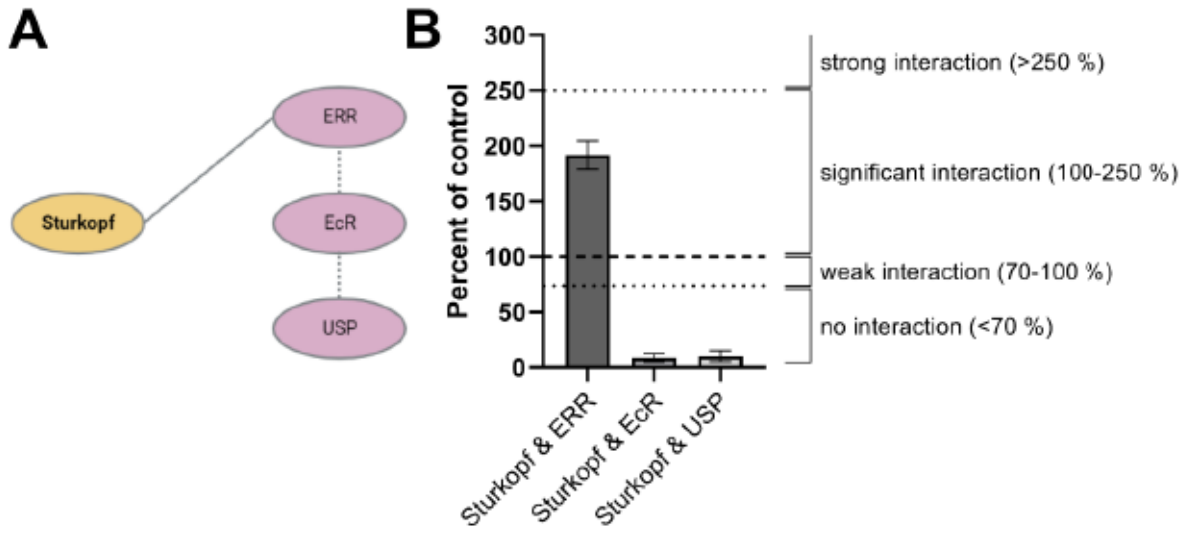

Figure 26: (**A**) Interaction analysis of sturkopf, EcR, ERR, and USP using a split luciferase complementation assay. Continuous lines represent significant/strong interactions identified within the scope of this work, dotted lines show interactions which were identified by others (Yao et al. 1992; Yao et al. 1993b; Yoo et al. 2021; Kovalenko et al. 2019). sturkopf was tested for interaction with all depicted proteins. (**B**) Complementation data of the depicted interactions in (A). Data was normalized to the known zipper-zipper interaction (Kolkhof et al. 2017) and thresholds for the determination of interactions were set accordingly (Kolkhof et al. 2017).

Protein-protein-interaction studies between sturkopf and ERR, EcR, and USP revealed a strong interaction between sturkopf and ERR, while no direct interaction between sturkopf with EcR as well as USP could be determined (figure 26). This data suggest that there is no direct regulation through an interaction of the EcR via sturkopf. This result does, however, not necessarily disconfirm an indirect regulation of EcR by sturkopf.

2.3.3 Investigation of EcR protein stability in cultured cells

The murine sturkopf homolog LDAH regulates the stability of the major TAG lipase ATGL via enhancement of its proteasomal degradation under TAG storage conditions (Goo et al. 2017). Furthermore, circumstantial evidence associates sturkopf with the ubiquitination machinery, as proven by the direct interaction of sturkopf and ubiquitin (Kolkhof et al. 2017). This association is further underpinned by the abolishment of the sturkopf-mediated LD clustering phenotype upon overexpression when C-terminal lysines are exchanged to arginines (Thiel et al. 2013; Kolkhof et al. 2017) and thus unable to be ubiquitinated (Pickart 2001). In addition, it was previously shown that the EcR also gets ubiquitinated and subsequently degraded via the proteasome (Gradilla et al. 2011).

To investigate a potential sturkopf-mediated regulation on protein stability of the EcR it was tested whether it was possible to demonstrate the general ubiquitination of the EcR as reported previously (Gradilla et al. 2011) performing a cycloheximide pulse-chase experiment. S2R+ cells were treated with cycloheximide (25 µg/ml) to monitor protein degradation (Buchanan et al. 2016), with the proteasome inhibitor MG132 (20 µM) to prevent proteasomal degradation (Lee and Goldberg 1998) and Pyr-41 (20 µM). The latter is an inhibitor of ubiquitin-activating enzyme (E1) (Yang et al. 2007) resulting in the inhibition of ubiquitination-mediated proteasomal degradation. DMSO-treated cells served as solvent control. Treatment was monitored over 2 days in different time intervals. Cells were then lysed, and cell extracts were subjected to western blot to analyze EcR protein abundance upon treatment (figure 27).

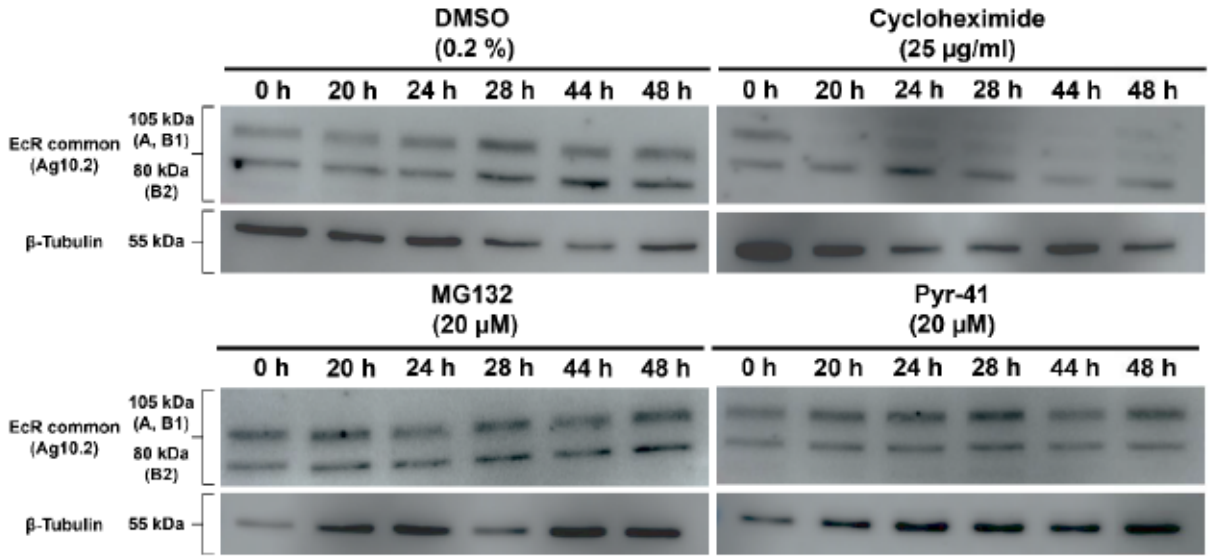

Figure 27: Detection of common EcR via immunoblotting with the Ag10.2 antibody in S2R+ cells. Cells were treated with either 0.2 % DMSO, cycloheximide (25 µg/ml), MG132 (20 µM) or Pyr-41 (20 µM) and sampled over the time course of 2 days at timepoint t_0 (0 h), t_1 (20 h), t_2 (24 h), t_3 (28 h) t_4 (44 h) and t_5 (48 h). Cell lysates were generated and subsequently measured for whole protein levels by means of BCA and equal amounts of protein were loaded. The Ag10.2 antibody detects all EcR isoforms, resulting in the presence of multiple signals (EcR A, B1 ~105 kDa, EcR B2 ~80kDa). Ubiquitously expressed β-tubulin (55 kDa) served as loading control. The depicted blots show representative images from at least three independent repetitions.

The DMSO-treated control showed a slight increase in EcR protein abundance over time for all isoforms detected with the Ag10.2 antibody. For cycloheximide treatment, an instant disappearing of the signal of EcR isoform A/B1 was noticeable, while signals for isoform B2 slowly faded over time. However, both, the treatment with MG132 as well as Pyr-41, did not result in a striking increase in EcR protein

abundance in comparison to the DMSO-treated control. These experiments were performed several times. Each time, the obtained results were comparable to those depicted in figure 27. Thus, no clear-cut conclusion could be drawn concerning an inhibition of proteasomal degradation using MG132 and Pyr-41.

Besides the hypothesized reduction in ecdysone signaling in *sturkopf* mutant animals, the data presented in figure 25 indicate a reduction in 20HE hemolymph titers suggesting an impairment in ecdysone signaling. To investigate whether sturkopf affects EcR protein stability, which would support the hypothesis of an impairment in ecdysone signaling, EcR protein abundance was analyzed in the cultured cells stably overexpressing different sturkopf variants (compare figure 6).

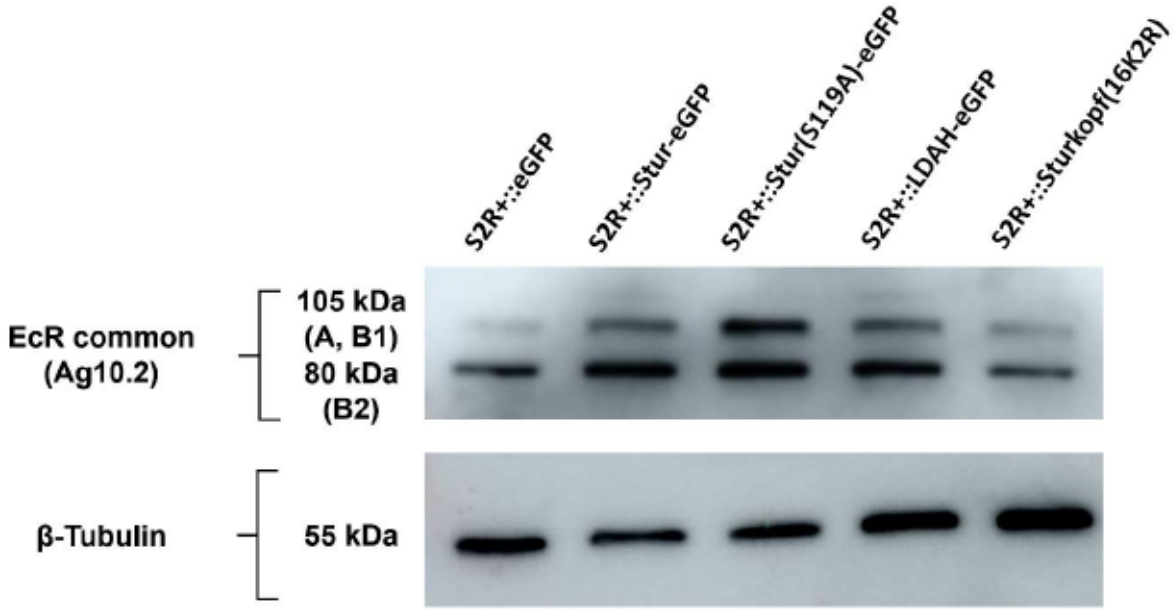

Figure 28: Detection of common EcR via immunoblotting with the Ag10.2 antibody in cell culture extracts from generated S2R+::eGFP, S2R+::sturkopf-eGFP, S2R+::sturkopf(S119A)-eGFP, S2R+::LDAH-eGFP and S2R+::sturkopf(16K2R)-eGFP polyclonal cell lines. Cell lysates were measured for whole protein levels by means of BCA and equal amounts of protein were loaded. The Ag10.2 antibody detects all EcR isoforms, resulting in the presence of multiple signals (EcR A, B1 ~105 kDa, EcR B2 ~80kDa). Ubiquitously expressed β-tubulin (55 kDa) served as loading control. Note that it is the same blot as depicted in figure 6, but this time the membrane was probed for the EcR. The depicted blot shows a representative image of at least two independent repetitions.

The detection of the EcR in the polyclonal cell lines S2R+::eGFP, S2R+::sturkopf-eGFP, S2R+::sturkopf(S119A)-eGFP, S2R+::LDAH-eGFP and S2R+::sturkopf(16K2R)-eGFP revealed isoform- and cell line-specific differences in EcR protein abundance. While EcR isoform A and/or B1 as well as B2 protein

abundance was increased in wild type sturkopf overexpressing cells as well as in sturkopf(S119A) and *hsLDAH* overexpressing cells, all EcR isoforms in sturkopf(16K2R)-overexpressing cells showed a protein abundance comparable to the control cell line (figure 28). This data suggest a stabilizing role of wild type sturkopf overexpression for the different EcR isoforms. Furthermore, both sturkopf(S119A) and *hs*LDAH overexpression increased isoform-specific protein abundance of EcR A/B1 in comparison to the control. sturkopf(16K2R) overexpression is the only condition which showed no difference in EcR protein abundance compared to the control.

It was initially planned to perform cycloheximide pulse-chase experiments with these cell lines, too. However, these experiments were not executed due to the not very convincing data obtained from the cycloheximide chase experiments including MG132 and Pyr-41 treatment performed using S2R+ cells (figure 27).

EcR protein abundance was also checked *in vivo* using lysates of wandering L3 larvae and 7-days old female and male flies of the genotypes *sturkopf* Ctrl and *sturkopf[35.7]*. However, the EcR signal could only be detected in L3 larvae but due to extremely high levels of background signal it was impossible to draw conclusions from this data set (data not shown). Furthermore, EcR-specific antibody stainings were performed to test for differences in isoform-specific EcR protein abundance in *sturkopf* null mutant animals. This data did likewise not result in clear-cut differences towards EcR protein abundance (data not shown).

2.4 Manipulation of sturkopf protein levels *in vivo*

Within the scope of this work the *sturkopf* LOF was identified as the reason for the observed loss of SC phenotype in the accessory glands (figures 12A and 16). The phenotype was further investigated as it was completely unclear whether the observed phenotype results from a tissue or even cell specific sturkopf mode of action or whether it is based on a long-range effect in another tissue and, thus, affecting numbers of SCs in the AGs.

2.4.1 Single molecule FISH for the determination of *sturkopf* transcription site

Sturkopf was identified as LDAP shuttling between the endoplasmic reticulum and LDs once these become available (Thiel et al. 2013). Furthermore, it is known to be

highly enriched in fat storing tissue such as the *Drosophila* fat body where it also was initially identified (Beller et al. 2006). Thus, the localization of overexpressed sturkopf previously was assessed in the fat body of wandering L3 larvae.

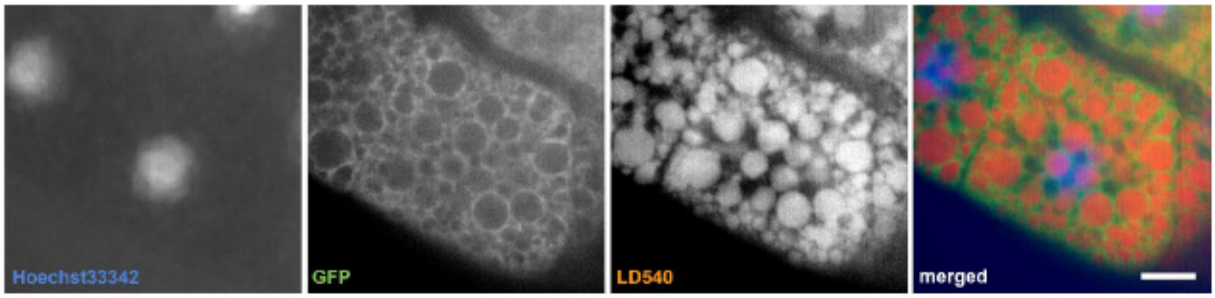

Figure 29: Localization of overexpressed sturkopf C-terminally tagged with GFP using a fat body Gal4 specific driver line and a sturkopf overexpression effector line. Fat bodies were additionally stained with LD540 to mark lipids. Images were recorded with the Operetta CLS High Content Analysis System using a 5x air objective to identify and select tissues and a 40x air objective to obtain high resolution images of the selected fields. Scale bar = 20 µm. (Figure was adapted from (Chartschenko et al. 2021) with permission of the journal.

The localization of overexpressed sturkopf in the larval fat body is limited to the lipid droplets present in the fat body (figure 29). However, although its localization pattern is known, the actual site of protein expression or gene transcription remained elusive. To address this question, single molecule (smi-)FISH experiments were performed to identify the transcription sites of *sturkopf* in the AGs of male flies. The smiFISH probe design as well as experimental procedure was performed according to Tsanov et al. and Calvo et al. (Tsanov et al. 2016; Calvo et al. 2021). For this purpose, 7 days-old, mated males of the genotypes *sturkopf* Ctrl and the *sturkopf[35.7]* null mutant line were used.

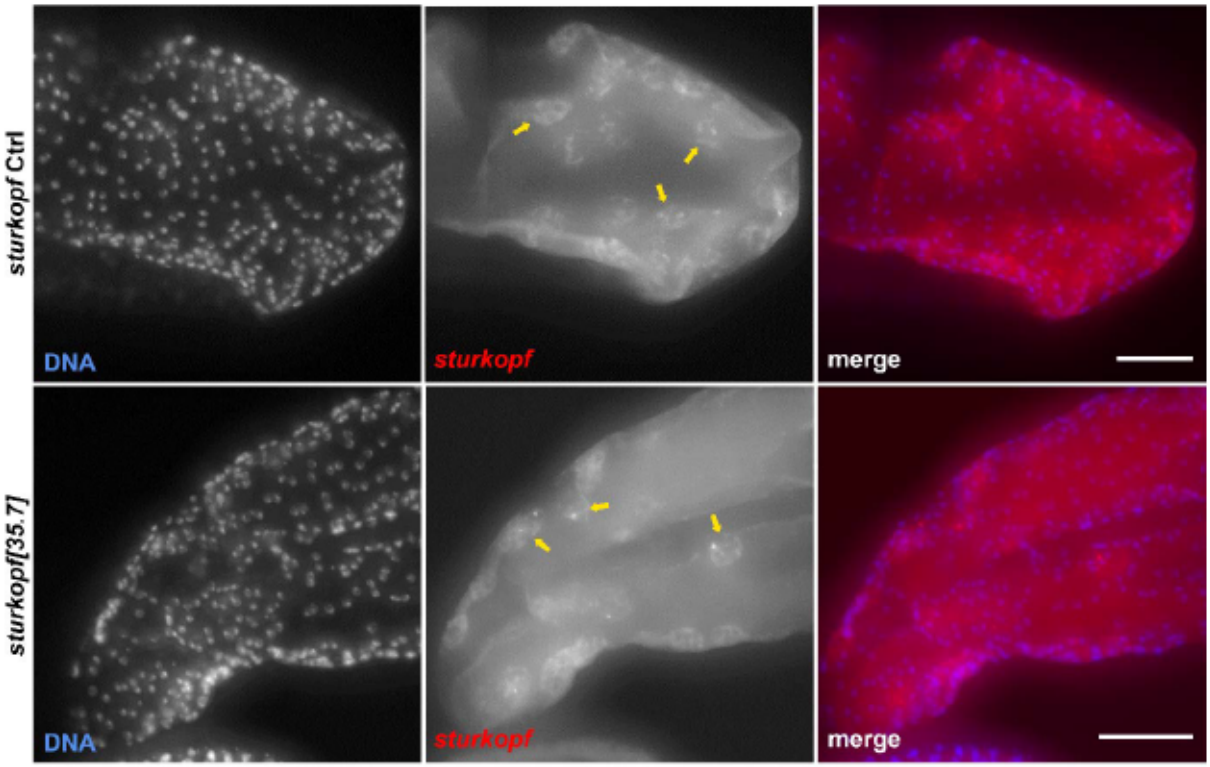

Figure 30: Representative maximum intensity projections of accessory glands lobe tips of 7 days-old, mated males of the genotypes *sturkopf* Ctrl and *sturkopf[35.7]* for the detection of sturkopf mRNA transcripts performing smi-FISH. DNA was stained using Hoechst33342 and *sturkopf* mRNA detection was performed with a set of 24 *sturkopf*-specific probes which were previously hybridized with the FLAP X probe which was C- and N-terminally tagged with Cy3. Yellow arrow heads mark signal limited to secondary cells. Images were recorded with the Operetta CLS High Content Analysis System using a 5x air objective to identify and select tissues and a 40x air objective to obtain high resolution images of the selected fields. Scale bar = 50 µm.

The smiFISH experiments performed on AGs did not result in clear-cut differences comparing to, both, the *sturkopf* Ctrl and *sturkopf[35.7]* null mutant line (figure 30). In both cases, a distinct signal was obtained which was limited to the SCs of the accessory gland. However, in case of a successful hybridization, the signal should be exclusive to the *sturkopf* Ctrl line. As a signal was obtained for both genotypes, it could be concluded that the smiFISH approach was not successful to determine the transcription site of *sturkopf* mRNA. Previously performed FISH experiments for the detection of *Drosophila* gut bacteria *in vitro* and *vivo*, however, were successful as depicted in figure 31 (Akhtar et al. 2021).

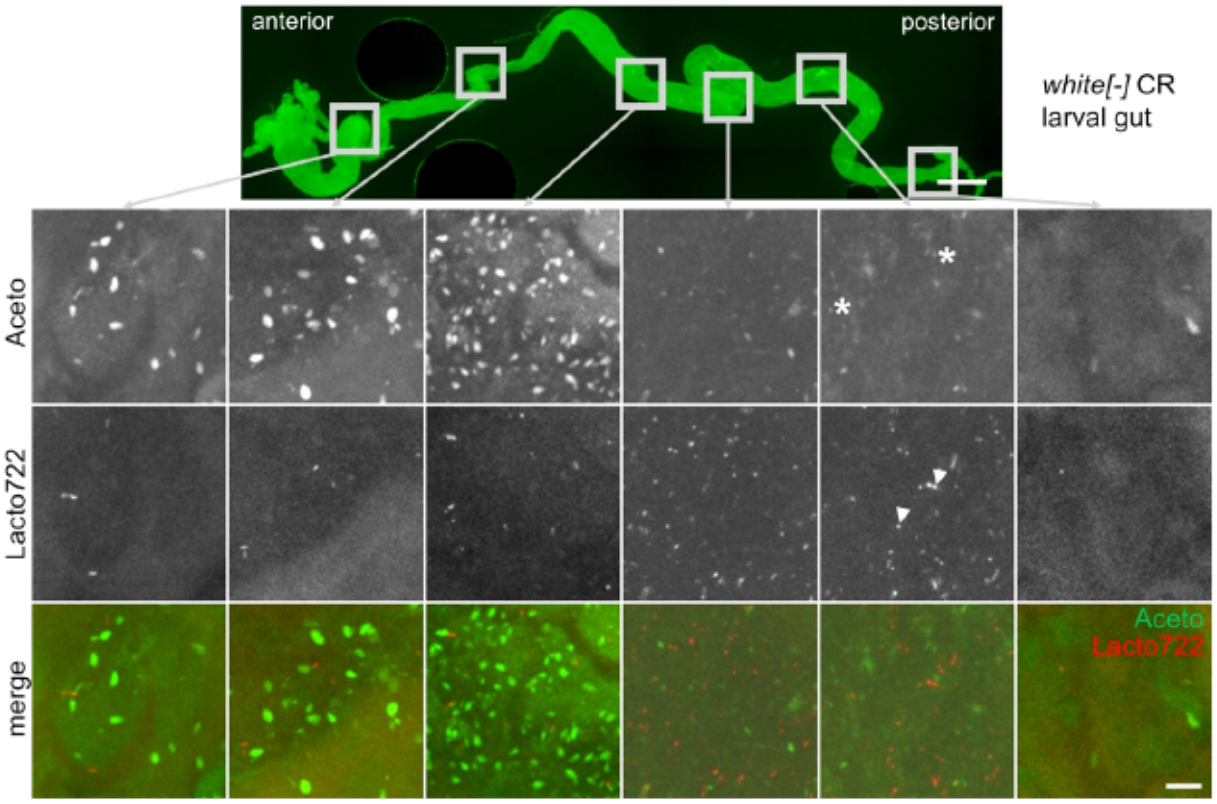

Figure 31: Fluorescence *in situ* hybridization of a representative larval *Drosophila* gut. FISH was performed with Carnoy's solution-fixed larval *Drosophila* guts using the genera-specific probes Aceto (green) and Lacto722 (red). An overview of the entire gut was imaged and detailed zoom-ins of 6 different regions are shown. Exemplary *Acetobacter* cells are marked with asterisks and *Lactobacillus* cells are indicated by arrowheads. Scalebars = 500 µm (overview); 10 µm (zoom-ins). (Figure was taken from with (Akhtar et al. 2021) with permission of the journal, as it "is under the terms of Creative Commons CC-BY (CC-BY 4.0) license which permits unrestrictive use […] provided the original work is properly cited" Copyright Clearance Center, Inc.).

2.4.2 Organismic sturkopf protein modulation

To investigate sturkopf's phenocritic tissue, sturkopf protein level abundance was altered by a RNAi-mediated knockdown of *sturkopf* in an ubiquitous manner. This means enabled detecting whether organismal depletion of the protein exhibited a similar loss of SCs as observed for the *sturkopf* null mutant background previously (compare figures 12A and 16). Therefore, the Gal4/UAS system was harnessed by means of an *actin Gal4* driver line in order to drive *sturkopf* RNAi transgene activation and, thus, deplete sturkopf protein levels on an organismic scale.

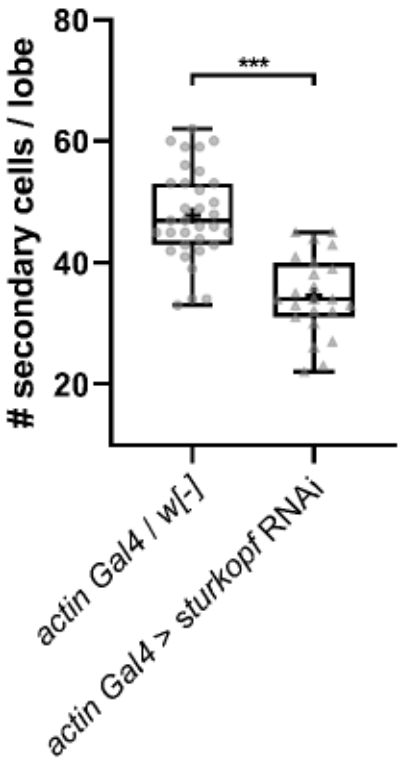

Figure 32: Quantification of SC number per lobe of 7-days old mated male flies of the crossings *actin Gal4 / w[-]* (n=33 lobes) and *actin Gal4 > sturkopf* RNAi (n=23 lobes). Analysis was performed based on an Abd-B antibody staining which specifically marks nuclei of SCs. Depicted data is based on at least three biologically independent experiments. Experimental procedure and data analysis was performed by Dilara Bursa (master student). All p values were obtained by an unpaired two-sample t test with significance levels: n.s., $p \geq 0.05$, *$p < 0.05$, **$p < 0.01$, ***$p < 0.001$.

Figure 32 shows the ubiquitous depletion of sturkopf protein levels. Compared to the control crossing *actin Gal4 / w[-]* which showed similar SC numbers compared to the different sturkopf control lines (compare figures 12A and 16), the RNAi-mediated knockdown of *sturkopf* phenocopied the *sturkopf* null mutant loss of SC phenotype as a highly significant reduction in SC numbers was identified (compare figures 12A, 16 and 32).

2.4.3 Fat body- and main cell specific sturkopf protein level modulation

Next it was tested whether modulation of sturkopf protein levels in a fat body- or main cell (MC)-specific manner resulted in differentially regulated SC numbers in the AG. To answer this, sturkopf was knocked down in an RNAi-specific manner in the fat body using a fat body-specific fat body Gal4 driver line (Grönke et al. 2003). The fat body is the pendant to the adipose tissue in mammals and it is the tissue in which

sturkopf was initially identified and where sturkopf is known to be highly expressed (Beller et al. 2006).

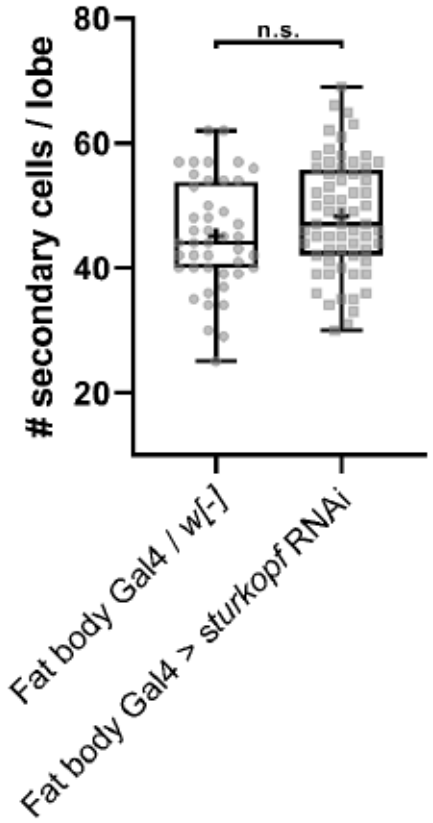

Figure 33: Quantification of SC number per lobe of 7-days old mated male flies of the crossings fat body Gal4 / *w[-]* (n=44 lobes) and fat body Gal4 > *sturkopf* RNAi (n=64 lobes). Analysis was performed based on an Abd-B antibody staining which specifically marks nuclei of SCs. Depicted data is based on at least three biologically independent experiments. Experimental procedure and data analysis was performed by Dilara Bursa (master student). All p values were obtained by an unpaired two-sample t test with significance levels: n.s., $p \geq 0.05$, *$p < 0.05$, **$p < 0.01$, ***$p < 0.001$.

Upon quantification of SCs, no significant differences in total SC number were found comparing fat body Gal4 > *sturkopf* RNAi and the corresponding control crossing fat body-Gal4 / *w[-]* (figure 33). The latter condition had similar numbers of SCs as determined before (compare figures 12A, 16, and 32).

The accessory gland of *Drosophila* is only comprised of two distinct cell types, i.e., MCs and SCs (Bertram et al. 1992). Therefore, the assumption is legitimate that manipulation of sturkopf protein levels in the tissue, in which the phenotype was identified, may have an effect on SC abundance. Therefore, the main cell driver line

Acp26Aa Gal4 driver line (Chapman et al. 2003) was used to modulate sturkopf protein levels in a MC-specific manner.

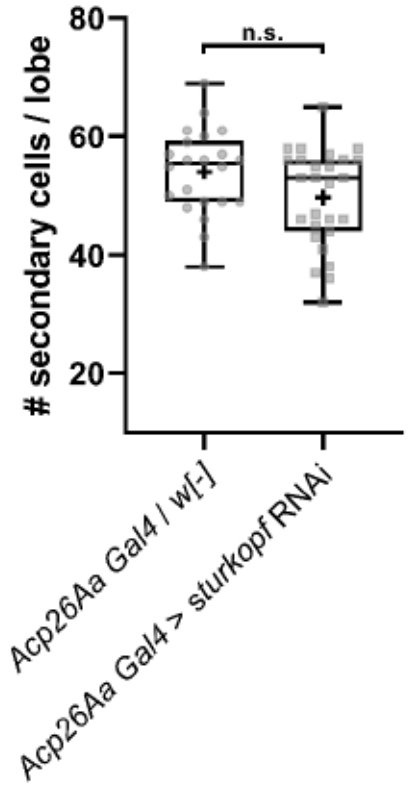

Figure 34: Quantification of SCs per lobe of 7-days old mated male flies of the crossings *Acp26Aa Gal4 / w[-]* (n=22 lobes) and *Acp26Aa Gal4 > sturkopf* RNAi (n=71 lobes). Analysis was performed based on an Abd-B antibody staining which specifically marks nuclei of SCs. Depicted data is based on at least three biologically independent experiments. Experimental procedure and data analysis was performed by Dilara Bursa (master student). All p values were obtained by an unpaired two-sample t test with significance levels: n.s., $p \geq 0.05$, *$p < 0.05$, **$p < 0.01$, ***$p < 0.001$.

Using the *Acp26Aa Gal4* driver line, the main cell-driven knockdown of *sturkopf* did not reveal significant differences in the total number of SCs when compared to the corresponding control crossing *Acp26Aa Gal4 / w[-]* (figure 34). The control crossing showed similar numbers of SCs as observed before (compare figures 12A, 16, 32 and 33). This data suggests that there is no long-range effect of sturkopf coming from the fat body or MCs affecting the number of SCs in the accessory gland thereby. However, it could not be ruled out that potential long-range effects of sturkopf from other tissues can have an impact on the number of SCs.

2.4.4 Secondary cell-specific sturkopf protein level modulation ("standard shift")

To investigate the impact location of sturkopf, the protein was further overexpressed and knocked down in a SC-specific manner. As the loss of SC phenotype observed for *sturkopf* mutant animals affects the SCs themselves, the possibility of a SC-specific sturkopf place of action was tested. To do this, the SC-specific *esg;Ctrl* and *esg;35.7* driver lines were used. These lines were also used for the identification of the loss of SC phenotype (figure 12A). Transgene expression using these driver lines also takes place in other cells expressing the *escargot* transcription factor, such as intestinal stem cells (Korzelius et al. 2014). However, inside the AGs the expression is limited to the SCs, which is why, from here on, transgene expression using *esg;Gal4* constructs is termed SC-specific.

In preliminary experiments it became clear that upon crossing and, thus, heterozygosity of the *escargot* constructs, the endogenous and SC-specific expression of GFP diminished. Not all SCs were expressing GFP robustly which became particularly clear in conditions in which transgene expression was additionally monitored by further means, e.g., by antibody staining. An exemplary picture of an AG derived from an *esg;Ctrl*-crossed animal is depicted in figure 35. The HA-tagged *sturkopf* overexpression was verified by antibody staining against the HA-tag.

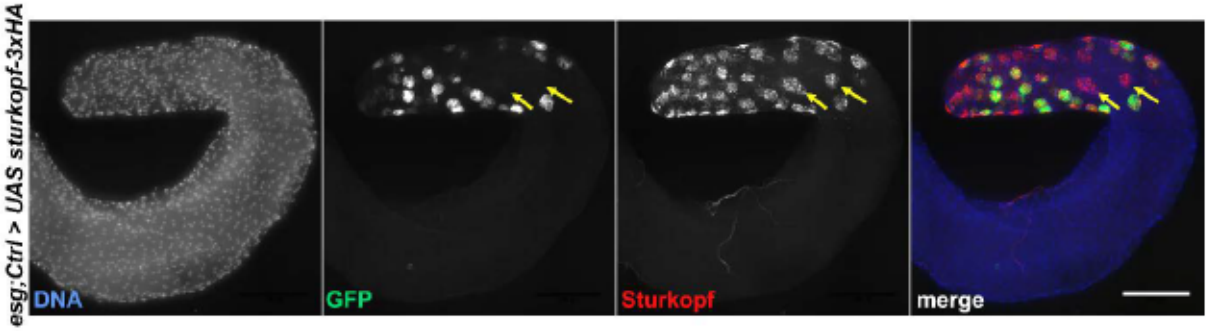

Figure 35: Representative maximum intensity projection of an accessory gland's lobe of a 7-days old, mated fly of the crossing *esg;Ctrl* > *UAS sturkopf-3xHA* antibody stained against HA of at least three biologically independent experiments. DNA was stained with Hoechst33342 (blue), SCs are marked by endogenous GFP expression (green) and sturkopf overexpression is detected by usage of an Alexa647-coupled secondary antibody (red). Note that the GFP and HA signals show no 1:1 overlap indicated by yellow arrows. Images were recorded with the Operetta CLS High Content Analysis

System using a 5x air objective to identify and select tissues and a 40x air objective to obtain high resolution images of the selected fields. Scale bar = 200 µm.

The analysis of these tissues revealed that not all SCs overexpressing *sturkopf* (anti-HA staining) also expressed GFP as it has been the case for, both, *esg;Ctrl*- (figure 35) and *esg;35.7*-driven expression (data not shown) driven crossings. However, SC quantification of homozygous *esg;Ctrl* and *esg;35.7* fly lines showed either a complete signal overlap when co-stained with an α-ANCE antibody (compare e.g., figure 14) or SC numbers were comparable to those obtained by antibody stainings against Abd-B or ANCE in the *sturkopf* Ctrl and *sturkopf[35.7]* fly lines (compare data from figures 16, 32, 33 and 34). Further crossings of the *esg;Ctrl* and *esg;35.7* with other effector lines revealed the same issue of insufficient SC-specific GFP expression (data not shown). Thus, it needed to be assumed that upon heterozygosity of the *escargot* construct not all SCs express GFP robustly. The quantification of SCs on the mere GFP expression was, hence, not sufficient to obtain robust data in crossings using the *esg;Ctrl* or *esg;35.7* driver lines to drive transgene expression. Therefore, additional antibody stainings were performed. As described in 4.2.5.1, animals of the genotype *esg;Ctrl* and *esg;35.7* as well as crossings with these lines require the cultivation on 18 °C until hatching and then get shifted to 29 °C to ensure Gal4/UAS-mediated transgene expression. The expression is blocked at 18 °C based on a temperature-sensitive $Gal80^{ts}$ protein inhibiting Gal4. Both available SC markers, ANCE and Abd-B were tested in this respect. However, both failed to detect SCs in the temperature-shifted crossings (figure 36).

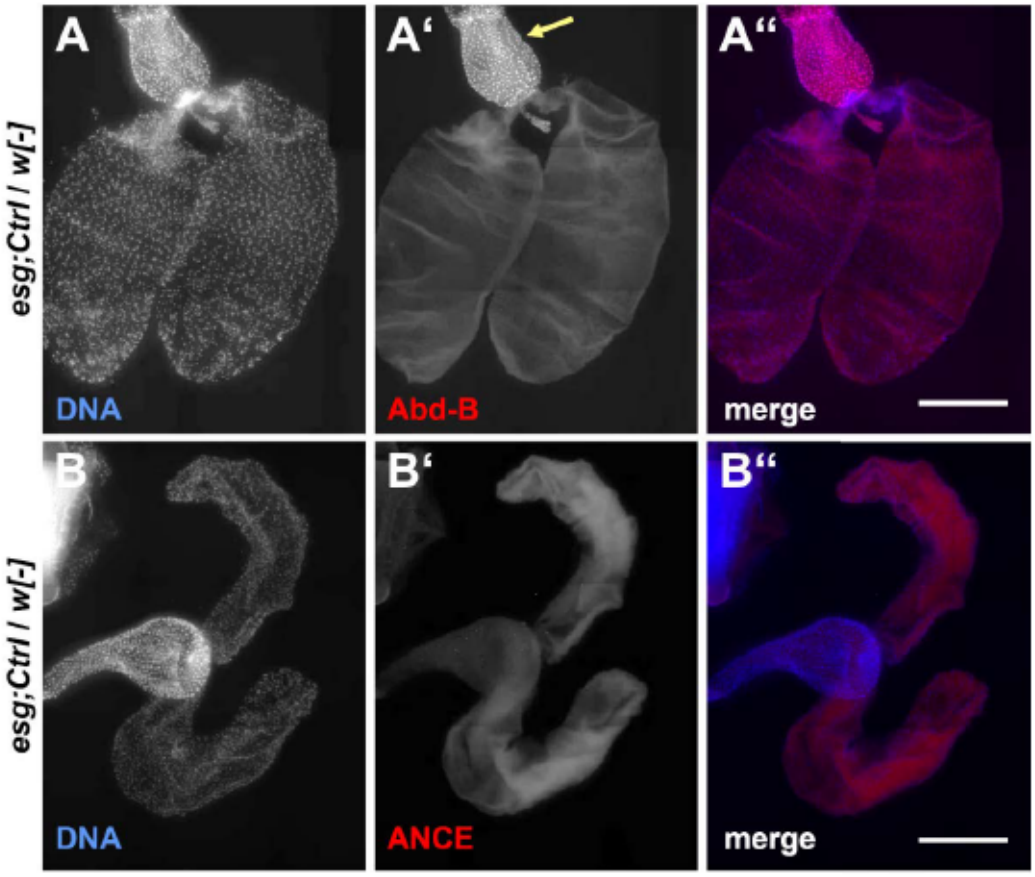

Figure 36: Representative maximum intensity projections of accessory glands of 7-days old flies of the crossing *esg;Ctrl / w[-]* antibody stained against (**A**) Abd-B and (**B**) ANCE. DNA was stained with Hoechst33342 (blue), SCs were counterstained with either ANCE (**A'**) or Abd-B (**B'**) using an Alexa647-coupled secondary antibody (red) due to insufficient endogenous SC-specific GFP expression (channel not shown). Abd-B-positive ejaculatory duct cells are indicated by a yellow arrow (**A'**). Images were recorded with the Operetta CLS High Content Analysis System using a 5x air objective to identify and select tissues and a 40x air objective to obtain high resolution images of the selected fields. Scale bar = 200 µm.

The antibody-stained tissue using ANCE to detect SCs (figure 36B') completely failed to mark the SCs. Utilization of Abd-B also failed to mark SCs in AGs, however, marked the cells of the ejaculatory duct, which are also Abd-B positive serving as internal control for a successful antibody staining *per se* (figure 36A'). The temperature shift to 29 °C represents a stressor for *Drosophila* and may serve as explanation for the unsuccessful staining of the SCs. To circumvent this issue, crossings of the driver lines *esg;Ctrl* or *esg;35.7* with the appropriate effector lines were reared as usual. However, after transgene expression for 7 days, flies were put back to the restrictive temperature of 18 °C for three days. The subsequent dissection of AGs and antibody staining against Abd-B resulted in a successful

marking of SCs in crossings using the driver lines *esg;Ctrl* and *esg;35.7* consequently. Figure 37 displays a representative AG, in which SCs were positively marked using an Abd-B-specific antibody. The ejaculatory duct cells, which are also Abd-B-positive, served again as an internal control for a successful antibody staining.

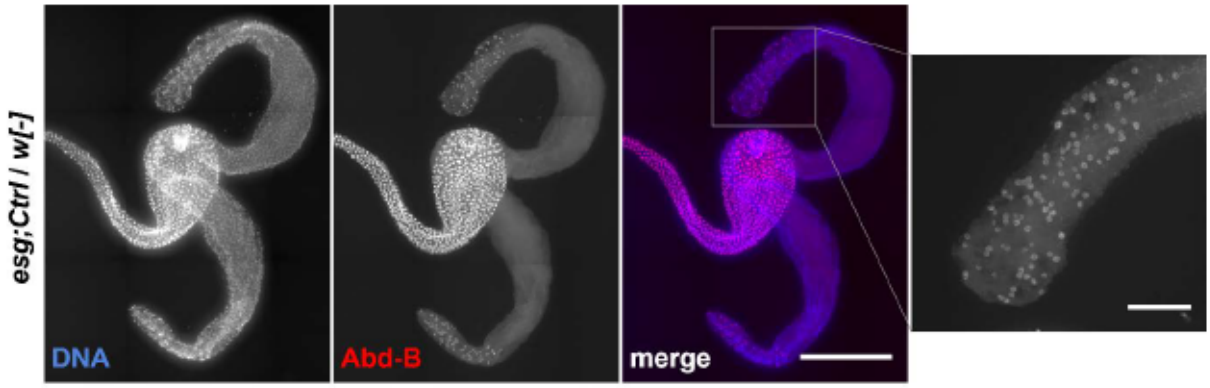

Figure 37: Representative maximum intensity projection of an accessory gland of a 7-days old fly of the crossing *esg;Ctrl / w[-]* antibody stained against Abd-B. DNA was stained with Hoechst33342 (blue), SCs were counterstained with Abd-B using an Alexa647-coupled secondary antibody (red) due to insufficient endogenous SC-specific GFP expression (channel not shown). *esg*-based crossings were reared as usual but after transgene expression for 7 days, flies were put back to the restrictive temperature of 18 °C for three days. The grey box demarcates the area used for zoom-in. Images were recorded with the Operetta CLS High Content Analysis System using a 5x air objective to identify and select tissues and a 40x air objective to obtain high resolution images of the selected fields. Scale bar = 200 µm (overview) and 50 µm (zoom-in).

Besides crossings between *esg;Ctrl* or *esg;35.7* with *w[-]* as control crossings, homozygous animals of both driver lines were additionally carried along as controls for the antibody staining. First, crossings with *esg;Ctrl* were used to investigate whether the RNAi-mediated SC-specific *sturkopf* knockdown results in a phenocopy of the *sturkopf* null mutant phenotype (figure 38).

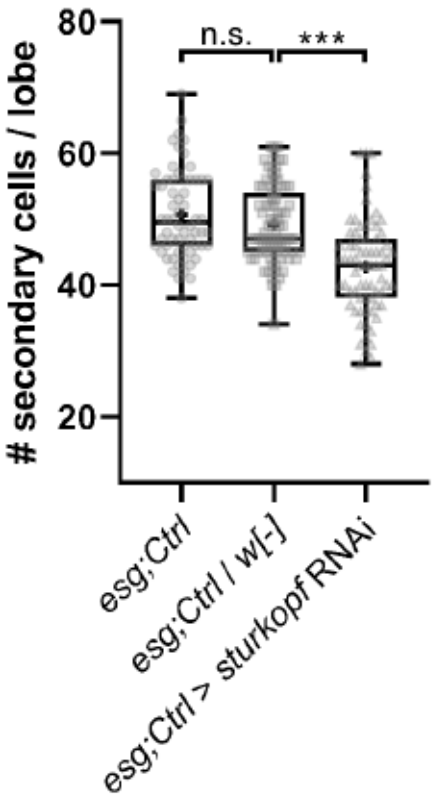

Figure 38: Quantification of SCs per lobe in mated male flies of the genotype *esg;Ctrl* (n=62 lobes) and of the crossings *esg;Ctrl* / *w[-]* (n=89 lobes) and *esg;Ctrl* > *sturkopf* RNAi (n=73 lobes) based on an Abd-B antibody staining. Flies were kept on 29 °C for 7 days to ensure transgene expression and afterwards put back to the restrictive temperature of 18 °C for 3 additional days. Depicted data is based on at least three biologically independent experiments. All p values were obtained by an unpaired two-sample t test with significance levels: n.s., $p \geq 0.05$, *$p < 0.05$, **$p < 0.01$, ***$p < 0.001$.

The secondary cell-specific RNAi-mediated knockdown of *sturkopf* resulted in highly significant decrease of SC numbers compared to both the control crossing *esg;Ctrl* / *w[-]* as well as the homozygous driver line *esg;Ctrl*. The obtained data for both controls were similar to those obtained previously (figures 12A and 16). The RNAi-mediated *sturkopf* knockdown resulted in a highly significant decrease of SCs which was comparable to the *sturkopf* null mutant situation (figures 12A and 16). These data together with the previously obtained results. This data suggests a secondary cell-specific sturkopf place of action.

As a significant decrease of SCs was obtained upon SC-specific *sturkopf* knockdown it was tested whether an overexpression of sturkopf resulted in an opposing phenotype of an increase of SCs next, since previously acquired data strongly suggest a SC-specific sturkopf mode of action.

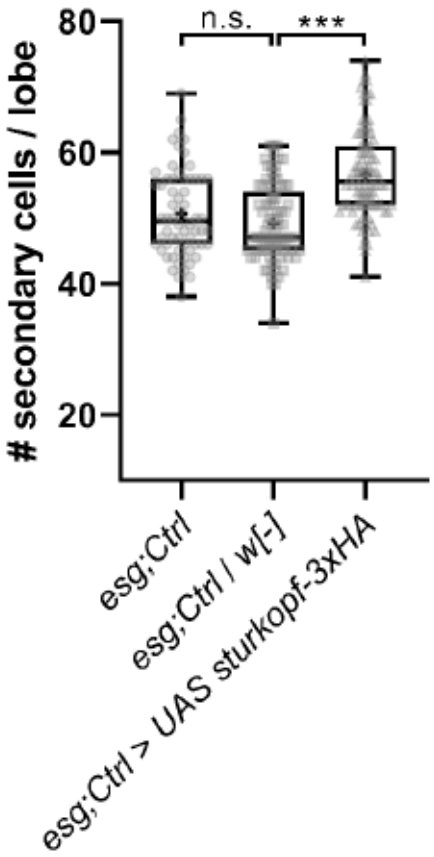

Figure 39: Quantification of SCs per lobe in mated male flies of the genotype *esg;Ctrl* (n=62 lobes) and of the crossings *esg;Ctrl / w[-]* (n=89 lobes) and *esg;Ctrl > UAS sturkopf-3xHA* (n=100 lobes) based on an Abd-B antibody staining. Flies were kept on 29 °C for 7 days to ensure transgene expression and afterwards put back to the restrictive temperature of 18 °C for 3 additional days. Depicted data is based on at least three biologically independent experiments. Note that the depicted controls are the same data as depicted in figure 38 as all conditions were carried along at the same time. All p values were obtained by an unpaired two-sample t test with significance levels: n.s., $p \geq 0.05$, *$p < 0.05$, **$p < 0.01$, ***$p < 0.001$.

Sturkopf overexpression in a SC-specific manner led to a highly significant increase in SC number compared to the control crossing *esg;Ctrl / w[-]* as well as the homozygous driver line *esg;Ctrl* (figure 39). Sturkopf overexpression resulted in an opposing phenotype as compared to the *sturkopf* RNAi-mediated knockdown (figure 38). These findings further suggest a SC-specific sturkopf mode of action. A frequency distribution analysis was additionally performed to reinforce the differences between sturkopf overexpression and RNAi-mediated knockdown in comparison to the control crossing *esg;Ctrl / w[-]*.

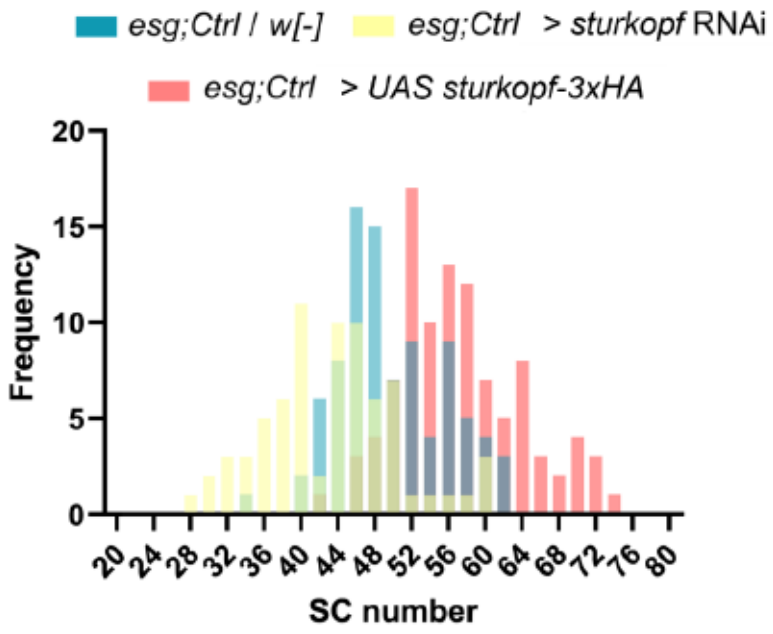

Figure 40: Frequency distribution analysis of secondary cell numbers per lobe of 7-days old animals of the crossings *esg;Ctrl / w[-]* (n=89 lobes), *esg;Ctrl > sturkopf* RNAi (n=73 lobes) and *esg;Ctrl > UAS sturkopf-3xHA* (n=100 lobes). Processed data are the same as depicted in figures 38 and 39.

The frequency distribution analysis depicted in figure 40 revealed three distinct populations representing the three different crossings *esg;Ctrl / w[-]*, *esg;Ctrl > sturkopf* RNAi and *esg;Ctrl > UAS sturkopf-3xHA*. While the RNAi-mediated knockdown of *sturkopf* showed the overall lowest numbers of SCs, the sturkopf overexpression showed the highest number of SCs, and the control crossing showed intermediate numbers of SCs. All data of the tested conditions showed an almost gaussian normal distribution.

Having identified that the sturkopf mode of action as SC-specific, the modulation of sturkopf protein abundance was tested in the *sturkopf* mutant background subsequently. Therefore, the *esg;35.7* driver line was utilized. First, it was tested whether it was possible to recapitulate the partial rescue by reintroducing at least one functional *sturkopf* allele via crossing with *w[-]* as before (compare figure 17). The homozygous *esg;35.7* driver line was carried along as antibody staining control and for comparison to the *sturkopf* null mutant state. For the sake of completeness, *esg;35.7* was also crossed with *sturkopf* RNAi with the results being depicted in figure 41.

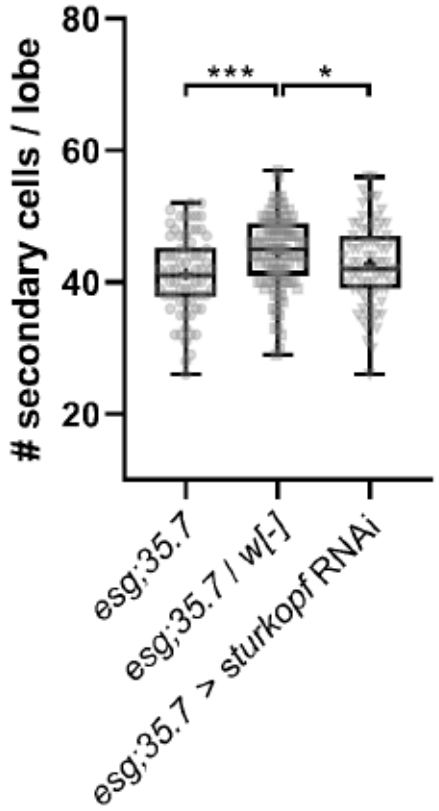

Figure 41: Quantification of SCs per lobe in mated male flies of the genotype *esg;35.7* (n=74 lobes) and of the crossings *esg;35.7 / w[-]* (n=111 lobes) and *esg;Ctrl > sturkopf* RNAi (n=77 lobes) based on an Abd-B antibody staining. Flies were kept on 29 °C for 7 days to ensure transgene expression and afterwards put back to the restrictive temperature of 18 °C for 3 additional days. Depicted data is based on at least three biologically independent experiments. Depicted data is based on at least three biologically independent experiments. All p values were obtained by an unpaired two-sample t test with significance levels: n.s., $p \geq 0.05$, *$p < 0.05$, **$p < 0.01$, ***$p < 0.001$.

As visible in figure 41, homozygous *sturkopf* mutant animals had SC numbers which were compatible with previously obtained data for *sturkopf* null mutant animals (compare figures 12A and 16). Interestingly, reintroduction of one functional *sturkopf* allele resulted in a highly significant increase in SC number as it is shown for the *esg;35.7 / w[-]* crossing. RNAi-mediated *sturkopf* knockdown in the *sturkopf* mutant background did not result in any differences in SC number as compared to the homozygous driver line but showed a significantly reduced number of SCs in comparison to the control crossing *esg.35.7 / w[-]*, with sturkopf being heterozygously expressed. This data suggests that reintroduction of one functional *sturkopf* allele partially rescues the loss SC phenotype while knockdown of *sturkopf* in this genetic background resulted in SC numbers comparable to the *sturkopf* null mutant line.

However, the heterozygous *sturkopf* mutant situation does not rescue the loss of SCs to control level as depicted in figure 42.

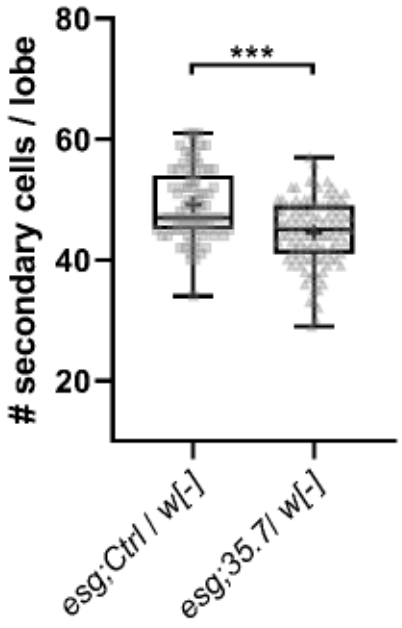

Figure 42: Comparison of SC number per lobe in mated male flies of the crossings *esg;Ctrl / w[-]* (n=89 lobes) *esg;35.7 / w[-]* (n=111 lobes) based on an Abd-B antibody staining. Flies were kept on 29 °C for 7 days to ensure transgene expression and afterwards put back to the restrictive temperature of 18 °C for 3 additional days. Depicted data is based on at least three biologically independent experiments. Depicted data is based on at least three biologically independent experiments. Note that the depicted controls are the same data as depicted in figure 38 and 41 as all conditions were carried along at the same time. All p values were obtained by an unpaired two-sample t test with significance levels: n.s., $p \geq 0.05$, *$p < 0.05$, **$p < 0.01$, ***$p < 0.001$.

Comparing the SC numbers of the crossings *esg;Ctrl / w[-]* with *esg;35.7 / w[-]* uncovered highly significant differences as numbers of SCs are highly reduced in the *sturkopf* heterozygous mutant situation as it is present in *esg;35.7 / w[-]*. This finding argues against a total rescue upon reintroduction of one *sturkopf* allele.

As a partial rescue of the loss of SC phenotype was achieved by expression of one functional copy of *sturkopf*, it was next tested whether sturkopf overexpression resulted in a complete rescue of the loss of SCs.

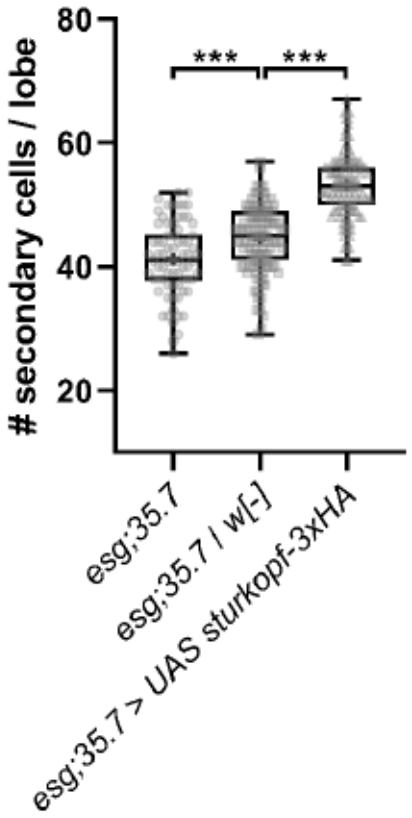

Figure 43: Quantification of SCs per lobe in mated male flies of the genotype *esg;35.7* (n=74 lobes) and of the crossings *esg;35.7 / w[-]* (n=111 lobes) and *esg;35.7 > UAS sturkopf-3xHA* (n=116 lobes) based on an Abd-B antibody staining. Flies were kept on 29 °C for 7 days to ensure transgene expression and afterwards put back to the restrictive temperature of 18 °C for 3 additional days. Depicted data is based on at least three biologically independent experiments. Note that the depicted controls are the same data as depicted in figure 41 as all conditions were carried along at the same time. All p values were obtained by an unpaired two-sample t test with significance levels: n.s., $p \geq 0.05$, *$p < 0.05$, **$p < 0.01$, ***$p < 0.001$.

Overexpression of sturkopf in the *sturkopf* null mutant background resulted in a highly significant increase in SC number compared to the *sturkopf* heterozygous mutant control crossing *esg;35.7 / w[-]* even exceeding SC numbers in fly lines expressing sturkopf wild type levels (e.g., figures 12A and 16).

A frequency distribution analysis was again performed to reinforce the differences between sturkopf overexpression and RNAi-mediated knockdown of *sturkopf* in comparison to the control crossing in the *sturkopf* mutant background.

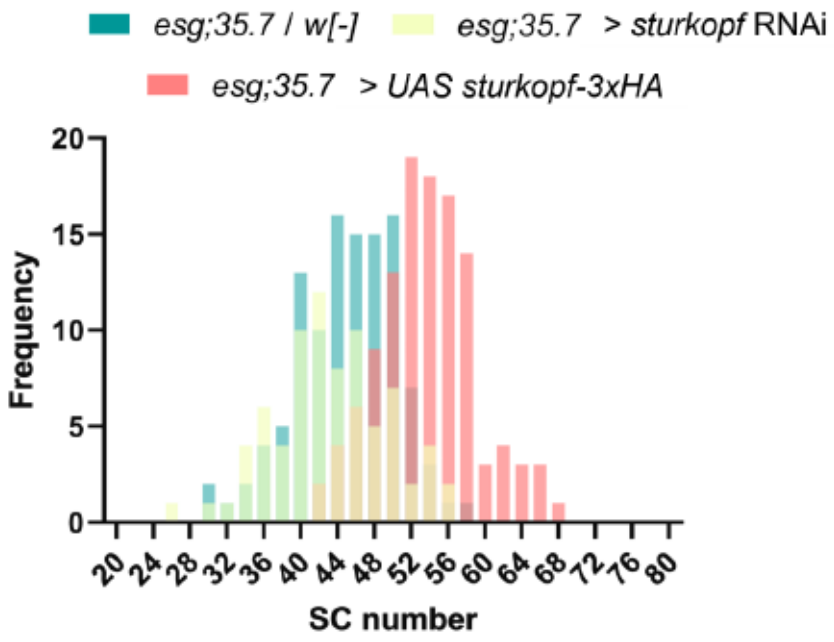

Figure 44: Frequency distribution analysis of secondary cell numbers per lobe of 7-days old animals of the crossings *esg;35.7 / w[-]* (n=111 lobes), *esg;35.7 > sturkopf* RNAi (n=77 lobes), and *esg;35.7 > UAS sturkopf-3xHA* (n=116 lobes). Processed data are the same as depicted in figures 41 and 43.

In contrast to the frequency distribution analysis in the *sturkopf* control background depicted in figure 40, frequency distribution analysis of crossings in the *sturkopf* mutant background allowed identifying only two distinct populations (figure 44). Frequency distribution of crossings between *esg;35.7 / w[-]* and *esg;35.7 > sturkopf* RNAi were mostly overlapping and only differed in the frequency of single SC number abundances. Frequency distribution of the crossing *esg;35.7 > UAS sturkopf-3xHA* represented the second distinguishable population. While the RNAi-mediated knockdown of *sturkopf* in the *sturkopf* mutant background showed the overall lowest numbers of SCs corresponding the null mutant state, the sturkopf overexpression showed the highest number of SCs. The control crossing had a similar distribution pattern as the *esg;35.7 > sturkopf* RNAi condition which may be attributable to the *sturkopf* heterozygous mutant state. The data of all tested conditions showed a gaussian normal distribution mostly.

As a result, it was worthwhile to investigate whether the overexpression of sturkopf in the mutant background rescued the loss of SC phenotype to control level. Therefore, the data was compared as can be seen in figure 45.

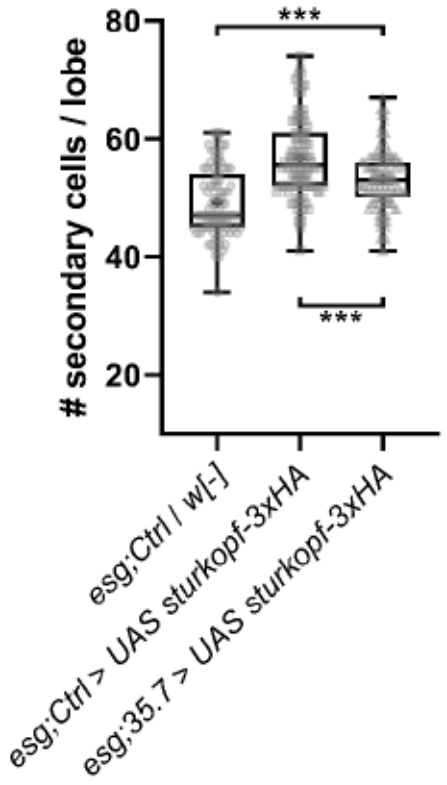

Figure 45: Comparison of SCs per lobe in mated male flies of the crossings *esg;Ctrl / w[-]* (n=89 lobes), *esg;Ctrl > UAS sturkopf-3xHA* (n=100 lobes), and *esg;35.7 > UAS sturkopf-3xHA* (n=116 lobes) based on an Abd-B antibody staining. Flies were kept on 29 °C for 7 days to ensure transgene expression and afterwards put back to the restrictive temperature of 18 °C for 3 additional days. Depicted data is based on at least three biologically independent experiments. Note that the depicted data are the same as used in figure 38, 39 and 43. All p values were obtained by an unpaired two-sample t test with significance levels: n.s., $p \geq 0.05$, *$p < 0.05$, **$p < 0.01$, ***$p < 0.001$.

Sturkopf overexpression in the *sturkopf* null mutant background resulted in a highly significant increase in SCs exceeding SC numbers of the *esg;Ctrl / w[-]* control crossing which had two functional *sturkopf* alleles. However, comparison of the overexpression in the *sturkopf* mutant background with sturkopf overexpression in the control background still showed significantly higher numbers of SCs suggesting a highly coordinated SC number regulation mediated and dependent on sturkopf protein levels.

2.4.5 Secondary cell-specific sturkopf protein modulation during the sensitive period of SC physiology (“L3 shift”)

As adult SCs are postmitotic (Taniguchi et al. 2014) and expression of all tested transgenes was driven post-eclosion (figures 38-45), the subsequent analysis discovered whether transgene expression during the last mitotic division of the SCs

halfway through pupation, from now on termed “sensitive phase of SC physiology” (Taniguchi et al. 2014; Kubo et al. 2018) affected the total SC number. In this approach, animals were raised at 18 °C and temperature-shifted to 29 °C once they reached the late L3 larvae/prepupal stage to ensure transgene expression during the sensitive period of SC physiology (Kubo et al. 2018) (figure 46).

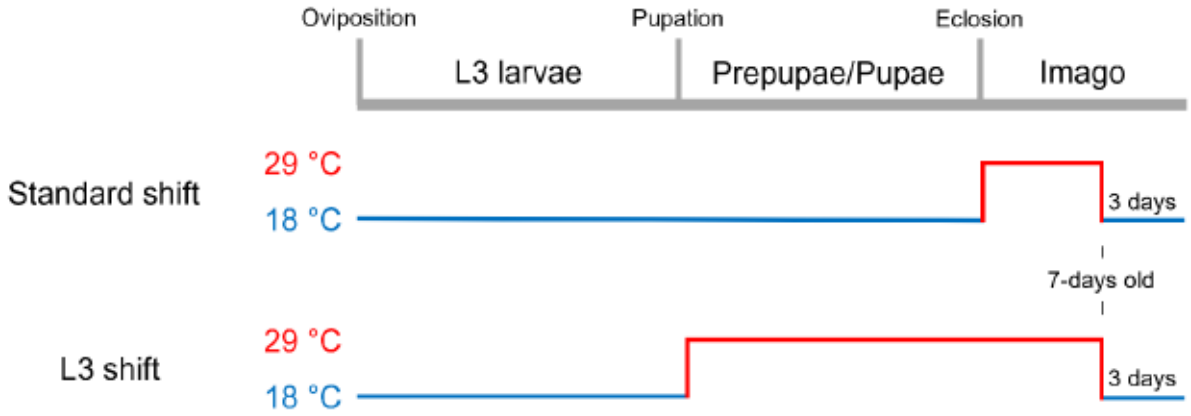

Figure 46: Differential temperature shift pattern to ensure transgene expression. While performing the standard shift, animals were raised on the restrictive temperature (18 °C) throughout their complete larval and pupal development and shifted to 29 °C post eclosion to enable transgene expression. After 7 days, animals were put back to the restrictive temperature. During the L3 shift, animals were raised on 18 °C as well, however shifted to 29 °C shortly during the time of pupation to ensure earlier transgene expression. Animals were kept on 29 °C until 7-days old and then put back to the restrictive 18 °C.

Otherwise, the experimental procedure was identical as for the experiments described before. To test for a potential impact of the timepoint of temperature shift on SC abundance, transgene expression was performed in the *sturkopf* control background using the *esg;Ctrl* driver line at first.

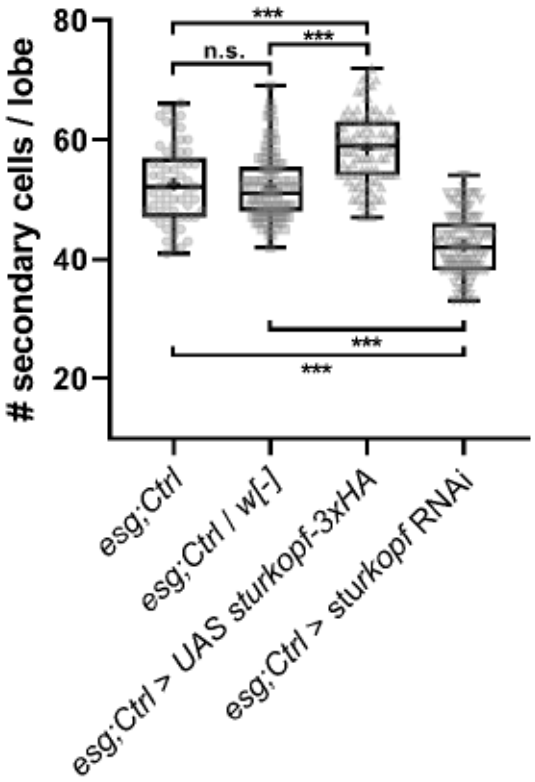

Figure 47: Quantification of SCs per lobe in mated male flies of the homozygous driver line *esg;Ctrl* (n=60 lobes) and the crossings *esg;Ctrl / w[-]* (n=106 lobes), *esg;Ctrl > UAS sturkopf-3xHA* (n=92 lobes), and *esg;Ctrl > sturkopf* RNAi (n=123 lobes) based on an Abd-B antibody staining following the L3 temperature shift. Late L3/prepupal were put on 29 °C and kept on this temperature for 7 days post eclosion to ensure transgene expression and afterwards put back to the restrictive temperature of 18 °C for 3 additional days. Depicted data is based on at least three biologically independent experiments. All p values were obtained by an unpaired two-sample t test with significance levels: n.s., $p \geq 0.05$, *$p < 0.05$, **$p < 0.01$, ***$p < 0.001$.

In general, the modified temperature shift ("L3 shift") and the consequent transgene expression during the sensitive phase for SC physiology (figure 47) resulted in SC numbers for each of the tested conditions comparable to those obtained for the standard temperature shift (figures 38 and 39). Both, the *esg;Ctrl* driver line and the crossing *esg;Ctrl / w[-]*, showed no significant differences in total SC numbers compared to the corresponding condition under standard shift conditions. A highly significant increase in SC numbers was again obtained when overexpressing sturkopf in a SC-dependent manner compared to the controls. However, this effect was also prevalent in both temperature shifts. This applied for the RNAi-mediated SC-specific *sturkopf* knockdown likewise. Again, a similar and highly significant reduction of SCs was obtained as compared to the controls to the data obtained for

the standard shift. Datasets for both the standard shift and the L3 shift were plotted together to test for potential differences.

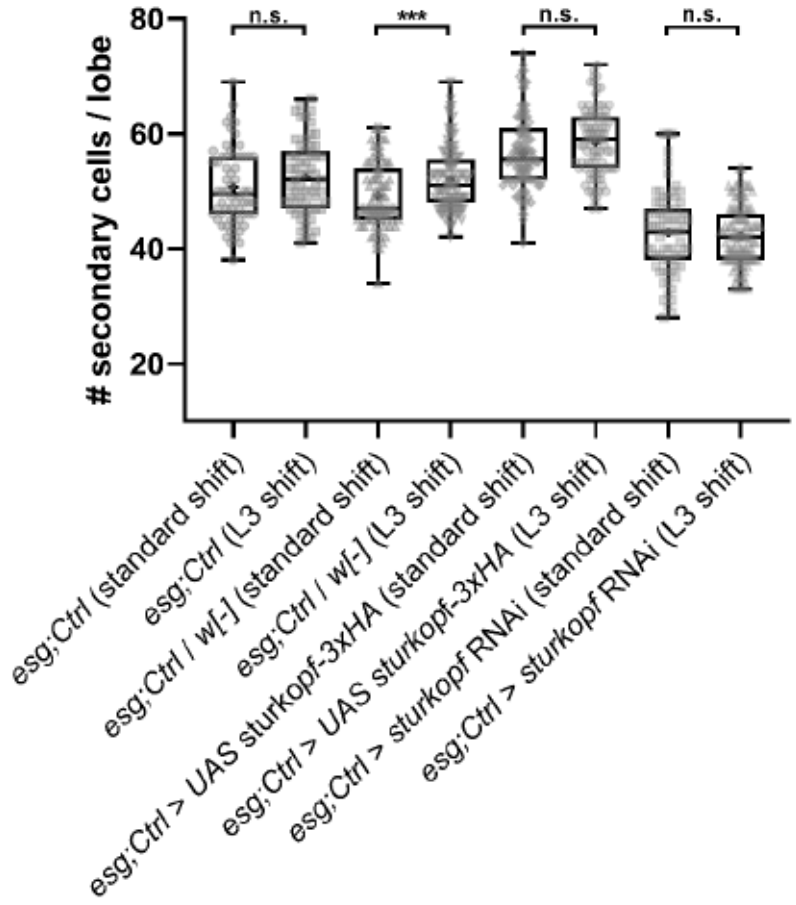

Figure 48: Comparison of quantified SCs per lobe of standard and L3-shifted mated male flies for of the homozygous driver line *esg;Ctrl* (standard shift: n=62 lobes; L3 shift: n=60 lobes) and the crossings *esg;Ctrl / w[-]* (standard shift: n=89 lobes; L3 shift: n=106 lobes), *esg;Ctrl > UAS sturkopf-3xHA* (standard shift: n=100 lobes; L3 shift: n=92 lobes) and *esg;Ctrl > sturkopf* RNAi (standard shift: n=73 lobes; L3 shift: n=123 lobes) based on an Abd-B antibody staining. Note that the depicted graph shows merged data already presented in figures 38, 39 and 47. Depicted data is based on at least three biologically independent experiments. All p values were obtained by an unpaired two-sample t test with significance levels: n.s., $p \geq 0.05$, *$p < 0.05$, **$p < 0.01$, ***$p < 0.001$.

Comparison of *esg;Ctrl*-mediated transgene expression of both temperature shifts (standard and L3) revealed no prominent differences of the corresponding crossings among each other (figure 48). However, for *esg;Ctrl / w[-]*, a highly significant increase in SC number was observed for L3-shifted male flies compared to the same crossing performing the standard shift.

Following the same strategy as for the standard shift, next transgene expression was driven using the *sturkopf* null mutant driver line *esg;35.7* following the L3 temperature shift pattern.

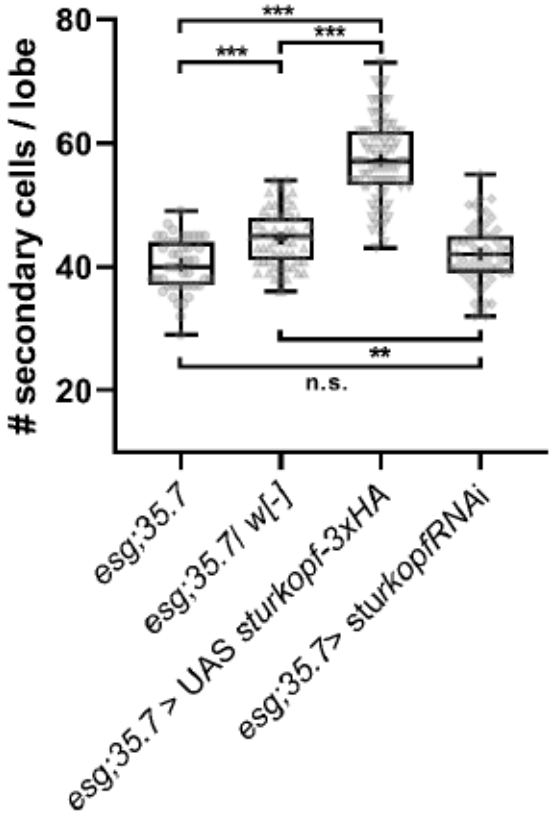

Figure 49: Quantification of SCs per lobe in mated male flies of the homozygous driver line *esg;35.7* (n=47 lobes) and the crossings *esg;35.7 / w[-]* (n=58 lobes), *esg;35.7 > UAS sturkopf-3xHA* (n=85 lobes) and *esg;35.7 > sturkopf* RNAi (n=57 lobes) based on an Abd-B antibody staining following the L3 temperature shift. Late L3/prepupal were put on 29 °C and kept on this temperature for 7 days post eclosion to ensure transgene expression and afterwards put back to the restrictive temperature of 18 °C for 3 additional days. Depicted data is based on at least three biologically independent experiments. All p values were obtained by an unpaired two-sample t test with significance levels: n.s., $p \geq 0.05$, *$p < 0.05$, **$p < 0.01$, ***$p < 0.001$.

The data obtained for L3-shifted *esg;35.7* crossings (figure 49) was comparable to the data assessed for the standard shift performing *esg;35.7*-driven transgene expression (figure 41 and 43). Homozygous *esg;35.7* showed highly reduced SC numbers compared to the control crossing *esg;35.7 / w[-]* in which one functional *sturkopf* allele was reintroduced. This resulted in a partial rescue of the *sturkopf* LOF-mediated SC loss as already demonstrated before for the same crossing performing

the standard shift (figures 41 and 43). Overexpression of sturkopf in a SC-specific manner led to a highly significant increase in SC number, corresponding to prior effects observed for the sturkopf overexpression in the *sturkopf* null mutant background following the standard shift pattern. RNAi-mediated knockdown of *sturkopf* in the null mutant background resulted in numbers of SCs comparable to the *sturkopf* null mutant, homozygous driver line *esg;35.7*. Again, the data from *esg;35.7*-driven transgene expression following the standard and L3 temperature shift was plotted for comparison purposes accordingly.

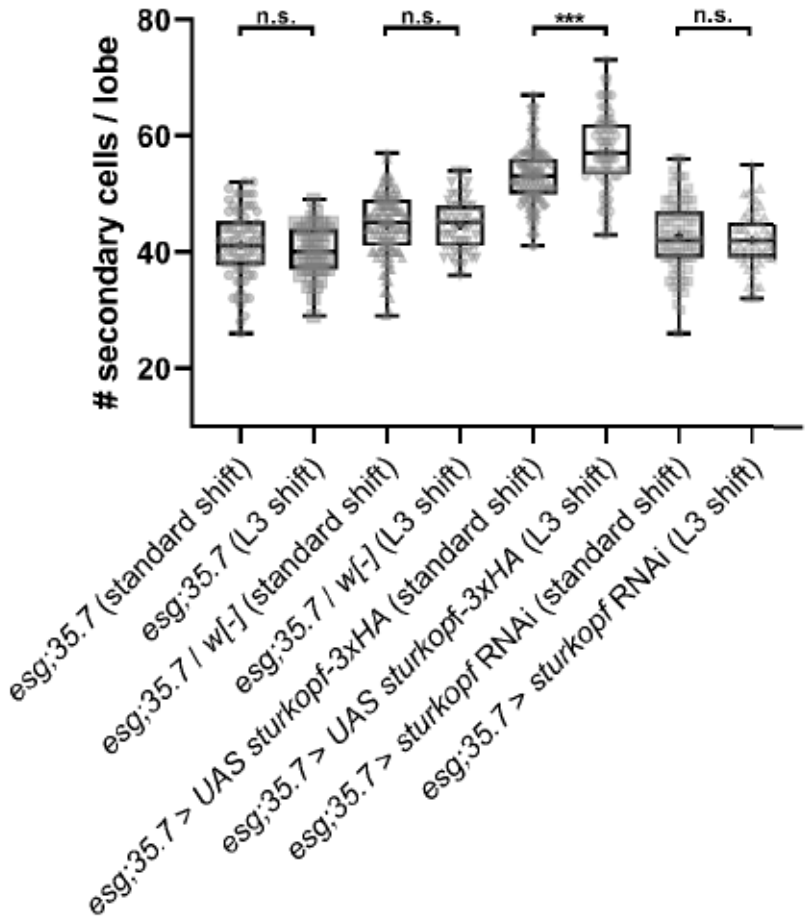

Figure 50: Comparison of quantified SCs per lobe of standard and L3-shifted mated male flies for of the homozygous driver line *esg;35.7* (standard shift: n=74 lobes; L3 shift: n=47 lobes) and the crossings *esg;35.7 / w[-]* (standard shift: n=111 lobes; L3 shift: n=58 lobes), *esg;35.7 > UAS sturkopf-3xHA* (standard shift: n=116 lobes; L3 shift: n=85 lobes) and *esg;35.7 > sturkopf RNAi* (standard shift: n=77 lobes; L3 shift: n=57 lobes) based on an Abd-B antibody staining. Note that the depicted graph is merged from the data presented in figures 41, 43 and 49. Depicted data is based on at least three biologically independent experiments. All p values were obtained by an unpaired two-sample t test with significance levels: n.s., $p \geq 0.05$, *$p < 0.05$, **$p < 0.01$, ***$p < 0.001$.

Comparison between SC numbers of standard and L3-shifted *esg;35.7* crossings revealed repeatedly no striking differences comparing data for both conditions (figure 50). However, for the L3-shifted sturkopf overexpression a highly significant increase in SC number was determined compared to the respective condition for the standard shift.

All in all, the data suggests that a temperature shift ensuring transgene expression during the sensitive phase of SC physiology did not alter the abundance of SCs following differential temperature shift patterns. Significant increases in SC abundance performing the L3 shift compared to the standard shift were only obtained for the control crossing *esg;Ctrl* / *w[-]* (figure 48) and for sturkopf overexpression in the *sturkopf* mutant background (figure 50).

2.5 Apoptosis-mediated regulation of SC abundance

2.5.1 Secondary cell-specific inhibition of apoptosis as possible regulator of SC number ("standard shift")

As all both cell types of the accessory gland are known to be postmitotic (Taniguchi et al. 2014), it was intriguing that the number of SCs changed depending on the abundance of sturkopf protein levels. This suggests a sturkopf-dependent regulation of SC number post eclosion and the last mitotic cycle of these cells taking place during the transition from L3 larvae to the prepupal stage. It was previously shown that the SC-specific overexpression of a constitutively active insulin receptor (InR) resulted in a highly significant increase in SC numbers (Kubo et al. 2018). However, this was only the case for the condition in which transgene expression was driven according to the L3 shift pattern. Further, a regulation of SC number via the inhibition of apoptosis was demonstrated as well (Kubo et al. 2018). Therefore, it was of great interest to investigate whether apoptosis was the underlying cellular process regulating SC number in case of modulation of sturkopf protein abundance post eclosion.

The viral apoptosis inhibitor p35 was overexpressed in a SC-specific manner using the *esg;Ctrl* and *esg;35.7* driver lines. At first p35 overexpression was tested in the *sturkopf* control background following the standard temperature shift pattern. The results are depicted in figure 51.

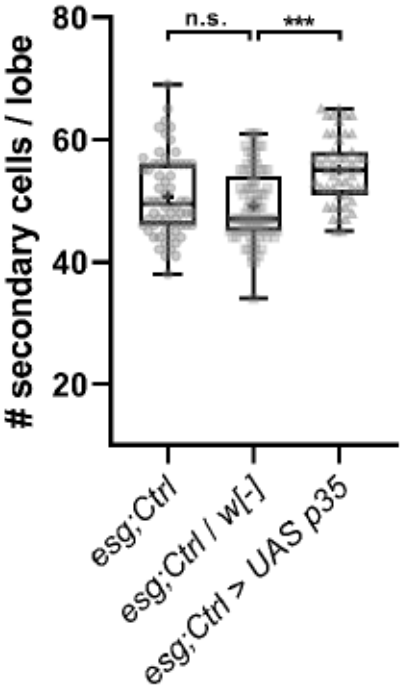

Figure 51: Quantification of SCs per lobe in mated male flies of the genotype *esg;Ctrl* (n=62 lobes) and the crossings *esg;Ctrl / w[-]* (n=89 lobes) and *esg;Ctrl > UAS p35* (n=51 lobes) based on an Abd-B antibody staining. Flies were kept on 29 °C for 7 days to ensure transgene expression and afterwards put back to the restrictive temperature of 18 °C for 3 additional days. Depicted data is based on at least three biologically independent experiments. Note that the depicted data for *esg;Ctrl* and *esg;Ctrl > w[-]* are the same as used in figure 38 as experiments were carried along at the same time. All p values were obtained by an unpaired two-sample t test with significance levels: n.s., $p \geq 0.05$, *$p < 0.05$, **$p < 0.01$, ***$p < 0.001$.

SC-specific overexpression of p35 resulted in a highly significant increase in SC numbers as compared to the respective control crossing *esg;Ctrl / w[-]*.

Of course, it was of particular interest, whether overexpression of the apoptosis inhibitor rescues the loss of SCs in the *sturkopf* null mutant background. This question was addressed by p35 overexpression using the *esg;35.7* driver line to test for a SC rescue.

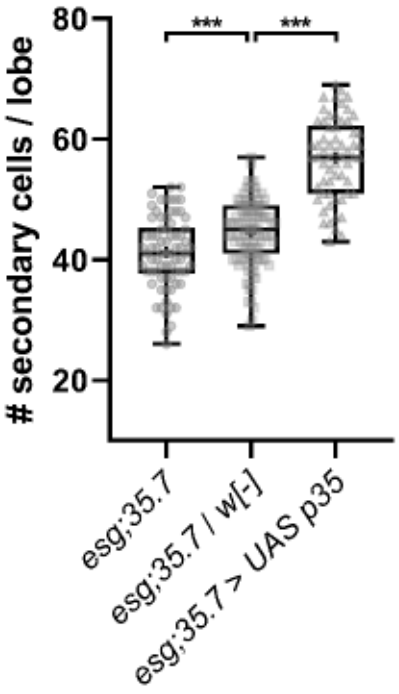

Figure 52: Quantification of SCs per lobe in mated male flies of the genotype *esg;35.7* (n=74 lobes) and the crossings *esg;35.7 / w[-]* (n=11 lobes) and *esg;35.7 > UAS p35* (n=62 lobes) based on an Abd-B antibody staining. Flies were kept on 29 °C for 7 days to ensure transgene expression and afterwards put back to the restrictive temperature of 18 °C for 3 additional days. Depicted data is based on at least three biologically independent experiments. Note that the depicted data for *esg;35.7* and *esg;35.7 > w[-]* are the same as used in figure 41 as experiments were carried along at the same time. All p values were obtained by an unpaired two-sample t test with significance levels: n.s., $p \geq 0.05$, *$p < 0.05$, **$p < 0.01$, ***$p < 0.001$.

SC-specific overexpression of p35 in the *sturkopf* mutant background resulted likewise in a highly significant increase in SC number compared to the control crossing *esg;35.7 / w[-]*. The p35-mediated rescue of SC loss which is comprehendible comparing the homozygous *sturkopf* mutant line *esg;35.7* and the control crossing *esg;35.7 / w[-]*, exceeded the number of SCs compared to both the homozygous *sturkopf* mutant line as well as the control crossing. For comparative purposes, SC-specific p35 overexpression in both the *sturkopf* control and mutant background was additionally plotted (figure 53).

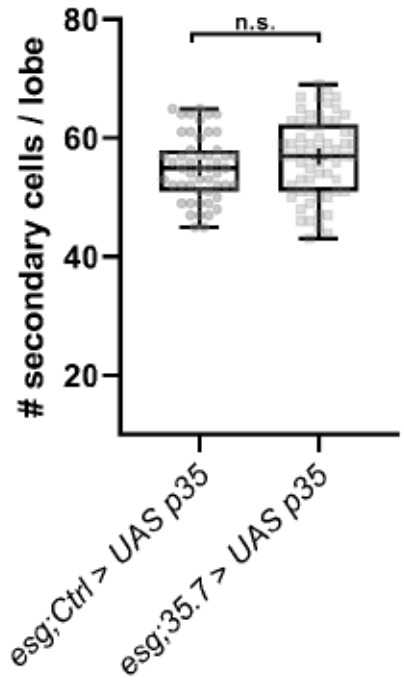

Figure 53: Comparison of SCs per lobe in mated male flies of the crossings *esg;Ctrl > UAS p35* (n=51 lobes) and *esg;35.7 > UAS p35* (n=62 lobes) based on an Abd-B antibody staining. Flies were kept on 29 °C for 7 days to ensure transgene expression and afterwards put back to the restrictive temperature of 18 °C for 3 additional days. Depicted data is based on at least three biologically independent experiments. Note that the depicted data are the same as used in figures 50 and 51 and only plotted for comparison purposes. All p values were obtained by an unpaired two-sample t test with significance levels: n.s., $p \geq 0.05$, *$p < 0.05$, **$p < 0.01$, ***$p < 0.001$.

No significant differences were found comparing SC-specific p35 overexpression in the *sturkopf* control and null mutant genetic background.

The data indicates that SC survival might be generally regulated via apoptotic processes which influence the abundance of secondary cells in the adult AG which is in line with previous findings (Kubo et al. 2018). Furthermore, the data suggests that loss of SCs in the *sturkopf* mutant background might occur due to differentially regulated apoptotic processes.

2.5.2 Secondary cell-specific inhibition of apoptosis during the sensitive phase of SC physiology as possible regulator of SC number (“L3 shift”)

Overexpression of p35 was also performed following the L3 temperature shift to test for potential differences in SC abundance based on earlier transgene expression

(figure 54) which was previously shown to be the case overexpressing the apoptosis inhibitor DIAP1 (Kubo et al. 2018).

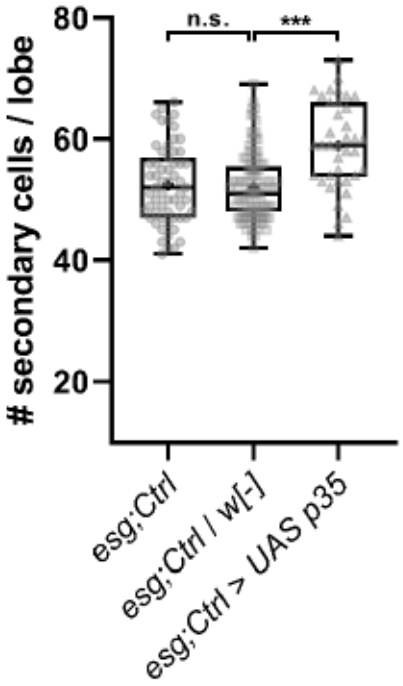

Figure 54: Quantification of SCs per lobe in mated male flies of the genotype *esg;Ctrl* (n=60 lobes) and the crossings *esg;Ctrl / w[-]* (n=106 lobes), and *esg;Ctrl > UAS p35* (n=39 lobes) based on an Abd-B antibody staining following the L3 temperature shift pattern. Late L3/prepupal were put on 29 °C and kept on this temperature for 7 days post eclosion to ensure transgene expression and afterwards put back to the restrictive temperature of 18 °C for 3 additional days. Depicted data is based on at least three biologically independent experiments. Note that the depicted data for *esg;Ctrl* and *esg;Ctrl > w[-]* are the same as used in figure 47 as experiments were carried along at the same time. All p values were obtained by an unpaired two-sample t test with significance levels: n.s., $p \geq 0.05$, *$p < 0.05$, **$p < 0.01$, ***$p < 0.001$.

Driving SC-specific p35 overexpression during the sensitive phase of SC physiology resulted in a highly significant increase in SC number in the *sturkopf* control background compared to the control crossing *esg;Ctrl / w[-]* in a similar manner as already observed for the standard shift (compare figures 51 and 54).

This early transgene expression was also performed in the *sturkopf* null mutant genetic background using the *esg;35.7* driver line (figure 55).

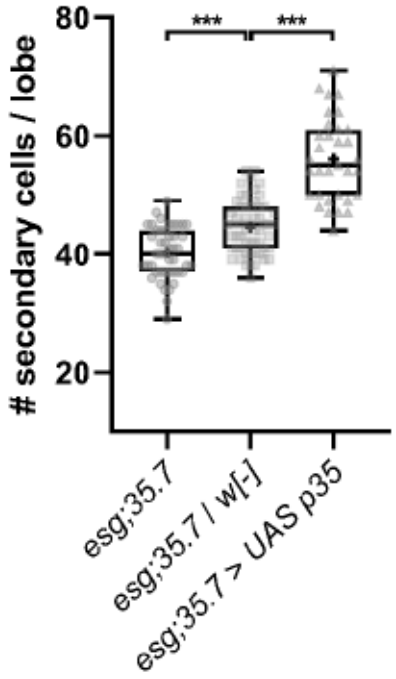

Figure 55: Quantification of SC number per lobe in mated male flies using the *sturkopf* null mutant driver line *esg;35.7* (n= 47 lobes), the control crossings *esg;35.7 / w[-]* (n= 58 lobes) and *esg;35.7 > UAS p35* (n= 34 lobes) based on an Abd-B antibody staining following the L3 temperature shift pattern. Late L3/prepupal were put on 29 °C and kept on this temperature for 7 days post eclosion to ensure transgene expression and afterwards put back to the restrictive temperature of 18 °C for 3 additional days. Depicted data is based on at least three biologically independent experiments. Note that the depicted data for *esg;Ctrl*, *esg;Ctrl > w[-]*, *esg;35.7*, *esg;35.7 > w[-]* are the same as used in figure 49 as experiments were carried along at the same time. All p values were obtained by an unpaired two-sample t test with significance levels: n.s., $p \geq 0.05$, *$p < 0.05$, **$p < 0.01$, ***$p < 0.001$.

Performing SC-specific p35 overexpression in the *sturkopf* mutant background led to a highly significant increase in SC number outrunning SC numbers compared to both homozygous *sturkopf* mutant line as well as the corresponding control crossing *esg;35.7 /w[-]* which is only heterozygous *sturkopf* mutant. Again, SC-specific p35 overexpression performing the L3 temperature shift in both the *sturkopf* control and null mutant background was visualized for comparative purposes (figure 56).

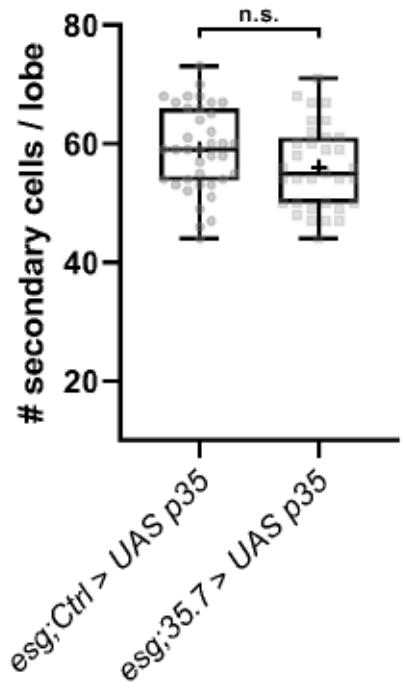

Figure 56: Comparison of SCs per lobe in mated male flies of the crossings *esg;Ctrl* > *UAS p35* (n=39 lobes), and *esg;35.7* > *UAS p35* (n=34 lobes) based on an Abd-B antibody staining following the L3 temperature shift pattern. Late L3/prepupal were put on 29 °C and kept on this temperature for 7 days post eclosion to ensure transgene expression and afterwards put back to the restrictive temperature of 18 °C for 3 additional days. Depicted data is based on at least three biologically independent experiments. Note that the depicted data are the same data used in figures 54 and 55 as experiments were carried along at the same time. All p values were obtained by an unpaired two-sample t test with significance levels: n.s., $p \geq 0.05$, *$p < 0.05$, **$p < 0.01$, ***$p < 0.001$.

Just as for the SC-specific p35 overexpression following the standard shift, no significant differences were observed comparing p35 overexpression, both, in the *sturkopf* control and mutant background. However, as these findings did not imply that there are no differences performing the two different temperature shifts, datasets for both the standard shift and the L3 shift were plotted together to test for potential differences mediated by the differential transgene expression timepoints.

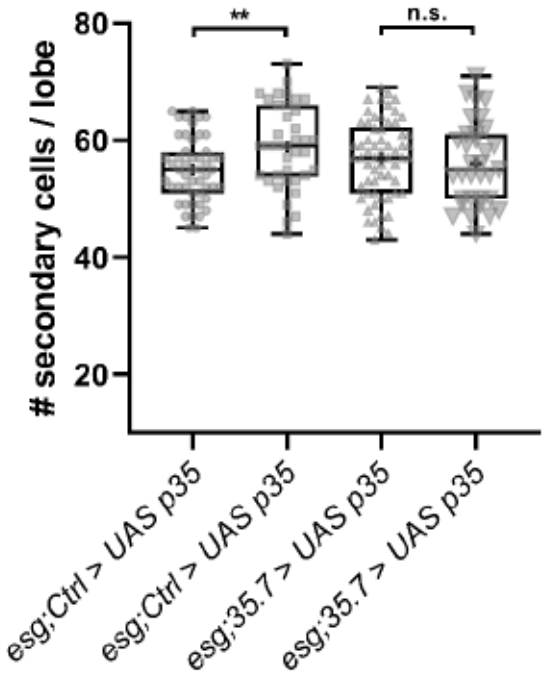

Figure 57: Comparison of quantified SCs per lobe of both standard and L3-shifted mated male flies of the crossing *esg;Ctrl* > *UAS p35* (standard shift: n=51 lobes; L3 shift: n=39 lobes) and *esg;35.7* > *UAS p35* (standard shift: n=62 lobes; L3 shift: n=34 lobes) based on an Abd-B antibody staining. Note that the depicted graph is merged from the data presented in figures 51, 52, 54 and 55. Depicted data is based on at least three biologically independent experiments. All p values were obtained by an unpaired two-sample t test with significance levels: n.s., $p \geq 0.05$, *$p < 0.05$, **$p < 0.01$, ***$p < 0.001$.

Comparing SC-specific p35 overexpression for both temperature shifts revealed a moderately significant increase in SC number overexpressing p35 in the *sturkopf* control background performing the L3 shift while no differences in the *sturkopf* mutant background were obtained (figure 57). These data suggest that a temperature shift timepoint-dependent p35 overexpression leads to higher abundance of SCs in presence of two functional sturkopf alleles, while only one sturkopf allele is not sufficient to alter SC abundance in a p35 overexpression setting.

2.6 Sturkopf and LDAH can be linked to the ubiquitination processes demonstrated for PCa

Sturkopf affects a variety of endocrine processes such as insulin and juvenile hormone signaling. Moreover, it may also affect ecdysone signaling (Werthebach et al. 2019). The EcR is a crucial factor for AG development and physiology and was shown to influence SC physiology in a 20HE-dependent and -independent manner. Beyond that, EcR signaling was hypothesized and in partially shown to share mechanistical parallels between the demonstrated physiological signaling switch

(Leiblich et al. 2019) and pathophysiological signaling switch of the androgen receptor (AR) well-known in PCa (Navarro et al. 2002). The dysregulation of the AR is a key factor in the promotion and progression of PCa (Navarro et al. 2002; Heinlein and Chang 2004; Culig and Santer 2014). Posttranslational modification, such as ubiquitination among others, contribute to PCa directly and indirectly via differential regulation of the AR (e.g., reviewed in (Li et al. 2014a). For instance, three lysine residues of the AR are known to be ubiquitinated by a variety of E3 ubiquitin ligases resulting in different E3 ligase-dependent outcomes for the receptor. The two C-terminal lysine residues K845 and K847 get ubiquitinated by RNF6, SIAH, SKP2, MDM, and CHIP (Li et al. 2014a) with ubiquitination by SKP2, MDM and CHIP resulting in proteasomal degradation of the AR, while RNF6- and SIAH2-mediated ubiquitination enhances the AR transcriptional activity (Li et al. 2014a). Moreover, one N-terminal lysine residue (K311) was recently identified to be ubiquitinated by SKP2 which was shown to be critical for AR protein stability and transcriptional activity (McClurg et al. 2017). Additional factors contributing to AR signaling regulation and AR stability such as the Canopy FGF signaling regulator 2 (CNPY2) were recently identified (Ito et al. 2018b). CNPY2 inhibits the ubiquitination of the AR through the E3 ubiquitin ligase myosin regulatory light chain interacting protein (MYLIP) via interaction with the E2 ubiquitin-conjugating enzyme UBE2D1 in prostate cancer cells (Ito et al. 2018b). As LDAH was recently shown to affect protein stability (Goo et al. 2017), which was also hypothesized for *Drosophila* sturkopf (Werthebach et al. 2019), it was of interest to investigate whether it is possible to use *Drosophila* not only as model to recapitulate the ubiquitination cascade demonstrated for PCa cells (Ito et al. 2018b), but also to integrate sturkopf or LDAH in this respect since LDAH was previously associated with PCa initiation, progression and invasiveness (Currall et al. 2018).

The *Drosophila* homologs of CNPY2, UBE2D1, and MYLIP namely seele, CG10862, and defense repressor 1 (dnr1) were tested for conserved inter- and intraspecies protein interactions. Sturkopf and human LDAH were also included utilizing the luciferase-fragment complementation assay (Kolkhof et al. 2017). Furthermore, *Drosophila* orthologs of several E3 ubiquitin ligases known to ubiquitinate the AR as well as the nuclear receptor proteins EcR and ERR as potential AR orthologs were part of this protein-protein interaction study. A visualization of the interactome

network is depicted in figures 58 and data for selected interactions in plotted in figure 59, respectively.

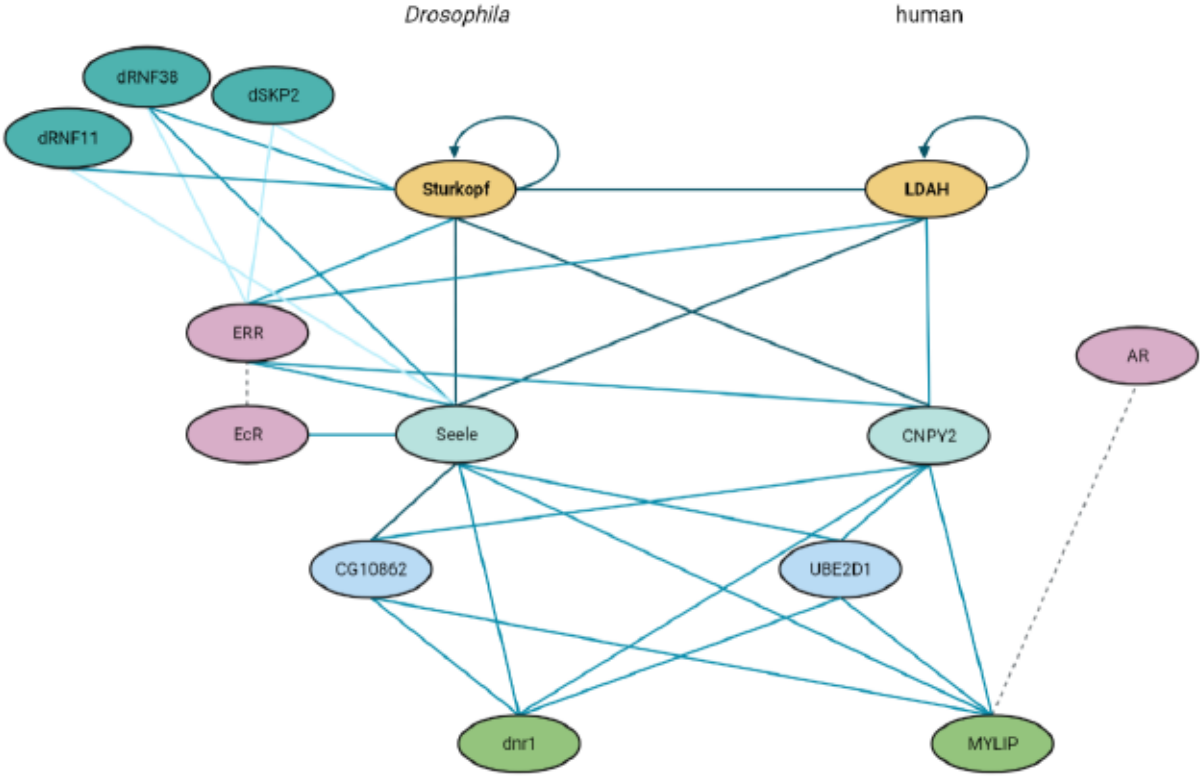

Figure 58: Representation of a conserved interactome of *Drosophila* proteins and the human counterparts of a ubiquitination cascade demonstrated in PCa. Continuous lines represent experimentally assessed interactions identified using the split luciferase complementation assay, dotted lines show interactions which were identified by others (Kovalenko et al. 2019; Ito et al. 2018b). Dark blue lines represent strong interactions, medium blue lines are showing interactions categorized as significant and light blue lines show weak interactions.

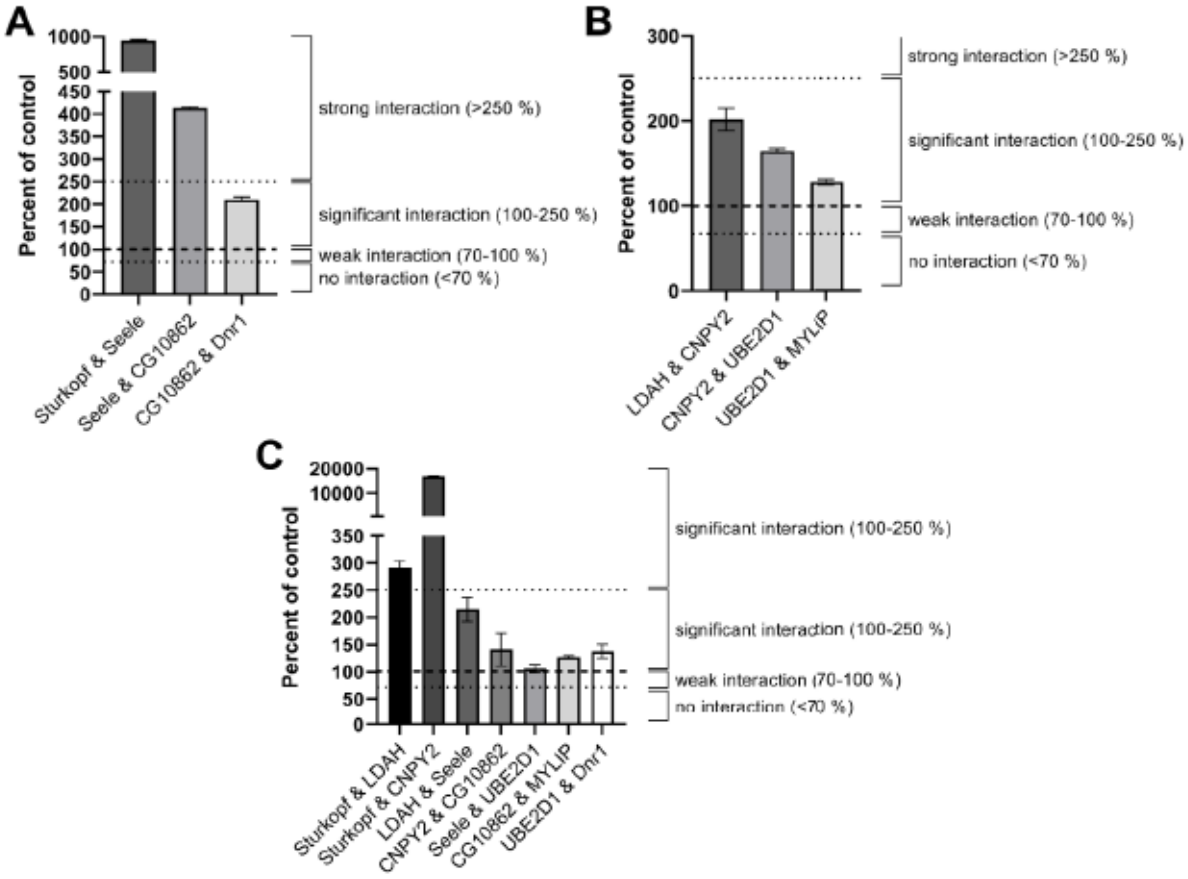

Figure 59: Selected protein-protein-interaction data of the interactome network presented in figure 58. (**A**) Conservation of protein-protein interactions in *Drosophila* of a ubiquitination cascade demonstrated in PCa (Ito et al. 2018b). (**B**) Recapitulation of the human protein-protein interactions demonstrated in PCa cells (Ito et al. 2018b). (**C**) Protein-protein interaction data to test for interspecies interaction conservation of the selected proteins shown in (A) and (B). Data was normalized to the known zipper-zipper interaction (Kolkhof et al. 2017) and thresholds for the determination of interactions were set accordingly (Kolkhof et al. 2017).

Significant protein-protein interactions between the human candidate proteins CNPY2, UBE2D1 and MYLIP as demonstrated by Ito and colleagues were identified using the split luciferase complementation assay (Ito et al. 2018b) (figures 58 and 59B). It was further possible to recapitulate this previously published interaction network using the *Drosophila* orthologs seele, CG10862, as well as dnr1 (figures 58 and 59A). Interactions were not only tested for intraspecies protein-protein interactions but also in an interspecies-dependent manner. The interspecies conservation between tested *Drosophila* and human proteins was identified when tested for interaction (figures 58 and 59C). Sturkopf and LDAH were also included in this respect due to the evidence that human LDAH was associated with the occurrence and progression of prostate cancer (Currall et al. 2018). Both, sturkopf and LDAH, are known to be linked to the ubiquitination machinery (Kolkhof et al.

2017; Goo et al. 2017). Both very strongly interacted with seele and/or CNPY2, which may point towards a role of sturkopf/LDAH in the tested interaction cascade. EcR and ERR were also included as potential orthologs of the AR (figure 58). Especially for ERR, an interaction network comprising sturkopf, seele, as well as LDAH and CNPY2 could be identified. The EcR was only identified to interact with seele within the scope of this protein-protein interaction study. Additionally, the *Drosophila* E3 ubiquitin ligases dSKP2, dRNF11 and dRNF38 which are orthologs of the human SKP2 and eventually RNF6 E3 ubiquitin ligases known to ubiquitinate the AR (Li et al. 2014b; Xu et al. 2009) were included. For these E3 ubiquitin ligases, interactions with sturkopf, seele, and ERR were identified within the presented interactome model.

All in all, the presented interactome model revealed intra- and interspecies conservation of the interaction network previously demonstrated in PCa cells (Ito et al. 2018b). Furthermore, the inclusion of sturkopf or LDAH within this network revealed strong interactions of both sturkopf and LDAH with the main component seele/CNPY2 as well as the nuclear receptor ERR and different E3 ubiquitin ligases. These results pave a path to evaluate a potential role of sturkopf or LDAH regarding ubiquitination processes and in PCa progression and/or initiation.

3 Discussion

Lipid droplets (LDs) have recently gained recognition as highly diverse and dynamic organelles. They have a unique structure comprising a hydrophobic core of neutral lipids which is enveloped by a phospholipid monolayer with proteins attached (Beller et al. 2006; Henne et al. 2018; Olzmann and Carvalho 2019). LDs are in charge of regulating storage and remobilization of neutral lipids on a cellular level (Farese and Walther 2009; Thiam and Beller 2017).

Besides playing a major role in lipid metabolism and energy homeostasis, LDs serve various other functions. They function as a reservoir for metabolic building blocks (Welte and Gould 2017), contribute to ER protein homeostasis (Welte and Gould 2017), and are involved in degradation or act as sequestration sites for proteins or lipids (Welte and Gould 2017). The LD-associated proteins (LDAPs) are key to LD functionality and diversity. While some LDAPs such as proteins of the perilipin-protein family (Greenberg et al. 1991; Londos et al. 1999; Brasaemle et al. 2009; Najt et al. 2022) have are well characterized and associated with lipid metabolism, other proteins and their functions are less known in this matters. Apart from lipid metabolism, some LDAPs were found to play important roles in diverse fundamental biological processes affecting organismal physiology profoundly (Werthebach et al. 2019; Currall et al. 2018). Thus, it is not surprising that a variety of pathophysiological conditions including various types of cancer are associated with LDs in general (Petan 2020) and with the deregulation of specific LDAP functions (Currall et al. 2018).

One LDAP affecting organismal physiology rather than lipid metabolism is the *Drosophila* LDAP sturkopf (Werthebach et al. 2019). This protein belongs to a highly evolutionary conserved protein family of annotated serine hydrolases/lipases harboring a typical catalytic triad with a putative catalytically active serine (Thiel et al. 2013; Goo et al. 2014). However, several studies argue against such an enzymatic function of the protein as no clear-cut effects on lipid metabolism were identified neither for sturkopf in *Drosophila* nor for the mammalian ortholog LDAH (lipid droplet associated hydrolase) in mice (Thiel et al. 2013; Kory et al. 2017; Werthebach et al. 2019). Interestingly, mutation in the gene locus of the mammalian homolog *LDAH* (*lipid droplet associated hydrolase*) correlate with the initiation and progression of prostate cancer (Takata et al. 2010; Innocenti et al. 2011; Lindström et al. 2012; Long

et al. 2012; Wang et al. 2013; Shui et al. 2014; Penney et al. 2015; Du et al. 2016; Currall et al. 2018). To date, the molecular mechanism of how loss of this LDAP is involved in prostate carcinogenesis is, however, not understood. Within the scope of this work, the *Drosophila* LDAH homolog sturkopf was, hence, studied to identify a potential molecular mechanism of how loss of *sturkopf* affects proliferation and endocrine physiology. The aim was to contribute to a better understanding of how loss of mammalian *LDAH* promotes prostate carcinogenesis. Various *in vitro* and *in vivo* approaches were applied to unravel the unclear role of this LDAP in tumorigenic processes. The work further illustrates how the *Drosophila* accessory gland and sturkopf can be used as means to model the role of human LDAH in the initiation and promotion of prostate carcinogenesis.

3.1 The *Drosophila* accessory gland as a model tissue to study prostate cancer-relevant aspects

Prostate cancer (PCa) is the second most frequent neoplastic malignancy affecting older men primarily and is the fifth leading cause for cancer-related deaths (Smith et al. 2000; Luining et al. 2022). Like many types of cancer, it is characterized by an uncontrolled growth of prostate cells, ultimately leading to pain or other symptoms affecting physiological processes such as urination or ejaculation (Rebello et al. 2021). Androgen signaling through the androgen receptor (AR) is known to be one of the key factors both for the normal prostate physiology as well as for prostate cancer. In early-stage PCa hormone-deprivation therapy is the therapeutic method of choice (Huggins and Hodges 1972) as emerging PCa depends on androgen signaling for its growth and metastatic capacity (Culig and Santer 2014). Over time, PCa cells acquire hormone-independence resulting in castration-resistant prostate cancer (CRPC) (Crowley et al. 2021). As manifestations in the initial phase of prostate carcinogenesis are likely asymptomatic, the disease often gets detected in late stages. More than 95 % of PCa are of epithelial origin, characterized as adenocarcinomas by definition, while less than 2 % of PCa derive from neuroendocrine cells of the prostate (Grignon 2004). The evolution of prostate cancer is marked by its initiation, promotion, and progression. The initiation is likely characterized by loss-of-function mutation in tumor suppressor genes of one cell, laying the foundation for carcinogenesis. Normally, a mutation cannot be repaired as it is possible for DNA damage caused by both endogenous and exogenous noxae

such as ionizing radiation or the exposure to chemicals (Saini 2015). The only way for the cell to abolish of the mutation is to undergo apoptosis, the programmed cell death (Ulukaya et al. 2011). The mutation in a tumor suppressor gene, such as *p53* or *PTEN*, results in excessive proliferation of the affected cell which is one of the most distinguishing features of cancer cells (Hanahan and Weinberg 2000). Genomic studies revealed more than 2000 genetic alterations for primary PCa and more than 9000 alterations for CRPC, illustrating the genetic heterogeneity of PCa (van Dessel et al. 2019). The most frequent genetic alterations of PCa include loss of function of different tumor suppressors such as *NKX3.1* (Bethel et al. 2006) or *PTEN* (Yue et al. 2014; Jamaspishvili et al. 2018), as well as gene fusions such as ETS-related gene *ERG* and serine protease *TMPRSS2* (TMPRSS2-ERG) being the most frequent fusion in PCa (Fang et al. 2022). Besides genetic factors characterizing the nature of the tumor, other factors including the tumor microenvironment as well as the immune system are key factors determining the diversity of PCa (Rambur et al. 2021). as well as these factors have significant impact on therapy success (Rambur et al. 2021). It is, therefore, of utmost importance to use suitable model systems to study different aspects of PCa accurately.

The existing model systems to study prostate cancer include different 2-D PCa cell lines, 3-D PCa organoids/spheroids and several mouse models including xenografts as well as genetic mouse models (Wilson et al. 2017; Rambur et al. 2021). These models have advantages and disadvantages depending on the research focus. While 2-D cell culture is routinely used to gain insight into functional and mechanistic processes, these models are unable to reproduce the entirety and complexity of the tumor (Rambur et al. 2021). Furthermore, cell lines are mainly derived from metastatic lesions, making them inappropriate measures to study early steps of prostate carcinogenesis (Rambur et al. 2021). 3-D cell culture models such as organoids and spheroids, in turn, represent cell culture models which are closer to the native tumor because of a (partial) conservation of tumor heterogeneity, cell morphology as well as cell-cell and cell-matrix interactions (Rambur et al. 2021). However, these 3-D cell models are not fully established PCa models and the usage of highly aggressive cell lines complicate the study of early steps of PCa (Rambur et al. 2021). *In vivo* mouse models represent a tool to study the complexity of prostatic tumors which take factors such as the tumor microenvironment, its heterogeneity, an intact immune system, and a functional interaction of the tissue with other organs

within a complex organism into account (Wilson et al. 2017; Rambur et al. 2021). However, disadvantages become obvious when taking the time-consuming process to develop a tumor, the differential organization of the mouse prostate, and genetic redundancies between humans and mice which complicate signaling pathway analysis into consideration (Wilson et al. 2017; Rambur et al. 2021).

For several decades, *Drosophila* has been used extensively to study various human diseases including different types of cancer (Halder and Mills 2011; Mirzoyan et al. 2019). More recently, the accessory gland of the fruit fly is used as model tissue for the study of aspects regarding prostate cancer (Ito et al. 2014). Since then, this organ became a widely accepted model to study different aspects of the human prostate and prostate cancer (Ito et al. 2014; Wilson et al. 2017; Leiblich et al. 2019; Rambur et al. 2020; Rambur et al. 2021). It is not only the functional analog of the human prostate contributing factors to the seminal fluid and to mating success (Gligorov et al. 2013; Sitnik et al. 2016), but is also entirely comprised of epithelial cells which are the known cellular origin of the majority of PCa (Grignon 2004). The gland consists of two dead-end lobes which are comprised of two binucleate and postmitotic cell types, i.e., the highly abundant main cells (MCs) comprising roughly 95 % of the entire gland, and the much less frequent secondary cells (SCs) with a proportion of only 5 % of the tissue (Bertram et al. 1992). The prostate, in contrast, comprises three different cell types (Long et al. 2005). Basal and luminal cells are the most abundant cells in the prostate, whereas neuroendocrine cells occur to a much smaller extent (Long et al. 2005). However, the lower cellular diversity of the accessory gland limits modelling the complexity of, both, the prostate and its microenvironment (Rambur et al. 2021), but represents a simplified model with few genetic redundancies to investigate generalized processes and mechanisms of epithelial carcinogenesis such as basal extrusion, on the other hand (Rambur et al. 2020).

Secondary cells have been particularly used to study prostate cancer-relevant aspects. For instance, they have been used as platform to perform a genetic screen with regulators of prostate cancer progression (Ito et al. 2014). Within this screen, three genes were identified which promoted SC growth and migration namely *seele*, *MrgBP* (*MRG/MORF4L binding protein*), and *Semp-1* (*seminal metalloprotease-1*) (Ito et al. 2014). For the human orthologs of these identified genes (*Canopy FGF signaling regulator 2* [*CNPY2*], *MRG domain binding protein* [*MRGBP*], and *Meprin A*

subunit α [*MEP1A*]), there is evidence showing an involvement in the initiation and/or progression of other cancers such as colorectal cancer (Rösmann et al. 2002; Yamaguchi et al. 2011) and glioma (Bornhauser and Lindholm 2005). These genes also promote invasion capacity in the 22Rv1 prostate cancer cell line (Ito et al. 2014), indicating that the SC of the AG can be used as a means to study AR signaling-independent aspects of PCa because androgen signaling through the androgen receptor is not present in *Drosophila* (Rambur et al. 2021).

SCs are filled with granules for the secretion of different factors into the seminal fluid via exosomes or regular excretion (Wilson et al. 2017). SC migration through the accessory gland is enhanced due to mating of the flies (Leiblich et al. 2012; Leiblich et al. 2019). Both, exosomes and migration have profound roles implicated in cancer biology (Dai et al. 2020; Liu et al. 2021; Friedl and Wolf 2003; Wu et al. 2021), thus offering the opportunity to use the accessory gland to study basal, however potentially conserved mechanisms of these processes. Growth or endoreplication of SCs was also observed in previous studies (Leiblich et al. 2012; Leiblich et al. 2019). Endoreplication is also a very common phenomenon of cancer cells (Zhang et al. 2022). In the SCs of the accessory gland, growth is dependent on the steroid hormone ecdysone in virgin male flies which switches to hormone-independent steroid receptor–mediated growth upon mating (Leiblich et al. 2019), suggesting mechanistic parallels between this physiological signaling switch and altered pathological signaling as it is known for CRPC (Leiblich et al. 2019). However, as signaling in the accessory gland of *Drosophila* is mediated through ecdysone and its corresponding receptor (EcR), and signaling in the human prostate, in turn, is dependent on testosterone and the androgen receptor (AR), studies regarding PCa mechanisms involving AR-signaling still appear difficult (Rambur et al. 2021).

All in all, the AGs of *Drosophila* represent suitable model to study certain aspects of prostate carcinogenesis. Its use as easily accessible, simplified *in vivo* model has the opportunity to study conserved fundamental processes including general steps of epithelial carcinogenesis or exosome biology (Rambur et al. 2021; Wilson et al. 2017). Recent research proved a causal association between the loss of the LDAP *LDAH* (lipid droplet associated hydrolase) and the initiation and progression of prostate cancer (Currall et al. 2018). Moreover, the *Drosophila* LDAH ortholog

sturkopf is prominently expressed in the AG and influences a variety of processes regulating organismal endocrine physiology (Werthebach et al. 2019).

As deregulation of endocrine signaling is a hallmark of prostate cancer (Heinlein and Chang 2004; Culig and Santer 2014; Michaud et al. 2015; Dai et al. 2017) the AG of *Drosophila* represents a suitable model system to study sturkopf-mediated effects of prostate cancer-relevant aspects such as a deregulation of ecdysone signaling. Ecdysone is known to mediate a variety of signaling processes which are essential for proper accessory gland development and function (Sharma et al. 2017). As stated earlier, it is not possible to homologize ecdysone signaling through the associated EcR and androgen signaling through the AR (Rambur et al. 2021). However, it is assumed that the regulation of both signaling pathways underlie at least partially conserved mechanisms (Leiblich et al. 2019). As an impairment of ecdysone signaling was hypothesized for *sturkopf* LOF animals (Werthebach et al. 2019), the accessory gland is an interesting model tissue to investigate effects of such deregulation mediated by *sturkopf* loss of function.

3.2 The role of sturkopf in cell proliferation

Genome-wide association studies have identified several prostate cancer risk-associated single-nucleotide polymorphisms (SNPs) in the gene locus of the human *sturkopf* orthologous gene, *C2orf43* (Takata et al. 2010; Innocenti et al. 2011; Lindström et al. 2012; Long et al. 2012; Wang et al. 2013; Shui et al. 2014; Penney et al. 2015; Du et al. 2016). However, these associations were first put into causal context in 2018, when Benjamin Currall and colleagues presented an early-onset prostate cancer patient with a *de novo*, germline, balanced chromosomal translocation in the *LDAH* gene (Currall et al. 2018). In this study, LDAH was also studied using different *in vitro* and *in vivo* approaches regarding its role in proliferation, migration and invasion capacity in prostate carcinogenesis (Currall et al. 2018). Changes in the aforementioned processes were analyzed by performing transient *LDAH* knockdown in RWPE-1 cells and LDAH overexpression in PC3 cells. The RWPE-1 cell line is a non-tumorigenic prostate cell line with a high endogenous LDAH expression, while the highly tumorigenic line PC3, in contrast, exhibits lower endogenous LDAH expression (Currall et al. 2018). While knockdown of *LDAH* was shown to highly increase proliferation of RWPE-1 cells, migration and invasion capacity was unaffected (Currall et al. 2018). On the contrary, overexpression of

LDAH in the PCa cell line PC3 resulted in the opposite effect as proliferation was significantly decreased in these cells (Currall et al. 2018). Furthermore, cell migration as well as invasion was significantly reduced upon LDAH overexpression (Currall et al. 2018) which are aspects usually characterizing this prostate cancer cell line (Zi et al. 2005; Tai et al. 2011; Raja Singh et al. 2017).

Analogous experiments regarding proliferation in *Drosophila* S2R+ cells using the *Drosophila* LDAH ortholog sturkopf revealed an impact of altered sturkopf protein levels on cell proliferation likewise (figures 7 and 8). Upon overexpression of wild type sturkopf in S2R+ cells, a significant decrease in cell proliferation was obtained which is in line with the overexpression of human LDAH in PC3 cells (Currall et al. 2018). Heterologously expressed human LDAH was unable to induce changes in proliferation behavior when overexpressed in *Drosophila* S2R+ cells. The overexpression of the sturkopf(S119A) truncation construct in which the hypothetical catalytic serine is mutated (Thiel et al. 2013) did not result in any significant changes regarding proliferation. The changes in proliferation observed for wild type sturkopf overexpression and also likely for human LDAH overexpression in prostate (cancer) cell lines (Currall et al. 2018) can, thus, be traced back to the putative enzymatic function of the proteins as the amino acid exchange S119A abolishes the increase in proliferation. The inclusion of the sturkopf(16K2R) construct in which all 16 lysines were mutated to arginines, 9 of which are located in the C-terminus (Kolkhof et al. 2017), revealed a significant increase in proliferation of the S2R+ cells. The C-terminus of sturkopf is of importance for the protein function as sturkopf overexpression was shown to induce a LD clustering phenotype (Thiel et al. 2013). At least two lysine residues (K271 and K280) located in the C-terminus of the protein can get ubiquitinated (Kolkhof et al. 2017). However, an amino acid exchange of these two lysine residues to arginines (K271R and K280R) is unable to abolish the LD clustering (Werthebach 2019). The amino acid exchange of all sturkopf lysine residues to arginines (16K2R) abolishes this clustering phenotype (Kolkhof et al. 2017; Werthebach 2019). This suggests that further lysine residues of the protein on top of the two residues K271 and K280 must be ubiquitinated, on the one hand, and that the C-terminal lysine residues are required for the induction of LD clustering, on the other hand, which is likely mediated through homo-dimerization of sturkopf (Kolkhof et al. 2017; Werthebach 2019). Considering the fact that the protein was presumably unable to be ubiquitinated (Kolkhof et al. 2017) the data obtained for

sturkopf(16K2R) regarding proliferation was particularly intriguing as this finding resembles the proliferation behavior observed in human cell culture upon *LDAH* knockdown (Currall et al. 2018). Hence, the mediated effects on proliferation might be dependent on a synergistic effect of the putative enzymatic function, the C-terminus of sturkopf as well as ubiquitination processes. Similarly, the C-terminus of mammalian LDAH was shown to be required for ubiquitination-dependent protein stability regulation of the major triacylglycerol lipase ATGL. In terms of proliferation, a similar sturkopf/LDAH-mediated stability regulation of an yet unknown target protein could have resulted in the observed proliferation decrease upon sturkopf (figure 7) and LDAH overexpression (Currall et al. 2018). Overexpression of sturkopf(S119A) did not alter the proliferation behavior of the cells, yet harboring a functional C-terminus (Thiel et al. 2013) arguing against a role of a functional C-terminus in proliferation. However, with regard to the LD clustering phenotype observed for sturkopf overexpression (Thiel et al. 2013), the point mutation of the putative catalytic serine S119 was demonstrated to counter-balance induction of LD clustering (Thiel et al. 2013). Consequently, the putative catalytic serine at position 119 and the C-terminus act in an antagonistic manner pertaining to LD clustering. This might also serve as an explanation for the inability of the sturkopf(S119A) construct to induce proliferation changes suggesting a synergistic effect mediated through both the still unknown enzymatic function of sturkopf and a fully functional C-terminus. To test this hypothesis, a double mutant construct both harboring the mutation in the putative catalytical serine at aa119 as well as the 16K2R modification could be generated to analyze whether this combination has a differential influence towards proliferation. It is noteworthy, that the described decrease in proliferation upon sturkopf overexpression could also be the result of increased cell death events as crystal violet experiments only assay cell presence. This possibility applies also to the analogous experiments in human cell culture (Currall et al. 2018) and should be addressed in future studies.

Interestingly, the proliferation behavior changed completely in response to OA loading of the cells (figures 9 and 10). The induction of LDs and, thus, the translocation of sturkopf on LDs (Thiel et al. 2013; Goo et al. 2017) resulted in a significant increase in cell proliferation upon wild type sturkopf overexpression, whereas all other tested constructs did not show any difference in proliferation behavior. These results suggest that sturkopf has different modes of action regarding

proliferation depending on its localization. While mostly located in the endoplasmic reticulum as it is probably the case for the data presented in figure 7, sturkopf overexpression suppressed proliferation of the cells. However, relocation of sturkopf onto LDs increased proliferation (figure 9) indicating that the observed suppression of proliferation upon sturkopf overexpression is regulated when localized in the ER, while sturkopf overexpression enhances proliferation upon lipid loading of the cells and translocation of sturkopf onto lipid droplets consequently (figure 9). However, for the overexpression of sturkopf(16K2R) it was expected to also promote proliferation of OA-treated cells similar to the untreated condition (figure 7). Assuming that the abolishment of C-terminal lysine residues is (co-)responsible for the proliferation increase as seen in figure 7, an increase in proliferation was also expected, which was, however, not the case. Overexpression of sturkopf(S119A) in OA-treated cells did not alter the proliferation behavior. Again, this finding points towards an important role of the hypothetical enzymatic function of sturkopf regarding proliferation. Alternatively, an antagonistic effect of the enzymatic core of sturkopf and its C-terminus (Thiel et al. 2013) is also here conceivable.

Certainly, it would also be of interest to investigate whether a *sturkopf* knockdown in S2R+ cells result in increased cell proliferation under basal conditions demonstrated for *LDAH* knockdown before (Currall et al. 2018). As the heterologous human LDAH overexpression did not alter the proliferation behavior of the cells in both tested conditions (figures 7 and 9), it could be supposed that human LDAH is not able to phenocopy the effects on proliferation which were obvious for sturkopf overexpression. This could be due to the cellular system used. The use of S2R+ cells, which are cells derived from male *Drosophila* embryos on the verge of hatching (Yanagawa et al. 1998), might not be ideal to study human LDAH-induced proliferation changes with regards to prostate cancer as demonstrated in prostate cell lines (Currall et al. 2018). Even sturkopf overexpression using this cellular system was not ideal considering a role of sturkopf in the accessory gland as model to study prostate cancer-relevant processes. Ideally, an accessory gland-derived cell line should be utilized in this particular case to be able to recapitulate the experiments shown for LDAH overexpression/knockdown and the effects on proliferation (Currall et al. 2018). However, the purpose of these experiments was to test for a potential capacity of *Drosophila* sturkopf to alter proliferation upon protein abundance alterations. As changes in sturkopf protein levels were shown to influence

proliferation regardless of the cellular system (figures 7 and 9), it allows for studying the role of a lipid droplet-associated protein in terms of proliferation changes in the context of prostate cancer in a different cellular model system.

3.3 The impact of sturkopf on ecdysone signaling

In a study of 2019, sturkopf was characterized towards its role in organismic physiology (Werthebach et al. 2019). An involvement of sturkopf in a variety of processes affecting endocrine physiology was demonstrated (Werthebach et al. 2019). Within this study a model of sturkopf's mode of action with regards to endocrine physiology regulation was proposed (figure 60).

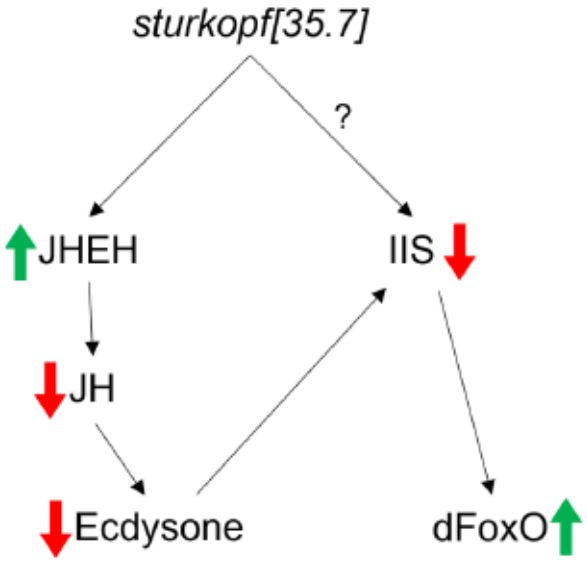

Figure 60: Hypothesized *sturkopf* LOF working model. The sturkopf mutant state JHEH activity is increased which in turns reduces JH signaling. IIS signaling is also reduced, potentially via lowered ecdysone signaling. The reduction in IIS signaling results in increased nuclear localization, and thus activity of dFoxO (modified from Werthebach et al. (2019) with permission of the journal, as it "is under the terms of Creative Commons CC-BY (CC-BY 4.0) license which permits unrestrictive use […] provided the original work is properly cited" Copyright Clearance Center, Inc.).

Without any concrete experimental evidence, it was hypothesized that ecdysone signaling might be reduced in the *sturkopf* mutant state (Werthebach et al. 2019). The putative reduction or impairment in ecdysone signaling was still to be proven. Besides juvenile hormone, ecdysone is one of the two major hormones regulating development by orchestrating developmental transitions, particularly during metamorphosis (Riddiford et al. 2000; Mirth and Shingleton 2012). It also fulfils diverse roles in adult flies (Schwedes and Carney 2012) by affecting the male

germline (Qian et al. 2014) and male courtship behavior (Ganter et al. 2011) amongst others. Furthermore, ecdysone and its associated receptor (EcR) are essential for the proper development of the accessory gland (Sharma et al. 2017; van Lommel et al. 2022). Endoreplication of SCs is dependent on the EcR and ecdysone signaling in virgin male flies (Leiblich et al. 2019). RNAi-mediated *EcR* knockdown leads to a highly significant reduction of nuclear growth in the secondary cells of the accessory gland upon (Leiblich et al. 2019). As a reduction in ecdysone signaling was proposed for *sturkopf* mutant animals, it was of interest to investigate whether the *sturkopf* LOF resulted in similar findings. Indeed, a highly significant reduction in nuclear size and, thus, of SCs was observed in *sturkopf* null mutant animals (figures 19B and 20) which might be due to lowered ecdysone signaling. Interestingly, the main cell nuclear area, which also needed to be determined for the evaluation of SC endoreplication, is significantly increased in the *sturkopf* mutant state (figure 19A). These cells are, as well as the SCs, of epithelial origin (Wilson et al. 2017; Rambur et al. 2021). While most studies focus on the SCs using the AGs as PCa model, the main cells might also be an interesting target to focus on in this specific regard. Main cells make up more than 95 % of the entire gland (Bertram et al. 1992) and the majority of prostate cancers arise from the most abundant cells in the prostate (Grignon 2004).

The alterations of endoreplication represented first tangible experimental data hinting towards perturbed ecdysone signaling in *sturkopf* mutant animals. The impairment in ecdysone signaling was further investigated via the measurement of 20-hydroxyecdysone hemolymph titers. A highly significant reduction in ecdysone hemolymph titers in *sturkopf* null mutant males could be discovered (figure 25). In female flies, however, no significant changes were observed (figure 25). Many of the phenotypes discovered in *sturkopf* mutant animals such as the early stochastic death are sex-specific and affect males more drastically than females (Werthebach et al. 2019). Taking the lowered ecdysone titers as well as the reduced endoreplication in *sturkopf* mutant males into consideration, this data partially indicate an impairment in ecdysone signaling. Further data such as the increase in trehalose levels which was exclusively found in *sturkopf* mutant males also hint towards this hypothesis (Werthebach et al. 2019). Trehalose is a nonreducing disaccharide and comprises the main sugar in insects hemolymph (Becker et al. 1996). Trehalose catabolism was shown to be regulated by ecdysone signaling in a dose-dependent manner

(Nishimura 2020; Li et al. 2020). The delay in developmental timing observed in *sturkopf* mutant animals was associated with altered JH signaling (Werthebach et al. 2019). However, it could also be an indication of perturbed ecdysone signaling which was also hypothesized (Werthebach et al. 2019). As juvenile hormone signaling and ecdysone signaling are closely interwoven during development especially (Dubrovsky 2005), further research is needed to discriminate between effects mediated by altered JH signaling and ecdysone signaling in *sturkopf* mutant animals.

The data obtained for differential expression of ecdysone target genes, however, argue against this hypothesis (figure 24). No significant differences in transcript expression of the ecdysone downstream target genes *E74A*, *E75A*, and *E75B* as well as the *EcR* were found in accessory glands *sturkopf* mutant males. However, these results require further revision due to the high standard deviation obtained assessing the gene expression data (figure 24). In contrast, the transcript expression of *juvenile hormone epoxide hydrolases* (*JHEH*) *1-3* revealed a 1.5-fold increase in *JHEH1* expression in *sturkopf* mutant accessory glands, while the expression of the other two *JHEH2* and *JHEH3* was unaffected (figure 23). JHEHs degrade juvenile hormone via hydrolysis of the functional epoxide group into diols (Ottea et al. 1987). Previously, interactions between all three JHEH and sturkopf were shown (Kolkhof et al. 2017; Werthebach et al. 2019; Guruharsha et al. 2011). Juvenile hormone regulates ecdysone synthesis (Mirth et al. 2014), providing another hint for impaired ecdysone signaling. A FACS-based isolation of SC RNA based on endogenous GFP reporter expression of genetically engineered male *Drosophila* (Immarigeon et al. 2019) may be used in future studies to analyze other target genes such as the Halloween genes, which are essential for ecdysone synthesis (Rewitz et al. 2006) and their expression in the *sturkopf* LOF background.

Ecdysone is primarily produced in the prothoracic glands (Huang et al. 2008). However, growing evidence suggest SCs as a site of ecdysone synthesis (Hentze et al. 2013; Leiblich et al. 2019) and ecdysone signaling was almost exclusively studied in SCs (Hentze et al. 2013; Sharma et al. 2017; Leiblich et al. 2019). Furthermore, a significant reduction in SCs was determined in *sturkopf* mutant males (e.g., figures 12 and 16), which will be discussed later in greater detail. It is, however, questionable in how far this reduction of SCs as potential sites of ecdysone synthesis might influence of the overall hemolymph ecdysone titers. Thus, the FACS-based isolation of SCs

(Immarigeon et al. 2019) could serve as helpful measure to study ecdysone signaling in SCs exclusively.

3.4 Sturkopf-mediated protein stability regulation

Sturkopf as well as LDAH have been assumed to regulate protein stability (Werthebach et al. 2019; Goo et al. 2017). For LDAH, an involvement in stability regulation of the major triacylglycerol lipase ATGL (adipocyte triglyceride lipase) (Zimmermann et al. 2004) was identified (Goo et al. 2017). Overexpression of LDAH results in an enhancement of ATGL polyubiquitination (Goo et al. 2017). This results in the proteasomal LDAH-mediated degradation of ATGL (Goo et al. 2017) via the proteasome-ubiquitin pathway consequently (Olzmann et al. 2013; Dai et al. 2013). However, ATGL is protected from proteasomal degradation when bound to LDs (Olzmann et al. 2013; Li et al. 2014c). In theory, this polyubiquitination could be traced back to a direct effect of LDAH on protein ubiquitination e.g., via a LDAH-mediated recruitment of E3 ubiquitin ligases. However, in the fruit fly sturkopf has a higher affinity to LDs than brummer (Thiel et al. 2013; Kory et al. 2015), i.e., the ATGL ortholog in *Drosophila*. Polyubiquitination of ATGL may emanate from physical properties such as competition of LD binding sites resulting in cytoplasmatic sequestration of the protein and hence its proteasomal degradation (Goo et al. 2017). However, the latter does not necessarily exclude a potential role of sturkopf/LDAH in ubiquitination processes because these results were mainly generated using overexpression constructs of sturkopf and brummer (Thiel et al. 2013; Kory et al. 2015) and not with endogenously expressed protein levels which may be more promising in identifying a putative role of sturkopf-/LDAH-mediated ubiquitination of brummer/ATGL. Furthermore, the hypothesis of protein crowding and competition of LD-binding sites would only apply to LDAPs. Sturkopf was assumed to reinforce protein stability of the JHEH enzymes as visualized in figure 60 (Werthebach et al. 2019). These enzymes do not belong to the family of LDAP. The sturkopf/LDAH-mediated regulation of protein stability might, thus, be due to an actual function of the proteins.

As mentioned before, *sturkopf* LOF was assumed (Werthebach et al. 2019) and proven by circumstantial evidence (figures 20 and 25) to impair ecdysone signaling. As ecdysone signaling functions through the binding of 20-hydroxyecdysone to its associated heterodimeric receptor, comprised of EcR and USP (ultraspiracle) (Yao et

al. 1992; Yao et al. 1993a), the impairment in ecdysone signaling due to *sturkopf* LOF may also be influenced by differentially regulated EcR protein abundance. Although transcript expression of *EcR* was not altered in accessory glands of *sturkopf* loss of function males (figure 24) this did not necessarily exclude a putative sturkopf-mediated influence on EcR protein stability. Investigating of EcR protein stability regulation aimed at monitoring protein degradation based on cycloheximide-chase experiments using S2R+ cells (figure 27) (Buchanan et al. 2016). To further test for ubiquitination-mediated proteasomal degradation of the EcR, cycloheximide-treatment was complemented using the proteasome inhibitor MG132 (Lee and Goldberg 1998). Furthermore, Pyr-41, as an inhibitor of ubiquitin-activating enzymes (E1) (Yang et al. 2007) for the inhibition of the ubiquitin-proteasome system was included. Using an antibody against common EcR isoforms, an instant isoform-specific reduction EcR-A/B1 protein signal could be observed, while EcR isoform B2 protein levels slowly reduced over the course of time (figure 27). EcR-A gets ubiquitinated and degraded via the proteasomal system (Gradilla et al. 2011). However, as no differences in the MG132- and Pyr-41-treated cells compared to the DMSO-treated control became apparent, it was impossible to draw conclusions on EcR protein stability regulation via ubiquitination of the different isoforms detected with the antibody. Originally, an increase in protein levels was expected for the MG132- and Pyr-41-treated conditions over time.

To test for differences in EcR protein levels directly, the stably transfected cells overexpressing different sturkopf variants were analyzed (figure 28). Interestingly, differences in EcR protein abundance were evident. Overexpression of wild type sturkopf, as well as sturkopf(S119A) and human LDAH increased the protein abundance of EcR A/B1. Overexpression of the sturkopf(16K2R) variant, in contrast, did not change EcR protein abundance at all. This indicates a stabilizing function of sturkopf on the EcR which might be associated with the C-terminal function of sturkopf and its capability to get ubiquitinated (Kolkhof et al. 2017). In line with the hypothesis that sturkopf(16K2R) overexpression “phenocopies” the *LDAH* knockdown in mammalian cell culture system resulting in an increase in cell proliferation (figure 7, (Currall et al. 2018)). A stabilizing role for EcR of this sturkopf variant could not be determined. As a result, this construct may function as a “dominant negative” sturkopf variant. In this case, one might expect a reduction in EcR protein abundance for this specific condition. However, these cells overexpress

sturkopf(16K2R) on top of endogenous sturkopf protein expression (FlyBase, version FB2022_05). The EcR protein expression apparent in figure 28 for sturkopf(16K2R) overexpression does not differ from EcR protein levels in the control cell line. The absence of a sturkopf(16K2R)-mediated effect could also be a result of the overexpression magnitude of this construct as it showed the weakest overexpression of all stable cell lines generated (figure 6).

Beyond that, a direct interaction of sturkopf and EcR as well as USP, as the second component of a functional EcR heterodimeric nuclear receptor, was tested (figure 26). This protein could serve as an additional indication of a *sturkopf* LOF-associated impairment in ecdysone signaling. No direct interaction between sturkopf and neither EcR, nor USP, was identified (figure 26B). Interestingly, a direct interaction between sturkopf and the estrogen-related receptor (ERR) was found in this context. This receptor is considered a potential ortholog of the human androgen receptor compared to the EcR (FlyBase, version FB2022_05). However, as stated before, the regulation of the EcR and/or USP might function indirectly through the recruitment of other components, which, in turn, directly regulate EcR protein stability.

EcR is the only steroid receptor in *Drosophila* (Koelle et al. 1991). Attempts were made to investigate parallels between EcR signaling and AR signaling (Leiblich et al. 2019). Although the EcR is not the ortholog of the human AR (FlyBase, version FB2022_05), it shares similar functions as the AR. For instance, it is responsible for proper accessory gland development (Sharma et al. 2017), which also applies to the AR in the prostate as it heavily relies on testicular androgen signaling during its development and for the maintenance of tissue integrity (Vickman et al. 2020). Thus, it is not completely impossible that stability regulation of these two nuclear receptors might be conserved. It was, for instance, shown that various lysine residues in the AR get ubiquitinated by several E3 ubiquitin ligases (Xu et al. 2009; Li et al. 2014a; Li et al. 2014b; McClurg et al. 2017; Ito et al. 2018b). The fate of the AR is dependent on which E3 ubiquitin ligase ubiquitinates which lysine residue. Ubiquitination of the C-terminal lysine residues K845 and K847 via the E3 ubiquitin ligases SKP2 (S-phase kinase-associated protein-2), CHIP (C-terminus of Hsc70-interacting protein) and MDM2 (mouse double minute 2 homolog) leads to the proteasomal degradation of the AR (Li et al. 2014a; Li et al. 2014b). In contrast, ubiquitination of the K845 and K857 lysine residues by SKP2 and SIAH2 (seven in absentia homolog 2) results in

enhanced AR transcriptional activity (Li et al. 2014a). The N-terminal K311 residue was recently shown to get ubiquitinated by SKP2 which is crucial for both AR stability and transcriptional activity (McClurg et al. 2017). Another E3 ligase, namely MYLIP/IDOL (myosin regulatory light chain interacting protein/inducible degrader of the LDL-receptor) was also identified to ubiquitinate the AR (Ito et al. 2018b). In this study, CNPY2 was shown to inhibit MYLIP-mediated AR degradation through an interaction with the E2-conjugating enzyme UBE2D1 promoting prostate cancer cell growth (Ito et al. 2018b). Moreover, an increase in CNPY2-mediated MYLIP degradation was previously identified as well (Do et al. 2012). The CNPY2 *Drosophila* ortholog seele promotes SC migration in the accessory gland (Ito et al. 2014). As ER-resident protein, seele was tested for interaction with sturkopf performing protein-protein interaction studies using the luciferase complementation assay. This assay revealed a highly significant interaction between sturkopf and seele (figure 58 and 59A). As this interaction on top of the recent causal association of LDAH and prostate cancer (Currall et al. 2018) was intriguing, the interactions within the ubiquitination cascade identified for MYLIP-mediated AR ubiquitination before (Ito et al. 2018b), were recapitulated with the human proteins (figures 58 and 59B). Furthermore, the *Drosophila* orthologs of each component were also tested in protein-protein interaction assays (figures 58 and 59A). It was possible to not only mirror the interactions needed for ubiquitination using the *Drosophila* orthologs and thus uncover a conservation of the interaction cascade as demonstrated for the human proteins (Ito et al. 2018b), but also to identify inter-species interactions between the single components which highly suggests conservation of the protein-protein-interactions tested (figures 58 and 59C). Furthermore, as a significantly strong interaction between sturkopf and seele, as well as LDAH and CNPY2 was uncovered. This could be one of the sturkopf/LDAH binding partners or recruited components which help to regulate protein stability. CNPY2 was also shown to promote proliferation, migration and angiogenesis of colorectal cancer cells via apoptosis inhibition through negative regulation of the p53 pathway (Yan et al. 2016). p53 is also known as the “guardian of the genome” and is one of the most studied tumor suppressors best known for maintaining genome integrity and preventing tumorigenesis (Lane 1992). UBE2D1 is the identified E2 ubiquitin-conjugating enzyme in the ubiquitination cascade mediating p53 proteasomal degradation (Zhou et al. 2018). Interestingly, UBE2D1 is also the E2 ubiquitin-conjugating enzyme

interacting with CNPY2 and, thus, inhibiting AR protein degradation in prostate cancer cells (Ito et al. 2018b). Thus, an involvement of CNPY2 in the regulation of p53 appears likely. Additionally, mutations in the *p53* gene are among the most frequent genetic aberrations in cancer, including prostate cancer (Wan et al. 2018). A conceivable explanation could be a sequestration or binding of CNPY2 through/to LDAH enabling e.g., MYLIP-mediated protein degradation of the AR which would be the case for prostate cancer (Ito et al. 2018b).

LDAH was assumed to exhibit cholesteryl ester hydrolase activity in murine macrophages (Goo et al. 2014). Besides another study of the LDAH yeast ortholog Ypr147cp finding similar results (Naresh Kumar et al. 2018), several other studies were unable to identify this enzymatic function for mammalian LDAH (Kory et al. 2017) as well as *Drosophila* sturkopf (Thiel et al. 2013; Werthebach et al. 2019). Within the scope of the protein-protein interactions, however, highly significant interactions were identified between sturkopf and the lipophorin receptor 1 and 2 (appendix, figure 61). These receptors are the orthologs of human (V)LDLR ([very] low density lipoprotein receptor) which are cholesterol receptors (Jeon and Blacklow 2005). MYLIP and CNPY2 also play demonstrated roles in cholesterol metabolism. MYLIP is also known as inducible degrader of LDL receptor (IDOL) and was shown to be induced by the sterol-responsive nuclear receptor LXR (liver X receptor) (Zelcer et al. 2009), which, interestingly, happens to be the human homolog of the EcR (Willy et al. 1995) and CNPY2 was shown to negatively regulate MYLIP-mediated ubiquitination and thus proteasomal degradation of the LDLR (Do et al. 2012). Taking the interactions between sturkopf/LDAH with seele/CNPY2 (figure 59), between sturkopf and LpR1/LpR2 receptors (appendix, figure 61), as well as sturkopf's putative role in EcR protein regulation into consideration, an involvement of sturkopf/LDAH in the context of cholesterol homeostasis might appear reasonable also considering its predicted function as lipolytic enzyme (Thiel et al. 2013; Goo et al. 2014). However, as several lines of evidence argue against a role in the canonical lipid metabolism (Thiel et al. 2013; Kory et al. 2017; Werthebach et al. 2019), a function in lipid metabolism might just be an additional function on top of its still unknown main function. Such a putative auxiliary function of LDAH has been shown by others previously (Dubey et al. 2020). LDAH was identified as mediator of hydrolysis of lasonolide A (LasA), a marine sponge-derived macrolide with anti-cancer properties, to its active and toxic metabolite LasF (Wright et al. 2004; Dubey

et al. 2020). Although the authors underline the specificity of LDAH-mediated LasA hydrolysis rather than being a product of generic ester hydrolysis (Dubey et al. 2020), it is questionable whether this LDAH-mediated hydrolysis is indeed a specific enzymatic reaction of the dedicated enzyme and its physiological target substrate as these macrolides are absent in humans, *Drosophila*, and other species. However, what cannot be ruled out is an evolutionary adaptation of a putative ortholog of sturkopf/LDAH in the marine sponge *Forcepia sp.*, making LasA the physiological substrate of the enzyme. Furthermore, it is possible that LasA coincidentally shares similar properties as the still unknown physiological substrate(s) of sturkopf/LDAH thus resulting in the formation of a functional enzyme-substrate-complex.

3.5 Sturkopf protein level modulation in the *Drosophila* AG and its effect on SC number

The number of SCs has been previously used in a genetic screen as a readout to study effects of *Drosophila* orthologs of known human prostate cancer mediators (Ito et al. 2014). These cells have the ability to migrate (Leiblich et al. 2012; Ito et al. 2014), endoreplicate (Leiblich et al. 2012; Leiblich et al. 2019) and are a suitable platform to study exosome biology (Corrigan et al. 2014; Redhai et al. 2016). All these aspects are also important and deregulated in prostate cancer (Wilson et al. 2017; Rambur et al. 2021). As it is still in question where exactly sturkopf is expressed in the AG, smiFISH experiments were performed to identify the origin of *sturkopf* transcript expression (figure 30). However, the data obtained for *sturkopf* transcript expression is hard to interpret. The signals obtained for smiFISH experiments were, while nicely limited to the SCs, also detected in the *sturkopf* null mutant situation (figure 30). It is highly likely that the obtained signal in both conditions is due to unspecific binding of the probes as no discrimination can be made between the *sturkopf* null mutant background and the respective control. Although residual *sturkopf* transcripts are present in the *sturkopf* null mutant condition, it rather does not explain the obtained signal, as the partial transcripts is fairly short (Werthebach et al. 2019) and a substantial number of smiFISH probes are necessary for robust detection of mRNA transcripts (Calvo et al. 2021).

However, one main aim of this dissertation was to identify whether it is possible to model and translate the *LDAH* loss-mediated PCa association (Currall et al. 2018) using the *Drosophila* accessory gland and sturkopf. *LDAH* knockdown promotes

proliferation, whereas LDAH overexpression reduces cell proliferation as well as migration and invasion capacity in cultured cells (Currall et al. 2018). *LDAH* loss *in vivo* results in prostate carcinogenesis (Currall et al. 2018). It was, thus, assumed that modulation of sturkopf protein abundance in the *Drosophila* accessory gland also results in differences in cell abundancies. While cell abundance of the main cells was not tested, loss of *sturkopf* was significantly lowered SC numbers (e.g., figures 12 and 16) which was a counterintuitive result as excessive proliferation is one of the key features of cancer cells in general (Feitelson et al. 2015) and loss of *LDAH* was associated with prostate carcinogenesis and over-proliferation of the PCa cells consequently (Currall et al. 2018). However, as this SC loss phenotype was shown to be sturkopf- (figures 17 and 18) and presumably SC-specific (compare figures 33 and 34 with figure 38) it was investigated further. It is worthwhile to mention that in all experiments including transgene activation in a "SC-specific" manner using the *esg;Ctrl* and *esg;35.7*, transgene activation took also place in other cell types expressing the *escargot* transcription factor e.g., intestinal stem cells (Korzelius et al. 2014). These *esgcargot*-based driver lines are advertised in scientific literature to be SC-specific inside the accessory glands, however, completely neglecting the possibility of transgene expression in other cells expressing *escargot* (Leiblich et al. 2019; Leiblich et al. 2012; Hopkins et al. 2019). Thus, the possibility of a long-range effect mediated by cells of another tissue/cell type expressing *escargot* cannot be entirely ruled out and requires further investigation. Here, a driver line which functions and drives transgene expression in SCs exclusively is required to fully rule out any long-range effects which might be mediated by other cells expressing *escargot*. However, as these driver lines are advertised to function in a SC-specific manner, it was also assumed for the results presented in this study.

Upon SC quantification of crossings between the SC-specific driver line *esg;Ctrl* expressing wild type sturkopf protein levels or *esg;35.7* as a *sturkopf* mutant SC-specific driver line with any effector fly line to ensure SC-specific transgene expression inside the AGs, the problem of diminishing GFP expression was encountered (e.g., figure 35). GFP expression was only expressed by a few, if any, SCs. A similar observation was made by others (Leiblich et al. 2012). However, in this case, the diminishing SC-specific GFP expression was traced back to the genetic system used which enabled the SC-specific GFP expression only in the first day of adulthood (Micchelli and Perrimon 2006; Jiang and Edgar 2009). The use of a

combination of an *esg*^{ts} *Flp-Out* (*F/O*) system (Jiang et al. 2009) and an ubiquitously expressed, temperature-sensitive form of the *GAL4* inhibitor *GAL80* (*tub-GAL80*^{ts}) and an interrupted copy of an *actin Gal4* construct (McGuire et al. 2004) was supposedly circumventing this issue (Leiblich et al. 2012). The *actin Gal4* construct is activated by *UAS-FLP*-mediated recombination (Leiblich et al. 2012). The temperature shift of the animals induce a conformational change of the Gal80^{ts} enabling *escargot*-Gal4 regulated, *FLP*-induced events in all SCs (Leiblich et al. 2012). However, also using this SC-specific driver line resulted in partial/impaired GFP-expression (data not shown). Thus, SCs of temperature-shifted animals, independent of the performed temperature shift (figure 46), needed to be counterstained against SC-specific markers (Abd-B (Gligorov et al. 2013; Kubo et al. 2018) or ANCE (Houard et al. 1998; Rylett et al. 2007) [e.g., figure 15]) due to the insufficient expression of GFP in all SCs. An explanation for this issue could be the heterozygous state of the *escargot* construct as SCs in animals homozygous for this construct robustly expressed GFP in all SCs as confirmed by counterstaining (figure 15). However, also using SC-specific marker-antibodies required a variation of the routinely performed standard shift. Animals needed to be additionally shifted back to the restrictive temperature for 3 days. This suggests that temperature plays a decisive role in the detection of the SC-specific markers used. However, this means enabled the robust marking of SC nuclei staining the tissue against Abd-B (figure 37) allowing for an analysis of SC number in animals heterozygous for the constructs *esg;Ctrl* and *esg;35.7*, respectively.

Reintroduction of one functional *sturkopf* allele in the null mutant background resulted in a partial rescue of the SC loss phenotype as expected (e.g., figures 17 and 41). In contrast, sturkopf overexpression resulted in a highly significant increase in the number of SCs, both in the *sturkopf* control background (figure 39) as well as in the *sturkopf* mutant background (figure 43). This result suggests that sturkopf protein levels regulate the number of SCs in a sturkopf dose-dependent manner. As secondary cells are postmitotic undergoing their last mitotic cycle halfway through pupariation (Taniguchi et al. 2014; Kubo et al. 2018), the only possible way of how *sturkopf* LOF can affect SC abundance post eclosion is through regulation of apoptosis. Apoptosis was previously shown to regulate SC abundance (Minami et al. 2012; Kubo et al. 2018). Inhibition of apoptosis leads to increase in SC number by approximately 1.8 fold suggesting that apoptosis might be a major regulator of SC

abundance (Kubo et al. 2018). Consequently, it was assumed that sturkopf regulate these apoptotic processes of the SCs in the AG. Within the scope of this work, the viral apoptosis inhibitor p35 was overexpressed to test for apoptotic regulation of SC numbers (figures 51 and 52). In case of a sturkopf-mediated regulation of apoptosis it would be expected that its inhibition in the *sturkopf* control background would result in an increase in numbers of SCs as previously demonstrated by others (Kubo et al. 2018). Inhibition of apoptosis in a *sturkopf* mutant background should in a rescue of SCs comparable to the assumed increase in SC number in the *sturkopf* control background upon p35 overexpression and would suggest a role of sturkopf in apoptotic processes. Not only did the p35 overexpression led to significantly increased numbers of SCs in a *sturkopf* wild type background (figure 51), but also overexpression of the same transgene in the *sturkopf* mutant background resulted in SC numbers which were comparable to those in the *sturkopf* control background (figure 52) indicating a role of sturkopf in apoptosis regulation. Sturkopf interacts with the polyubiquitin precursor Ubiquitin-63E (Ubi-p63E) (Kolkhof et al. 2017) which, in turn, was demonstrated to interact with Dronc (Death regulator Nedd2-like caspase) (Kamber Kaya et al. 2017). It represents an initiator caspase essential for caspase-dependent apoptosis and is, interestingly, induced by ecdysone (Dorstyn et al. 1999) which again could create a reference to an impairment in ecdysone signaling. Dronc is the *Drosophila* ortholog of the human caspase 2, which is involved in the regulation of the androgen receptor and cell cycle in prostate cancer cells (Taghiyev et al. 2011). A negative regulation of caspases in cell death control is equally important as regulation of processes promoting cell death (Kornbluth and White 2005). This is mainly mediated by the caspase inhibitor protein family IAPs (inhibitors of apoptosis) which are capable of binding and inhibiting caspases (Salvesen and Duckett 2002; Vaux and Silke 2005). In *Drosophila*, DIAP1 is one of the major regulators of inhibition of the caspase Dronc. DIAP1, as dedicated E3 ubiquitin ligase, targets Dronc for proteasomal degradation in living cells and promotes DIAP1 degradation via autoubiquitination which is selectively regulated by the protein Reaper under apoptotic conditions (Ryoo et al. 2002; Wilson et al. 2002; Ryoo et al. 2004). Sturkopf and LDAH are associated with the ubiquitination machinery (Kolkhof et al. 2017; Goo et al. 2017) and likely to be involved in protein stability regulation (Goo et al. 2017; Werthebach et al. 2019) (figure 28). Thus, investigating sturkopf's role in apoptosis regulation might be an interesting target for future studies. Given the fact that loss of

LDAH promotes proliferation and prostate carcinogenesis (Currall et al. 2018) results in the hypothesis that *LDAH* is a novel proto-oncogene in the context of prostate cancer. *Drosophila* sturkopf and the accessory glands can be used to model certain aspects in this respect.

3.6 Outlook

The molecular mechanism of how the loss of a lipid droplet associated protein such as *LDAH* promotes prostate carcinogenesis is still not understood.

The data presented in this work for sturkopf overexpression on cell proliferation in cultured cells were in accordance with the data presented for human LDAH overexpression (Currall et al. 2018). It would be interesting to analyze whether a *sturkopf* knockdown or knockout affects proliferation behavior in a similar fashion as the knockdown of *LDAH* did by promoting proliferation (Currall et al. 2018). Furthermore, as induction of LDs also forced proliferation in wild type sturkopf-overexpressing cells, the study calls for research focusing on the suggested dual role of sturkopf based on its localization. As this was not put into consideration in the study of Currall and colleagues (Currall et al. 2018) and induction of LDs promoted proliferation of sturkopf-overexpressing cells in the present work in a similar manner as *LDAH* knockout did in human cell culture (Currall et al. 2018), it would be compelling to study this hypothesis in mammalian cell culture via the induction of LDs in the mammalian system (Currall et al. 2018). Here, it should be assessed in dependence of the location of sturkopf/LDAH whether proteins regulating proliferation such as p53 or xeele/CNPY2 are differentially expressed or show altered activity. Furthermore, it should be analyzed whether the mere translocation of LDAH to LDs is already sufficient to promote proliferation as shown for sturkopf overexpression. As a result, over-proliferation and prostate carcinogenesis in general might be favored when LDAH is simply not located in the ER but on LDs and thereby unable to control the activity of target proteins. CNPY2, for instance, is an ER-resident saposin like protein (Do et al. 2012) and a known oncogene (Yan et al. 2016; Ito et al. 2018b). It is suggested that CNPY2 activity is released upon loss of *LDAH* promoting prostate carcinogenesis. This hypothesis is based on the strong interaction between sturkopf/LDAH and seele/CNPY2 and the putative sturkopf/LDAH-mediated protein stability regulation which should be investigated in the future particularly. Furthermore, the very strong interaction between LDAH and the oncogene *CNPY2*

(Yan et al. 2016) support the hypothesized LDAH-mediated sequestration or stability regulation of seele/CNPY2, preventing CNPY2 from the inhibition of the ubiquitination of the AR in prostate cancer cells in order to be proteasomally degraded (Ito et al. 2018b). This data also may help to understand the role of sturkopf/LDAH in ubiquitination processes and the accompanying protein stability regulation further.

Moreover, CNPY2 negatively regulates p53 activity and stability and thereby contributing to carcinogenesis as demonstrated for liver and colorectal cancer (Hong et al. 2022; Yan et al. 2016). The transcription factor p53 is often referred to as "guardian of the genome" by regulating the expression of genes involved in DNA repair, cell cycle progression and induction of apoptosis (Lane 1992) and is frequently mutated in a variety of cancers (Lane 1992). A sturkopf-meditated effect on apoptosis, SC endoreplication as well as SC abundance was identified in this work. SC number is regulated by apoptosis as shown here and by others (Kubo et al. 2018). Endoreplication of various *Drosophila* cells is dependent on Cyclin E (CycE) (Edgar et al. 2014), including the SCs of the accessory gland (Leiblich et al. 2019). The reduction in SC endoreplication as well as the decrease in SC abundance identified in accessory glands of *sturkopf* mutant males might thus be a result of a disturbed cell cycle regulation. Within the scope of this work, it was hypothesized that loss of *sturkopf/LDAH* might release CNPY2/seele activity and thereby contribute to prostate carcinogenesis as shown before (Ito et al. 2018b). As loss of *LDAH* was associated with the initiation and progression of prostate cancer (Currall et al. 2018) the protein might contribute either directly or indirectly to maintain genome stability through the regulation of CNPY2 activity. If this contribution holds true, CNPY2 could serve as potential therapeutic target in *LDAH* LOF prostate cancer by regulating CNPY2 activity/stability via a therapeutic drug in case LDAH would be the major regulator of CNPY2 activity. *LDAH* was identified to be among the most frequently downregulated genes in both primary and metastatic PCa samples, even surpassing well-known tumor suppressor genes such as *PTEN* or *NKX3-1* (Currall et al. 2018) proposing a role of *LDAH* as a novel tumor suppressor gene in prostatic carcinomas.

CNPY2 and MYLIP, which is an E3 ubiquitin ligase regulating AR protein stability by proteasomal degradation (Ito et al. 2018b), is also involved in the regulation of low density lipoprotein receptors (LDLR) (Do et al. 2012). The strong interaction of sturkopf and the *Drosophila* LDLR orthologs (LpR1/LpR2) found (appendix, figure

61), may suggest a role of sturkopf/LDAH in cholesterol metabolism by regulating the stability of these receptors and, thus, cellular cholesterol levels. This lipid entity was shown to be accumulated in prostate cancer cells (Yue et al. 2014) and is also known to be essential for the synthesis of both testosterone (Eacker et al. 2008) as well as ecdysone (Svoboda et al. 1975; Igarashi et al. 2018).

Although ecdysone signaling through the EcR in the AG of *Drosophila* cannot be homologized to androgen signaling through the AR in the human prostate (see 3.1), fundamental and potentially conserved mechanisms were already hypothesized (Leiblich et al. 2019). The *in vivo* data for the ecdysone hemolymph titers suggests that *sturkopf* LOF either impairs the synthesis of ecdysone or alters its maintenance/turnover. However, in either case, ecdysone signaling is likely to be impaired. Future research may test whether this reduction in ecdysone titers is a direct or an indirect effect of *sturkopf* LOF. In case of a direct effect, *sturkopf* LOF might alter the regulation of the cytochrome P450 enzymes encoded by the Halloween genes, namely *phantom*, *disembodied*, *shadow*, and *shade* which function in a sequential manner during ecdysone synthesis (Rewitz et al. 2006). In case of an indirect effect *sturkopf* LOF might result in an altered stability regulation of target proteins regulating ecdysone synthesis. It would be intriguing to answer whether such deregulation in hormone titers also applies to androgen levels in a *LDAH* knockout mouse since the synthesis of mammalian testosterone is partially regulated via cytochrome p450 enzymes (Eacker et al. 2008). Deregulation of the AR is another key feature of prostate cancer cells (Heinlein and Chang 2004; Culig and Santer 2014; Dai et al. 2017). It would be interesting to investigate whether loss of *LDAH* in a mammalian *in vitro* and *in vivo* system alters the abundance of the androgen receptor in a similar manner as altered sturkopf protein levels directly influence EcR protein levels via a putative stability regulation. In this case it is pivotal to finally prove that sturkopf protein abundance indeed alters the abundance of EcR protein levels *in vivo* at first. However, as stability of other target proteins such as ATGL were shown to be regulated via the mammalian sturkopf ortholog LDAH (Goo et al. 2017), a putative sturkopf-mediated stability regulation of the EcR via ubiquitination appears possible, especially as it was previously shown that the EcR protein stability is regulated via ubiquitination and subsequent proteasomal degradation (Gradilla et al. 2011).

4 Materials and Methods

4.1 Materials

4.1.1 Chemicals and reagents

Table 1: Used chemicals and reagents.

Designation	Manufacturer
Agar	Becton, Dickinson and Company
D-(+)-Glucose monohydrate	Sigma-Aldrich/Merck
Prolong Gold antifade reagent	Thermo Fisher Scientific
LE Agarose	Biozym Scientific
Magnesium chloride x 6 H_2O	Grüssing
Magnesium sulfate heptahydrate	Grüssing
Methyl-4-hydroxybenzoate	Sigma-Aldrich/Merck
Propionic acid	Sigma-Aldrich/Merck
Milk powder	Carl Roth
Paraformaldehyde	Grüssing
Peptone	Becton, Dickinson and Company
Potassium chloride	Grüssing
Potassium acetate	Grüssing
Sodium acetate	Grüssing
Sodium chloride	Sigma-Aldrich/Merck
Sodium hydroxide	Sigma-Aldrich/Merck
Sodium dodecyl sulfate	Sigma-Aldrich/Merck
Triton X-100	Sigma-Aldrich/Merck
Trizma Base	Sigma-Aldrich/Merck
Tryptone	Becton, Dickinson and Company
Tween20	Sigma-Aldrich/Merck
Yeast extract	Becton, Dickinson and Company
Dimethyl sulfoxide	Sigma-Aldrich/Merck

Designation	Manufacturer
Glycerol	Carl Roth
di-Potassium hydrogen phosphate	PanReac AppliChem
Potassium dihydrogenphosphate	Grüssing
di-Sodium hydrogen phosphate dihydrate	PanReac AppliChem
EGTA	PanReac AppliChem
EDTA	PanReac AppliChem
Ethanol absolute	Sigma-Aldrich/Merck
Midori Green Advanced DNA stain	Nippon Genetics
6x DNA loading dye	Thermo Fisher Scientific
Rotiphorese Gel 30 (37.5:1)	Carl Roth
N,N,N',N'-tetramethylethylenediamine	Sigma-Aldrich/Merck
Methanol	Sigma-Aldrich/Merck
Restore Western Blot Stripping Buffer	Thermo Fisher Scientific
Dithiothreitol	Carl Roth
Propionic acid	Sigma-Aldrich/Merck
Bisbenzimide H33342	Sigma-Aldrich/Merck
Chloroform	VWR International
Bovine serum albumin, fatty acid-free	Sigma-Aldrich/Merck
Bovine serum albumin	Sigma-Aldrich/Merck
Calcium chloride hexahydrate	Sigma-Aldrich/Merck
Glycine	VWR International
GeneRuler Mix	Thermo Fisher Scientific
Propan-2-ol	Fisher Scientific
Glacial acetic acid	VWR International
Monopotassium phoshate	Sigma-Aldrich/Merck
Bromphenol blue sodium salt	Carl Roth
D-(-)-α-Aminobenzylpenecillin	PanReac AppliChem
Kanamycin sulfate	PanReac AppliChem
Streptomycin sulfate	PanReac AppliChem
Sodium deoxycholate	Sigma-Aldrich/Merck
Ammonium persulfate	Carl Roth
BODIPY 558/568 C12	Thermo Fisher Scientific
HEPES	Carl Roth

Designation	Manufacturer
cOmplete Protease inhibitor, EDTA-free	Roche Diagnostics
Crystal violet, 1 % aqueous solution	Sigma-Aldrich/Merck
Normal goat serum	Sigma-Aldrich/Merck
Tris-HCl	Sigma-Aldrich/Merck
Trizma Base	Sigma-Aldrich/Merck
E. coli tRNA	Roche Diagnostics
Herring sperm DNA	Promega
Ribonucleoside vanadyl complex	New England Biolabs
Trisodium citrate	Thermo Fisher Scientific
Formamide	Thermo Fisher Scientific
Dextran sulfate (MW 6.500-10.000)	Fisher Scientific

4.1.2 Buffers, solutions, and gels

Table 2: Used buffers and solutions with information regarding their components.

Tris-acetate-EDTA (TAE) buffer	2 M	Trizma Base
(50x)	1 M	Glacial acetic acid
	0.5 M	EDTA, pH 8.0
	ad 1 l	dH_2O
Phosphate-buffered saline (PBS)	1.37 M	Sodium chloride
pH 7.4 (10x)	27 mM	Potassium chloride
	100 mM	Disodium phosphate
	20 mM	Monopotassium phosphate
	ad 1 l	dH_2O
for PBT	add 0.1 %	Tween 20 to 1x PBS
for PBST	add 0.1 %	Triton X-100

Sample (Laemmli) buffer	250 mM	Tris-HCl, pH 6.8
(5x)	500 mM	Dithiothritol
	10 %	Sodium dodecyl sulfate
	0.5 %	Bromphenol blue sodium salt
	5 ml	Glycerol
	ad 10 ml	dH_2O
SDS PAGE Running buffer	250 mM	Tris-HCl
(10x)	1.92 M	Glycine
	1 %	Sodium dodecyl sulfate
	ad 1 l	dH_2O
SDS PAGE Transfer buffer	250 mM	Tris-HCl
(10x)	1.92 M	Glycine
	ad 1 l	dH_2O
for 1x Transfer buffer	add 10 %	Methanol
RNAfix	10 %	10x PBS
pH 7.0	10 %	0.5 M EGTA, pH 8.0
	10 %	Paraformaldehyde
	ad 1 l	dH_2O
before use dilute	1:1 with	1x PBS
Lysogeny broth (LB)	1 %	Tryptone
pH 7.5	0.5 %	Yeast extract
	1 %	Sodium chloride
	ad 1 l	dH_2O
for LB_{AMP}	100 µg/ml	Ampicillin
for $LB_{STREPTO}$	50 µg/ml	Streptomycin
for LB_{KANA}	100 µg/ml	Kanamycin
for agar plates	add 15 %	Agar

Radioimmunoprecipitation buffer	10 mM	Tris-HCl, pH 8.0
(RIPA buffer)	1 mM	EDTA
	0.5 mM	EGTA
	1 %	Triton X-100
	0.1 %	Sodium deoxycholate
	0.1 %	Sodium dodecyl sulfate
	140 mM	Sodium chloride
Lysis buffer	50 mM	HEPES, pH 7.5
	150 mM	Sodium chloride
	1.5 mM	Magnesium chloride
	500 µM	EGTA
	0.5 %	Triton X-100
before use add	1:100	Protease inhibitor cocktail
Super optimal broth (SOB)	2 %	Tryptone
	0.5 %	Yeast extract
	8.56 mM	Sodium chloride
	2.5 mM	Potassium chloride
	10 mM	Magnesium chloride
	10 mM	Magnesium sulfate
	ad 1 l	dH_2O
Squishing buffer	10 mM	Tris-HCl, pH 8.2
	1 mM	EDTA
	25 mM	Natrium chloride
before use add	200 µg/ml	Proteinase K
NEB 3	1 M	Sodium chloride
(10x), pH 7.9	500 mM	Tris-HCl
	100 mM	Magnesium chloride

SSC buffer	3 M	Sodium chloride
(20x), pH 7.3	300 mM	Trisodium citrate
smiFISH wash buffer	2x	SSC buffer
	10 %	deionized formamide
smiFISH hybridization buffer	2x	SSC buffer
	10 % w/v	Dextran sulfate
	10 %	deionized formamide
Alkaline lysis buffer P1	50 mM	Tris-HCl, pH 8.0
	10 mM	ETDA, pH 8.0
Alkaline lysis buffer P2	0.2 M	Sodium hydroxide
	1 %	Sodium dodecyl sulfate
Alkaline lysis buffer N3	3 M	Potassium acetate, pH 5.5

Table 3: Used gels with information regarding their components.

Agarose gel	1 g	Agarose
(1 %)	100 ml	dH_2O
Stacking gel	3.4 ml	dH_2O
(5 %, 5 ml)	830 µl	Rotiphorese Gel 30
	630 µl	1 M Tris-HCl, pH 6.8
	50 µl	10 % Sodium dodecyl sulfate
	50 µl	10 % Ammonium persulfate
	5 µl	TEMED

Separating gel	4 ml	dH_2O
(10 %, 10 ml)	3.3 ml	Rotiphorese Gel 30
	2.5 ml	1.5 M Tris-HCl, pH 8.8
	100 µl	10 % Sodium dodecyl sulfate
	100 µl	10 % Ammonium persulfate
	4 µl	TEMED

4.1.3 Enzymes

Table 4: Used enzymes and their corresponding buffers.

Designation	Manufacturer
Phusion High Fidelity DNA Polymerase	New England Biolabs
Phusion HF buffer, 5x	New England Biolabs
Q5 High Fidelity DNA Polymerase	New England Biolabs
Q5 Reaction Buffer, 5x	New England Biolabs
NotI HF	New England Biolabs
AscI	New England Biolabs
EcoRV HF	New England Biolabs
Cutsmart Buffer, 10x	New England Biolabs
T4 DNA Ligase	New England Biolabs
T4 DNA Ligase Reaction Buffer	New England Biolabs
Proteinase K	Thermo Fisher Scientific

4.1.4 Oligonucleotides

All nucleotides were used for ORF amplification and were purchased from Sigma-Aldrich/Merck.

Table 5: Used oligonucleotides with information regarding their designation (fwd: forward, rev: reverse) sequence, usage, and reference.

Designation	Sequence (5‘-3‘)	Reference
hsUBE2D1 fwd	GCTTGCGGCCGCCACCATGGCGCTGAAGA GGATTCAGAAAG	This work
hsUBE2D1 rev	GCAAGGCGCGCCCCATTGCATATTTCTGAG TCCATTCTC	This work

Designation	Sequence (5‘-3‘)	Reference
hsTRIM28 fwd	GCTTGCGGCCGCCACCATGGCGGCCTCCG CGGCGGCAG	This work
hsTRIM28 rev	GCAAGGCGCGCCCGGGGCCATCACCAGGG CCACC	This work
hsMYLIP fwd	GCTTGCGGCCGCCACCATGCTGTGTTATGT GACGAGGCCG	This work
hsMYLIP rev	GCAAGGCGCGCCCGATTACAGTCAGATTGA GAAGACTG	This work
mmCNPY2 fwd	GCTTGCGGCCGCCACCATGCGAGCGTCAG AGGCTGTG	This work
mmCNPY2 rev	GCAAGGCGCGCCCTAGCTCATCGTGAGATC TGTGC	This work
hsCNPY2 fwd	GCTTGCGGCCGCCACCATGAAAGGCTGGG GTTGGCTG	This work
hsCNPY2 rev	GCAAGGCGCGCCCTAGCTCATCATGCGATA TGTGC	This work
hsLDAH fwd	GCTTGCGGCCGCCACCATGGACTCAGAACT CAAGGAAG	This work
hsLDAH rev	GCAAGGCGCGCCCCATTTTGGACAAGTCAT CCTTTAG	This work
Ariadne1 fwd	GCTTGCGGCCGCCACCATGGACTCGGACAA TGACAATG	This work
Ariadne1 rev	GCAAGGCGCGCCCTTCTGTGTACTCCCACC ACTC	This work
pUbiP-Seq1	CCTCTAGACTAGCTAGC	Our group
pUbiP-Seq2	CGTCTGATTTCGTACTAATTTTCCAC	Our group
rp49 fwd	ATCGGTTACGGATCGAACAA	(Liu et al. 2016)
rp49 rev	GACAATCTCCTTGCGCTTCT	(Liu et al. 2016)
JHEH1 fwd	CAGTCTCCACCCTGGATAAAGAA	(Guio et al. 2014)

Designation	Sequence (5‘-3‘)	Reference
JHEH1 rev	AGTTTACCAGGTTATGGCTGGTC	(Guio et al. 2014)
JHEH2 fwd	AGGCCATCCTACCCTTCGACATCA	(Guio et al. 2014)
JHEH2 rev	ATTGGAAACCCACACCCTCCAGTG	(Guio et al. 2014)
JHEH3 fwd	CATCACAGTGGCCATTTCAG	(Guio et al. 2014)
JHEH3 rev	CATGCTAACCAAGCACTCAAAC	(Guio et al. 2014)
E74A fwd	AGAAACTTCGAGGCAATAGGGT	(Zipper et al. 2020)
E74A rev	TGTGCGGCCTCATCTCAAG	(Zipper et al. 2020)
E75A fwd	CCTGTGCCAGAAGTTCGATGA	(Zipper et al. 2020)
E75A rev	AAGAATCCATCGGCATCTTCGT	(Zipper et al. 2020)
E75B fwd	CGTCTAGCTCGATTCCTGATCTA	(Zipper et al. 2020)
E75B rev	CGGAAGAATCCCTTGCAACC	(Zipper et al. 2020)
EcR fwd	GTGTTCGGTGAAAAACGCAA	(Zipper et al. 2020)
EcR rev	TCCTAGCAACTGAGCTTTTGTAGAC	(Zipper et al. 2020)
smiFISH stur1	CTGGATCATGTCTCTTACGATTACAGCCACC TCCTAAGTTTCGAGCTGGACTCAGTG	This work
smiFISH stur2	GGTCGATCTTCTTGGTGTCCAGCTGGGCCT CCTAAGTTTCGAGCTGGACTCAGTG	This work
smiFISH stur3	CATAGTAGGAGATTGGTACCCATCCTGCGG CCTCCTAAGTTTCGAGCTGGACTCAGTG	This work

Designation	Sequence (5‘-3‘)	Reference
smiFISH stur4	ACTTTAGGGCGGTGCCCAGAACTGTCGCCT CCTAAGTTTCGAGCTGGACTCAGTG	This work
smiFISH stur5	GCATATAGCGCTTTTGGATGCGACTCCGCC TCCTAAGTTTCGAGCTGGACTCAGTG	This work
smiFISH stur6	GGATCTTGACATCACTTGGCACGTATTTCTC CTCCTAAGTTTCGAGCTGGACTCAGTG	This work
smiFISH stur7	AAATTGAAGAGCTCCTCGTTGCCGCTGACC TCCTAAGTTTCGAGCTGGACTCAGTG	This work
smiFISH stur8	TTGCCAGTTATGCAGATGACGATCTCCTCCT CCTAAGTTTCGAGCTGGACTCAGTG	This work
smiFISH stur9	GATTCCCAAGTCTATTGGCATGGATGGATTA CCTCCTAAGTTTCGAGCTGGACTCAGTG	This work
smiFISH stur10	TAATGGACAGGGCTGATTGTCTGGGCCCCT CCTAAGTTTCGAGCTGGACTCAGTG	This work
smiFISH stur11	GCTCTACAATCTCCCTTTGAATCCCGCCTCC TAAGTTTCGAGCTGGACTCAGTG	This work
smiFISH stur12	CGCTCGTTTTCCAGCAGCTGCAGGATCCTC CTAAGTTTCGAGCTGGACTCAGTG	This work
smiFISH stur13	ATGAAGGCGATTTTATGCCGGATTTGTCCGT CCTCCTAAGTTTCGAGCTGGACTCAGTG	This work
smiFISH stur14	TGAGGAACCTCCCGAATACTGGCCTCCCTC CTAAGTTTCGAGCTGGACTCAGTG	This work
smiFISH stur15	TCGGTTATGGTCTCCTCAATCCACCTCCTCC TAAGTTTCGAGCTGGACTCAGTG	This work
smiFISH stur16	CCCATGTGAATATGTGGGTGGGAATGGAGT TGCCTCCTAAGTTTCGAGCTGGACTCAGTG	This work
smiFISH stur17	GTTGACGTAGGCCTCCTGCATATTTTCCCCT CCTAAGTTTCGAGCTGGACTCAGTG	This work
smiFISH stur18	ATCAATCGGCACCTGTGTTGATCCCACCTCC TAAGTTTCGAGCTGGACTCAGTG	This work
smiFISH stur19	CTTTTCACACGCGATGAGTTGTCTAATCCCC CTCCTAAGTTTCGAGCTGGACTCAGTG TGGCAACCGGTTTTCCTTTGTCCAACCACCT	This work

Designation	Sequence (5'-3')	Reference
smiFISH stur20	CCTAAGTTTCGAGCTGGACTCAGTG	This work
smiFISH stur21	TCGGCTGCAGCCTTTCACGAGTTTCAAACCT CCTAAGTTTCGAGCTGGACTCAGTG	This work
smiFISH stur22	TCCACCTTGGGGTAGTCTTTTTTGAGCTGCC TCCTAAGTTTCGAGCTGGACTCAGTG	This work
smiFISH stur23	ACCTTCTCCGCTACCGATGGTTTGGACCTC CTAAGTTTCGAGCTGGACTCAGTG	This work
smiFISH stur24	CCACCTTGGTGAACACCCATCCATTGCCTC CTAAGTTTCGAGCTGGACTCAGTG	This work
FLAP-X	CACTGAGTCCAGCTCGAAACTTAGGAGG	Biomers.net GmBH

4.1.5 Plasmids

Table 6: Used plasmids with information concerning their usage and reference. PPI: protein-protein-interaction, GR: gateway recombination, CLG: cell line generation.

Designation	Usage	Reference
pCO Blast	CLG	Thermo Fisher Scientific
pDONR bonus-RB	GR	Harvard FlyBi plasmid collection
pDONR Lpr1-RD	GR	Harvard FlyBi plasmid collection
pDONR Lpr1-RH	GR	Harvard FlyBi plasmid collection
pDONR Lpr2-RD	GR	Harvard FlyBi plasmid collection
pDONR Lpr2-RE	GR	Harvard FlyBi plasmid collection
pDONR Lpr2-RF	GR	Harvard FlyBi plasmid collection
pDONR221-EcR	GR	Addgene KHBD00332
pDONR-mura-RC	GR	Harvard FlyBi plasmid collection
pENTR/Ariadne1	GR	This work
pENTR/D-TOPO	Cloning	Thermo Fisher Scientific

Designation	Usage	Reference
pENTR/hsCNPY2_var1	GR	This work
pENTR/TRIM28	GR	This work
pENTR-hsLDAH_var1	GR	This work
pENTR-mmCNPY2pred_var2	GR	This work
pENTR-MYLIP	GR	This work
pENTR-UBE2D1	GR	This work
pUbi-CG9186(S119A):eGFP	CLG	(Kolkhof et al. 2017)
pUbi-CG9186-eGFP	CLG	(Kolkhof et al. 2017)
pUbiP- hGLuc(1)-rfA	GR	(Kolkhof et al. 2017)
pUbiP- hGLuc(2)-rfA	GR	(Kolkhof et al. 2017)
pUbiP_CG32850_hGluc(1)	PPI	This work
pUbiP_CG9772_hGluc(1)	PPI	This work
pUbiP_CG9772_hGluc(2)	PPI	This work
pUbiP_hGluc(1)_CG32850	PPI	This work
pUbiP_hGluc(2)_CG32850	PPI	This work
pUbiP_hGluc(2)_CG9772	PPI	This work
pUbiP-Ari-hGLuc(1)	PPI	This work
pUbiP-Ari-hGLuc(2)	PPI	This work
pUbiP-bonus-RB-hGLuc(1)	PPI	This work
pUbiP-bonus-RB-hGLuc(2)	PPI	This work
pUbiP-CG10862-hGLuc(1)	PPI	This work
pUbiP-CG10862-hGLuc(2)	PPI	This work
pUbiP-CG32850-hGLuc(2)	PPI	This work

Designation	Usage	Reference
pUbiP-CG9186(16K2R)-eGFP	CLG	(Kolkhof et al. 2017)
pUbiP-CG9186(16K2R)-hGLuc(1)	PPI	(Kolkhof et al. 2017)
pUbiP-CG9186(16K2R)-hGLuc(2)	PPI	(Kolkhof et al. 2017)
pUbiP-CG9186-hGLuc(1)	PPI	(Kolkhof et al. 2017)
pUbiP-CG9186-hGLuc(2)	PPI	(Kolkhof et al. 2017)
pUbiP-dnr1-hGLuc(1)	PPI	This work
pUbiP-dnr1-hGLuc(2)	PPI	This work
pUbiP-EcR-eGFP	CLG	This work
pUbiP-EcR-hGLuc(1)	PPI	This work
pUbiP-EcR-hGLuc(2)	PPI	This work
pUbiP-eGFP-EcR	CLG	This work
pUbiP-ERR-hGLuc(1)	PPI	This work
pUbiP-ERR-hGLuc(2)	PPI	This work
pUbiP-hGLuc(1)-Ari	PPI	This work
pUbiP-hGLuc(1)-bonus-RB	PPI	This work
pUbiP-hGLuc(1)-CG10862	PPI	This work
pUbiP-hGLuc(1)-CG9186	PPI	(Kolkhof et al. 2017)
pUbiP-hGLuc(1)-CG9772	PPI	This work
pUbiP-hGLuc(1)-dnr1	PPI	This work
pUbiP-hGluc(1)-EcR	PPI	This work
pUbiP-hGLuc(1)-ERR	PPI	This work
pUbiP-hGLuc(1)-hsCNPY2_var1	PPI	This work
pUbiP-hGLuc(1)-hsLDAHvar1	PPI	This work
pUbiP-hGLuc(1)-Lpr1-RD	PPI	This work
pUbiP-hGLuc(1)-Lpr1-RH	PPI	This work

Designation	Usage	Reference
pUbiP-hGLuc(1)-Lpr2-RD	PPI	This work
pUbiP-hGLuc(1)-Lpr2-RE	PPI	This work
pUbiP-hGLuc(1)-Lpr2-RF	PPI	This work
pUbiP-hGLuc(1)-mmCG9186	PPI	(Kolkhof et al. 2017)
pUbiP-hGLuc(1)-mmCNPY2predvar2	PPI	This work
pUbiP-hGluc(1)-mura(RA)	PPI	This work
pUbiP-hGLuc(1)-mura(RC)	PPI	This work
pUbiP-hGLuc(1)-MYLIP	PPI	This work
pUbiP-hGLuc(1)-TRIM28	PPI	This work
pUbiP-hGLuc(1)-UBE2D1	PPI	This work
pUbiP-hGLuc(2)-Ari	PPI	This work
pUbiP-hGLuc(2)-bonus-RB	PPI	This work
pUbiP-hGLuc(2)-CG10862	PPI	This work
pUbiP-hGLuc(2)-CG9186	PPI	(Kolkhof et al. 2017)
pUbiP-hGLuc(2)-CG9186(16K2R)	PPI	(Kolkhof et al. 2017)
pUbiP-hGLuc(2)-dnr1	PPI	This work
pUbiP-hGLuc(2)-EcR	PPI	This work
pUbiP-hGLuc(2)-ERR	PPI	This work
pUbiP-hGLuc(2)-hsCNPY2_var1	PPI	This work
pUbiP-hGLuc(2)-hsLDAHvar1	PPI	This work
pUbiP-hGLuc(2)-Lpr1-RD	PPI	This work
pUbiP-hGLuc(2)-Lpr1-RH	PPI	This work
pUbiP-hGLuc(2)-Lpr2-RD	PPI	This work
pUbiP-hGLuc(2)-Lpr2-RE	PPI	This work

Designation	Usage	Reference
pUbiP-hGLuc(2)-Lpr2-RF	PPI	This work
pUbiP-hGLuc(2)-mmCG9186	PPI	(Kolkhof et al. 2017)
pUbiP-hGLuc(2)-mmCNPY2predvar2	PPI	This work
pUbiP-hGluc(2)-mura(RA)	PPI	This work
pUbiP-hGLuc(2)-mura(RC)	PPI	This work
pUbiP-hGLuc(2)-MYLIP	PPI	This work
pUbiP-hGLuc(2)-TRIM28	PPI	This work
pUbiP-hGLuc(2)-UBE2D1	PPI	This work
pUbiP-hsCNPY2_var1-hGLuc(1)	PPI	This work
pUbiP-hsCNPY2_var1-hGLuc(2)	PPI	This work
pUbiP-hsLDAHvar1-eGFP	CLG	This work
pUbiP-hsLDAHvar1-hGLuc(1)	PPI	This work
pUbiP-hsLDAHvar1-hGLuc(2)	PPI	This work
pUbiP-Lpr1-RD-hGLuc(1)	PPI	This work
pUbiP-Lpr1-RD-hGLuc(2)	PPI	This work
pUbiP-Lpr1-RH-hGLuc(1)	PPI	This work
pUbiP-Lpr1-RH-hGLuc(2)	PPI	This work
pUbiP-Lpr2-RD-hGLuc(1)	PPI	This work
pUbiP-Lpr2-RD-hGLuc(2)	PPI	This work
pUbiP-Lpr2-RE-hGLuc(1)	PPI	This work
pUbiP-Lpr2-RE-hGLuc(2)	PPI	This work
pUbiP-Lpr2-RF-hGLuc(1)	PPI	This work
pUbiP-Lpr2-RF-hGLuc(2)	PPI	This work

Designation	Usage	Reference
pUbiP-mmCNPY2predvar2-hGLuc(1)	PPI	This work
pUbiP-mmCNPY2predvar2-hGLuc(2)	PPI	This work
pUbiP-mura(RA)-hGluc(1)	PPI	This work
pUbiP-mura(RA)-hGluc(2)	PPI	This work
pUbiP-mura(RC)-hGLuc(1)	PPI	This work
pUbiP-mura(RC)-hGLuc(2)	PPI	This work
pUbiP-MYLIP-hGLuc(1)	PPI	This work
pUbiP-MYLIP-hGLuc(2)	PPI	This work
pUbiP-rfA-eGFP	CLG	Alf Herzig, MPIbpc, Göttingen
pUbiP-rfA-hGLuc(1)	GR	(Kolkhof et al. 2017)
pUbiP-rfA-hGLuc(2)	GR	(Kolkhof et al. 2017)
pUbiP-TRIM28-hGLuc(1)	PPI	This work
pUbiP-TRIM28-hGLuc(2)	PPI	This work
pUbiP-UBE2D1-hGLuc(1)	PPI	This work
pUbiP-UBE2D1-hGLuc(2)	PPI	This work

4.1.6 Bacterial strains

Table 7: Used bacterial strains including a brief description of their properties.

Designation	**Description**	**Reference**
***ccdB* survival cells**	*Escherichia coli* strain with a mutation in the *gyrA* gene	(Bernard and Couturier 1992)
DH5α	*Escherichia coli* strain with mutations in *recA1*, *endA1* and *lacZΔM15*	(Hanahan et al. 1991)

4.1.7 Antibodies

Table 8: Used primary antibodies with information regarding their target proteins, organismal origin, used dilution, and reference.

Designation	Target	Origin	Dilution	Reference
1A2E9	Abdominal-B	Mouse	1:10	DSHB
Ag10.2	Ecdysone receptor (common)	Mouse	1:1000	DSHB
ANCE	Angiotensin-converting enzyme	Rat	1:500	(Rylett et al. 2007)
ANCE	Angiotensin-converting enzyme	Rabbit	1:500	Kerafast, Boston, USA
C29F4 mAb#3724	HA	Rabbit	1:500	Cell Signaling Technlogy
CG9186 2419 #1	Sturkopf	Rat	1:3000	(Thiel et al. 2013)
E7	β-Tubulin	Mouse	1:3000	DSHB
Purified rabbit α-GFP	GFP	Rabbit	1:2000	Torrey Pines Biolabs, Secaucus, USA
α-dFoxO	FoxO	Rabbit	1:500	(Delanoue et al. 2010)

Table 9: Used secondary antibodies with information regarding their organismal origin, used dilution, and reference.

Designation	Origin	Dilution	Reference
α-mouse-Alexa488	Goat	1:100	Jacksonville ImmunoResearch
α-mouse-Alexa594	Goat	1:100	Jacksonville ImmunoResearch
α-mouse-Alexa647	Goat	1:100	Jacksonville ImmunoResearch
α-mouse-HRP	Donkey	1:10.000	Jacksonville ImmunoResearch
α-rabbit-Alexa488	Goat	1:500	Jacksonville ImmunoResearch
α-rabbit-Alexa594	Goat	1:100	Jacksonville ImmunoResearch
α-rabbit-HRP	Goat	1:10.000	Jacksonville ImmunoResearch
α-rat-Alexa488	Goat	1:100	Jacksonville ImmunoResearch
α-rat-Alexa594	Goat	1:100	Jacksonville ImmunoResearch
α-rat-HRP	Goat	1:10.000	Jacksonville ImmunoResearch

4.1.8 Molecular biological and biochemical kits

Table 10: Used molecular biological and biochemical kits.

Designation	Manufacturer
Effectene Transfection Reagent	Qiagen
Gateway LR Clonase II Enzyme Mix	Thermo Fisher Scientific
Gaussia-Juice Luciferase Assay	PJK Biotech
GoTaq 2-Step RT-qPCR System	Promega
HiScribe T7 in vitro Transcription Kit	New England Biolabs
Nucleospin Gel and Purification Kit	Macherey-Nagel
Pierce BCA Protein Assay Kit	Thermo Fisher Scientific
QIAprep Spin Miniprep Kit	Qiagen
QIAquick PCR Purification Kit	Qiagen
Rneasy Mini Kit	Qiagen
SuperSignal West Pico Chemiluminescent Substrate	Thermo Fisher Scientific

4.1.9 Cell culture media

Table 11: Used cell culture media and reagents.

Designation	Manufacturer
Blasticidin S hydrochloride	PanReac AppliChem
DMEM (Dulbecco's minimal essential medium)	PAN-Biotech
Fetal calf serum (FCS)	PAN-Biotech
Oleic acid	Sigma-Aldrich/Merck
Penicillin-Streptomycin	Sigma-Aldrich/Merck
Schneider's *Drosophila* medium	PAN-Biotech
Trypsin / EDTA (0.05 % / 0.02 % in PBS)	PAN-Biotech

Table 12: Used cell culture media with information regarding their composition.

Schneider's complete medium,	89 %	Schneider's *Drosophila* medium
sterile filtered	10 %	FCS, heat-inactivated
	1 %	Penicillin-Streptomycin

BLAST selection medium,	89 %	Schneider's *Drosophila* medium
sterile filtered	10 %	FCS, heat-inactivated
	1 %	Penicillin-Streptomycin
for selection	30 µg/ml	Blasticidin S hydrochloride
for maintenance	10 µg/ml	Blasticidin S hydrochloride
DMEM complete medium,	89 %	DMEM medium
sterile filtered	10 %	FCS, heat-inactivated
	1 %	Penicillin-Streptomycin
Cell freezing medium,	90 %	FCS, heat-inactivated
sterile filtered	10 %	Dimethyl sulfoxide
Oleic acid solution	2.8 g	BSA, fatty acid-free
(12.5 mM)	20 ml	0.1 M Tris-HCl, pH 8.0
	78 µl	oleic acid

4.1.10 Cell lines

Table 13: Used cell lines with information regarding cell line characteristics and their reference.

Designation	Description	Reference
HEK-293	Human embryonic kidney cells	(Graham and Pick 2017); kind gift from Matias Zurbriggen
Kc167	Female embryonic cells from disaggregated young embryos (8-12 h old)	(Echalier and Ohanessian 1969), Harvard RNAi Screening center
S2R+	Cells derived from whole male embryos on the verge of hatching; express the *Drosophila* frizzled 1 and 2 proteins (Dfz1/2)	(Yanagawa et al. 1998), kind gift of Sven Bogdan

Designation	Description	Reference
S2R+::eGFP	S2R+ cells stably overexpressing eGFP (pUbiP-rfa-eGFP), Blasticidin-resistant	This work
S2R+::LDAH-eGFP	S2R+ cells stably overexpressing C-terminally eGFP-tagged human LDAH (pUbiP-LDAH-eGFP), Blasticidin-resistant	This work
S2R+::sturkopf (16K2R)-eGFP	S2R+ cells stably overexpressing C-terminally eGFP-tagged sturkopf(16K2R) (pUbiP-sturkopf(16K2R)-eGFP), Blasticidin-resistant	This work
S2R+::sturkopf (S119A)-eGFP	S2R+ cells stably overexpressing C-terminally eGFP-tagged sturkopf(S119A) (pUbiP-sturkopf(S119A)-eGFP), Blasticidin-resistant	This work
S2R+::sturkopf-eGFP	S2R+ cells stably overexpressing C-terminally eGFP-tagged sturkopf eGFP (pUbiP-sturkopf-eGFP), Blasticidin-resistant	This work

4.1.11 *Drosophila* culture medium

Table 14: Used *Drosophila* culture media with information regarding their composition.

Standard diet (100 ml)	0.5 g	Agar
	7.1 g	Polenta
	0.95 g	Soy flour
	1.68 g	Dry yeast
	4 g	Sugar beet molasses
	4.5 g	Malt extract
	1.5 ml	10 % Nipagin in 70 % EtOH
	450 µl	Propionic acid

Standard diet (AG Jäckle)	0.63 g	Agar
(100 ml)	8 g	Polenta
	1 g	Soy flour
	1.8 g	Dry yeast
	2.2 g	Sugar beet molasses
	8 g	Malt extract
	1.5 ml	10 % Nipagin in 70 % EtOH
	630 µl	Propionic acid

4.1.12 Fly lines

Table 15: Used *Drosophila* lines with information regarding their genotype and reference.

Designation	Genotype	Reference
Acp26Aa Gal4	*z1w11e4{Acp26Aa-P-Gal4};UAS-lacZ*	(Chapman et al. 2003), kind gift from Clive Wilson
actin Gal4	*P{Act5C-GAL4}25FO1*	BL4414
Df(3L)BSC250	*w[1118];Df(3L)BSC250/TM6C, Sb[1] cu[1]*	(Cook 2012), BL23150
Df(3L)BSC363	*w[1118];Df(3L)BSC363/TM6C, Sb[1] cu[1]*	(Cook 2012), BL24387
Df(3L)ED202	*w[1118];Df(3L)ED202,P{w[+mW.Scer\FRT.hs3]=3'.RS5+3.3'}ED202/TM6C, cu[1] Sb[1]*	(Cook 2012), BL8051
esg;Gal4	*w;esg-Gal4,tub-Gal80^{ts},UAS-GFP$_{nls}$/CyO:UAS-flp act>CD2>Gal4/Tm6*	(Leiblich et al. 2012)
esg;Ctrl	*w;esg;Gal4,UASserGFP,tubGal80^{ts};+*	(Werthebach et al. 2019)
esg;sturkopf[35.7]	*w;esg;Gal4,UASserGFP,tubGal80^{ts};sturkopf[35.7]*	(Werthebach et al. 2019)
Fat body Gal4	*w*; P{w[+mW.hs]=GawB}FB+SNS*	(Grönke et al. 2003)

Designation	Genotype	Reference
sturkopf Ctrl	*w1118;;*	(Werthebach et al. 2019)
sturkopf[35.7]	*w1118;;sturkopf$^{35.7}$/ sturkopf$^{35.7}$*	(Werthebach et al. 2019)
UAS-p35	*w[*]; P{w[+mC]=UAS-p35.H}BH1*	BL5072
UAS-sturkopf-ORF-3xHA	*yw; +/+; UAS-CG9186 / Tm3 Sb Ser*	FlyORF F004457
sturkopf-RNAi	*P{KK108771}VIE-260B*	(Dietzl et al. 2007), VDRC105945
White[-] (*w-*)	*w[1118]*	VDRC60000

4.1.13 Devices

Table 16: Used devices with information regarding the model type.

Designation	Model type	Manufacturer
Binocular	EZ4D	Leica
Biological safety cabinet	Safe2020 Class 2	Thermo Fisher Scientific
Cell counter	Luna automated cell counter	Logos Biosystems
Centrifuge	Heraeus Fresco 21	Thermo Fisher Scientific
Centrifuge	Pico 21	Thermo Fisher Scientific
Centrifuge	5804 R	Eppendorf AG
Confocal laser scanning microscope	LSM 710	Carl Zeiss Microscopy
Gel documentation system	FAS-Digi PRO	Nippon Genetics
Gel imager	Amersham Imager 680	GE Healthcare
Heating block	THERMOCELL	Hangzhou Bioer Technology
Heating block	Thermomixer compact	Eppendorf AG
High content analysis system	Operetta CLS	PerkinElmer
High precision scale	ABJ-NM/ABS-N	Kern & Sohn GmbH
Incubation Shaker	Ecotron	Infors GmbH

Designation	Model type	Manufacturer
Incubator	Heraeus B12	Thermo Fisher Scientific
Incubator	IPP110 Plus	Memmert GmbH
Laboratory shaker	RS-OS5	Phoenix Instrument
Magnetic stirrer	MR3001	Heidolph Instruments
Magnetic stirrer	VMS-A	VWR International
Microplate reader	Synergy Mx	BioTek Instruments
pH-meter	Basic pH meter pb-11	Sartorius AG
Power supply	Biometra Power Pack P25	Analytik Jena
Power supply	PowerPac Hc Mini-PROTEAN Tetra Cell	Bio-Rad Laboratories
Precision scale	EW-N/EG-N	Kern & Sohn GmbH
Real time PCR detection system	CFX Connect	Bio-Rad Laboratories
Sonication device	Bioruptor Plus	Diagenode SA
Spectrophotometer	Nanodrop 2000c	Thermo Fisher Scientific
Thermal cycler	Biometra TAdvanced	Analytik Jena
Tissue grinder	Pellet Pestle	Gerresheimer AG
Vortexer	Vortexgenie 2	Scientific Industries Inc.

4.1.14 Software

Table 17: Used software with information regarding the used version.

Designation	Version	Manufacturer
Bio-Rad CFX Manager	3.1	Bio-Rad Laboratories
CellCounter	-	Jürgen Schönborn, group member
FAS Digi PRO	1.5	Nippon Genetics
FinchTV	1.4.0	Geospiza Inc.
Gen5	2.07	BioTek Instruments
GraphPad Prism	8.3.0	GraphPad Software Inc.
Harmony	4.8	PerkinElmer
ImageJ	1.51n	National Institute of Health
MS Office	2207	Microsoft Corporation

Designation	Version	Manufacturer
Nanodrop 2000	1.0	Thermo Fisher Scientific
Rest2009	1.0	Qiagen N.V.
Sequence Massager	-	Attotron Biosensor Corporation
Serial Cloner	2.6	SerialBasics
TeamViewer	14	Teamviewer GmbH
Zeiss Zen Blue	2.5	Carl Zeiss Microscopy

4.1.15 Consumables

Pipettes, reaction tubes/flasks and other not listed apparatuses, materials and consumables were standard laboratory equipment and of research grade and were primarily purchased from Sarstedt Inc., VWR International, or Neolab Migge GmbH.

4.2 Methods

4.2.1 Cell biological methods

4.2.1.1 General cell culture conditions

All cell biological work stages were performed under a sterile bench.

4.2.1.1.1 *Drosophila* cell lines

The used *Drosophila* cell lines (table 13) were routinely cultivated in 25 cm^2 cell culture flasks at 25 °C in the appropriate growth medium (table 12) without the need of external CO_2 supply. The cells were passaged in a 1:5 ratio every 2-3 days upon reaching confluency of approximately <80 %. As the used Kc167 and S2R+ cells were only weakly adherent, the detachment of the cells was performed merely due to weak shear forces based on pipetting. Cells were cultivated up to a passage of ~50 and then replaced with freshly thawed cells.

4.2.1.1.2 Human cell lines

HEK293 cells were cultivated 25 cm^2 cell culture flasks in DMEM complete medium (table 12) at constant 37 °C with 5 % CO_2 supply. Cells were passaged every 2-3 days upon reaching a confluency of approximately <80 % by washing cells once with PBS and trypsination of the cells. Upon detachment of the cells, fresh DMEM was added to the cells to stop the enzymatic process.

4.2.1.2 Freezing cells

In order to freeze cells for later usage, the cells were either grown to sub-confluency of roughly 1-2*10^7 cells/ml or the remaining cell suspension from the routinely passaging was used. The cells were centrifuged for 5 minutes at 1200 rpm in order to pellet the cells. Afterwards the medium was aspirated, and the pelleted cells were resuspended in freezing medium. The suspension was aliquoted in cryovials and put into a foam box at -80 °C. After 2-3 days, the vials were transferred to normal boxes at -80 °C for long term storage.

4.2.1.3 Thawing cells

Frozen cells were quickly thawed in a water bath. Upon thawing, the cells were transferred into 5 ml of fresh medium and centrifuged for 5 minutes at 1200 rpm. The medium was aspirated, and the pelleted cells were resuspended in 5 ml of fresh medium. The cell suspension was plated into a new 25 cm^2 cell culture flask. Initially, freshly thawed cells were passaged at irregular intervals.

4.2.1.4 Cell counting

For cell counting, 10 µl of cells resuspended for passaging were pipetted into a cell counting slide and put into an automated cell counter. The device was used for the determination of cell number and further utilized to calculate required cell numbers and dilutions depending on the experiment performed.

4.2.1.5 Transient and stable plasmid DNA transfection

For both types of transfection, the Effectene Transfection Reagent Kit was used. The first step of the Effectene-DNA complex formation is the condensation of the DNA by interaction with the Enhancer in a defined buffer system. Upon addition of Effectene, the condensed DNA starts to complex with the Effectene Reagent by building micelle-like structures. Complexing of the DNA and the reagent allows an overcoming of the electrostatic repulsion of cell membranes. DNA containing micelles with a positively charged surface can then fuse with the negatively charged plasma membrane of living cells.

Transient transfections were performed to conduct luciferase complementation assays to monitor for protein-protein interactions (4.2.3.6). For transient transfections within the scope of luciferase complementation assays, Kc167 or S2R+ cells were seeded in a 96 well plate with a cell density of approximately 5.5*10^4 cells per well in

100 µl of Schneider's complete medium. After incubation overnight at 25 °C, the transfection mix was prepared by adjusting the DNA concentration of each putative interactor to 75 ng/µl and 6 µl of each plasmid was pipetted into a 1.5 ml reaction tube. To this mixture 81.6 µl of EC buffer were added, followed by the addition of 2.1 µl of Enhancer. The mixture was then vortexed and incubated for 5 minutes at room temperature. Then, 3.6 µl of Effectene were added and the mixture was again vortexed and incubated at room temperature for 15 minutes. Finally, 31 µl of transfection mix were pipetted to the cells in technical triplicates for each putative interaction.

Stable transfections were performed within the scope of the generation of polyclonal cell lines (4.2.1.6) to perform crystal violet proliferation assays (4.2.1.7) and to generate protein lysates for western blot (4.2.3.1). In order to generate stable polyclonal *Drosophila* cell lines, $1*10^6$ S2R+ cells in 4 ml Schneider's complete medium in 25 cm^2 cell culture flask. The next day, a transfection mix containing the expression plasmid (2 µg), pCO Blast (50 ng) and EC buffer in a final volume of 140 µl was produced. Upon addition of 16 µl Enhancer, the mixture was vortexed and incubated for 5 minutes at room temperature. Afterwards, 20 µl Effectene were added, vortexed and incubated for 15 minutes. Then, 840 µl of Schneider's complete medium were added and the complete mix was added to the cells.

4.2.1.6 Generation of stable polyclonal *Drosophila* cell lines

The transfection procedure for the generation of stable polyclonal *Drosophila* cell lines was performed as described in 4.2.1.5. The cells grew for 3 days, and dead cells were brought in suspension upon swirling the flasks carefully. The medium was aspirated and replaced with Schneider's complete medium containing additional 30 µg/ml Blasticidin (BLAST selection medium). This process was repeated every 3 days until Blasticidin-resistant colonies grew confluent. If necessary, Blasticidin-resistant colonies were transferred to a new 25 cm^2 cultivation flask. Once confluent, cells were then resuspended in 5 ml BLAST selection medium (30 µg/ml) and plated in a 25 cm^2 flask. From now on, cells were passaged under standard conditions using BLAST selection medium (10 µg/ml) for maintenance. Newly generated polyclonal cell lines were monitored for a successful transfection of the respective expression construct via western blot.

4.2.1.7 Crystal violet proliferation assay

Crystal violet assays were performed in order to determine differences in proliferative behavior of stably generated cell lines (see 4.1.10, table 13). Crystal violet binds to DNA and proteins inside the cell. Cells undergoing cell death will also be stained. However, cell death results in the detachment of the cells from the culture plate. Thus, these cells will be washed off during the washing steps of the procedure. The protocol was adapted from Feoktiskova *et al.*, 2016.

Stably transfected cell lines were seeded in a density of $5x10^4$ cells/ml in a 24 well plate in technical triplicates and incubated at 25 °C for 24 h. Cells were either cultured under basal conditions or with the supplementation of 400 µM oleic acid per well. Over the course of 5 days, cells were stained and fixed with 200 µl 0.1 % crystal violet solution for 20 minutes under constant agitation. Cells were then carefully washed with 1 ml PBS thrice for 10 minutes each under constant agitation. Crystal violet-dyed cells were airdried overnight at 25 °C. Extraction of crystal violet dye was performed by using 500 µl methanol for 20 minutes under constant agitation. Finally, 300 µl of each well were pipetted into a new 24 well plate and optical density was measured at a wavelength of 570 nm. To three wells, 1 ml of BLAST selection medium without cells was used as control for non-specific binding of crystal violet to the 24 well plate.

4.2.2 Molecular biological methods

4.2.2.1 Production of chemically competent DH5α bacteria

5 µl of a DH5α *E. coli* stock were inoculated in 5 ml SOB medium and incubated overnight at 37°C under constant shaking (220 rpm). The next day, 2 ml of the liquid overnight culture were inoculated in 200 ml SOB medium. The culture was incubated for approximately 2 h at 37°C until reaching an optical density (OD) of OD_{600}=0.4-0.6. For measuring the optical density (OD) of the bacterial culture, 1 ml of that suspension was put into a cuvette and measured using the Nanodrop 2000c. OD_{600}-measurements were performed every 45 minutes until the desired optical density was reached. The suspension was aliquoted in four 50 ml falcons and incubated for 20 minutes on ice. Meanwhile, the centrifuge was cooled down on 4°C and the calcium chloride solutions were prepared. The cells were centrifuged for 10 minutes at 3500 rpm at 4°C. The supernatant was decanted, and the falcons were put back on ice. The residual cell pellets were resuspended in 12 ml ice-cold, sterile filtered 0.1 M

$CaCl_2$. Afterwards, an incubation step of 30 minutes on ice followed. The cells were then centrifuged again for 10 minutes at 3.500 rpm at 4°C. The supernatant was again decanted, and the pelleted cells were resuspended in 3 ml ice-cold 0.1 M $CaCl_2$ containing 15% glycerol. The suspension was then aliquoted in 100 µl batches in prechilled reaction tubes and shock frozen at -80°C.

4.2.2.2 Plasmid DNA transformation

To perform a transformation, bacterial cells were thawed on ice. Then, 100 ng of plasmid DNA were put to a 100 µl aliquot of DH5α or *ccdB* survival *E. coli* and incubated for 15 minutes on ice. Afterwards, the bacteria were heat-shocked at 42°C for 90 seconds and put back on ice for 2 minutes. Then, 500 µl of SOB medium were added to the bacteria and incubated at 37°C for 30 minutes under constant shaking. Following this incubation, the bacteria were plated on LB plates containing the appropriate antibiotic.

4.2.2.3 Mini-preparation

In order to perform a mini-preparation, a plasmid DNA transformation was performed beforehand (4.2.2.2). Single colonies of transformed bacteria plated on agar plates containing the appropriate antibiotic were picked and put into a test tube containing 5 ml of LB medium also containing the suitable antibiotic. The picked bacteria were then incubated for 12 to 16h at 37 °C. To purify the plasmid DNA, the QIAprep Spin Miniprep Kit was used according to the manufacturer's protocol. The purified DNA was eluted in 30-50 µl dH_2O. The DNA concentration was then determined by spectrophotometry using the NanoDrop2000c spectrophotometer and the plasmid DNA integrity was checked by an analytical restriction digestion using an appropriate restriction enzyme according to the manufacturer's instructions (4.1.3).

4.2.2.4 Alkaline lysis

Alkaline lysis is a fast and crude method of preparing plasmid DNA from bacteria. It underlies the same principle as in the mini-preparation namely the alkaline lysis. This method was preferred, when testing many colonies in order to prevent excessive usage of the purification columns which are provided by the Miniprep kit.

2 ml of a 5 ml overnight culture were centrifuged for 1 minute at 13.000 rpm. The pelleted cells was resuspended in 300 µl of alkaline lysis buffer P1. Then, 300 µl of the alkaline lysis buffer P2 were added and the tubes were inverted several times. The mixture incubated for 5 minutes at room temperature. Afterwards, 300 µl of

alkaline lysis buffer N3 were added, mixed, and the mixture was then centrifuged for 10 minutes at 13.000 rpm. The supernatant was transferred into a new reaction tube and mixed with 0.7 volumes of isopropyl by vortexing. After 15 minutes of centrifugation at 13.000 rpm, the isopropyl was discarded and the pellet was washed with 70% EtOH. After that, the air-dried pellet was resuspended in 20-50 µl of dH_2O and the concentration was measured using the Nanodrop2000c. Upon restriction digestion and a subsequent agarose gel electrophoresis, the residual overnight culture of positive clones could be used in an actual mini-preparation to obtain a clean plasmid DNA sample.

4.2.2.5 Polymerase chain reaction (PCR)

The PCR is being used to enzymatically amplify specific DNA sequences *in vitro*. Within the scope of this work PCRs were performed in order to amplify ORFs for the generation of expression plasmids. The following protocol was routinely used:

Mixture:		Cycle:		
1 µl	cDNA template	98 °C	30 sec	
2.5 µl	fwd primer [10 pmol/µl]	98 °C	10 min	
2.5 µl	rev primer [10 pmol/µl]	primer-specific	30 sec	30x
1 µl	dNTPs [10 mM]	72 °C	amplicon-specific	
10 µl	Phusion HF/Q5 reaction buffer [5x]	72 °C	30 sec	
0.5 µl	Phusion HF/Q5 HF polymerase	8 °C	∞	
32.5 µl	dH_2O			

The annealing temperature as well as the elongation times varied depending on the oligonucleotide properties and the size of the amplicon generated.

4.2.2.6 Agarose gel electrophoresis

Agarose gel electrophoresis was routinely performed after plasmid DNA preparation and subsequent analytical restriction digestion either by mini-preparation or alkaline lysis or after an ORF amplification by means of PCR and a subsequent preparative restriction digestion. The electrophoresis was performed using a 1 % agarose gel at 80-100 V for ~30 minutes by default.

4.2.2.7 Gel extraction / PCR purification

A gel extraction is performed following a gel electrophoresis to extract and purify DNA of interest from an agarose gel. The desired gel fragment was cut, and the extraction was performed using the Nucleospin Gel and PCR clean-up kit according to the manufacturer's protocol.

PCR purifications were performed following a prior PCR with the Nucleospin Gel and PCR clean-up kit and all steps were executed according to the manufacturer's protocol.

4.2.2.8 Gateway cloning

The cloning of expression plasmids was performed due to the generation of an entry vector (pENTR) by amplifying the desired ORFs based on cDNA (see appendix) via PCR from either *Drosophila* accessory gland-derived RNA or HEK-293 cell-derived RNA. To accomplish that, oligonucleotides with overhang sequences containing *NotI* and *AscI* restriction sites were used (4.1.4, table 5). The obtained amplicon was digested with *NotI* and *AscI* and ligated into the pENTR/D-TOPO plasmid, according to the manufacturer's instructions, respectively. Several *Drosophila* transcripts were obtained pre-cloned in a pDONR backbone vector from the Harvard FlyBi gene expression plasmid collection and also used for recombination. Desired ORFs were recombined into destination vectors using the Gateway LR Clonase II Enzyme Mix with the following adaptions to the manufacturer's protocol:

Mixture:		Cycle:	
1-3 µl	Entry clone [50-150 ng]	25 °C	1 h
1 µl	Destination vector [150 ng]		
1 µl	Clonase enzyme mix		
ad 4 µl	dH_2O		
1 µl	Proteinase K	37 °C	10 min

The entire mixture was then transformed into DH5α *E. coli* and then used as described in 4.2.2.2.

4.2.2.9 DNA sequencing

DNA sequencing was carried out by MWG Eurofins. For sequencing of pDONR and pENTR constructs the universal sequencing primer M13 uni (-21) and M13 rev (-29) provided by MWG Eurofins were used. For sequencing of generated pUbiP vectors, the sequencing primer pUbiP-Seq1 and pUbiP-Seq2 (4.1.4) were used. Sequencing was always performed for both DNA strands.

4.2.2.10 RNA isolation

The isolation of RNA was performed using the Rneasy Mini Kit.

4.2.2.10.1 RNA isolation from cultured cells

RNA from *Drosophila* S2R+ cells and human HEK-293 cells was isolated prior to cDNA synthesis. For that, cultured cells were centrifuged at 1200 rpm for 5 minutes

and the cell pellet was resuspended in PBS and again centrifuged for 5 minutes at 1200 rpm. The supernatant was aspirated, the pellet was resuspended in 100 µl PBS and frozen at -80 °C. The cell suspension was thawed on ice and 400 µl RLT buffer (provided with the Rneasy Mini Kit) with 20 mM DTT were added. The mixture was centrifuged at 13.000 rpm for 3 minutes and the supernatant was put into a new 1.5 reaction tube. The following steps were according to the Rneasy Mini Kit protocol.

4.2.2.10.2 RNA isolation from *Drosophila* accessory glands

RNA isolation of *Drosophila* AGs was performed prior to cDNA synthesis and optionally subsequent qRT-PCR experiments. Roughly 30 glands were dissected in ice-cold PBS and collected in 100 µl RLT buffer (provided with the Rneasy Mini Kit) with 40 mM DTT in a 1.5 ml reaction tube. The following steps were according to the Rneasy Mini Kit protocol.

4.2.2.11 Reverse transcription and cDNA synthesis

Complementary DNA (cDNA) synthesis was performed following a prior RNA extraction using the GoTaq 2-Step RT-qPCR System kit according to the manufacturers' protocol.

Mixture:		Cycle:	
≤ 5 µg	RNA	70 °C	5 min
1 µl	Primer [Oligo(dT)$_{15}$ Primer]	4 °C	5 min
1 µl	Random Primer		
ad 10 µl	dH_2O		

The following mixture was prepared and added to the denatured RNA/reverse transcription primer mix to generate cDNA:

Mixture:		Cycle:	
10 µl	denatured RNA	25 °C	5 min
1.5 µl	dH_2O	42 °C	1 h
4 µl	GOScript 5x Reaction Buffer	70 °C	15 min
2 µl	$MgCl_2$,25 mM	4 °C	∞
1 µl	PCR Nucleotide Mix, 10 mM		
0.5 µl	Recombinant RNasin		
1 µl	Reverse Transcriptase		

The obtained cDNA was either used directly or frozen at -20 °C for later use.

4.2.2.12 Quantitative real time-polymerase chain reaction (qRT-PCR)

The quantitative real rime-PCR (qRT-PCR) was used to determine differences in the expression of specific genes. For this, RNA was isolated from male accessory glands as described in (4.2.2.10.2). Afterwards, the RNA was used as template to synthesize cDNA as described in (4.2.2.11). The oligonucleotides for the respective genes are listed in (4.1.4, table 5). Every condition to be analyzed was assayed in triplicates and for each well of the 96 well assay plate the following mix was prepared:

Mixture:		Cycle:	
12.5 µl	GoTaq MasterMix	95 °C	2 min
0.5 µl	Forward primer [10 µM]	95 °C	15 sec
0.5 µl	Reverse primer [10 µM]	60 °C	1 min
6.5 µl	dH_2O	95 °C	1 min
5 µl	cDNA	58 °C	1 min
		65-95 °C	+0.5 °C/5 sec

Afterwards, the assay plate was sealed with a foil, shortly centrifuged, and samples were measured using the Real Time PCR Detection System. Subsequent data analysis was performed using the CFX-manager and REST2009.

4.2.2.13 Isolation of genomic DNA (gDNA)

To isolate genomic DNA (gDNA) from single *w[-] Drosophila*, single flies were put in reaction tubes. Upon addition of 50 µl of squishing buffer the flies were homogenized using the tissue grinder. The homogenate got incubated for 20-30 minutes at 37 °C prior to activation of the proteinase K by heating up the homogenate to 95 °C for 2 minutes. The homogenate was shortly centrifuged, and the supernatant was transferred to a new reaction tube and stored at -20 °C.

4.2.3 Biochemical methods

4.2.3.1 Sample preparation for western blots

Cultured Cells:

For protein analyses using cultured cells, cells were harvested and centrifuged at 1200 rpm for 5 minutes and the cell pellet was resuspended in PBS and again centrifuged for 5 minutes at 1200 rpm. The supernatant was aspirated, the pellet was resuspended in 100 µl PBS and frozen at -80 °C. Upon thawing, the cell suspension

was additionally sonicated to break down the cells further (7 cycles, 40 seconds/cycle). For each western blot performed, total protein amounts were determined performing a BCA assay (4.2.3.5).

In order to denature the proteins, 20 µl of 5x sample (Laemmli-) buffer were added to the suspension, mixed, and then incubated for 10 minutes at 95 °C. Shortly before usage of the samples, the suspension was briefly centrifuged to pellet cell components and to fragment nucleic acids. Upon centrifugation, the proteins are eluted in the aqueous phase of the suspension which was used in a SDS-PAGE with subsequent western blot.

Whole *Drosophila* Flies:

To generate lysates from adult *Drosophila* flies, the flies got immobilized at -20 °C for 5 minutes and 3-5 flies were collected in a 1.5 ml reaction tube. 50-100 µl of RIPA or lysis buffer were added to each tube and the flies were homogenized using the tissue grinder. The homogenate was centrifuged for 3 minutes at 13.000 rpm, the supernatant was transferred to a new tube, sonicated as described before, and 40 µl of the supernatant was mixed with 10 µl Laemmli buffer, incubated for 10 minutes at 95 °C and frozen at -80 °C.

4.2.3.2 Sodium dodecyl sulfate polyacrylamide gel electrophoresis

The SDS-PAGE is a biochemical electrophoresis method to separate proteins according to their hydrodynamic radius. In this work, discontinuous Tris-glycine gels were made and used. The protein samples were focused in a 5 % stacking gel at 70 V for ~20 minutes and then separated in a 10 % separating gel at 140 V for approximately 1.5 h using the SDS-PAGE Tank-Blot-System Mini-PROTEAN Tetra Cell.

4.2.3.3 Western blot

Equal amounts of protein were separated using standard SDS-PAGE. Separated proteins were transferred from the carrier matrix (polyacrylamide gel) onto a membrane (polyvinylidene fluoride [PVDF]) by using electric voltage. Prior to transfer, the membrane needed to be activated by soaking in methanol to reduce its hydrophobicity. The implementation of the blot followed the protocol of (Towbin et al. 1979). The Tank-Blot-System Mini-PROTEAN Tetra Cell was used for blotting, using

an electric current of 150 mA for 1 h. After blotting proteins onto a PVDF membrane, the membrane was washed with PBT for 10 minutes and afterwards blocked with 5 % milk powder in PBT overnight at 4 °C to block free protein binding sites on the membrane.

4.2.3.4 Immunodetection using chemiluminescence

PVDF membranes from western blot experiments were washed for 20 minutes with PBT, following the incubation with a primary antibody diluted in 2.5 % milk powder in PBT for up to 24 h under constant agitation using a laboratory shaker. The used antibodies and dilutions can be comprehended in 4.1.7, table 8 and 9. Following 3 PBT washing steps of 10 minutes each, the membrane was incubated with the secondary antibody diluted in 2.5% milk powder in PBT for up to 24 h at 4 °C. After that, the membrane was washed again with PBT for 3 times of 10 minutes each. Subsequently, the immunodetection using chemiluminescence was performed using the SuperSignal West Pico Chemiluminescent Substrate kit. Luminol exhibits chemiluminescence when activated with an oxidant. In this case the oxidizing agent was a peroxide solution which was mixed in a ratio of 1:1 with the luminol solution both provided with the kit. The mixture was dropped onto the membrane and as the horseradish peroxidase catalyzes the oxidation of luminol, emitting light at 428 nm, the light could be detected using the Amersham680 Gel Imager. In case of multiple antibody probing per membrane, the membrane was washed with PBT for 10 minutes followed by an incubation with stripping buffer for 15 minutes. Afterwards, the membrane was washed again with PBT and incubated with 5 % milk powder in PBT at 4 °C overnight.

4.2.3.5 Bicinchoninic acid assay (BCA)

The BCA assay was performed prior to every western blot and within the scope of luciferase complementation assays for normalization purposes using the Pierce BCA assay kit according to the manufacturer's protocol. Defined amounts of BSA were used as standard. For the measurement of the total protein amount of cell lysates and whole *Drosophila* flies for later western blot analysis, dilutions of the lysates have been generated (1:5, 1:50, 1:500) and 50 µl of each dilution were measured. For luciferase complementation assays 10 µl of cell lysates were used. Samples were incubated at 37°C for 30-45 minutes and measured by a microplate reader at a wavelength of 562 nm.

4.2.3.6 Luciferase complementation assay

Luciferase complementation assays were performed to test candidate proteins for protein-protein interactions (PPI). The underlying principle is the generation of measurable chemiluminescence generated by the enzymatic conversion of coelenterazine by the enzyme luciferase. The *Gaussia princeps* luciferase enzyme is split into two similarly sized fragments. To test for interacting proteins, each of the putative interactor of one interaction pair was fused to one half of the luciferase enzyme via Gateway recombination (4.2.2.8). Luciferase fragments were C- and N-terminally fused to each putative interactor to test for interactions in *cis*- and *trans*-configuration. Putative interaction partner transcripts were co-transfected in either Kc167 or S2R+ cells. Cells were routinely treated with 400 µM oleic acid and incubated for 4 days. In case of an interaction, both luciferase fragments complement to a fully functional luciferase enzyme, thus being able to convert coelenterazine and thereby emitting light. Dimerized yeast GCN4 leucine zipper served as positive control and for normalization purposes. Untransfected cells served as assay baseline. Complementation results were categorized in strong interactions (>250 % of zipper-zipper reads), significant interactions (100-250 % of zipper-zipper reads), weak interactions (70-100 % of zipper-zipper reads), and no interaction (<70 % of zipper-zipper reads). The detailed method is described in Kolkhof *et al.*, (2017).

4.2.3.7 20-Hydroxyecdysone (20HE) ELISA

The 20HE ELISA was performed to determine 20HE hemolymph titers of 7 days old virgin and mated female and male *sturkopf* Ctrl and *sturkopf;35.7* animals. Hemolymph preparation was performed as described in (4.2.5.2) and the 20HE ELISA was performed using the 20-Hydroxyecdysone Enzyme Immunoassay kit and according to the indicated manufacturer's instructions. 20HE hemolymph titers were normalized to the hemolymph yield.

4.2.4 Histological methods and confocal microscopy

4.2.4.1 Immunostaining

For antibody staining of *Drosophila* accessory glands, the protocol described in Sharma *et al.*, (2017) was adapted. Accessory glands were dissected in ice-cold 0.1 % PBST and collected in cold 0.1 % PBST in a separate preparation dish until all tissues of flies of the appropriate genotype were dissected. Tissues were then fixed using RNAfix for 30 minutes and afterwards washed thrice with 0.1 % PBST for at

least 10 minutes each. Tissues were then incubated in a blocking solution containing 4 % BSA in 0.1 % PBST for 30 minutes. Primary antibodies were diluted appropriately (4.1.7, table 8) in the blocking solution and incubated overnight at 4 °C. Tissues were washed thrice with 0.1 % PBST for at least 10 minutes each. Secondary antibodies were diluted accordingly (table 9) in 0.1 % PBST and incubated overnight at 4 °C. Tissues were washed thrice with 0.1 % PBST for at least 10 minutes each and stained for DNA with Hoechst33342 [10 mg/ml] diluted 1:2000 in PBS for 30-60 minutes. Tissues were then mounted using Prolong Gold antifade reagent.

4.2.4.2 Measurement of endoreplication

Endoreplication was measured as described in Leiblich *et al.*, (2012). Accessory glands of 7 days-old *esg;Ctrl* and *esg;35.7* mated males were stained with Hoechst33342 as described in (4.2.4.1) and recorded using the LSM710 confocal microscope. Nuclear areas of one secondary cell and 3 surrounding main cells were measured using the ZEN blue 2.5 software. A minimum of 4 clusters per lobe of each genotype were measured and a minimum of 6 lobes per genotype were used the determine the SC/MC nuclear ratio.

4.2.4.3 Single molecule fluorescence *in situ* hybridization

smiFISH was used as means to visualize RNA molecules by using a set of unlabeled, gene-specific primary probes and a fluorescently labelled secondary detector oligonucleotide according to Tsanov et al. and Calvo et al. (Tsanov et al. 2016; Calvo et al. 2021). *sturkopf*-specific primary probes were selected using the Stellaris Probe designer tool (https://www.biosearchtech.com/support/tools/design-software/stellaris-probe-design). 24 sturkopf-specific primary probes (100 µM) were brought into equimolar solution and afterwards diluted 1:5 in dH_2O to obtain a total concentration of ~0.833 µM/probe. 100 µM of the detector oligonucleotide FLAP-X was annealed with the primary probe mixture using a thermal cycler.

Mixture:		Cycle:	
4 µl	Primary probe mix [0.833 µM/probe]	85 °C	3 min
1 µl	FLAP-X probe [100 µM]	65 °C	3 min
2 µl	NEB 3 (10x)	25 °C	5 min
13 µl	dH_2O		

Annealed probes were either put on ice for direct use or stored at -20 °C.

Accessory glands of 7 days-old *sturkopf* Ctrl and *sturkopf[35.7]* males were dissected, fixed and permeabilized as described in 4.2.4.1. Annealed probes were diluted in smiFISH hybridization buffer to a final concentration of 80 nM. Prior to the hybridization reaction, competitor DNA was prepared by combining 100 µl of 10 mg/ml herring sperm DNA with 100 µl of 10 mg/ml *E. coli* tRNA. A hybridization reaction was performed subsequently.

Mixture:

23 µl	Urea [14 M]
8 µl	SSC buffer (20x)
40 µl	Dextran sulfate (20 %)
3.5 µl	Ribonucleoside vanadyl complex
1.5 µl	Competitor DNA
2 µl	hybridized probes
ad 80 µl	dH_2O

Tissues were hybridized for 14 h at 37 °C and samples were protected from light. Afterwards, tissues were washed thrice for 10 minutes using smiFISH wash buffer and lastly washed once with PBST for 10 minutes. Finally, tissues were stained for DNA using Hoechst33342 (1:200) for 30-60 minutes, washed once with PBS and mounted using Prolong Gold.

4.2.4.4 Confocal microscopy

Confocal microscopy was performed using the LSM 710 Confocal Laser Scanning Microscope (63x oil immersion objective) and the Operetta CLS High Content Analysis System (5x and 40x air objective). All samples were recorded in Z-stacks. The analysis of the specimens was performed using maximum intensity projections and by means of the Zen Blue or Harmony software.

4.2.5 *Drosophila melanogaster* methods

4.2.5.1 Fly husbandry and genetics

Flies were kept according to the methods of Ashburner (Ashburner 1989) in cultivation tubes on standard diet (4.1.11, table 14), in a 12 hour:12-hour light-dark cycle at 25 °C and 50–60 % humidity. Unless stated differently, all experiments were performed using 7 days-old mated male flies. The used fly lines are listed in 4.1.12, table 15.

For crossings, at least 5 female virgin flies were put together with 2 male flies in a new cultivation tube. For an increased number of descendants, the number of female and male flies was adapted.

Homozygous *esg;Ctrl* and *esg;35.7* were reared on 18 °C as the constructs include a temperature sensitive Gal80^{ts} repressor which represses Gal4 transgene activation. 1-day old flies were transferred to 29 °C. The temperature shift induces a conformational change of the Gal80^{ts} resulting its inability to repress Gal4, thus ensuring transgene expression. *esg;Ctrl* and *esg;35.7* were reared for 6 days on 29 °C.

Crossings involving *esg;Ctrl* and *esg;35.7* were reared as described before. Crosses were kept for 6 days at 29 °C. Afterwards, the crosses were put back to the restrictive temperature of 18 °C for 3 days.

To test for a timepoint-dependent impact of the temperature shift, late L3 larvae or prepupal animals reared on 18 °C, were transferred to and kept on 29 °C until the adults were 7 days old (Kubo et al. 2018). Afterwards, the crosses were put back to the restrictive temperature of 18 °C for 3 days.

4.2.5.2 Isolation of adult *Drosophila* hemolymph

Isolation of adult *Drosophila* hemolymph was performed for the measurement of 20-hydroxyecdysone (20HE) hemolymph titers of 7 days old virgin and mated female and male *sturkopf* Ctrl and *sturkopf;35.7* animals. For each biological replicate, 3x30 animals per sex, genotype and mating status were pierced in the thorax with a fine needle and transferred to a 200 µl bottom-punctured PCR tube. The PCR tube was put into a 1.5 ml reaction tube and hemolymph was then harvested by centrifugation for 5 minutes at 5000x g for 5 minutes at room temperature. The total weight of flies and reaction tubes was determined prior to and after the centrifugation. Animal preparation was performed at similar day times to minimize circadian rhythm-dependent 20HE fluxes. 500 µl methanol were added to isolated hemolymph samples and centrifuged at 12.000x g and 4 °C for 20 minutes. The supernatant was transferred to a new 1.5 ml reaction tube and hemolymph was lyophilized by evaporation of the methanol and 20HE was resuspended in 100 µl EIA buffer (provided with the 20-Hydroxyecdysone Enzyme Immunoassay kit) and stored at -20 °C.

4.2.6 Data analysis and statistics

Unless stated differently, data analyses were performed using Microsoft Excel and GraphPad Prism. Statistical analyses of independent samples were performed using a two-tailed, unpaired t-test, if not stated differently. Significant differences were marked by asterisks with the following significance levels: p-value>0.05 not significant (n.s.), p<0.05 *, p<0.01 **, p<0.001 ***.

5 Appendix

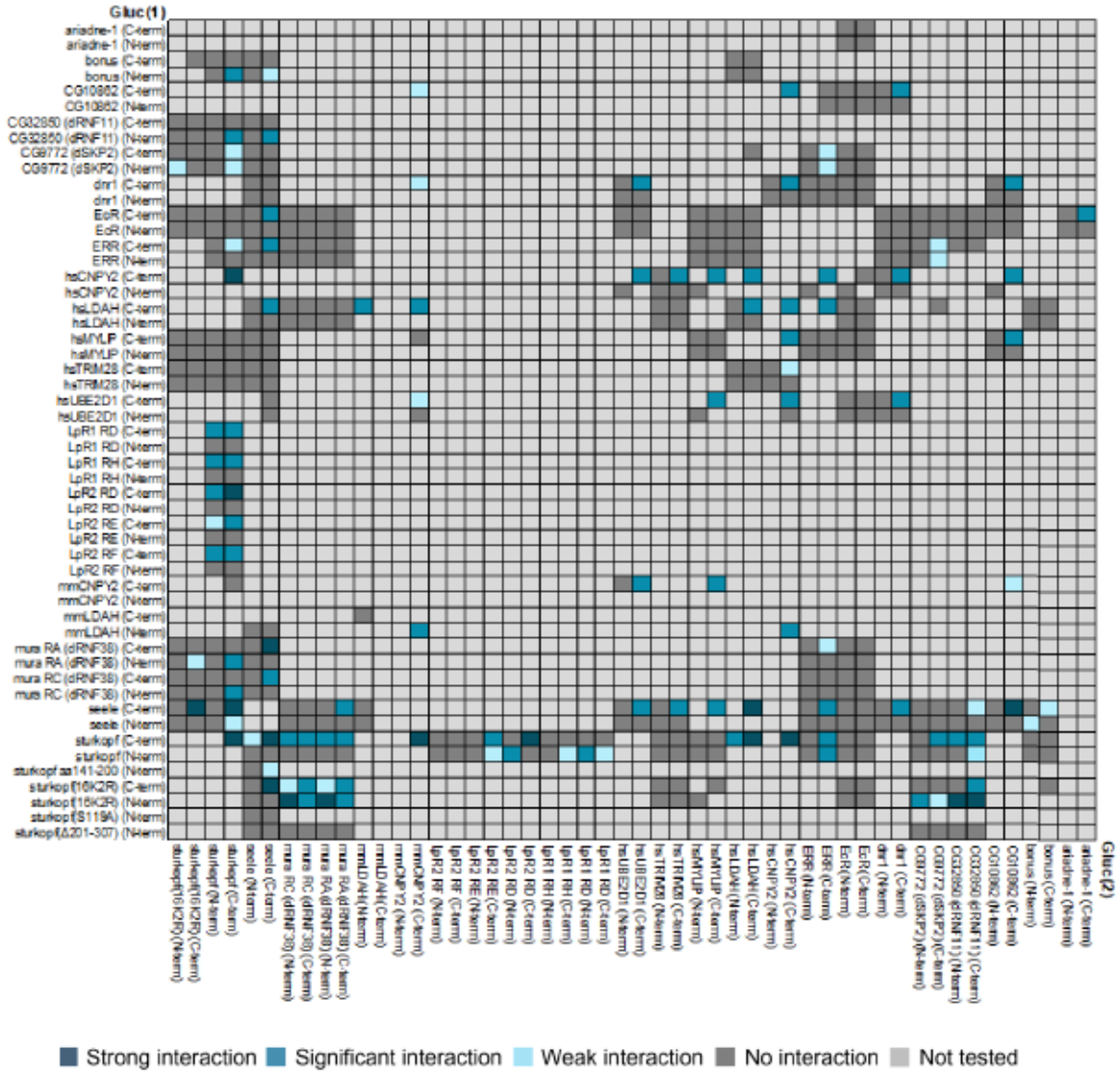

Figure 61: Complete split luciferase complementation PPI results. Split luciferase complementation assay results for co-expression of the indicated proteins in the presence of 400 µM OA for 4 days in *Drosophila* S2R+ cells. A legend explaining the color coding is included in the panel. Threshold levels are indicated as in 4.2.3.6.

Figure 62: Sequencing results from resequencing of pUbiP-sturkopf(S119A)-eGFP to check for the integrity of the construct. The sequencing result shows the amino acid exchange from serine to alanine at position aa119 (marked by yellow square) thus confirming the correctness of the plasmid.

Original sturkopf protein sequence (source: Uniprot)

MQEAYVNINSIPTHIFTWGRWIEETITEKEIVICITGNPGLPGFYTEFAGTLQKELGDL
PVWVIGHAGHDDPPEASIREVPQLSGNEELFNLDGQIRHKIAFIEKYVPSDVKIHLIG
HSIGAWMILQLLENERIRSRIQKCYMLFPTVERMMESPNGWVFTKVAMPLYSVFGYI
FFSFFNFLPVWLRLMLIQIYFLIFSIPRQFLGTALKYSKPSVAEKVVFLADDEMARVRG
IQREIVEQNLDLLKFYYGTTDGWVPISYYDQLKKDYPKVDAQLDTKKIDHAFVLRHS
QPMAVIVRDMIQQHRRV

➔ **Sequencing data of pUbiP-sturkopf(S119A)-eGFP (fwd sequencing)**

TLVTTLTYGVQCFSRYPDHMKQHDFFKSAMPEGYVQERTIFFKDDGNYKTRAEVKF
EGDTLVNRIEKGIDFKEDGNILGHKLEYNYNSHNVYIMADKQNGIKVNFKIRHNIEDG
SVQLADHYQQNTPIGDGPVLLPDNHYLSTQSALSKDPNEKRDHMVLLEFVTAAGITL
RMDELYKASDITSLYKKAGSAAATMQEAYVNINSIPTHIFTWGRWIEETITEKEIVICIT
GNPGLPGFYTEFAGTLQKELGDLPVWVIGHAGHDDPPEASIREVPQLSGNEELFNL
DGQIRHKIAFIEKYVPSDVKIHLIGHA

Coding sequences for molecular cloning of target genes:

dmAriadne (source: FlyBase):

ATGGACTCGGACAATGACAATGATTTCTGCGATAATGTCGATTCGGGCAACGTCTCCTC
GGGCGACGACGGCGATGATGACTTTGGCATGGAGGTGGACCTGCCAAGCTCCGCGGA
CCGCCAGATGGACCAAGATGACTACCAGTACAAGGTGCTCACCACCGATGAGATTGTG
CAACACCAGCGCGAGATCATCGACGAAGCCAATCTGCTGCTGAAGCTACCCACACCCA
CCACACGGATACTGCTAAATCACTTCAAGTGGGACAAGGAGAAGCTATTGGAGAAGTAC
TTCGACGACAACACTGATGAGTTCTTCAAATGCGCACATGTCATAAATCCTTTCAACGCC
ACCGAAGCGATCAAACAAAAGACCTCACGCAGTCAGTGCGAAGAGTGCGAAATATGCTT
TTCACAGCTCCCGCCAGATTCCATGGCCGGGCTGGAATGCGGACACCGATTCTGCATG
CCCTGTTGGCACGAGTATCTGTCAACGAAGATCGTGGCGGAGGGTCTGGGCCAGACCA
TTTCGTGCGCGGCGCACGGCTGTGATATCCTGGTGGACGACGTGACCGTCGCCAACCT
AGTGACGGACGCACGGGTGCGGGTCAAGTACCAGCAGCTGATCACCAATAGCTTTGTG
GAGTGCAACCAGCTGCTGCGCTGGTGTCCGTCCGTCGACTGCACCTATGCGGTGAAGG
TGCCGTACGCGGAGCCACGTCGCGTCCATTGCAAATGCGGCCATGTCTTCTGCTTTGC
CTGCGGCGAGAACTGGCACGATCCGGTCAAGTGCCGTTGGCTAAAGAAGTGGATCAAG
AAGTGTGACGACGACTCGGAGACGTCCAACTGGATCGCGGCCAATACCAAAGAGTGTC
CCAGGTGCAGCGTGACCATCGAGAAGGACGGCGGCTGCAACCACATGGTGTGCAAGA
ACCAGAACTGCAAAAACGAGTTCTGCTGGGTGTGCCTCGGTTCTTGGGAGCCGCACGG
CTCCTCCTGGTACAACTGCAATCGCTATGACGAGGACGAGGCCAAGACGGCCCGCGAT
GCTCAGGAGAAGCTGCGCTCCTCGCTGGCCAGATATCTCCACTACTACAATCGCTACAT
GAACCACATGCAGTCGATGAAGTTTGAGAACAAATTGTATGCATCTGTGAAGCAAAAGA
TGGAGGAGATGCAACAGCACAACATGTCATGGATTGAGGTGCAGTTTCTGAAAAAGGCT
GTCGACATACTTTGCCAGTGCCGTCAGACTCTCATGTACACGTACGTGTTTGCATATTAC
TTGAAAAAGAACAATCAATCCATGATATTCGAGGATAATCAAAAGGACTTGGAGTCGGCA
ACCGAGATGTTGTCGGAGTATTTGGAACGTGATATTACATCCGAGAATTTGGCTGATATT
AAGCAGAAAGTGCAAGATAAATACAGGTATTGTGAAAAGCGGTGCTCTGTTCTGCTGAA
GCACGTGCACGAGGGGTACGACAAGGAGTGGTGGGAGTACACAGAATGA

hsCNPY2 (variant 1, source: NCBI):

ATGAAAGGCTGGGGTTGGCTGGCCCTGCTTCTGGGGGCCCTGCTGGGAACCGCCTGG
GCTCGGAGGAGCCAGGATCTCCACTGTGGAGCATGCAGGGCTCTGGTGGATGAACTAG
AATGGGAAATTGCCCAGGTGGACCCCAAGAAGACCATTCAGATGGGATCTTTCCGGATC
AATCCAGATGGCAGCCAGTCAGTGGTGGAGGTGCCTTATGCCCGCTCAGAGGCCCACC
TCACAGAGCTGCTGGAGGAGATATGTGACCGGATGAAGGAGTATGGGGAACAGATTGA
TCCTTCCACCCATCGCAAGAACTACGTACGTGTAGTGGGCCGGAATGGAGAATCCAGT
GAACTGGACCTACAAGGCATCCGAATCGACTCAGATATTAGCGGCACCCTCAAGTTTGC

GTGTGAGAGCATTGTGGAGGAATACGAGGATGAACTCATTGAATTCTTTTCCCGAGAGG
CTGACAATGTTAAAGACAAACTTTGCAGTAAGCGAACAGATCTTTGTGACCATGCCCTG
CACATATCGCATGATGAGCTATGA

hsLDAH (variant 1, source: NCBI):

ATGGACTCAGAACTCAAGGAAGAAATTCCTGTGCATGAGGAATTCATTTTGTGTGGTGG
AGCCGAAACCCAGGTTCTAAAATGTGGGCCCTGGACAGACCTCTTTCATGATCAAAGTG
TCAAAAGGCCTAAGCTGCTTATTTTCATTATTCCTGGTAACCCAGGTTTTTCTGCCTTTTA
TGTGCCATTTGCAAAGGCTTTATACTCTTTGACAAACAGACGCTTTCCAGTTTGGACTAT
CAGTCATGCTGGGCATGCGTTGGCTCCCAAAGACAAGAAGATTCTTACAACATCAGAGG
ATTCAAACGCTCAAGAAATTAAGGACATTTATGGACTAAATGGACAAATAGAGCACAAAC
TAGCTTTCCTGAGAACTCATGTGCCAAAGGACATGAAACTTGTGCTCATTGGCCATTCAA
TAGGCAGCTATTTCACACTTCAGATGCTGAAGCGAGTCCCTGAGCTCCCGGTAATTCGT
GCCTTTCTGCTCTTTCCAACAATTGAACGAATGTCTGAGTCACCCAATGGCAGAATTGCC
ACTCCACTTTTGTGCTGGTTTCGATATGTTCTCTATGTTACTGGCTACTTATTATTGAAAC
CGTGTCCTGAGACAATCAAGTCCTTGCTAATCAGAAGGGGCCTTCAAGTAATGAACCTA
GAGAATGAATTTTCACCATTGAATATATTAGAACCATTCTGCCTTGCTAATGCTGCCTAC
CTTGGGGGCCAAGAAATGATGGAGGTGGTGAAGAGAGATGACGAAACCATAAAGGAGC
ATTTATGTAAGCTTACATTTTATTATGGTACTATAGATCCTTGGTGTCCAAAAGAGTACTA
TGAAGACATTAAGAAGGATTTTCCAGAAGGAGACATTCGACTCTGTGAGAAAAACATAC
CTCATGCTTTCATCACCCATTTTAACCAGGAAATGGCAGACATGATTGCTGACTCCCTAA
AGGATGACTTGTCCAAAATGTAA

mmCNPY2 (predicted variant 2, source: NCBI):

ATGCGAGCGTCAGAGGCTGTGGGCGCACTGAGGTGGAGCGACCCTGTTACACTAAAGA
TGAAAGGCTGGGGTTGGCTAGCCCTACTTTTGGGGGTCCTGCTGGGAACTGCCTGGGC
TCGAAGGAGCCAAGATCTACACTGTGGAGCTTGCAGGGCTCTGGTGGATGAATTAGAG
TGGGAAATTGCCCGCGTGGACCCCAAGAAGACCATTCAGATGGGATCCTTCCGAATCA
ATCCAGATGGCAGCCAGTCAGTTGTGGAGGTACCTTATGCCCGCTCAGAGGCCCACCT
CACAGAGTTGCTTGAGGAGGTGTGTGACCGAATGAAGGAGTACGGGGAACAGATTGAC
CCTTCTACCCACCGCAAGAACTACGTACGCGTCGTGAGCCGGAATGGAGAATCCAGTG
AACTAGACTTACAGGGCATCCGAATTGACTCAGATATCAGCGGCACCCTCAAGTTTGCG
TGTGAGAGCATTGTGGAAGAATACGAGGATGAGCTTATCGAATTCTTCTCCAGAGAGGC
TGACAACGTTAAAGACAAACTTTGCAGTAAGCGGACAGATCTATGTGACCATGCCCTGC
ACAGATCTCACGATGAGCTATGA

hsMYLIP (source: Kegg, #29116):

ATGCTGTGTTATGTGACGAGGCCGGACGCGGTGCTGATGGAGGTGGAGGTGGAGGCG
AAAGCCAACGGCGAGGACTGCCTCAACCAGGTGTGCAGGCGACTGGGAATCATAGAAG
TTGACTATTTTGGACTGCAGTTTACGGGTAGCAAAGGTGAAAGTTTATGGCTAAACCTGA

GAAACCGGATCTCCCAGCAGATGGATGGGCTAGCCCCTTACAGGCTTAAACTTAGAGTC
AAGTTCTTCGTGGAGCCTCATCTCATCTTACAGGAGCAGACTAGGCATATCTTTTTCTTG
CACATCAAGGAGGCCCTCTTGGCAGGCCACCTCTTGTGTTCCCCAGAGCAGGCAGTGG
AACTCAGTGCCCTCCTGGCCCAGACCAAGTTTGGAGACTACAACCAGAACACTGCCAA
GTATAACTATGAGGAGCTCTGTGCCAAGGAGCTCTCCTCTGCCACCTTGAACAGCATTG
TTGCAAAACATAAGGAGTTGGAGGGGACCAGCCAGGCTTCAGCTGAATACCAAGTTTTG
CAGATTGTGTCGGCAATGGAAAACTATGGCATAGAATGGCATTCTGTGCGGGATAGCGA
AGGGCAGAAACTGCTCATTGGGGTTGGACCTGAAGGAATCTCAATTTGTAAAGATGACT
TTAGCCCAATTAATAGGATAGCTTATCCTGTGGTGCAGATGGCCACCCAGTCAGGAAAG
AATGTATATTTGACGGTCACCAAGGAATCTGGGAACAGCATCGTGCTCTTGTTTAAAATG
ATCAGCACCAGGGCGGCCAGCGGGCTCTACCGAGCGATAACAGAGACGCACGCATTCT
ACAGGTGTGACACAGTGACCAGCGCCGTGATGATGCAGTATAGCCGTGACTTAAGGGC
CACTTGGCATCTCTGTTTCTGAATGAAAACATTAACCTTGGCAAGAAATATGTCTTTGATA
TTAAAAGAACATCAAAGGAGGTGTATGACCATGCCAGGAGGGCTCTGTACAATGCTGGC
GTTGTGGACCTCGTTTCAAGAAACAACCAGAGCCCTTCACACTCGCCTCTGAAGTCCTC
AGAAAGCAGCATGAACTGCAGCAGCTGCGAGGGCCTCAGCTGCCAGCAGACCCGGGT
GCTGCAGGAGAAGCTACGCAAGCTGAAGGAAGCCATGCTGTGCATGGTGTGCTGCGAG
GAGGAGATCAACTCCACCTTCTGTCCCTGTGGCCACACTGTGTGCTGTGAGAGCTGCG
CCGCCCAGCTACAGTCATGTCCCGTCTGCAGGTCGCGTGTGGAGCATGTCCAGCACGT
CTATCTGCCAACGCACACCAGTCTTCTCAATCTGACTGTAATCTAA

hsTRIM28 (source: Kegg, #10155):

ATGGCGGCCTCCGCGGCGGCAGCCTCGGCAGCAGCGGCCTCGGCCGCCTCTGGCAG
CCCGGGCCCGGGCGAGGGCTCCGCTGGCGGCGAAAAGCGCTCCACCGCCCCTTCGG
CCGCAGCCTCGGCCTCTGCCTCAGCCGCGGCGTCGTCGCCCGCGGGGGGCGGCGCC
GAGGCGCTGGAGCTGCTGGAGCACTGCGGCGTGTGCAGAGAGCGCCTGCGACCCGA
GAGGGAGCCCCGCCTGCTGCCCTGTTTGCACTCGGCCTGTAGTGCCTGCTTAGGGCCC
GCGGCCCCCGCCGCCGCCAACAGCTCGGGGGACGGCGGGGCGGCGGGCGACGGCA
CCGTGGTGGACTGTCCCGTGTGCAAGCAACAGTGCTTCTCCAAAGACATCGTGGAGAA
TTATTTCATGCGTGATAGTGGCAGCAAGGCTGCCACCGACGCCCAGGATGCGAACCAG
TGCTGCACTAGCTGTGAGGATAATGCCCCAGCCACCAGCTACTGTGTGGAGTGCTCGG
AGCCTCTGTGTGAGACCTGTGTAGAGGCGCACCAGCGGGTGAAGTACACCAAGGACCA
TACTGTGCGCTCTACTGGGCCAGCCAAGTCTCGGGATGGTGAACGTACTGTCTATTGCA
ACGTACACAAGCATGAACCCCTTGTGCTGTTTTGTGAGAGCTGTGATACTCTCACCTGC
CGAGACTGCCAGCTCAATGCCCACAAGGACCACCAGTACCAGTTCTTAGAGGATGCAG
TGAGGAACCAGCGCAAGCTCCTGGCCTCACTGGTGAAGCGCCTTGGGGACAACATGCA
ACATTGCAGAAGAGCACCAAGGAGGTTCGCAGCTCAATCCGCCAGGTGTCTGACGTAC
AGAAGCGTGTGCAAGTGGATGTCAAGATGGCCATCCTGCAGATCATGAAGGAGCTGAA

TAAGCGGGGCCGTGTGCTGGTCAATGATGCCCAGAAGGTGACTGAGGGGCAGCAGGA
GCGCCTGGAGCGGCAGCACTGGACCATGACCAAGATCCAGAAGCACCAGGAGCACATT
CTGCGCTTTGCCTCTTGGGCTCTGGAGAGTGACAACAACACAGCCCTTTTGCTTTCTAA
GAAGTTGATCTACTTCCAGCTGCACCGGGCCCTCAAGATGATTGTGGATCCCGTGGAG
CCACATGGCGAGATGAAGTTTCAGTGGGACCTCAATGCCTGGACCAAGAGTGCCGAGG
CCTTTGGCAAGATTGTGGCAGAGCGTCCTGGCACTAACTCAACAGGCCCTGCACCCAT
GGCCCCTCCAAGAGCCCCAGGGCCCCTGAGCAAGCAGGGCTCTGGCAGCAGCCAGCC
CATGGAGGTGCAGGAAGGCTATGGCTTTGGGTCAGGAGATGATCCCTACTCAAGTGCA
GAGCCCCATGTGTCAGGTGTGAAACGGTCCCGCTCAGGTGAGGGCGAGGTGAGCGGC
CTTATGCGCAAGGTGCCACGAGTGAGCCTTGAACGCCTGGACCTGGACCTCACAGCTG
ACAGCCAGCCACCCGTCTTCAAGGTCTTCCCAGGCAGTACCACTGAGGACTACAACCTT
ATTGTTATTGAACGTGGCGCTGCCGCTGCAGCTACCGGCCAGCCAGGGACTGCGCCTG
CAGGAACCCCTGGTGCCCCACCCCTGGCTGGCATGGCCATTGTCAAGGAGGAGGAGA
CGGAGGCTGCCATTGGAGCCCCTCCTACTGCCACTGAGGGCCCTGAGACCAAACCTGT
GCTTATGGCTCTTGCGGAGGGTCCTGGTGCTGAGGGTCCCCGCCTGGCCTCACCTAGT
GGCAGCACCAGCTCAGGGCTGGAGGTGGTGGCTCCTGAGGGTACCTCAGCCCCAGGT
GGTGGCCCGGGAACCCTGGATGACAGTGCCACCATTTGCCGTGTCTGCCAGAAGCCAG
GCGATCTGGTTATGTGCAACCAGTGTGAGTTTTGTTTCCACCTGGACTGTCACCTGCCG
GCCCTGCAGGATGTACCAGGGGAGGAGTGGAGCTGCTCACTCTGCCATGTGCTCCCTG
ACCTGAAGGAGGAGGATGGCAGCCTCAGCCTGGATGGTGCAGACAGCACTGGCGTGG
TGGCCAAGCTCTCACCAGCCAACCAGCGGAAATGTGAGCGTGTACTGCTGGCCCTATT
CTGTCACGAACCCTGCCGCCCCCTGCATCAGCTGGCTACCGACTCCACCTTCTCCCTG
GACCAGCCCGGTGGCACCCTGGATCTGACCCTGATCCGTGCCCGCCTCCAGGAGAAG
TTGTCACCTCCCTACAGCTCCCCACAGGAGTTTGCCCAGGATGTGGGCCGCATGTTCAA
GCAATTCAACAAGTTAACTGAGGACAAGGCAGACGTGCAGTCCATCATCGGCCTGCAG
CGCTTCTTCGAGACGCGCATGAACGAGGCCTTCGGTGACACCAAGTTCTCTGCTGTGC
TGGTGGAGCCCCCGCCGATGAGCCTGCCTGGTGCTGGCCTGAGTTCCCAGGAGCTGT
CTGGTGGCCCTGGTGATGGCCCCTGA

hsUBE2D1 (source: Kegg, #7321):

ATGGCGCTGAAGAGGATTCAGAAAGAATTGAGTGATCTACAGCGCGATCCACCTGCTCA
CTGTTCAGCTGGACCTGTGGGAGATGACTTGTTCCACTGGCAAGCCACTATTATGGGGC
CTCCTGATAGCGCATATCAAGGTGGAGTCTTCTTTCTCACTGTACATTTTCCGACAGATT
ATCCTTTTAAACCACCAAAGATTGCTTTCACAACAAAAATTTACCATCCAAACATAAACAG
TAATGGAAGTATTTGTCTCGATATTCTGAGGTCACAATGGTCACCAGCTCTGACTGTATC
AAAAGTTTTATTGTCCATATGTTCTCTACTTTGTGATCCTAATCCAGATGACCCCTTAGTA
CCAGATATTGCACAAATCTATAAATCAGACAAAGAAAAATACAACAGACATGCAAGAGAA
TGGACTCAGAAATATGCAATGTAA

Acknowledgements

I would like to express my gratitude to all the people who stood by me and supported me during my doctoral thesis.

In the first place, I would like to express my greatest thanks to my supervisor Dr. Mathias Beller who gave me the opportunity to work on this dissertation in his group. I especially appreciated his constructive criticism and the fact that he offered me the space to work autonomously on the project and to contribute to it with my own ideas. Even in the very stressful final phase of the doctoral thesis, he proved to be an engaging and eager mentor in many respects.

Second, I want to thank Prof. Dr. Thomas Klein for being the second referee of this doctoral thesis. Furthermore, I would like to thank the entire AG Klein and the AG Reiff for providing premises, materials, as well as samples for my work.

My infinite gratitude goes to my working group. You have been a really great team and I had lots of fun working with you. It's a pity that we did not have the chance to work side by side and support each other until the end. Petra, I owe you a lot, not only for your professional competence, but also just for your personality and your emotional support. Words cannot express how grateful I am for everything. Andrea, you have been such a great team member as well, always ready to help when help was needed. And lastly, Jürgen, without you as my colleague, office buddy and friend, it would have been much harder to get through all this. I also thank all of my students I supervised during my doctoral thesis. I also want to thank Nida for our unforgettable times and emotional support during our “Pausen”. The same applies to Jule and Kathi aka the “Selbsthilfe e.V.”.

Not least, I want to thank my family and friends for the moral support I received during my studies and doctorate at Heinrich-Heine-Universität Düsseldorf. Especially, Besart and Silvia, I cannot say more than thank you for being there for me all the time. You have always been the biggest support for me during this journey.

Publication bibliography

Adeyo, Oludotun; Horn, Patrick J.; Lee, Sungkyung; Binns, Derk D.; Chandrahas, Anita; Chapman, Kent D.; Goodman, Joel M. (2011): The yeast lipin orthologue Pah1p is important for biogenesis of lipid droplets. In *The Journal of cell biology* 192 (6), pp. 1043–1055. DOI: 10.1083/jcb.201010111.

Akhtar, Irfan; Stewart, Fiona A.; Härle, Anna; Droste, Andrea; Beller, Mathias (2021): Visualization of endogenous gut bacteria in Drosophila melanogaster using fluorescence in situ hybridization. In *PloS one* 16 (2), e0247376. DOI: 10.1371/journal.pone.0247376.

Alexander, Caroline M.; Kasza, Ildiko; Yen, C-L. Eric; Reeder, Scott B.; Hernando, Diego; Gallo, Richard L. et al. (2015): Dermal white adipose tissue: a new component of the thermogenic response. In *Journal of lipid research* 56 (11), pp. 2061–2069. DOI: 10.1194/jlr.R062893.

Álvarez-Garcia, Virginia; Tawil, Yasmine; Wise, Helen M.; Leslie, Nicholas R. (2019): Mechanisms of PTEN loss in cancer: It's all about diversity. In *Seminars in cancer biology* 59, pp. 66–79. DOI: 10.1016/j.semcancer.2019.02.001.

Aoyagi, Tomoyoshi; Terracina, Krista P.; Raza, Ali; Matsubara, Hisahiro; Takabe, Kazuaki (2015): Cancer cachexia, mechanism and treatment. In *World journal of gastrointestinal oncology* 7 (4), pp. 17–29. DOI: 10.4251/wjgo.v7.i4.17.

Asgari, Yazdan; Zabihinpour, Zahra; Salehzadeh-Yazdi, Ali; Schreiber, Falk; Masoudi-Nejad, Ali (2015): Alterations in cancer cell metabolism: the Warburg effect and metabolic adaptation. In *Genomics* 105 (5-6), pp. 275–281. DOI: 10.1016/j.ygeno.2015.03.001.

Ashburner, Michael (1989): Drosophila: A Laboratory Handbook and Manual. Cold Spring Harbor, NY: Cold Spring Harbor Laboratory Press.

Ashburner, Michael; Bergman, Casey M. (2005): Drosophila melanogaster: a case study of a model genomic sequence and its consequences. In *Genome research* 15 (12), pp. 1661–1667. DOI: 10.1101/gr.3726705.

Badalament, R. A.; O'Toole, R. V.; Young, D. C.; Drago, J. R. (1991): DNA ploidy and prostate-specific antigen as prognostic factors in clinically resectable prostate cancer.

In *Cancer* 67 (12), pp. 3014–3023. DOI: 10.1002/1097-0142(19910615)67:12<3014::aid-cncr2820671215>3.0.co;2-u.

Bai, Rubing; Rebelo, Artur; Kleeff, Jörg; Sunami, Yoshiaki (2021): Identification of prognostic lipid droplet-associated genes in pancreatic cancer patients via bioinformatics analysis. In *Lipids Health Dis* 20 (1). DOI: 10.1186/s12944-021-01476-y.

Bairati, A. (1967): Struttura ed ultrastruttura dell'apparato genitale maschile di Drosophila melanogaster Meig. I. Il testicolo. In *Zeitschrift fur Zellforschung und mikroskopische Anatomie (Vienna, Austria : 1948)* 76 (1), pp. 56–99.

Bangi, Erdem; Murgia, Claudio; Teague, Alexander G. S.; Sansom, Owen J.; Cagan, Ross L. (2016): Functional exploration of colorectal cancer genomes using Drosophila. In *Nature Communications* 7, p. 13615. DOI: 10.1038/ncomms13615.

Becker, A.; Schlöder, P.; Steele, J. E.; Wegener, G. (1996): The regulation of trehalose metabolism in insects. In *Experientia* 52 (5), pp. 433–439. DOI: 10.1007/BF01919312.

Beller, Mathias; Riedel, Dietmar; Jänsch, Lothar; Dieterich, Guido; Wehland, Jürgen; Jäckle, Herbert; Kühnlein, Ronald P. (2006): Characterization of the Drosophila lipid droplet subproteome. In *Molecular & cellular proteomics : MCP* 5 (6), pp. 1082–1094. DOI: 10.1074/mcp.M600011-MCP200.

Bender, M.; Imam, F. B.; Talbot, W. S.; Ganetzky, B.; Hogness, D. S. (1997): Drosophila ecdysone receptor mutations reveal functional differences among receptor isoforms. In *Cell* 91 (6), pp. 777–788. DOI: 10.1016/s0092-8674(00)80466-3.

Bernard, P.; Couturier, M. (1992): Cell killing by the F plasmid CcdB protein involves poisoning of DNA-topoisomerase II complexes. In *Journal of molecular biology* 226 (3), pp. 735–745. DOI: 10.1016/0022-2836(92)90629-x.

Bertram, M. J.; Akerkar, G. A.; Ard, R. L.; Gonzalez, C.; Wolfner, M. F. (1992): Cell type-specific gene expression in the Drosophila melanogaster male accessory gland. In *Mechanisms of Development* 38 (1), pp. 33–40. Available online at http://dx.doi.org/10.1016/0925-4773(92)90036-J.

Bertram, M. J.; Neubaum, D. M.; Wolfner, M. F. (1996): Localization of the Drosophila male accessory gland protein Acp36DE in the mated female suggests a role in sperm storage. In *Insect biochemistry and molecular biology* 26 (8-9), pp. 971–980. DOI: 10.1016/s0965-1748(96)00064-1.

Bethel, Carlise R.; Faith, Dennis; Li, Xiang; Guan, Bin; Hicks, Jessica L.; Lan, Fusheng et al. (2006): Decreased NKX3.1 protein expression in focal prostatic atrophy, prostatic intraepithelial neoplasia, and adenocarcinoma: association with gleason score and chromosome 8p deletion. In *Cancer research* 66 (22), pp. 10683–10690. DOI: 10.1158/0008-5472.CAN-06-0963.

Bharucha, Kamal N. (2009): The epicurean fly: using Drosophila melanogaster to study metabolism. In *Pediatric research* 65 (2), pp. 132–137. DOI: 10.1203/PDR.0b013e318191fc68.

Bohnert, Maria (2020): Tether Me, Tether Me Not-Dynamic Organelle Contact Sites in Metabolic Rewiring. In *Developmental cell* 54 (2), pp. 212–225. DOI: 10.1016/j.devcel.2020.06.026.

Bornhauser, B. C.; Lindholm, D. (2005): MSAP enhances migration of C6 glioma cells through phosphorylation of the myosin regulatory light chain. In *Cellular and molecular life sciences* 62 (11), pp. 1260–1266. DOI: 10.1007/s00018-005-5055-x.

Brasaemle, Dawn L.; Subramanian, Vidya; Garcia, Anne; Marcinkiewicz, Amy; Rothenberg, Alexis (2009): Perilipin A and the control of triacylglycerol metabolism. In *Molecular and cellular biochemistry* 326 (1-2), pp. 15–21. DOI: 10.1007/s11010-008-9998-8.

Buch, Susanne; Melcher, Christoph; Bauer, Matthias; Katzenberger, Joerg; Pankratz, Michael J. (2008): Opposing effects of dietary protein and sugar regulate a transcriptional target of Drosophila insulin-like peptide signaling. In *Cell metabolism* 7 (4), pp. 321–332. DOI: 10.1016/j.cmet.2008.02.012.

Buchanan, Bryce W.; Lloyd, Michael E.; Engle, Sarah M.; Rubenstein, Eric M. (2016): Cycloheximide Chase Analysis of Protein Degradation in Saccharomyces cerevisiae. In *Journal of visualized experiments : JoVE* (110). DOI: 10.3791/53975.

Buhman, K. K.; Chen, H. C.; Farese, R. V. (2001): The enzymes of neutral lipid synthesis. In *The Journal of biological chemistry* 276 (44), pp. 40369–40372. DOI: 10.1074/jbc.R100050200.

Bujdoso, Raymond; Smith, Andrew; Fleck, Oliver; Spiropoulos, John; Andréoletti, Olivier; Thackray, Alana M. (2022): Prion disease modelled in Drosophila. In *Cell and tissue research*. DOI: 10.1007/s00441-022-03586-0.

Caldwell, Philip E.; Walkiewicz, Magdalena; Stern, Michael (2005): Ras activity in the Drosophila prothoracic gland regulates body size and developmental rate via ecdysone release. In *Current biology : CB* 15 (20), pp. 1785–1795. DOI: 10.1016/j.cub.2005.09.011.

Calvo, Llilians; Ronshaugen, Matthew; Pettini, Tom (2021): smiFISH and embryo segmentation for single-cell multi-gene RNA quantification in arthropods. In *Communications biology* 4 (1), p. 352. DOI: 10.1038/s42003-021-01803-0.

Cannon, Barbara; Nedergaard, Jan. (2004): Brown Adipose Tissue: Function and Physiological Significance. In *Physiological Reviews* 84 (1), pp. 277–359. DOI: 10.1152/physrev.00015.2003.

Carman, George M.; Han, Gil-Soo (2009): Phosphatidic acid phosphatase, a key enzyme in the regulation of lipid synthesis. In *The Journal of biological chemistry* 284 (5), pp. 2593–2597. DOI: 10.1074/jbc.R800059200.

Carney, G. E.; Bender, M. (2000): The Drosophila ecdysone receptor (EcR) gene is required maternally for normal oogenesis. In *Genetics* 154 (3), pp. 1203–1211. DOI: 10.1093/genetics/154.3.1203.

Castle, W. E. (1906): INBREEDING, CROSS-BREEDING AND STERILITY IN DROSOPHILA. In *Science (New York, N.Y.)* 23 (578), p. 153. DOI: 10.1126/science.23.578.153.

Celniker, Susan E.; Dillon, Laura A. L.; Gerstein, Mark B.; Gunsalus, Kristin C.; Henikoff, Steven; Karpen, Gary H. et al. (2009): Unlocking the secrets of the genome. In *Nature* 459 (7249), pp. 927–930. DOI: 10.1038/459927a.

Cermelli, Silvia; Guo, Yi; Gross, Steven P.; Welte, Michael A. (2006): The lipid-droplet proteome reveals that droplets are a protein-storage depot. In *Current biology : CB* 16 (18), pp. 1783–1795. DOI: 10.1016/j.cub.2006.07.062.

Chapman, K. B.; Wolfner, M. F. (1988): Determination of male-specific gene expression in Drosophila accessory glands. In *Developmental Biology* 126 (1), pp. 195–202. Available online at http://dx.doi.org/10.1016/0012-1606(88)90253-9.

Chapman, Tracey; Bangham, Jenny; Vinti, Giovanna; Seifried, Beth; Lung, Oliver; Wolfner, Mariana F. et al. (2003): The sex peptide of Drosophila melanogaster: female post-mating responses analyzed by using RNA interference. In *Proceedings of the National Academy of Sciences of the United States of America* 100 (17), pp. 9923–9928. DOI: 10.1073/pnas.1631635100.

Chartschenko, Eugenia; Hugenroth, Marie; Akhtar, Irfan; Droste, Andrea; Kolkhof, Petra; Bohnert, Maria; Beller, Mathias (2021): CG32803 is the fly homolog of LDAF1 and influences lipid storage in vivo. In *Insect biochemistry and molecular biology* 133, p. 103512. DOI: 10.1016/j.ibmb.2020.103512.

Chatterjee, Nirmalya; Perrimon, Norbert (2021): What fuels the fly: Energy metabolism in Drosophila and its application to the study of obesity and diabetes. In *Science advances* 7 (24). DOI: 10.1126/sciadv.abg4336.

Chen, Fang; Yan, Bing; Ren, Jie; Lyu, Rui; Wu, Yanfang; Guo, Yuting et al. (2021): FIT2 organizes lipid droplet biogenesis with ER tubule-forming proteins and septins. In *The Journal of cell biology* 220 (5). DOI: 10.1083/jcb.201907183.

Chen, S. y.; Wang, J.; Yu, G. q.; Liu, W.; Pearce, D. (1997): Androgen and glucocorticoid receptor heterodimer formation. A possible mechanism for mutual inhibition of transcriptional activity. In *The Journal of biological chemistry* 272 (22), pp. 14087–14092. DOI: 10.1074/jbc.272.22.14087.

Chintapalli, Venkateswara R.; Wang, Jing; Dow, Julian A. T. (2007): Using FlyAtlas to identify better Drosophila melanogaster models of human disease. In *Nature genetics* 39 (6), pp. 715–720. DOI: 10.1038/ng2049.

Cinti, S. (2005): The adipose organ. In *Prostaglandins, Leukotrienes and Essential Fatty Acids* 73 (1), pp. 9–15. DOI: 10.1016/j.plefa.2005.04.010.

Cinti, Saverio (2009): Transdifferentiation properties of adipocytes in the adipose organ. In *American journal of physiology. Endocrinology and metabolism* 297 (5), E977-E986. DOI: 10.1152/ajpendo.00183.2009.

Colombani, Julien; Bianchini, Laurence; Layalle, Sophie; Pondeville, Emilie; Dauphin-Villemant, Chantal; Antoniewski, Christophe et al. (2005): Antagonistic actions of ecdysone and insulins determine final size in Drosophila. In *Science (New York, N.Y.)* 310 (5748), pp. 667–670. DOI: 10.1126/science.1119432.

Cook, R. Kimberley (2012): The generation of chromosomal deletions to provide extensive coverage and subdivision of the Drosophila melanogaster genome. In *Genome biology* 13 (3), pp. 1–14. DOI: 10.1186/gb-2012-13-3-r21.

Corrigan, Laura; Redhai, Siamak; Leiblich, Aaron; Fan, Shih-Jung; Perera, Sumeth M. W.; Patel, Rachel et al. (2014): BMP-regulated exosomes from Drosophila male reproductive glands reprogram female behavior. In *The Journal of cell biology* 206 (5), pp. 671–688. DOI: 10.1083/jcb.201401072.

Costello, L. C.; Franklin, R. B.; Feng, Pei (2005): Mitochondrial function, zinc, and intermediary metabolism relationships in normal prostate and prostate cancer. In *Mitochondrion* 5 (3), pp. 143–153. DOI: 10.1016/j.mito.2005.02.001.

Costello, Leslie C.; Franklin, Renty B. (2011): Zinc is decreased in prostate cancer: an established relationship of prostate cancer! In *Journal of biological inorganic chemistry : JBIC : a publication of the Society of Biological Inorganic Chemistry* 16 (1), pp. 3–8. DOI: 10.1007/s00775-010-0736-9.

Crowley, Fionnuala; Sterpi, Michelle; Buckley, Conor; Margetich, Lauren; Handa, Shivani; Dovey, Zach (2021): A Review of the Pathophysiological Mechanisms Underlying Castration-resistant Prostate Cancer. In *Research and reports in urology* 13, pp. 457–472. DOI: 10.2147/RRU.S264722.

Cruz, André L. S.; Barreto, Ester de A.; Fazolini, Narayana P. B.; Viola, João P. B.; Bozza, Patricia T. (2020): Lipid droplets: platforms with multiple functions in cancer hallmarks. In *Cell death & disease* 11 (2), p. 105. DOI: 10.1038/s41419-020-2297-3.

Culig, Zoran; Santer, Frédéric R. (2014): Androgen receptor signaling in prostate cancer. In *Cancer metastasis reviews* 33 (2-3), pp. 413–427. DOI: 10.1007/s10555-013-9474-0.

Currall, Benjamin B.; Chen, Ming; Sallari, Richard C.; Cotter, Maura; Wong, Kristen E.; Robertson, Nahid G. et al. (2018): Loss of LDAH associated with prostate cancer and hearing loss. In *Human molecular genetics* 27 (24), pp. 4194–4203. DOI: 10.1093/hmg/ddy310.

Dai, Charles; Heemers, Hannelore; Sharifi, Nima (2017): Androgen Signaling in Prostate Cancer. In *Cold Spring Harbor perspectives in medicine* 7 (9). DOI: 10.1101/cshperspect.a030452.

Dai, Jie; Su, Yangzhou; Zhong, Suye; Cong, Li; Liu, Bang; Yang, Junjun et al. (2020): Exosomes: key players in cancer and potential therapeutic strategy. In *Signal transduction and targeted therapy* 5 (1), p. 145. DOI: 10.1038/s41392-020-00261-0.

Dai, Zhiyu; Qi, Weiwei; Li, Cen; Lu, Juling; Mao, Yuling; Yao, Yachao et al. (2013): Dual regulation of adipose triglyceride lipase by pigment epithelium-derived factor: a novel mechanistic insight into progressive obesity. In *Molecular and cellular endocrinology* 377 (1-2), pp. 123–134. DOI: 10.1016/j.mce.2013.07.001.

Dansako, Hiromichi; Hiramoto, Hiroki; Ikeda, Masanori; Wakita, Takaji; Kato, Nobuyuki (2014): Rab18 is required for viral assembly of hepatitis C virus through trafficking of the core protein to lipid droplets. In *Virology* 462-463, pp. 166–174. DOI: 10.1016/j.virol.2014.05.017.

Deep, Gagan; Schlaepfer, Isabel R. (2016): Aberrant Lipid Metabolism Promotes Prostate Cancer: Role in Cell Survival under Hypoxia and Extracellular Vesicles Biogenesis. In *International journal of molecular sciences* 17 (7). DOI: 10.3390/ijms17071061.

Deitch, A. D.; Miller, G. J.; deVere White, R. W. (1993): Significance of abnormal diploid DNA histograms in localized prostate cancer and adjacent benign prostatic tissue. In *Cancer* 72 (5), pp. 1692–1700. DOI: 10.1002/1097-0142(19930901)72:5<1692::aid-cncr2820720533>3.0.co;2-8.

Delanoue, Rénald; Slaidina, Maija; Léopold, Pierre (2010): The steroid hormone ecdysone controls systemic growth by repressing dMyc function in Drosophila fat cells. In *Developmental cell* 18 (6), pp. 1012–1021. DOI: 10.1016/j.devcel.2010.05.007.

DiAngelo, Justin R.; Birnbaum, Morris J. (2009): Regulation of fat cell mass by insulin in Drosophila melanogaster. In *Molecular and cellular biology* 29 (24), pp. 6341–6352. DOI: 10.1128/MCB.00675-09.

Dietzl, Georg; Chen, Doris; Schnorrer, Frank; Su, Kuan-Chung; Barinova, Yulia; Fellner, Michaela et al. (2007): A genome-wide transgenic RNAi library for conditional gene inactivation in Drosophila. In *Nature* 448 (7150), pp. 151–156. DOI: 10.1038/nature05954.

Do, Hai Thi; Tselykh, Timofey V.; Mäkelä, Johanna; Ho, Tho Huu; Olkkonen, Vesa M.; Bornhauser, Beat C. et al. (2012): Fibroblast growth factor-21 (FGF21) regulates

low-density lipoprotein receptor (LDLR) levels in cells via the E3-ubiquitin ligase Mylip/Idol and the Canopy2 (Cnpy2)/Mylip-interacting saposin-like protein (Msap). In *The Journal of biological chemistry* 287 (16), pp. 12602–12611. DOI: 10.1074/jbc.M112.341248.

Dorstyn, L.; Colussi, P. A.; Quinn, L. M.; Richardson, H.; Kumar, S. (1999): DRONC, an ecdysone-inducible Drosophila caspase. In *Proceedings of the National Academy of Sciences of the United States of America* 96 (8), pp. 4307–4312. DOI: 10.1073/pnas.96.8.4307.

Du, Meijun; Tillmans, Lori; Gao, Jianzhong; Gao, Ping; Yuan, Tiezheng; Dittmar, Rachel L. et al. (2016): Chromatin interactions and candidate genes at ten prostate cancer risk loci. In *Scientific reports* 6, p. 23202. DOI: 10.1038/srep23202.

Dubey, Ramin; Stivala, Craig E.; Nguyen, Huy Quoc; Goo, Young-Hwa; Paul, Antoni; Carette, Jan E. et al. (2020): Lipid droplets can promote drug accumulation and activation. In *Nature chemical biology* 16 (2), pp. 206–213. DOI: 10.1021/ja411270d.

Dubrovsky, Edward B. (2005): Hormonal cross talk in insect development. In *Trends in endocrinology and metabolism: TEM* 16 (1), pp. 6–11. DOI: 10.1016/j.tem.2004.11.003.

Eacker, Stephen M.; Agrawal, Nalini; Qian, Kun; Dichek, Helén L.; Gong, Eun-Yeung; Lee, Keesook; Braun, Robert E. (2008): Hormonal Regulation of Testicular Steroid and Cholesterol Homeostasis. In *Molecular Endocrinology* 22 (3), pp. 623–635. DOI: 10.1210/me.2006-0534.

Echalier, G.; Ohanessian, A. (1969): Isolement, en cultures in vitro, de lignées cellulaires diploïdes de Drosophila melanogaster. In *Comptes rendus hebdomadaires des seances de l'Academie des sciences. Serie D: Sciences naturelles* 268 (13), pp. 1771–1773.

Edgar, B. A.; Orr-Weaver, T. L. (2001): Endoreplication cell cycles: more for less. In *Cell* 105 (3), pp. 297–306. DOI: 10.1016/s0092-8674(01)00334-8.

Edgar, Bruce A.; Zielke, Norman; Gutierrez, Crisanto (2014): Endocycles: a recurrent evolutionary innovation for post-mitotic cell growth. In *Nature reviews. Molecular cell biology* 15 (3), pp. 197–210. DOI: 10.1038/nrm3756.

Eidelman, Eric; Twum-Ampofo, Jeffrey; Ansari, Jamal; Siddiqui, Mohummad Minhaj (2017): The Metabolic Phenotype of Prostate Cancer. In *Frontiers in oncology* 7, p. 131. DOI: 10.3389/fonc.2017.00131.

Enomoto, T.; Tanuma, S.; Yamada, M. A. (1981): ATP requirement for the processes of DNA replication in isolated HeLa cell nuclei. In *Journal of biochemistry* 89 (3), pp. 801–807. DOI: 10.1093/oxfordjournals.jbchem.a133262.

Fang, Lei; Li, Dongmei; Yin, JuanJuan; Pan, Hong; Ye, Huihui; Bowman, Joel et al. (2022): TMPRSS2-ERG promotes the initiation of prostate cancer by suppressing oncogene-induced senescence. In *Cancer gene therapy* 29 (10), pp. 1463–1476. DOI: 10.1038/s41417-022-00454-5.

Farese, Robert V.; Walther, Tobias C. (2009): Lipid droplets finally get a little R-E-S-P-E-C-T. In *Cell* 139 (5), pp. 855–860. DOI: 10.1016/j.cell.2009.11.005.

Fawcett, Don Wayne (1966): An atlas of fine structure. The cell, its organelles, and inclusions. Philadelphia: W. B. Saunders Co.

Fei, Weihua; Shui, Guanghou; Gaeta, Bruno; Du, Ximing; Kuerschner, Lars; Li, Peng et al. (2008): Fld1p, a functional homologue of human seipin, regulates the size of lipid droplets in yeast. In *The Journal of cell biology* 180 (3), pp. 473–482. DOI: 10.1083/jcb.200711136.

Feinerman, Ofer (2021): Animal Behavior: Drosophila melanogaster Goes Social. In *Current biology : CB* 31 (3), R138-R140. DOI: 10.1016/j.cub.2020.11.047.

Feitelson, Mark A.; Arzumanyan, Alla; Kulathinal, Rob J.; Blain, Stacy W.; Holcombe, Randall F.; Mahajna, Jamal et al. (2015): Sustained proliferation in cancer: Mechanisms and novel therapeutic targets. In *Seminars in cancer biology* 35 Suppl (Suppl), S25-S54. DOI: 10.1016/j.semcancer.2015.02.006.

Feoktistova, Maria; Geserick, Peter; Leverkus, Martin (2016): Crystal Violet Assay for Determining Viability of Cultured Cells. In *Cold Spring Harbor protocols* 2016 (4), pdb.prot087379. DOI: 10.1101/pdb.prot087379.

Flatt, J. P. (1987): The difference in the storage capacities for carbohydrate and for fat, and its implications in the regulation of body weight. In *Annals of the New York Academy of Sciences* 499, pp. 104–123. DOI: 10.1111/j.1749-6632.1987.tb36202.x.

Flatt, J. P. (1995): Use and storage of carbohydrate and fat. In *The American journal of clinical nutrition* 61 (4 Suppl), 952S-959S. DOI: 10.1093/ajcn/61.4.952S.

Fox, Donald T.; Duronio, Robert J. (2013): Endoreplication and polyploidy: insights into development and disease. In *Development (Cambridge, England)* 140 (1), pp. 3–12. DOI: 10.1242/dev.080531.

Franz, M-C; Anderle, P.; Bürzle, M.; Suzuki, Y.; Freeman, M. R.; Hediger, M. A.; Kovacs, G. (2013): Zinc transporters in prostate cancer. In *Molecular aspects of medicine* 34 (2-3), pp. 735–741. DOI: 10.1016/j.mam.2012.11.007.

Friedl, Peter; Wolf, Katarina (2003): Tumour-cell invasion and migration: diversity and escape mechanisms. In *Nature reviews. Cancer* 3 (5), pp. 362–374. DOI: 10.1038/nrc1075.

Friguls, B.; Coroleu, W.; del Alcazar, R.; Hilbert, P.; van Maldergem, L.; Pintos-Morell, G. (2009): Severe cardiac phenotype of Berardinelli-Seip congenital lipodystrophy in an infant with homozygous E189X BSCL2 mutation. In *European journal of medical genetics* 52 (1), pp. 14–16. DOI: 10.1016/j.ejmg.2008.10.006.

Ganter, G. K.; Panaitiu, A. E.; Desilets, J. B.; Davis-Heim, J. A.; Fisher, E. A.; Tan, L. C. H. et al. (2011): Drosophila male courtship behavior is modulated by ecdysteroids. In *Journal of insect physiology* 57 (9), pp. 1179–1184. DOI: 10.1016/j.jinsphys.2011.05.007.

Ghosh, J.; Myers, C. E. (1997): Arachidonic acid stimulates prostate cancer cell growth: critical role of 5-lipoxygenase. In *Biochemical and biophysical research communications* 235 (2), pp. 418–423. DOI: 10.1006/bbrc.1997.6799.

Giancotti, Filippo G. (2013): Mechanisms governing metastatic dormancy and reactivation. In *Cell* 155 (4), pp. 750–764. DOI: 10.1016/j.cell.2013.10.029.

Gilchrist, A. S.; Partridge, L. (2000): Why it is difficult to model sperm displacement in Drosophila melanogaster: the relation between sperm transfer and copulation duration. In *Evolution; international journal of organic evolution* 54 (2), pp. 534–542. DOI: 10.1111/j.0014-3820.2000.tb00056.x.

Gligorov, Dragan; Sitnik, Jessica L.; Maeda, Robert K.; Wolfner, Mariana F.; Karch, François (2013): A novel function for the Hox gene Abd-B in the male accessory

gland regulates the long-term female post-mating response in Drosophila. In *PLoS genetics* 9 (3), e1003395. DOI: 10.1371/journal.pgen.1003395.

Goh, Vera J.; Silver, David L. (2013): The lipid droplet as a potential therapeutic target in NAFLD. In *Seminars in liver disease* 33 (4), pp. 312–320. DOI: 10.1055/s-0033-1358521.

Goo, Young-Hwa; Son, Se-Hee; Kreienberg, Paul B.; Paul, Antoni (2014): Novel lipid droplet-associated serine hydrolase regulates macrophage cholesterol mobilization. In *Arteriosclerosis, thrombosis, and vascular biology* 34 (2), pp. 386–396. DOI: 10.1161/ATVBAHA.113.302448.

Goo, Young-Hwa; Son, Se-Hee; Paul, Antoni (2017): Lipid Droplet-Associated Hydrolase Promotes Lipid Droplet Fusion and Enhances ATGL Degradation and Triglyceride Accumulation. In *Scientific reports* 7 (1), p. 2743. DOI: 10.1038/s41598-017-02963-y.

Gradilla, Ana-Citlali; Mansilla, Alicia; Ferrús, Alberto (2011): Isoform-specific regulation of a steroid hormone nuclear receptor by an E3 ubiquitin ligase in Drosophila melanogaster. In *Genetics* 189 (3), pp. 871–883. DOI: 10.1534/genetics.111.132191.

Graham, P.; Pick, L. (2017): Drosophila as a Model for Diabetes and Diseases of Insulin Resistance. In *Current topics in developmental biology* 121, pp. 397–419. DOI: 10.1016/bs.ctdb.2016.07.011.

Gramates, L. Sian; Marygold, Steven J.; Santos, Gilberto Dos; Urbano, Jose-Maria; Antonazzo, Giulia; Matthews, Beverley B. et al. (2017): FlyBase at 25: looking to the future. In *Nucleic acids research* 45 (D1), D663-D671. DOI: 10.1093/nar/gkw1016.

Greenberg, A. S.; Egan, J. J.; Wek, S. A.; Garty, N. B.; Blanchette-Mackie, E. J.; Londos, C. (1991): Perilipin, a major hormonally regulated adipocyte-specific phosphoprotein associated with the periphery of lipid storage droplets. In *The Journal of biological chemistry* 266 (17), pp. 11341–11346.

Griffin, J. E. (1992): Androgen resistance--the clinical and molecular spectrum. In *The New England journal of medicine* 326 (9), pp. 611–618. DOI: 10.1056/NEJM199202273260906.

Grignon, David J. (2004): Unusual subtypes of prostate cancer. In *Modern pathology : an official journal of the United States and Canadian Academy of Pathology, Inc* 17 (3), pp. 316–327. DOI: 10.1038/modpathol.3800052.

Grönke, Sebastian; Beller, Mathias; Fellert, Sonja; Ramakrishnan, Hariharasubramanian; Jäckle, Herbert; Kühnlein, Ronald P. (2003): Control of fat storage by a Drosophila PAT domain protein. In *Current biology : CB* 13 (7), pp. 603–606. DOI: 10.1016/s0960-9822(03)00175-1.

Gross, David A.; Zhan, Chenyang; Silver, David L. (2011): Direct binding of triglyceride to fat storage-inducing transmembrane proteins 1 and 2 is important for lipid droplet formation. In *Proceedings of the National Academy of Sciences of the United States of America* 108 (49), pp. 19581–19586. DOI: 10.1073/pnas.1110817108.

Grouleff, Julie; Irudayam, Sheeba Jem; Skeby, Katrine K.; Schiøtt, Birgit (2015): The influence of cholesterol on membrane protein structure, function, and dynamics studied by molecular dynamics simulations. In *Biochimica et biophysica acta* 1848 (9), pp. 1783–1795. DOI: 10.1016/j.bbamem.2015.03.029.

Guio, Lain; Barrón, Maite G.; González, Josefa (2014): The transposable element Bari-Jheh mediates oxidative stress response in Drosophila. In *Molecular ecology* 23 (8), pp. 2020–2030. DOI: 10.1111/mec.12711.

Guo, Yi; Cordes, Kimberly R.; Farese, Robert V.; Walther, Tobias C. (2009): Lipid droplets at a glance. In *Journal of cell science* 122 (Pt 6), pp. 749–752. DOI: 10.1242/jcs.037630.

Guruharsha, K. G.; Rual, Jean-François; Zhai, Bo; Mintseris, Julian; Vaidya, Pujita; Vaidya, Namita et al. (2011): A protein complex network of Drosophila melanogaster. In *Cell* 147 (3), pp. 690–703. DOI: 10.1016/j.cell.2011.08.047.

Halder, G.; Mills, G. B. (2011): Drosophila in cancer research: to boldly go where no one has gone before. In *Oncogene* 30 (39), pp. 4063–4066. DOI: 10.1038/onc.2011.128.

Hanahan, D.; Jessee, J.; Bloom, F. R. (1991): Plasmid transformation of Escherichia coli and other bacteria. In *Methods in enzymology* 204, pp. 63–113. DOI: 10.1016/0076-6879(91)04006-a.

Hanahan, D.; Weinberg, R. A. (2000): The hallmarks of cancer. In *Cell* 100 (1), pp. 57–70. DOI: 10.1016/s0092-8674(00)81683-9.

Harnish, J. Michael; Link, Nichole; Yamamoto, Shinya (2021): Drosophila as a Model for Infectious Diseases. In *International journal of molecular sciences* 22 (5). DOI: 10.3390/ijms22052724.

He, W. W.; Sciavolino, P. J.; Wing, J.; Augustus, M.; Hudson, P.; Meissner, P. S. et al. (1997): A novel human prostate-specific, androgen-regulated homeobox gene (NKX3.1) that maps to 8p21, a region frequently deleted in prostate cancer. In *Genomics* 43 (1), pp. 69–77. DOI: 10.1006/geno.1997.4715.

Hedstrom, Lizbeth (2002): An overview of serine proteases. In *Current protocols in protein science* Chapter 21, Unit 21.10. DOI: 10.1002/0471140864.ps2110s26.

Heid, Hans; Franke, Werner (2014): On the formation of lipid droplets in human adipocytes. The organization of the perilipin-vimentin cortex. In *PloS one*. DOI: 10.1371/journal.pone.0090386.

Heinlein, Cynthia A.; Chang, Chawnshang (2004): Androgen receptor in prostate cancer. In *Endocrine reviews* 25 (2), pp. 276–308. DOI: 10.1210/er.2002-0032.

Henne, W. Mike; Reese, Michael L.; Goodman, Joel M. (2018): The assembly of lipid droplets and their roles in challenged cells. In *The EMBO journal* 37 (12). DOI: 10.15252/embj.201898947.

Hentze, Julie L.; Moeller, Morten E.; Jørgensen, Anne F.; Bengtsson, Meghan S.; Bordoy, Anna M.; Warren, James T. et al. (2013): Accessory gland as a site for prothoracicotropic hormone controlled ecdysone synthesis in adult male insects. In *PloS one* 8 (2), e55131. DOI: 10.1371/journal.pone.0055131.

Herker, Eva; Vieyres, Gabrielle; Beller, Mathias; Krahmer, Natalie; Bohnert, Maria (2021): Lipid Droplet Contact Sites in Health and Disease. In *Trends in cell biology* 31 (5), pp. 345–358. DOI: 10.1016/j.tcb.2021.01.004.

Hink, M. A.; Griep, R. A.; Borst, J. W.; van Hoek, A.; Eppink, M. H.; Schots, A.; Visser, A. J. (2000): Structural dynamics of green fluorescent protein alone and fused with a single chain Fv protein. In *The Journal of biological chemistry* 275 (23), pp. 17556–17560. DOI: 10.1074/jbc.M001348200.

Hollander, M. Christine; Blumenthal, Gideon M.; Dennis, Phillip A. (2011): PTEN loss in the continuum of common cancers, rare syndromes and mouse models. In *Nature reviews. Cancer* 11 (4), pp. 289–301. DOI: 10.1038/nrc3037.

Holtze, Susanne; Gorshkova, Ekaterina; Braude, Stan; Cellerino, Alessandro; Dammann, Philip; Hildebrandt, Thomas B. et al. (2021): Alternative Animal Models of Aging Research. In *Frontiers in molecular biosciences* 8, p. 660959. DOI: 10.3389/fmolb.2021.660959.

Hong, Feng; Lin, Ching Ying; Yan, Jingyue; Dong, Yizhou; Ouyang, Yuli; Kim, Doyeon et al. (2022): Canopy Homolog 2 contributes to liver oncogenesis by promoting unfolded protein response-dependent destabilization of tumor protein P53. In *Hepatology (Baltimore, Md.)*. DOI: 10.1002/hep.32318.

Hopkins, Ben R.; Sepil, Irem; Bonham, Sarah; Miller, Thomas; Charles, Philip D.; Fischer, Roman et al. (2019): BMP signaling inhibition in Drosophila secondary cells remodels the seminal proteome and self and rival ejaculate functions. In *Proceedings of the National Academy of Sciences of the United States of America* 116 (49), pp. 24719–24728. DOI: 10.1073/pnas.1914491116.

Horton, Paul A.; Koehn, Frank E.; Longley, Ross E.; McConnell, Oliver J. (1994): Lasonolide A, A New Cytotoxic Macrolide from the Marine Sponge Forcepia sp. In *J. Am. Chem. Soc.* 116 (13), pp. 6015–6016. DOI: 10.1021/ja00092a081.

Houard, X.; Williams, T. A.; Michaud, A.; Dani, P.; Isaac, R. E.; Shirras, A. D. et al. (1998): The Drosophila melanogaster-related angiotensin-I-converting enzymes Acer and Ance--distinct enzymic characteristics and alternative expression during pupal development. In *European journal of biochemistry* 257 (3), pp. 599–606. DOI: 10.1046/j.1432-1327.1998.2570599.x.

Hsieh, Kai; Lee, Yun Kyung; Londos, Constantine; Raaka, Bruce M.; Dalen, Knut Tomas; Kimmel, Alan R. (2012): Perilipin family members preferentially sequester to either triacylglycerol-specific or cholesteryl-ester-specific intracellular lipid storage droplets. In *Journal of cell science* 125 (Pt 17), pp. 4067–4076. DOI: 10.1242/jcs.104943.

Huang, I-Ping; Sun, Shu-Pin; Cheng, Shih-Hsun; Lee, Chia-Hung; Wu, Chia-Yan; Yang, Chung-Shi et al. (2011): Enhanced chemotherapy of cancer using pH-sensitive mesoporous silica nanoparticles to antagonize P-glycoprotein-mediated drug

resistance. In *Molecular cancer therapeutics* 10 (5), pp. 761–769. DOI: 10.1158/1535-7163.MCT-10-0884.

Huang, Weiwei; Gao, Fei; Zhang, Yuting; Chen, Tianhui; Xu, Chen (2022): Lipid Droplet-Associated Proteins in Cardiomyopathy. In *Annals of nutrition & metabolism* 78 (1), pp. 1–13. DOI: 10.1159/000520122.

Huang, Xun; Warren, James T.; Gilbert, Lawrence I. (2008): New players in the regulation of ecdysone biosynthesis. In *Journal of genetics and genomics = Yi chuan xue bao* 35 (1), pp. 1–10. DOI: 10.1016/S1673-8527(08)60001-6.

Huggins, C.; Hodges, C. V. (1972): Studies on prostatic cancer. I. The effect of castration, of estrogen and androgen injection on serum phosphatases in metastatic carcinoma of the prostate. In *CA: a cancer journal for clinicians* 22 (4), pp. 232–240. DOI: 10.3322/canjclin.22.4.232.

Hughes-Fulford, M.; Chen, Y.; Tjandrawinata, R. R. (2001): Fatty acid regulates gene expression and growth of human prostate cancer PC-3 cells. In *Carcinogenesis* 22 (5), pp. 701–707. DOI: 10.1093/carcin/22.5.701.

Hwangbo, Dae Sung; Gershman, Boris; Gersham, Boris; Tu, Meng-Ping; Palmer, Michael; Tatar, Marc (2004): Drosophila dFOXO controls lifespan and regulates insulin signalling in brain and fat body. In *Nature* 429 (6991), pp. 562–566. DOI: 10.1038/nature02549.

Igarashi, Fumihiko; Ogihara, Mari H.; Iga, Masatoshi; Kataoka, Hiroshi (2018): Cholesterol internalization and metabolism in insect prothoracic gland, a steroidogenic organ, via lipoproteins. In *Steroids* 134, pp. 110–116. DOI: 10.1016/j.steroids.2018.01.012.

Ikura, Yoshihiro; Caldwell, Stephen H. (2015): Lipid droplet-associated proteins in alcoholic liver disease: a potential linkage with hepatocellular damage. In *International journal of clinical and experimental pathology* 8 (8), pp. 8699–8708.

Immarigeon, Clément; Karch, François; Maeda, Robert K. (2019): A FACS-based Protocol to Isolate RNA from the Secondary Cells of Drosophila Male Accessory Glands. In *Journal of visualized experiments : JoVE* (151). DOI: 10.3791/60218.

Innocenti, Federico; Cooper, Gregory M.; Stanaway, Ian B.; Gamazon, Eric R.; Smith, Joshua D.; Mirkov, Snezana et al. (2011): Identification, replication, and

functional fine-mapping of expression quantitative trait loci in primary human liver tissue. In *PLoS genetics* 7 (5), e1002078. DOI: 10.1371/journal.pgen.1002078.

Ito, Saya; Kayukawa, Naruhiro; Ueda, Takashi; Taniguchi, Hidefumi; Morioka, Yukako; Hongo, Fumiya; Ukimura, Osamu (2018a): MRGBP promotes AR-mediated transactivation of KLK3 and TMPRSS2 via acetylation of histone H2A.Z in prostate cancer cells. In *Biochimica et biophysica acta. Gene regulatory mechanisms*. DOI: 10.1016/j.bbagrm.2018.07.014.

Ito, Saya; Ueda, Takashi; Ueno, Akihisa; Nakagawa, Hideo; Taniguchi, Hidefumi; Kayukawa, Naruhiro; Miki, Tsuneharu (2014): A genetic screen in Drosophila for regulators of human prostate cancer progression. In *Biochemical and biophysical research communications* 451 (4), pp. 548–555. DOI: 10.1016/j.bbrc.2014.08.015.

Ito, Saya; Ueno, Akihisa; Ueda, Takashi; Nakagawa, Hideo; Taniguchi, Hidefumi; Kayukawa, Naruhiro et al. (2018b): CNPY2 inhibits MYLIP-mediated AR protein degradation in prostate cancer cells. In *Oncotarget* 9 (25), pp. 17645–17655. DOI: 10.18632/oncotarget.24824.

Jackson, Catherine L. (2019): Lipid droplet biogenesis. In *Current opinion in cell biology* 59, pp. 88–96. DOI: 10.1016/j.ceb.2019.03.018.

Jaeger, K. E.; Dijkstra, B. W.; Reetz, M. T. (1999): Bacterial biocatalysts: molecular biology, three-dimensional structures, and biotechnological applications of lipases. In *Annual review of microbiology* 53, pp. 315–351. DOI: 10.1146/annurev.micro.53.1.315.

Jamaspishvili, Tamara; Berman, David M.; Ross, Ashley E.; Scher, Howard I.; Marzo, Angelo M. de; Squire, Jeremy A.; Lotan, Tamara L. (2018): Clinical implications of PTEN loss in prostate cancer. In *Nature reviews. Urology* 15 (4), pp. 222–234. DOI: 10.1038/nrurol.2018.9.

Jamnagerwalla, Juzar (2017): Serum cholesterol and risk of high-grade prostate cancer: results from the REDUCE study. In *Prostate cancer and prostatic diseases* 21 (2), pp. 252–259. DOI: 10.1038/s41391-017-0030-9.

Jeon, Hyesung; Blacklow, Stephen C. (2005): Structure and physiologic function of the low-density lipoprotein receptor. In *Annual review of biochemistry* 74, pp. 535–562. DOI: 10.1146/annurev.biochem.74.082803.133354.

Jiang, Huaqi; Edgar, Bruce A. (2009): EGFR signaling regulates the proliferation of Drosophila adult midgut progenitors. In *Development (Cambridge, England)* 136 (3), pp. 483–493. DOI: 10.1242/dev.026955.

Jiang, Huaqi; Patel, Parthive H.; Kohlmaier, Alexander; Grenley, Marc O.; McEwen, Donald G.; Edgar, Bruce A. (2009): Cytokine/Jak/Stat signaling mediates regeneration and homeostasis in the Drosophila midgut. In *Cell* 137 (7), pp. 1343–1355. DOI: 10.1016/j.cell.2009.05.014.

Joyce, C. M.; Steitz, T. A. (1995): Polymerase structures and function: variations on a theme? In *Journal of bacteriology* 177 (22), pp. 6321–6329. DOI: 10.1128/jb.177.22.6321-6329.1995.

Kadereit, Bert; Kumar, Pradeep; Wang, Wen-Jun; Miranda, Diego; Snapp, Erik L.; Severina, Nadia et al. (2008): Evolutionarily conserved gene family important for fat storage. In *Proceedings of the National Academy of Sciences of the United States of America* 105 (1), pp. 94–99. DOI: 10.1073/pnas.0708579105.

Kamber Kaya, Hatem Elif; Ditzel, Mark; Meier, Pascal; Bergmann, Andreas (2017): An inhibitory mono-ubiquitylation of the Drosophila initiator caspase Dronc functions in both apoptotic and non-apoptotic pathways. In *PLoS genetics* 13 (2), e1006438. DOI: 10.1371/journal.pgen.1006438.

Kamita, Shizuo G.; Hammock, Bruce D. (2010): Juvenile hormone esterase: biochemistry and structure. In *Journal of pesticide science* 35 (3), pp. 265–274. DOI: 10.1584/jpestics.R10-09.

Kellner-Weibel, G.; Geng, Y. J.; Rothblat, G. H. (1999): Cytotoxic cholesterol is generated by the hydrolysis of cytoplasmic cholesteryl ester and transported to the plasma membrane. In *Atherosclerosis* 146 (2), pp. 309–319. DOI: 10.1016/s0021-9150(99)00155-0.

Kellner-Weibel, G.; Jerome, W. G.; Small, D. M.; Warner, G. J.; Stoltenborg, J. K.; Kearney, M. A. et al. (1998): Effects of intracellular free cholesterol accumulation on macrophage viability: a model for foam cell death. In *Arteriosclerosis, thrombosis, and vascular biology* 18 (3), pp. 423–431. DOI: 10.1161/01.atv.18.3.423.

Kelstrup, Hans C.; Hartfelder, Klaus; Esterhuizen, Nanike; Wossler, Theresa C. (2017): Juvenile hormone titers, ovarian status and epicuticular hydrocarbons in

gynes and workers of the paper wasp Belonogaster longitarsus. In *Journal of insect physiology* 98, pp. 83–92. DOI: 10.1016/j.jinsphys.2016.11.014.

Kelstrup, Hans C.; Hartfelder, Klaus; Nascimento, Fabio S.; Riddiford, Lynn M. (2014): The role of juvenile hormone in dominance behavior, reproduction and cuticular pheromone signaling in the caste-flexible epiponine wasp, Synoeca surinama. In *Frontiers in zoology* 11 (1), pp. 1–19. DOI: 10.1186/s12983-014-0078-5.

Kim, Ryeo Jin (2016): The GxSxG motif of Arabidopsis monoacylglycerol lipase (MAGL6 and MAGL8) is essential for their enzyme activities. In *Applied biological chemistry* 59 (6), pp. 833–840. DOI: 10.1007/s13765-016-0232-1.

Klingenberg, Marcel; Becker, Jürgen; Eberth, Sonja; Kube, Dieter; Wilting, Jörg (2014): The NADPH oxidase inhibitor imipramine-blue in the treatment of Burkitt lymphoma. In *Molecular cancer therapeutics* 13 (4), pp. 833–841. DOI: 10.1158/1535-7163.MCT-13-0688.

Koelle, M. R.; Talbot, W. S.; Segraves, W. A.; Bender, M. T.; Cherbas, P.; Hogness, D. S. (1991): The Drosophila EcR gene encodes an ecdysone receptor, a new member of the steroid receptor superfamily. In *Cell* 67 (1), pp. 59–77. DOI: 10.1016/0092-8674(91)90572-g.

Kolkhof, Petra; Werthebach, Michael; van de Venn, Anna; Poschmann, Gereon; Chen, Lili; Welte, Michael et al. (2017): A Luciferase-fragment Complementation Assay to Detect Lipid Droplet-associated Protein-Protein Interactions. In *Molecular & cellular proteomics : MCP* 16 (3), pp. 329–345. DOI: 10.1074/mcp.M116.061499.

Kornbluth, Sally; White, Kristin (2005): Apoptosis in Drosophila: neither fish nor fowl (nor man, nor worm). In *Journal of cell science* 118 (Pt 9), pp. 1779–1787. DOI: 10.1242/jcs.02377.

Kory, Nora; Farese, Robert V.; Walther, Tobias C. (2016): Targeting Fat: Mechanisms of Protein Localization to Lipid Droplets. In *Trends in cell biology* 26 (7), pp. 535–546. DOI: 10.1016/j.tcb.2016.02.007.

Kory, Nora; Grond, Susanne; Kamat, Siddhesh S.; Li, Zhihuan; Krahmer, Natalie; Chitraju, Chandramohan et al. (2017): Mice lacking lipid droplet-associated hydrolase, a gene linked to human prostate cancer, have normal cholesterol ester metabolism. In *Journal of lipid research* 58 (1), pp. 226–235. DOI: 10.1194/jlr.M072538.

Kory, Nora; Thiam, Abdou-Rachid; Farese, Robert V.; Walther, Tobias C. (2015): Protein Crowding Is a Determinant of Lipid Droplet Protein Composition. In *Developmental cell* 34 (3), pp. 351–363. DOI: 10.1016/j.devcel.2015.06.007.

Korzelius, Jerome; Naumann, Svenja K.; Loza-Coll, Mariano A.; Chan, Jessica Sk; Dutta, Devanjali; Oberheim, Jessica et al. (2014): Escargot maintains stemness and suppresses differentiation in Drosophila intestinal stem cells. In *The EMBO journal* 33 (24), pp. 2967–2982. DOI: 10.15252/embj.201489072.

Kotian, Nirupama; Troike, Katie M.; Curran, Kristen N.; Lathia, Justin D.; McDonald, Jocelyn A. (2022): A Drosophila RNAi screen reveals conserved glioblastoma-related adhesion genes that regulate collective cell migration. In *G3 (Bethesda, Md.)* 12 (1). DOI: 10.1093/g3journal/jkab356.

Kovalenko, Elena V.; Mazina, Marina Yu; Krasnov, Aleksey N.; Vorobyeva, Nadezhda E. (2019): The Drosophila nuclear receptors EcR and ERR jointly regulate the expression of genes involved in carbohydrate metabolism. In *Insect biochemistry and molecular biology* 112, p. 103184. DOI: 10.1016/j.ibmb.2019.103184.

Krahmer, Natalie; Farese, Robert V.; Walther, Tobias C. (2013a): Balancing the fat: lipid droplets and human disease. In *EMBO Mol Med* 5 (7), pp. 973–983. DOI: 10.1002/emmm.201100671.

Krahmer, Natalie; Hilger, Maximiliane; Kory, Nora; Wilfling, Florian; Stoehr, Gabriele; Mann, Matthias et al. (2013b): Protein correlation profiles identify lipid droplet proteins with high confidence. In *Molecular & cellular proteomics : MCP* 12 (5), pp. 1115–1126. DOI: 10.1074/mcp.M112.020230.

Krahmer, Natalie; Najafi, Bahar; Schueder, Florian; Quagliarini, Fabiana; Steger, Martin; Seitz, Susanne et al. (2018): Organellar Proteomics and Phospho-Proteomics Reveal Subcellular Reorganization in Diet-Induced Hepatic Steatosis. In *Developmental cell* 47 (2), 205-221.e7. DOI: 10.1016/j.devcel.2018.09.017.

Krause, Robert G. E.; Goldring, J. P. Dean (2019): Crystal violet stains proteins in SDS-PAGE gels and zymograms. In *Analytical biochemistry* 566, pp. 107–115. DOI: 10.1016/j.ab.2018.11.015.

Kubo, Ayuko; Matsuka, Mirai; Minami, Ryunosuke; Kimura, Fumika; Sakata-Niitsu, Rumi; Kokuryo, Akihiko et al. (2018): Nutrient conditions sensed by the reproductive organ during development optimize male fecundity in Drosophila. In *Genes to cells :*

devoted to molecular & cellular mechanisms 23 (7), pp. 557–567. DOI: 10.1111/gtc.12600.

Lane, D. P. (1992): Cancer. p53, guardian of the genome. In *Nature* 358 (6381), pp. 15–16. DOI: 10.1038/358015a0.

Le Wang; Lu, Bin; He, Mengjie; Wang, Youqing; Wang, Zongping; Du, Lingbin (2022): Prostate Cancer Incidence and Mortality: Global Status and Temporal Trends in 89 Countries From 2000 to 2019. In *Frontiers in public health* 10, p. 811044. DOI: 10.3389/fpubh.2022.811044.

Lee, D. H.; Goldberg, A. L. (1998): Proteasome inhibitors: valuable new tools for cell biologists. In *Trends in cell biology* 8 (10), pp. 397–403. DOI: 10.1016/s0962-8924(98)01346-4.

Lee, Hangnoh; McManus, C. Joel; Cho, Dong-Yeon; Eaton, Matthew; Renda, Fioranna; Somma, Maria Patrizia et al. (2014): DNA copy number evolution in Drosophila cell lines. In *Genome biology* 15 (8), R70. DOI: 10.1186/gb-2014-15-8-r70.

Lee, Y. F.; Shyr, C. R.; Thin, T. H.; Lin, W. J.; Chang, C. (1999): Convergence of two repressors through heterodimer formation of androgen receptor and testicular orphan receptor-4: a unique signaling pathway in the steroid receptor superfamily. In *Proceedings of the National Academy of Sciences of the United States of America* 96 (26), pp. 14724–14729. DOI: 10.1073/pnas.96.26.14724.

Leiblich, Aaron; Hellberg, Josephine E. E. U.; Sekar, Aashika; Gandy, Carina; Mendes, Claudia C.; Redhai, Siamak et al. (2019): Mating induces switch from hormone-dependent to hormone-independent steroid receptor-mediated growth in Drosophila secondary cells. In *PLoS biology* 17 (10), e3000145. DOI: 10.1371/journal.pbio.3000145.

Leiblich, Aaron; Marsden, Luke; Gandy, Carina; Corrigan, Laura; Jenkins, Rachel; Hamdy, Freddie; Wilson, Clive (2012): Bone morphogenetic protein- and mating-dependent secretory cell growth and migration in the Drosophila accessory gland. In *Proceedings of the National Academy of Sciences of the United States of America* 109 (47), pp. 19292–19297. DOI: 10.1073/pnas.1214517109.

Lengyel, F.; Westerlund, S. A.; Kaib, M. (2007): Juvenile hormone III influences task-specific cuticular hydrocarbon profile changes in the ant Myrmicaria eumenoides. In *Journal of chemical ecology* 33 (1), pp. 167–181. DOI: 10.1007/s10886-006-9185-x.

Levine, Benjamin D.; Cagan, Ross L. (2016): Drosophila Lung Cancer Models Identify Trametinib plus Statin as Candidate Therapeutic. In *Cell reports* 14 (6), pp. 1477–1487. DOI: 10.1016/j.celrep.2015.12.105.

Li, Bo; Lu, Wenfu; Chen, Zhenbang (2014a): Regulation of Androgen Receptor by E3 Ubiquitin Ligases: for More or Less. In *Receptors & clinical investigation* 1 (5). DOI: 10.14800/rci.122.

Li, Bo; Lu, Wenfu; Yang, Qing; Yu, Xiuping; Matusik, Robert J.; Chen, Zhenbang (2014b): Skp2 regulates androgen receptor through ubiquitin-mediated degradation independent of Akt/mTOR pathways in prostate cancer. In *The Prostate* 74 (4), pp. 421–432. DOI: 10.1002/pros.22763.

Li, J.; Yen, C.; Liaw, D.; Podsypanina, K.; Bose, S.; Wang, S. I. et al. (1997): PTEN, a putative protein tyrosine phosphatase gene mutated in human brain, breast, and prostate cancer. In *Science (New York, N.Y.)* 275 (5308), pp. 1943–1947. DOI: 10.1126/science.275.5308.1943.

Li, Shuai; Zhou, Ti; Li, Cen; Dai, Zhiyu; Di Che; Yao, Yachao et al. (2014c): High metastaticgastric and breast cancer cells consume oleic acid in an AMPK dependent manner. In *PloS one* 9 (5), e97330. DOI: 10.1371/journal.pone.0097330.

Li, Ya-Na; Liu, Yu-Bo; Xie, Xue-Qin; Zhang, Jia-Ning; Li, Wen-Li (2020): The Modulation of Trehalose Metabolism by 20-Hydroxyecdysone in Antheraea pernyi (Lepidoptera: Saturniidae) During its Diapause Termination and Post-Termination Period. In *Journal of insect science (Online)* 20 (5). DOI: 10.1093/jisesa/ieaa108.

Li, Yang; Gao, Junyuan; Lu, Zhongju; McFarland, Kelli; Shi, Jingyi; Bock, Kevin et al. (2013): Intracellular ATP binding is required to activate the slowly activating K+ channel I(Ks). In *Proceedings of the National Academy of Sciences of the United States of America* 110 (47), pp. 18922–18927. DOI: 10.1073/pnas.1315649110.

Liberti, Maria V.; Locasale, Jason W. (2016): The Warburg Effect: How Does it Benefit Cancer Cells? In *Trends in biochemical sciences* 41 (3), pp. 211–218. DOI: 10.1016/j.tibs.2015.12.001.

Lindström, Sara; Schumacher, Fredrick R.; Campa, Daniele; Albanes, Demetrius; Andriole, Gerald; Berndt, Sonja I. et al. (2012): Replication of five prostate cancer loci identified in an Asian population--results from the NCI Breast and Prostate Cancer Cohort Consortium (BPC3). In *Cancer epidemiology, biomarkers & prevention : a publication of the American Association for Cancer Research, cosponsored by the American Society of Preventive Oncology* 21 (1), pp. 212–216. DOI: 10.1158/1055-9965.EPI-11-0870-T.

Liu, Huanfa; Kubli, Eric (2003): Sex-peptide is the molecular basis of the sperm effect in Drosophila melanogaster. In *Proceedings of the National Academy of Sciences of the United States of America* 100 (17), pp. 9929–9933. DOI: 10.1073/pnas.1631700100.

Liu, Pingsheng; Ying, Yunshu; Zhao, Yingming; Mundy, Dorothy I.; Zhu, Meifang; Anderson, Richard G. W. (2004): Chinese hamster ovary K2 cell lipid droplets appear to be metabolic organelles involved in membrane traffic. In *The Journal of biological chemistry* 279 (5), pp. 3787–3792. DOI: 10.1074/jbc.M311945200.

Liu, Yang; Shi, Ke; Chen, Yong; Wu, Xianrui; Chen, Zheng; Cao, Ke et al. (2021): Exosomes and Their Role in Cancer Progression. In *Frontiers in oncology* 11, p. 639159. DOI: 10.3389/fonc.2021.639159.

Liu, Yiting; Liao, Sifang; Veenstra, Jan A.; Nässel, Dick R. (2016): Drosophila insulin-like peptide 1 (DILP1) is transiently expressed during non-feeding stages and reproductive dormancy. In *Scientific reports* 6, p. 26620. DOI: 10.1038/srep26620.

Londos, C.; Brasaemle, D. L.; Schultz, C. J.; Segrest, J. P.; Kimmel, A. R. (1999): Perilipins, ADRP, and other proteins that associate with intracellular neutral lipid droplets in animal cells. In *Seminars in cell & developmental biology* 10 (1), pp. 51–58. DOI: 10.1006/scdb.1998.0275.

Long, Qing-Zhi; Du, Yue-Feng; Ding, Xiao-Ying; Li, Xiang; Song, Wen-Bin; Yang, Yong et al. (2012): Replication and fine mapping for association of the C2orf43, FOXP4, GPRC6A and RFX6 genes with prostate cancer in the Chinese population. In *PloS one* 7 (5), e37866. DOI: 10.1371/journal.pone.0037866.

Long, Ronan M.; Morrissey, Colm; Fitzpatrick, John M.; Watson, R. William G. (2005): Prostate epithelial cell differentiation and its relevance to the understanding

of prostate cancer therapies. In *Clinical science (London, England : 1979)* 108 (1), pp. 1–11. DOI: 10.1042/CS20040241.

Losada-Pérez, María; Hernández García-Moreno, Mamen; García-Ricote, Irene; Casas-Tintó, Sergio (2022): Synaptic components are required for glioblastoma progression in Drosophila. In *PLoS genetics* 18 (7), e1010329. DOI: 10.1371/journal.pgen.1010329.

Lü, Feng-Gong; Fu, Kai-Yun; Guo, Wen-Chao; Li, Guo-Qing (2015): Characterization of two juvenile hormone epoxide hydrolases by RNA interference in the Colorado potato beetle. In *Gene* 570 (2), pp. 264–271. DOI: 10.1016/j.gene.2015.06.032.

Luining, Wietske I.; Cysouw, Matthijs C. F.; Meijer, Dennie; Hendrikse, N. Harry; Boellaard, Ronald; Vis, André N.; Oprea-Lager, Daniela E. (2022): Targeting PSMA Revolutionizes the Role of Nuclear Medicine in Diagnosis and Treatment of Prostate Cancer. In *Cancers* 14 (5). DOI: 10.3390/cancers14051169.

Luo, Wenqin; Wang, Huan; Ren, Liangliang; Lu, Zeyi; Zheng, Qiming; Ding, Lifeng et al. (2022): Adding fuel to the fire: The lipid droplet and its associated proteins in cancer progression. In *Int. J. Biol. Sci.* 18 (16), pp. 6020–6034. DOI: 10.7150/ijbs.74902.

Marjot, Thomas; Moolla, Ahmad; Cobbold, Jeremy F.; Hodson, Leanne; Tomlinson, Jeremy W. (2020): Nonalcoholic Fatty Liver Disease in Adults: Current Concepts in Etiology, Outcomes, and Management. In *Endocrine reviews* 41 (1). DOI: 10.1210/endrev/bnz009.

Martin, Ina V.; MacNeill, Stuart A. (2002): ATP-dependent DNA ligases. In *Genome biology* 3 (4), REVIEWS3005. DOI: 10.1186/gb-2002-3-4-reviews3005.

Martínez-Sánchez, Noelia (2020): There and Back Again: Leptin Actions in White Adipose Tissue. In *IJMS* 21 (17), p. 6039. DOI: 10.3390/ijms21176039.

Martorell, Òscar; Merlos-Suárez, Anna; Campbell, Kyra; Barriga, Francisco M.; Christov, Christo P.; Miguel-Aliaga, Irene et al. (2014): Conserved mechanisms of tumorigenesis in the Drosophila adult midgut. In *PloS one* 9 (2), e88413. DOI: 10.1371/journal.pone.0088413.

McClurg, Urszula L.; Cork, David M. W.; Darby, Steven; Ryan-Munden, Claudia A.; Nakjang, Sirintra; Mendes Côrtes, Leticia et al. (2017): Identification of a novel K311

ubiquitination site critical for androgen receptor transcriptional activity. In *Nucleic acids research* 45 (4), pp. 1793–1804. DOI: 10.1093/nar/gkw1162.

McGuire, Sean E.; Mao, Zhengmei; Davis, Ronald L. (2004): Spatiotemporal gene expression targeting with the TARGET and gene-switch systems in Drosophila. In *Science's STKE : signal transduction knowledge environment* 2004 (220), pl6. DOI: 10.1126/stke.2202004pl6.

Meiselman, Matthew; Lee, Sang Soo; Tran, Raymond-Tan; Dai, Hongjiu; Ding, Yike; Rivera-Perez, Crisalejandra et al. (2017): Endocrine network essential for reproductive success in Drosophila melanogaster. In *Proceedings of the National Academy of Sciences of the United States of America* 114 (19), E3849-E3858. DOI: 10.1073/pnas.1620760114.

Meunier, Nicolas; Belgacem, Yesser Hadj; Martin, Jean-René (2007): Regulation of feeding behaviour and locomotor activity by takeout in Drosophila. In *The Journal of experimental biology* 210 (Pt 8), pp. 1424–1434. DOI: 10.1242/jeb.02755.

Micchelli, Craig A.; Perrimon, Norbert (2006): Evidence that stem cells reside in the adult Drosophila midgut epithelium. In *Nature* 439 (7075), pp. 475–479. DOI: 10.1038/nature04371.

Michaud, Jason E.; Billups, Kevin L.; Partin, Alan W. (2015): Testosterone and prostate cancer: an evidence-based review of pathogenesis and oncologic risk. In *Therapeutic advances in urology* 7 (6), pp. 378–387. DOI: 10.1177/1756287215597633.

Minami, Ryunosuke; Wakabayashi, Miyuki; Sugimori, Seiko; Taniguchi, Kiichiro; Kokuryo, Akihiko; Imano, Takao et al. (2012): The homeodomain protein defective proventriculus is essential for male accessory gland development to enhance fecundity in Drosophila. In *PloS one* 7 (3), e32302. DOI: 10.1371/journal.pone.0032302.

Mirth, Christen; Truman, James W.; Riddiford, Lynn M. (2005): The role of the prothoracic gland in determining critical weight for metamorphosis in Drosophila melanogaster. In *Current biology : CB* 15 (20), pp. 1796–1807. DOI: 10.1016/j.cub.2005.09.017.

Mirth, Christen Kerry; Shingleton, Alexander W. (2012): Integrating body and organ size in Drosophila: recent advances and outstanding problems. In *Frontiers in endocrinology* 3, p. 49. DOI: 10.3389/fendo.2012.00049.

Mirth, Christen Kerry; Tang, Hui Yuan; Makohon-Moore, Sasha C.; Salhadar, Samy; Gokhale, Rewatee H.; Warner, Raechel D. et al. (2014): Juvenile hormone regulates body size and perturbs insulin signaling in Drosophila. In *Proceedings of the National Academy of Sciences of the United States of America* 111 (19), pp. 7018–7023. DOI: 10.1073/pnas.1313058111.

Mirzoyan, Zhasmine; Sollazzo, Manuela; Allocca, Mariateresa; Valenza, Alice Maria; Grifoni, Daniela; Bellosta, Paola (2019): Drosophila melanogaster: A Model Organism to Study Cancer. In *Frontiers in genetics* 10, p. 51. DOI: 10.3389/fgene.2019.00051.

Misra, Snigdha; Pandey, Anuj Kumar; Gupta, Snigdha; Kumar, Ajay; Khanna, Priyanka; Shankar, Jai; Ravi Ram, Kristipati (2017): Estrogen related receptor is required for the testicular development and for the normal sperm axoneme/mitochondrial derivatives in Drosophila males. In *Scientific reports* 7, p. 40372. DOI: 10.1038/srep40372.

Mitra, Ranjana; Le, Thuc T.; Gorjala, Priyatham; Goodman Jr., Oscar B. (2017): Positive regulation of prostate cancer cell growth by lipid droplet forming and processing enzymes DGAT1 and ABHD5. In *BMC cancer* 17 (1), pp. 1–12. DOI: 10.1186/s12885-017-3589-6.

Murphy, D. J. (2001): The biogenesis and functions of lipid bodies in animals, plants and microorganisms. In *Progress in lipid research* 40 (5), pp. 325–438. DOI: 10.1016/s0163-7827(01)00013-3.

Murtola, Teemu J. (2018): Serum cholesterol and prostate cancer risk in the Finnish randomized study of screening for prostate cancer. In *Prostate cancer and prostatic diseases*, pp. 1–11. DOI: 10.1038/s41391-018-0087-0.

Musselman, Laura Palanker; Kühnlein, Ronald P. (2018): Drosophila as a model to study obesity and metabolic disease. In *The Journal of experimental biology* 221 (Pt Suppl 1). DOI: 10.1242/jeb.163881.

Najt, Charles P.; Devarajan, Mahima; Mashek, Douglas G. (2022): Perilipins at a glance. In *Journal of cell science* 135 (5). DOI: 10.1242/jcs.259501.

Naresh Kumar, M.; Thunuguntla, V B S C; Chandra Sekhar, B.; Bondili, J. S. (2018): Saccharomyces cerevisiae lipid droplet associated enzyme Ypr147cp shows both TAG lipase and ester hydrolase activities. In *The Journal of general and applied microbiology* 64 (2), pp. 76–83. DOI: 10.2323/jgam.2017.08.001.

Navarro, Domingo; Luzardo, Octavio P.; Fernández, Leandro; Chesa, Nicolás; Díaz-Chico, Bonifacio N. (2002): Transition to androgen-independence in prostate cancer. In *The Journal of steroid biochemistry and molecular biology* 81 (3), pp. 191–201. DOI: 10.1016/s0960-0760(02)00064-x.

Nishimura, Takashi (2020): Feedforward Regulation of Glucose Metabolism by Steroid Hormones Drives a Developmental Transition in Drosophila. In *Current biology : CB* 30 (18), 3624-3632.e5. DOI: 10.1016/j.cub.2020.06.043.

Nöthiger, Rolf; Dübendorfer, Andreas; Epper, Felix (1977): Gynandromorphs reveal two separate primordia for male and female genitalia inDrosophila melanogaster. In *Wilhelm Roux's archives of developmental biology* 181 (4), pp. 367–373. DOI: 10.1007/BF00848062.

Novak, Ivana (2003): ATP as a signaling molecule: the exocrine focus. In *News in physiological sciences : an international journal of physiology produced jointly by the International Union of Physiological Sciences and the American Physiological Society* 18, pp. 12–17. DOI: 10.1152/nips.01409.2002.

Olzmann, James A.; Carvalho, Pedro (2019): Dynamics and functions of lipid droplets. In *Nature reviews. Molecular cell biology* 20 (3), pp. 137–155. DOI: 10.1038/s41580-018-0085-z.

Olzmann, James A.; Richter, Caleb M.; Kopito, Ron R. (2013): Spatial regulation of UBXD8 and p97/VCP controls ATGL-mediated lipid droplet turnover. In *Proceedings of the National Academy of Sciences of the United States of America* 110 (4), pp. 1345–1350. DOI: 10.1073/pnas.1213738110.

Osman, Dani; Gobert, Vanessa; Ponthan, Frida; Heidenreich, Olaf; Haenlin, Marc; Waltzer, Lucas (2009): A Drosophila model identifies calpains as modulators of the human leukemogenic fusion protein AML1-ETO. In *Proceedings of the National Academy of Sciences of the United States of America* 106 (29), pp. 12043–12048. DOI: 10.1073/pnas.0902449106.

Ottea, J. A.; Harshman, L. G.; Hammock, B. (1987): Patterns of epoxide metabolism by epoxide hydrolase and glutathione S-transferase associated with age and genotype in Drosophila melanogaster. In *Mutation research* 177 (2), pp. 247–254. DOI: 10.1016/0027-5107(87)90007-8.

Pandey, Udai Bhan; Nichols, Charles D. (2011): Human disease models in Drosophila melanogaster and the role of the fly in therapeutic drug discovery. In *Pharmacological reviews* 63 (2), pp. 411–436. DOI: 10.1124/pr.110.003293.

Pang, Yan Ling Joy; Poruri, Kiranmai; Martinis, Susan A. (2014): tRNA synthetase: tRNA aminoacylation and beyond. In *Wiley interdisciplinary reviews. RNA* 5 (4), pp. 461–480. DOI: 10.1002/wrna.1224.

Penney, Kathryn L.; Sinnott, Jennifer A.; Tyekucheva, Svitlana; Gerke, Travis; Shui, Irene M.; Kraft, Peter et al. (2015): Association of prostate cancer risk variants with gene expression in normal and tumor tissue. In *Cancer epidemiology, biomarkers & prevention : a publication of the American Association for Cancer Research, cosponsored by the American Society of Preventive Oncology* 24 (1), pp. 255–260. DOI: 10.1158/1055-9965.EPI-14-0694-T.

Petan, Toni (2020): Lipid Droplets in Cancer. In *Reviews of physiology, biochemistry and pharmacology*. DOI: 10.1007/112_2020_51.

Pickart, C. M. (2001): Mechanisms underlying ubiquitination. In *Annual review of biochemistry* 70, pp. 503–533. DOI: 10.1146/annurev.biochem.70.1.503.

Ploier, Birgit; Scharwey, Melanie; Koch, Barbara; Schmidt, Claudia; Schatte, Jessica; Rechberger, Gerald et al. (2013): Screening for hydrolytic enzymes reveals Ayr1p as a novel triacylglycerol lipase in Saccharomyces cerevisiae. In *The Journal of biological chemistry* 288 (50), pp. 36061–36072. DOI: 10.1074/jbc.M113.509927.

Prinz, William A.; Toulmay, Alexandre; Balla, Tamas (2020): The functional universe of membrane contact sites. In *Nature reviews. Molecular cell biology* 21 (1), pp. 7–24. DOI: 10.1038/s41580-019-0180-9.

Qian, Yue; Dominado, Nicole; Zoller, Richard; Ng, Chun; Kudyba, Karl; Siddall, Nicole A. et al. (2014): Ecdysone signaling opposes epidermal growth factor signaling in regulating cyst differentiation in the male gonad of Drosophila melanogaster. In *Developmental Biology* 394 (2), pp. 217–227. DOI: 10.1016/j.ydbio.2014.08.019.

Raftopulos, Nikki L.; Washaya, Tinashe C.; Niederprüm, Andreas; Egert, Antonia; Hakeem-Sanni, Mariam F.; Varney, Bianca et al. (2022): Prostate cancer cell proliferation is influenced by LDL-cholesterol availability and cholesteryl ester turnover. In *Cancer & metabolism* 10 (1), pp. 1–15. DOI: 10.1186/s40170-021-00278-1.

Raja Singh, Paulraj; Sugantha Priya, Elayapillai; Balakrishnan, Solaimuthu; Arunkumar, Ramachandran; Sharmila, Govindaraj; Rajalakshmi, Manikkam; Arunakaran, Jagadeesan (2017): Inhibition of cell survival and proliferation by nimbolide in human androgen-independent prostate cancer (PC-3) cells: involvement of the PI3K/Akt pathway. In *Molecular and cellular biochemistry* 427 (1-2), pp. 69–79. DOI: 10.1007/s11010-016-2898-4.

Rajakumari, Sona; Daum, Günther (2010): Multiple functions as lipase, steryl ester hydrolase, phospholipase, and acyltransferase of Tgl4p from the yeast Saccharomyces cerevisiae. In *The Journal of biological chemistry* 285 (21), pp. 15769–15776. DOI: 10.1074/jbc.M109.076331.

Rambur, Amandine; Lours-Calet, Corinne; Beaudoin, Claude; Buñay, Julio; Vialat, Marine; Mirouse, Vincent et al. (2020): Sequential Ras/MAPK and PI3K/AKT/mTOR pathways recruitment drives basal extrusion in the prostate-like gland of Drosophila. In *Nature Communications* 11 (1), p. 2300. DOI: 10.1038/s41467-020-16123-w.

Rambur, Amandine; Vialat, Marine; Beaudoin, Claude; Lours-Calet, Corinne; Lobaccaro, Jean-Marc; Baron, Silvère et al. (2021): Drosophila Accessory Gland: A Complementary In Vivo Model to Bring New Insight to Prostate Cancer. In *Cells* 10 (9). DOI: 10.3390/cells10092387.

Ravi Ram, K.; Wolfner, Mariana F. (2007): Seminal influences: Drosophila Acps and the molecular interplay between males and females during reproduction. In *Integrative and comparative biology* 47 (3), pp. 427–445. DOI: 10.1093/icb/icm046.

Rebello, Richard J.; Oing, Christoph; Knudsen, Karen E.; Loeb, Stacy; Johnson, David C.; Reiter, Robert E. et al. (2021): Prostate cancer. In *Nature reviews. Disease primers* 7 (1), p. 9. DOI: 10.1038/s41572-020-00243-0.

Redhai, Siamak; Hellberg, Josephine E. E. U.; Wainwright, Mark; Perera, Sumeth W.; Castellanos, Felix; Kroeger, Benjamin et al. (2016): Regulation of Dense-Core

Granule Replenishment by Autocrine BMP Signalling in Drosophila Secondary Cells. In *PLoS genetics* 12 (10), e1006366. DOI: 10.1371/journal.pgen.1006366.

Reschly, Erica J.; Ai, Ni; Welsh, William J.; Ekins, Sean; Hagey, Lee R.; Krasowski, Matthew D. (2008): Ligand specificity and evolution of liver X receptors. In *The Journal of steroid biochemistry and molecular biology* 110 (1-2), pp. 83–94. DOI: 10.1016/j.jsbmb.2008.02.007.

Rewitz, K. F.; Rybczynski, R.; Warren, J. T.; Gilbert, L. I. (2006): The Halloween genes code for cytochrome P450 enzymes mediating synthesis of the insect moulting hormone. In *Biochemical Society transactions* 34 (6), pp. 1256–1260. DOI: 10.1042/BST0341256.

Riddiford, L. M.; Cherbas, P.; Truman, J. W. (2000): Ecdysone receptors and their biological actions. In *Vitamins and hormones* 60, pp. 1–73. DOI: 10.1016/s0083-6729(00)60016-x.

Rösmann, Sandra; Hahn, Dagmar; Lottaz, Daniel; Kruse, Markus-N; Stöcker, Walter; Sterchi, Erwin E. (2002): Activation of human meprin-alpha in a cell culture model of colorectal cancer is triggered by the plasminogen-activating system. In *The Journal of biological chemistry* 277 (43), pp. 40650–40658. DOI: 10.1074/jbc.M206203200.

Rylett, Caroline M.; Walker, Michael J.; Howell, Gareth J.; Shirras, Alan D.; Isaac, R. Elwyn (2007): Male accessory glands of Drosophila melanogaster make a secreted angiotensin I-converting enzyme (ANCE), suggesting a role for the peptide-processing enzyme in seminal fluid. In *The Journal of experimental biology* 210 (Pt 20), pp. 3601–3606. DOI: 10.1242/jeb.009035.

Ryoo, Hyung Don; Bergmann, Andreas; Gonen, Hedva; Ciechanover, Aaron; Steller, Hermann (2002): Regulation of Drosophila IAP1 degradation and apoptosis by reaper and ubcD1. In *Nature cell biology* 4 (6), pp. 432–438. DOI: 10.1038/ncb795.

Ryoo, Hyung Don; Gorenc, Travis; Steller, Hermann (2004): Apoptotic cells can induce compensatory cell proliferation through the JNK and the Wingless signaling pathways. In *Developmental cell* 7 (4), pp. 491–501. DOI: 10.1016/j.devcel.2004.08.019.

Saad, Fred; Miller, Kurt (2015): Current and Emerging Immunotherapies for Castration-resistant Prostate Cancer. In *Urology* 85 (5), pp. 976–986. DOI: 10.1016/j.urology.2014.12.029.

Sadeghi et al. (2014): Targeting prostate cancer cell metabolism: impact of hexokinase and CPT-1 enzymes. In *Tumor biology* 36 (4), pp. 2893–2905. DOI: 10.1007/s13277-014-2919-4.

Saely, Christoph H.; Geiger, Kathrin; Drexel, Heinz (2012): Brown versus white adipose tissue: a mini-review. In *Gerontology* 58 (1), pp. 15–23. DOI: 10.1159/000321319.

Saini, Natalie (2015): The journey of DNA repair. In *Trends in cancer* 1 (4), pp. 215–216. DOI: 10.1016/j.trecan.2015.11.001.

Saito, Yasumasa; Kamita, Shizuo G.; Hammock, Bruce D.; Kunimi, Yasuhisa; Inoue, Maki N.; Nakai, Madoka (2015): Juvenile hormone (JH) esterase activity but not JH epoxide hydrolase activity is downregulated in larval Adoxophyes honmai following nucleopolyhedroviruses infection. In *Journal of insect physiology* 80, pp. 71–80. DOI: 10.1016/j.jinsphys.2015.02.005.

Salloum, Shadi; Wang, Hongliang; Ferguson, Charles; Parton, Robert G.; Tai, Andrew W. (2013): Rab18 binds to hepatitis C virus NS5A and promotes interaction between sites of viral replication and lipid droplets. In *PLoS pathogens* 9 (8), e1003513. DOI: 10.1371/journal.ppat.1003513.

Salo, Veijo T.; Belevich, Ilya; Li, Shiqian; Karhinen, Leena; Vihinen, Helena; Vigouroux, Corinne et al. (2016): Seipin regulates ER-lipid droplet contacts and cargo delivery. In *The EMBO journal* 35 (24), pp. 2699–2716. DOI: 10.15252/embj.201695170.

Salo, Veijo T.; Li, Shiqian; Vihinen, Helena; Hölttä-Vuori, Maarit; Szkalisity, Abel; Horvath, Peter et al. (2019): Seipin Facilitates Triglyceride Flow to Lipid Droplet and Counteracts Droplet Ripening via Endoplasmic Reticulum Contact. In *Developmental cell* 50 (4), 478-493.e9. DOI: 10.1016/j.devcel.2019.05.016.

Salvesen, Guy S.; Duckett, Colin S. (2002): IAP proteins: blocking the road to death's door. In *Nature reviews. Molecular cell biology* 3 (6), pp. 401–410. DOI: 10.1038/nrm830.

Sang, Tzu-Kang; Jackson, George R. (2005): Drosophila models of neurodegenerative disease. In *NeuroRx : the journal of the American Society for Experimental NeuroTherapeutics* 2 (3), pp. 438–446. DOI: 10.1602/neurorx.2.3.438.

Santhosh, H. T.; Krishna, M. S. (2013): Relationship between male age, accessory gland, sperm transferred, and fitness traits in Drosophila bipectinata. In *Journal of insect science (Online)* 13, p. 159. DOI: 10.1673/031.013.15901.

Scherer, Philipp E. (2006): Adipose Tissue. In *Diabetes* 55 (6), pp. 1537–1545. DOI: 10.2337/db06-0263.

Schwedes, Christoph C.; Carney, Ginger E. (2012): Ecdysone signaling in adult Drosophila melanogaster. In *Journal of insect physiology* 58 (3), pp. 293–302. DOI: 10.1016/j.jinsphys.2012.01.013.

Shai, Nadav; Yifrach, Eden; van Roermund, Carlo W. T.; Cohen, Nir; Bibi, Chen; IJlst, Lodewijk et al. (2018): Systematic mapping of contact sites reveals tethers and a function for the peroxisome-mitochondria contact. In *Nature Communications* 9 (1), pp. 1–13. DOI: 10.1038/s41467-018-03957-8.

Sharma, Vandana; Pandey, Anuj K.; Kumar, Ajay; Misra, Snigdha; Gupta, Himanshu P. K.; Gupta, Snigdha et al. (2017): Functional male accessory glands and fertility in Drosophila require novel ecdysone receptor. In *PLoS genetics* 13 (5), e1006788. DOI: 10.1371/journal.pgen.1006788.

Shui, Irene M.; Lindström, Sara; Kibel, Adam S.; Berndt, Sonja I.; Campa, Daniele; Gerke, Travis et al. (2014): Prostate cancer (PCa) risk variants and risk of fatal PCa in the National Cancer Institute Breast and Prostate Cancer Cohort Consortium. In *European urology* 65 (6), pp. 1069–1075. DOI: 10.1016/j.eururo.2013.12.058.

Sinenko, Sergey A.; Hung, Tony; Moroz, Tatiana; Tran, Quynh-Minh; Sidhu, Sohrab; Cheney, Matthew D. et al. (2010): Genetic manipulation of AML1-ETO-induced expansion of hematopoietic precursors in a Drosophila model. In *Blood* 116 (22), pp. 4612–4620. DOI: 10.1182/blood-2010-03-276998.

Siniossoglou, Symeon (2013): Phospholipid metabolism and nuclear function: roles of the lipin family of phosphatidic acid phosphatases. In *Biochimica et biophysica acta* 1831 (3), pp. 575–581. DOI: 10.1016/j.bbalip.2012.09.014.

Sitnik, Jessica L.; Gligorov, Dragan; Maeda, Robert K.; Karch, François; Wolfner, Mariana F. (2016): The Female Post-Mating Response Requires Genes Expressed in the Secondary Cells of the Male Accessory Gland in Drosophila melanogaster. In *Genetics* 202 (3), pp. 1029–1041. DOI: 10.1534/genetics.115.181644.

Smith, C. V.; Bauer, J. J.; Connelly, R. R.; Seay, T.; Kane, C.; Foley, J. et al. (2000): Prostate cancer in men age 50 years or younger: a review of the Department of Defense Center for Prostate Disease Research multicenter prostate cancer database. In *The Journal of urology* 164 (6), pp. 1964–1967. DOI: 10.1016/s0022-5347(05)66929-7.

Song, Jiunn; Mizrak, Arda; Lee, Chia-Wei; Cicconet, Marcelo; Lai, Zon Weng; Tang, Wei-Chun et al. (2022): Identification of two pathways mediating protein targeting from ER to lipid droplets. In *Nature cell biology*. DOI: 10.1038/s41556-022-00974-0.

Susic-Jung, Loreen; Hornbruch-Freitag, Christina; Kuckwa, Jessica; Rexer, Karl-Heinz; Lammel, Uwe; Renkawitz-Pohl, Renate (2012): Multinucleated smooth muscles and mononucleated as well as multinucleated striated muscles develop during establishment of the male reproductive organs of Drosophila melanogaster. In *Developmental Biology* 370 (1), pp. 86–97. DOI: 10.1016/j.ydbio.2012.07.022.

Suzuki, Michitaka; Shinohara, Yuki; Ohsaki, Yuki; Fujimoto, Toyoshi (2011): Lipid droplets: size matters. In *Journal of electron microscopy* 60 Suppl 1, S101-16. DOI: 10.1093/jmicro/dfr016.

Svoboda, J. A.; Kaplanis, J. N.; Robbins, W. E.; Thompson, M. J. (1975): Recent Developments in Insect Steroid Metabolism. In *Annu. Rev. Entomol.* 20 (1), pp. 205–220. DOI: 10.1146/annurev.en.20.010175.001225.

Szymanski, Kimberly M.; Binns, Derk; Bartz, René; Grishin, Nick V.; Li, Wei-Ping; Agarwal, Anil K. et al. (2007): The lipodystrophy protein seipin is found at endoplasmic reticulum lipid droplet junctions and is important for droplet morphology. In *Proceedings of the National Academy of Sciences of the United States of America* 104 (52), pp. 20890–20895. DOI: 10.1073/pnas.0704154104.

Taghiyev, Agshin F.; Rokhlin, Oskar W.; Glover, Rebecca B. (2011): Caspase-2-Based Regulation of the Androgen Receptor and Cell Cycle in the Prostate Cancer Cell Line LNCaP. In *Genes & cancer* 2 (7), pp. 745–752. DOI: 10.1177/1947601911426007.

Tai, Sheng; Sun, Yin; Squires, Jill M.; Zhang, Hong; Oh, William K.; Liang, Chao-Zhao; Huang, Jiaoti (2011): PC3 is a cell line characteristic of prostatic small cell carcinoma. In *The Prostate* 71 (15), pp. 1668–1679. DOI: 10.1002/pros.21383.

Takata, Ryo; Akamatsu, Shusuke; Kubo, Michiaki; Takahashi, Atsushi; Hosono, Naoya; Kawaguchi, Takahisa et al. (2010): Genome-wide association study identifies five new susceptibility loci for prostate cancer in the Japanese population. In *Nature genetics* 42 (9), pp. 751–754. DOI: 10.1038/ng.635.

Takeuchi, Kazuharu; Reue, Karen (2009): Biochemistry, physiology, and genetics of GPAT, AGPAT, and lipin enzymes in triglyceride synthesis. In *American journal of physiology. Endocrinology and metabolism* 296 (6), E1195-209. DOI: 10.1152/ajpendo.90958.2008.

Taniguchi, Kiichiro; Kokuryo, Akihiko; Imano, Takao; Minami, Ryunosuke; Nakagoshi, Hideki; Adachi-Yamada, Takashi (2014): Isoform-specific functions of Mud/NuMA mediate binucleation of Drosophila male accessory gland cells. In *BMC developmental biology* 14, p. 46. DOI: 10.1186/s12861-014-0046-5.

Tayler, Timothy D.; Pacheco, Diego A.; Hergarden, Anne C.; Murthy, Mala; Anderson, David J. (2012): A neuropeptide circuit that coordinates sperm transfer and copulation duration in Drosophila. In *Proceedings of the National Academy of Sciences of the United States of America* 109 (50), pp. 20697–20702. DOI: 10.1073/pnas.1218246109.

Tennessen, Jason M.; Baker, Keith D.; Lam, Geanette; Evans, Janelle; Thummel, Carl S. (2011): The Drosophila estrogen-related receptor directs a metabolic switch that supports developmental growth. In *Cell metabolism* 13 (2), pp. 139–148. DOI: 10.1016/j.cmet.2011.01.005.

Tewari, Reshu; Chhabra, Mohini; Natu, Shankar Madhavan; Goel, Apul; Dalela, Divakar; Goel, Madhu Mati; Rajender, Singh (2014): Significant association of metabolic indices, lipid profile, and androgen levels with prostate cancer. In *Asian Pacific journal of cancer prevention : APJCP* 15 (22), pp. 9841–9846. DOI: 10.7314/apjcp.2014.15.22.9841.

Thiam, Abdou Rachid; Beller, Mathias (2017): The why, when and how of lipid droplet diversity. In *Journal of cell science* 130 (2), pp. 315–324. DOI: 10.1242/jcs.192021.

Thiel, Katharina; Heier, Christoph; Haberl, Verena; Thul, Peter J.; Oberer, Monika; Lass, Achim et al. (2013): The evolutionarily conserved protein CG9186 is associated with lipid droplets, required for their positioning and for fat storage. In *Journal of cell science* 126 (Pt 10), pp. 2198–2212. DOI: 10.1242/jcs.120493.

Thul, Peter J.; Tschapalda, Kirsten; Kolkhof, Petra; Thiam, Abdou Rachid; Oberer, Monika; Beller, Mathias (2017): Targeting of the Drosophila protein CG2254/Ldsdh1 to a subset of lipid droplets. In *Journal of cell science* 130 (18), pp. 3141–3157. DOI: 10.1242/jcs.199661.

Tolwinski, Nicholas S. (2017): Introduction: Drosophila-A Model System for Developmental Biology. In *Journal of developmental biology* 5 (3). DOI: 10.3390/jdb5030009.

Towbin, H.; Staehelin, T.; Gordon, J. (1979): Electrophoretic transfer of proteins from polyacrylamide gels to nitrocellulose sheets: procedure and some applications. In *Proceedings of the National Academy of Sciences of the United States of America* 76 (9), pp. 4350–4354.

Tsanov, Nikolay; Samacoits, Aubin; Chouaib, Racha; Traboulsi, Abdel-Meneem; Gostan, Thierry; Weber, Christian et al. (2016): smiFISH and FISH-quant - a flexible single RNA detection approach with super-resolution capability. In *Nucleic acids research* 44 (22), e165. DOI: 10.1093/nar/gkw784.

Tseng, Yu-Hua (2023): Adipose tissue in communication: within and without. In *Nat Rev Endocrinol* 19 (2), pp. 70–71. DOI: 10.1038/s41574-022-00789-x.

Tsuda, Leo; Lim, Young-Mi (2018): Alzheimer's Disease Model System Using Drosophila. In *Advances in experimental medicine and biology* 1076, pp. 25–40. DOI: 10.1007/978-981-13-0529-0_3.

Twum-Ampofo, Jeffrey; Fu, De-Xue; Passaniti, Antonino; Hussain, Arif; Siddiqui, M. Minhaj (2016): Metabolic targets for potential prostate cancer therapeutics. In *Current opinion in oncology* 28 (3), pp. 241–247. DOI: 10.1097/CCO.0000000000000276.

Ulukaya, Engin; Acilan, Ceyda; Yilmaz, Yusuf (2011): Apoptosis: why and how does it occur in biology? In *Cell biochemistry and function* 29 (6), pp. 468–480. DOI: 10.1002/cbf.1774.

Valm, Alex M.; Cohen, Sarah; Legant, Wesley R.; Melunis, Justin; Hershberg, Uri; Wait, Eric et al. (2017): Applying systems-level spectral imaging and analysis to reveal the organelle interactome. In *Nature* 546 (7656), pp. 162–167. DOI: 10.1038/nature22369.

van Dessel, Lisanne F.; van Riet, Job; Smits, Minke; Zhu, Yanyun; Hamberg, Paul; van der Heijden, Michiel S. et al. (2019): The genomic landscape of metastatic castration-resistant prostate cancers reveals multiple distinct genotypes with potential clinical impact. In *Nature Communications* 10 (1), p. 5251. DOI: 10.1038/s41467-019-13084-7.

van Lommel, Joachim; Lenaerts, Cynthia; Delgouffe, Charlotte; Vanden Broeck, Jozef (2022): Knockdown of ecdysone receptor in male desert locusts affects relative weight of accessory glands and mating behavior. In *Journal of insect physiology* 138, p. 104368. DOI: 10.1016/j.jinsphys.2022.104368.

Vaux, David L.; Silke, John (2005): IAPs, RINGs and ubiquitylation. In *Nature reviews. Molecular cell biology* 6 (4), pp. 287–297. DOI: 10.1038/nrm1621.

Vickman, Renee E.; Franco, Omar E.; Moline, Daniel C.; Vander Griend, Donald J.; Thumbikat, Praveen; Hayward, Simon W. (2020): The role of the androgen receptor in prostate development and benign prostatic hyperplasia: A review. In *Asian journal of urology* 7 (3), pp. 191–202. DOI: 10.1016/j.ajur.2019.10.003.

Wan, Jiukai; Zhang, Jun; Zhang, Junqiang (2018): Expression of p53 and its mechanism in prostate cancer. In *Oncology letters* 16 (1), pp. 378–382. DOI: 10.3892/ol.2018.8680.

Wang, Huajin; Becuwe, Michel; Housden, Benjamin E.; Chitraju, Chandramohan; Porras, Ashley J.; Graham, Morven M. et al. (2016): Seipin is required for converting nascent to mature lipid droplets. In *eLife* 5. DOI: 10.7554/eLife.16582.

Wang, Na-Na; Xu, Yong; Yang, Kuo; Wei, Dong; Zhang, Yao-Guang; Liu, Ming et al. (2013): Susceptibility loci associations with prostate cancer risk in northern Chinese men. In *Asian Pacific journal of cancer prevention : APJCP* 14 (5), pp. 3075–3078. DOI: 10.7314/apjcp.2013.14.5.3075.

Wang, Sihui; Idrissi, Fatima-Zahra; Hermansson, Martin; Grippa, Alexandra; Ejsing, Christer; Carvalho, Pedro (2018): Seipin and the membrane-shaping protein Pex30 cooperate in organelle budding from the endoplasmic reticulum. In *Nature Communications* 9 (1), pp. 1–12. DOI: 10.1038/s41467-018-05278-2.

Warburg, Otto (1925): The metabolism of carcinoma cells. In *The Journal of Cancer Research* (9.1), pp. 148–163. DOI: 10.1158/jcr.1925.148.

Welte, Michael A.; Gould, Alex P. (2017): Lipid droplet functions beyond energy storage. In *Biochimica et biophysica acta. Molecular and cell biology of lipids* 1862 (10 Pt B), pp. 1260–1272. DOI: 10.1016/j.bbalip.2017.07.006.

Werthebach, Michael (2019): Charakterisierung des Lipidtröpfchen-assoziierten Proteins CG9186. Düsseldorf: Universitäts- und Landesbibliothek der Heinrich-Heine-Universität Düsseldorf.

Werthebach, Michael; Stewart, Fiona A.; Gahlen, Alisa; Mettler-Altmann, Tabea; Akhtar, Irfan; Maas-Enriquez, Kerstin et al. (2019): Control of Drosophila Growth and Survival by the Lipid Droplet-Associated Protein CG9186/Sturkopf. In *Cell reports* 26 (13), 3726-3740.e7. DOI: 10.1016/j.celrep.2019.02.110.

Wilfling, Florian; Haas, Joel T.; Walther, Tobias C.; Farese, Robert V. (2014): Lipid droplet biogenesis. In *Current opinion in cell biology* 29, pp. 39–45. DOI: 10.1016/j.ceb.2014.03.008.

Willy, P. J.; Umesono, K.; Ong, E. S.; Evans, R. M.; Heyman, R. A.; Mangelsdorf, D. J. (1995): LXR, a nuclear receptor that defines a distinct retinoid response pathway. In *Genes & development* 9 (9), pp. 1033–1045. DOI: 10.1101/gad.9.9.1033.

Wilson, C.; Leiblich, A.; Goberdhan, D. C. I.; Hamdy, F. (2017): The Drosophila Accessory Gland as a Model for Prostate Cancer and Other Pathologies. In *Current topics in developmental biology* 121, pp. 339–375. DOI: 10.1016/bs.ctdb.2016.06.001.

Wilson, Rebecca; Goyal, Lakshmi; Ditzel, Mark; Zachariou, Anna; Baker, David A.; Agapite, Julie et al. (2002): The DIAP1 RING finger mediates ubiquitination of Dronc and is indispensable for regulating apoptosis. In *Nature cell biology* 4 (6), pp. 445–450. DOI: 10.1038/ncb799.

Wisniewski, J. R.; Muszynska-Pytel, M.; Grzelak, K.; Kochman, M. (1987): Biosynthesis and degradation of juvenile hormone in corpora allata and imaginal wing discs of Galleria mellonella (L.). In *Insect Biochemistry* 17 (1), pp. 249–254. Available online at http://linkinghub.elsevier.com/retrieve/pii/0020-1790(87)90167-3.

Wright, Amy E.; Chen, Ying; Winder, Priscilla L.; Pitts, Tara P.; Pomponi, Shirley A.; Longley, Ross E. (2004): Lasonolides C-g, five new lasonolide compounds from the sponge Forcepia sp. In *Journal of natural products* 67 (8), pp. 1351–1355. DOI: 10.1021/np040028e.

Wu, Jia-Shun; Jiang, Jian; Chen, Bing-Jun; Wang, Ke; Tang, Ya-Ling; Liang, Xin-Hua (2021): Plasticity of cancer cell invasion: Patterns and mechanisms. In *Translational oncology* 14 (1), p. 100899. DOI: 10.1016/j.tranon.2020.100899.

Wu, Xinyu; Daniels, Garrett; Lee, Peng; Monaco, Marie E. (2014): Lipid metabolism in prostate cancer. In *American journal of clinical and experimental urology* 2 (2), pp. 111–120.

Xu, Kexin; Shimelis, Hermela; Linn, Douglas E.; Jiang, Richeng; Yang, Xi; Sun, Feng et al. (2009): Regulation of androgen receptor transcriptional activity and specificity by RNF6-induced ubiquitination. In *Cancer cell* 15 (4), pp. 270–282. DOI: 10.1016/j.ccr.2009.02.021.

Xu, Shimeng; Zhang, Xuelin; Liu, Pingsheng (2018): Lipid droplet proteins and metabolic diseases. In *Biochimica et Biophysica Acta (BBA) - Molecular Basis of Disease* 1864 (5), pp. 1968–1983. DOI: 10.1016/j.bbadis.2017.07.019.

Yamaguchi, Hideki; Wyckoff, Jeffrey; Condeelis, John (2005): Cell migration in tumors. In *Current opinion in cell biology* 17 (5), pp. 559–564. DOI: 10.1016/j.ceb.2005.08.002.

Yamaguchi, Kiyoshi; Sakai, Michihiro; Kim, JooHun; Tsunesumi, Shin-ichiro; Fujii, Tomoaki; Ikenoue, Tsuneo et al. (2011): MRG-binding protein contributes to colorectal cancer development. In *Cancer science* 102 (8), pp. 1486–1492. DOI: 10.1111/j.1349-7006.2011.01971.x.

Yamamoto, Shinya; Jaiswal, Manish; Charng, Wu-Lin; Gambin, Tomasz; Karaca, Ender; Mirzaa, Ghayda et al. (2014): A drosophila genetic resource of mutants to study mechanisms underlying human genetic diseases. In *Cell* 159 (1), pp. 200–214. DOI: 10.1016/j.cell.2014.09.002.

Yamazaki, H.; Schneider, E.; Myers, C. E.; Sinha, B. K. (1994): Oncogene overexpression and de novo drug-resistance in human prostate cancer cells. In *Biochimica et biophysica acta* 1226 (1), pp. 89–96. DOI: 10.1016/0925-4439(94)90063-9.

Yan, Ping; Gong, Hui; Zhai, Xiaoyan; Feng, Yi; Wu, Jun; He, Sheng et al. (2016): Decreasing CNPY2 Expression Diminishes Colorectal Tumor Growth and Development through Activation of p53 Pathway. In *The American journal of pathology* 186 (4), pp. 1015–1024. DOI: 10.1016/j.ajpath.2015.11.012.

Yanagawa, S.; Lee, J. S.; Ishimoto, A. (1998): Identification and characterization of a novel line of Drosophila Schneider S2 cells that respond to wingless signaling. In *The Journal of biological chemistry* 273 (48), pp. 32353–32359. DOI: 10.1074/jbc.273.48.32353.

Yang, Yili; Kitagaki, Jirouta; Dai, Ren-Ming; Tsai, Yien Che; Lorick, Kevin L.; Ludwig, Robert L. et al. (2007): Inhibitors of ubiquitin-activating enzyme (E1), a new class of potential cancer therapeutics. In *Cancer research* 67 (19), pp. 9472–9481. DOI: 10.1158/0008-5472.CAN-07-0568.

Yao, T. P.; Forman, B. M.; Jiang, Z.; Cherbas, L.; Chen, J. D.; McKeown, M. et al. (1993a): Functional ecdysone receptor is the product of EcR and Ultraspiracle genes. In *Nature* 366 (6454), pp. 476–479. DOI: 10.1038/366476a0.

Yao, T. P.; Forman, B. M.; Jiang, Z.; Cherbas, L.; Chen, J. D.; McKeown, M. et al. (1993b): Functional ecdysone receptor is the product of EcR and Ultraspiracle genes. In *Nature* 366 (6454), pp. 476–479. DOI: 10.1038/366476a0.

Yao, T. P.; Segraves, W. A.; Oro, A. E.; McKeown, M.; Evans, R. M. (1992): Drosophila ultraspiracle modulates ecdysone receptor function via heterodimer formation. In *Cell* 71 (1), pp. 63–72. DOI: 10.1016/0092-8674(92)90266-f.

Yap, Wei Sheng; Shyu, Peter; Gaspar, Maria Laura; Jesch, Stephen A.; Marvalim, Charlie; Prinz, William A. et al. (2020): The yeast FIT2 homologs are necessary to maintain cellular proteostasis and membrane lipid homeostasis. In *Journal of cell science* 133 (21). DOI: 10.1242/jcs.248526.

Yoo, Byoungjoo; Kim, Hae-Yoon; Chen, Xi; Shen, Weiping; Jang, Ji Sun; Stein, Shaianne N. et al. (2021): 20-hydroxyecdysone (20E) signaling regulates amnioserosa morphogenesis during Drosophila dorsal closure: EcR modulates gene expression in a complex with the AP-1 subunit, Jun. In *Biology open* 10 (8). DOI: 10.1242/bio.058605.

Yue, Shuhua; Li, Junjie; Lee, Seung-Young; Lee, Hyeon Jeong; Shao, Tian; Song, Bing et al. (2014): Cholesteryl ester accumulation induced by PTEN loss and PI3K/AKT activation underlies human prostate cancer aggressiveness. In *Cell metabolism* 19 (3), pp. 393–406. DOI: 10.1016/j.cmet.2014.01.019.

Yuen, Hiu-Fung; Chan, Yuen-Piu; Cheung, Wai-Lok; Wong, Yong-Chuan; Wang, Xianghong; Chan, Kwok-Wah (2008): The prognostic significance of BMP-6 signaling

in prostate cancer. In *Modern pathology : an official journal of the United States and Canadian Academy of Pathology, Inc* 21 (12), pp. 1436–1443. DOI: 10.1038/modpathol.2008.94.

Yuen, Hiu-Fung; McCrudden, Cian M.; Grills, Claire; Zhang, Shu-Dong; Huang, Yu-Han; Chan, Ka-Kui et al. (2012): Combinatorial use of bone morphogenetic protein 6, noggin and SOST significantly predicts cancer progression. In *Cancer science* 103 (6), pp. 1145–1154. DOI: 10.1111/j.1349-7006.2012.02252.x.

Zelcer, Noam; Hong, Cynthia; Boyadjian, Rima; Tontonoz, Peter (2009): LXR regulates cholesterol uptake through Idol-dependent ubiquitination of the LDL receptor. In *Science (New York, N.Y.)* 325 (5936), pp. 100–104. DOI: 10.1126/science.1168974.

Zhang, Congyan; Liu, Pingsheng (2019): The New Face of the Lipid Droplet: Lipid Droplet Proteins. In *Proteomics* 19 (10), p. 1700223. DOI: 10.1002/pmic.201700223.

Zhang, Jing; Qiao, Qing; Xu, Hong; Zhou, Ru; Liu, Xinzhe (2022): Human cell polyploidization: The good and the evil. In *Seminars in cancer biology* 81, pp. 54–63. DOI: 10.1016/j.semcancer.2021.04.005.

Zhang, Xiaoshuai; Li, Sheng; Liu, Suning (2021): Juvenile Hormone Studies in Drosophila melanogaster. In *Frontiers in physiology* 12, p. 785320. DOI: 10.3389/fphys.2021.785320.

Zhou, Chuanchuan; Bi, Fengrui; Yuan, Jihang; Yang, Fu; Sun, Shuhan (2018): Gain of UBE2D1 facilitates hepatocellular carcinoma progression and is associated with DNA damage caused by continuous IL-6. In *Journal of experimental & clinical cancer research* 37 (1), pp. 1–12. DOI: 10.1186/s13046-018-0951-8.

Zi, Xiaolin; Guo, Yi; Simoneau, Anne R.; Hope, Christopher; Xie, Jun; Holcombe, Randall F.; Hoang, Bang H. (2005): Expression of Frzb/secreted Frizzled-related protein 3, a secreted Wnt antagonist, in human androgen-independent prostate cancer PC-3 cells suppresses tumor growth and cellular invasiveness. In *Cancer research* 65 (21), pp. 9762–9770. DOI: 10.1158/0008-5472.CAN-05-0103.

Zimmermann, Robert; Strauss, Juliane G.; Haemmerle, Guenter; Schoiswohl, Gabriele; Birner-Gruenberger, Ruth; Riederer, Monika et al. (2004): Fat mobilization in adipose tissue is promoted by adipose triglyceride lipase. In *Science (New York, N.Y.)* 306 (5700), pp. 1383–1386. DOI: 10.1126/science.1100747.

Zipper, Lisa; Batchu, Sai; Kaya, Nida Hatice; Antonello, Zeus Andrea; Reiff, Tobias (2022): The MicroRNA miR-277 Controls Physiology and Pathology of the Adult Drosophila Midgut by Regulating the Expression of Fatty Acid β-Oxidation-Related Genes in Intestinal Stem Cells. In *Metabolites* 12 (4). DOI: 10.3390/metabo12040315.

Zipper, Lisa; Jassmann, Denise; Burgmer, Sofie; Görlich, Bastian; Reiff, Tobias (2020): Ecdysone steroid hormone remote controls intestinal stem cell fate decisions via the PPARγ-homolog Eip75B in Drosophila. In *eLife* 9. DOI: 10.7554/eLife.55795.

List of figures and tables

Abbreviations

20-hydroxyecdysone	20HE
abdominal-B	Abd-B
accessory gland	AG
amino acid	aa
ammonium persulfate	APS
androgen receptor	AR
angiotensin converting enzyme	ANCE
arginine	R
base pairs	bp
bovine serum albumin	BSA
castration-resistant prostate cancer	CRPC
centimorgan	cM
cholesteryl ester	CE
complementary DNA	cDNA
deficiency line	Df
degree Celsius	°C
deoxyribonucleic acid	DNA
dimethyl sulfoxide	DMSO
distilled water	dH2O
early 35 kDa protein	p35
ecdysone receptor	EcR
ecdysone-induced protein 74EF	E74A
ecdysone-induced protein 75A	E75A
ecdysone-induced protein 75B	E75B
endoplasmic reticulum	ER
escargot	esg
estrogen-related receptor	ERR
ethanol	EtOH
ethylene glycol-bis(β-aminoethyl ether)-N,N,N′,N′-tetraacetic acid	EGTA
ethylenediaminetetraacetic acid	EDTA
fat storage-inducing protein	FIT protein
fetal calf serum	FCS
gram	g

green fluorescent protein	GFP
hour	h
human influenza hemagglutinin	HA
insulin-like growth factor signaling	IIS
juvenile hormone	JH
juvenile hormone epoxide hydrolase	JHEH
kilodalton	kDa
lipid droplet	LD
lipid droplet associated protein	LDAP
lipid droplet-associated hydrolase	LDAH
loss of function	LOF
lysine	K
lysogeny broth	LB
main cell	MC
methanol	MeOH
microgram	µg
microliter	µl
micrometer	µm
micromolar	µM
milliampere	mA
milligram	mg
milliliter	ml
millimeter	mm
minute	min
myosin regulatory light chain interacting protein/ inducible degrader of the LDL receptor	MYLIP/ IDOL
nanogram	ng
nanometer	nm
oleic acid	OA
open reading frame	ORF
optical density	OD
paraformaldehyde	PFA
phosphatase and Tensin homolog	PTEN
phosphate-buffered saline	PBS

polyacrylamide gel electrophoresis	PAGE
polymerase chain reaction	PCR
polyunsaturated fatty acid	PUFA
prostate cancer	PCa
quantitative real-time polymerase chain reaction	qRT-PCR
ribonucleic acid	RNA
ribosomal protein 49	rp49
RNA interference	RNAi
rounds per minute	rpm
secondary cell	SC
seconds	sec
sodium dodecyl sulfate	SDS
(single molecule)fluorescence in situ hybridization	(smi)FISH
triacylglycerol	TAG
tumor protein p53	p53
ultraspiracle	USP
upstream activation sequence	UAS
(very) low density lipoprotein receptor	(V)LDLR
volts	V
mated females	MF
mated males	MM
virgin males	VM

Eidesstattliche Erklärung

Ich, Irfan Akhtar, versichere an Eides Statt, dass die vorliegende Dissertation von mir selbständig und ohne unzulässige fremde Hilfe unter Beachtung der „Grundsätze zur Sicherung guter wissenschaftlicher Praxis an der Heinrich-Heine-Universität Düsseldorf“ erstellt worden ist.

Düsseldorf, März 2023

_____

Irfan Akhtar